University of Alberta

Removal of Naphthenic Acids from Bitumen through Vapour-Phase Decarboxylation

by

Claudia Guarino Ⓒ

A thesis submitted to the Faculty of Graduate Studies and Research
in partial fulfillment of the requirements for the degree of

Master of Science
In
Chemical Engineering

Department of Chemical and Materials Engineering

Edmonton, Alberta
Fall 2006

Canada

ABSTRACT

Naphthenic acids in crude cause costly damage to equipment in refineries and upgrading plants due to corrosion, therefore, the elimination of these acids from oil has become a necessity. This research was focused on the removal of naphthenic acid by ketonic decarboxylation reactions using alkali metal and alkali earth metal carbonates and oxides, including Li_2CO_3, $MgCO_3$, MgO, $CaCO_3$, CaO, and $BaCO_3$. Butyric acid ($C_4H_8O_2$) was used as the model naphthenic acid compound, and the reagent powders were tested at 385 °C in a continuous flow reactor as well as in a batch reactor to determine their efficacy for ketonic decarboxylation. Precipitated $CaCO_3$ showed a higher rate of disappearance of butyric acid as well as higher rate of production of the main decarboxylation product, 4-heptanone. Other ketones, alkenes, CO_2, H_2O were also identified as products. Further analyses showed the formation of butyrate as an intermediate step in the formation of ketones.

ACKNOWLEDGMENT

I thank Dr. Gray for his valuable help and guidance through out my whole research. I am especially grateful to Brian Greenhalgh for his support, advice, patience and help through my entire masters. Research is rarely an individual effort, and I am indebted to Mildred Becerra, Walter Bodditz, Dimitre Karpuzov, Andree Koenig and Shihong Xu. Through my time at the University of Alberta I had the opportunity to share good times with great people: Alex Abraham, Joyce Funk, Abu Saleh Mohammad Junaid, Zhiming Liu, Mingyong Sun, Peter Unwin, Zhenhui Wang, Ling Yang and Shaofeng Yang. Finally, I also thank my parents for their support through my time here in Canada.

DEDICATION

A mi *hermanilla* Alejandra.

(To my sister Alejandra)

TABLE OF CONTENTS

CHAPTER 6: CONCLUSIONS AND RECOMMENDATIONS

LIST OF TABLES

LIST OF FIGURES

CHAPTER 4

LIST OF EQUATIONS

CHAPTER 4

NOMENCLATURE

A	Peak area reported by the gas chromatographer	arbitrary unit
d	Diameter of the particle	μ
F	Molar flow rate	(Mol / min)
f	Fraction of particles	
GHSV	Gas hourly space velocity	(h^{-1})
h	Planck's constant $(6.626068*10^{-34})$	(m^2*Kg/s)
M	Mass of reagent powder	(g)
MW	Molecular weight	(g/mol)
N	Number of moles	
P	Pressure	(atm)
Q	Volumetric flow rate	(scm^3)
T	Temperature	(^oC)
$R_{x/y}$	Ratio of x to y	
V	Volume	(cm^3)
WHSV	Weight hourly space velocity	(h^{-1})
X	Conversion	
y	Molar fraction in the vapour phase	

Subscripts

(A)	Acetone
(BA)	Butyric acid
C	Consumed
$E_{binding}$	Binding energy
$E_{kinetics}$	Kinetic energy

(H)	4-Heptanone
I	Inlet parameter
i	Group of particles with the same diameter
(N₂)	Nitrogen
O	Outlet parameter
P	Produced
RP	Reagent powder
RX	Reactor
SL	Sample loop of the 6-port valve installed in the gas chromatographer
(T)	Total

Greek letters

ϕ	Work function	
τ	Space-time at operating conditions	(s)
υ	Frequency of the exciting radiation	

INTRODUCTION

1.1. - Background and Motivation

Naphthenic acid is a general term used to describe the organic acids present in unrefined crude oil. Although the molecular weight and chemical formula of these acids can vary from one from specific acid to another, the general formula for all naphthenic acids is defined as R $(CH_2)_n$ COOH, where R is usually a cyclopentane or a cyclohexane ring (Slavcheva, et al. 1999) and n is usually larger than 12 (http://www.setlaboratories.com/naphthenic.htm).

According to Tseng-Pu (1991), naphthenic acids can be divided into seven major groups based on *hydrogen deficiency*. Hydrogen deficiency can be defined as the difference in hydrogen content between a cyclic and/or unsaturated acid and its saturated aliphatic analogue. In Figure 1-1, Z equal to 0 represents an aliphatic saturated carboxylic acid.
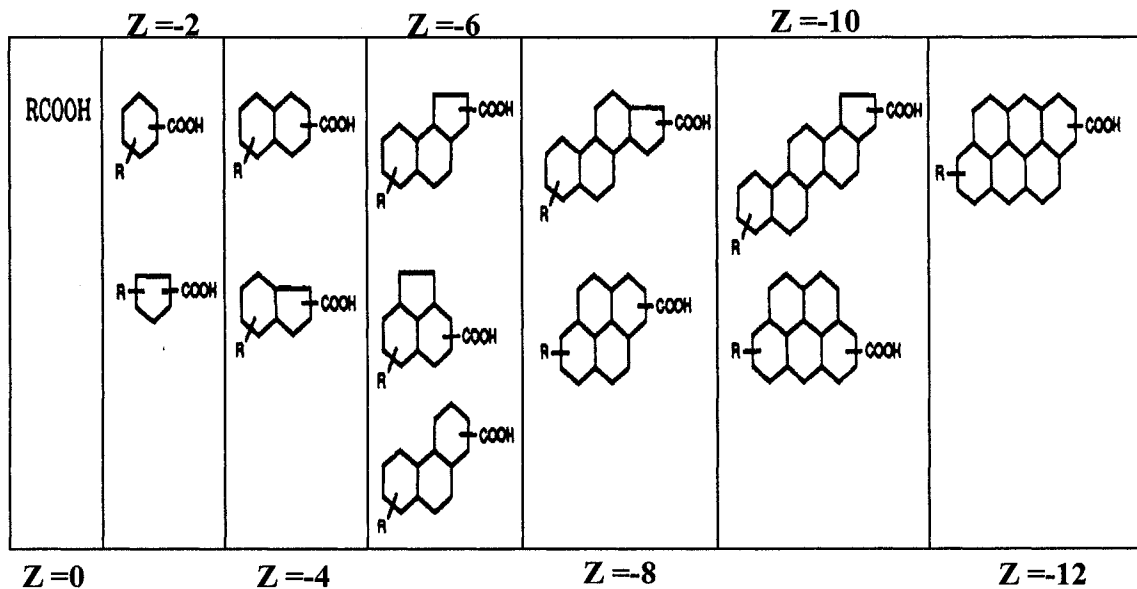
Figure 1-1: Different types of naphthenic acids and their corresponding hydrogen deficiency values. (Tseng-Pu, 1991)

Since the 1920s, naphthenic acids have been known to cause costly damage to equipment in crude refineries and upgrading plants due to corrosion (Piehi, 1988). Removal of these acids from oil has become a necessity, especially from untreated (non-hydrotreated) petroleum distillates.

The reaction mechanism through which naphthenic acids attack metal surfaces is unknown (Babaian-Kibala, 1994), however, Slavcheva et al. (1999) proposed the following corrosion reaction mechanism:

$$Fe + 2\,RCOOH \longrightarrow Fe\,(RCOO)_2 + H_2 \qquad (1\text{-}1)$$

$$Fe + H_2S \longrightarrow FeS + H_2 \qquad (1\text{-}2)$$

$$Fe\,(RCOO)_2 + H2S \longrightarrow FeS + 2\,RCOOH \qquad (1\text{-}3)$$
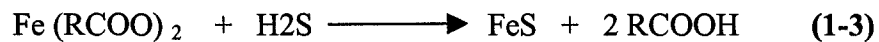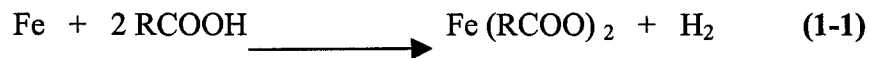
According to Slavcheva et al. (1999), the naphthenic acid reacts with the iron contained in the material of the equipment forming iron naphthenate, which is soluble in oil, thereby exposing further iron to degradation. However, iron sulphide can be formed in the presence of hydrogen sulphide (H_2S), which gives some protection to the surface of the material depending on the concentration of the naphthenic acids.

The boiling points of most naphthenic acids are between 200 and 370 °C, and as a result, they concentrate in the heavier cuts of the oil and are present in the hottest section of the crude refineries or upgrading plants (Babaian-Kibala, 1994). Naphthenic acid corrosion is favored by both high temperatures and high flow rates. Thus, such corrosion is usually found in the atmospheric and vacuum furnace and transfer lines, in the atmospheric and vacuum tower bottoms, and in pipelines where the temperature is higher than 200 °C (http://www.setlaboratories.com/naphthenic.htm; Babaian-Kibala, 1994).

Usually the concentration of naphthenic acid in crude oil is expressed by the Total Acid Number (TAN), which is defined as the milligrams of potassium hydroxide (KOH) required to neutralized 1 gram of oil (Blum et al., 2004). The TAN is determined according to the standard method ASTM D664, which has between 20 and 44%

2

reproducibility. However, this method cannot differentiate acidity due to carboxylic acids, phenols, carbon dioxide, hydrogen sulphide, or other compounds. (http://www.setlaboratories.com/naphthenic.htm).

Crude oils with a TAN lower than 0.2 are considered to be slightly to moderately corrosive (Blum et al., 2004). Crude oils whose TAN is equal to or higher than 0.5 are considered to be corrosive oils, and these crudes are discounted by about 0.50 $/TAN/BBL. Oil cuts with TAN higher than 1.5 are considered to be very corrosive at temperatures between 230 and 400 °C (Varadaraj 2002).

In order to reduce the effects of corrosion in crude refineries or upgrading plants, oil companies blend acidic crudes with non-acidic crudes to obtain a crude oil with a TAN lower than 0.5 (Varadaraj, 2002). Unfortunately, this alternative significantly decreases the value of the low TAN crude. Other alternatives to decrease the naphthenic acid corrosion are the addition of corrosion inhibitors, such as phosphate esters and the use of the construction materials based on chrome or molybdenum alloys (http://www.setlaboratories.com/naphthenic.htm; Babaian-Kibala, 1994). The disadvantages of these options are the high cost involved, and that the source of corrosion is not eliminated.

On the other hand, the removal of naphthenic acids from crude oil is a very attractive alternative since it would increase the value of the crude and reduce the capital and operation cost of the crude refineries and upgrading plants. Different approaches to the removal of naphthenic acids have been considered, such as thermal cracking of the naphthenic acids molecules (Moser et al., 1940). Emulsion techniques, such as the formation and separation of a water-in-oil emulsion by addition of alkoxylated amine (Varadaraj et al., 2000), or by the addition of solids such as silica, clay, coke, etc. have also been reported (Varadaraj et al., 2002). Chemical conversion of the acids to non-corrosive compounds such as esters by adding an alcohol and a group IA or IIA base to the acidic oil has been reported by Michael et al. (2001; 2004). Finally, Sartori et al. (2000) and Blum et al. (2004) have proposed the removal of these acids by neutralization.

Another way to remove naphthenic acids from crude oil suggested by Moser et al. (1940) and Zhang et al. (2004 and 2006) is via decarboxylation reactions. Senderens (1913) formulated the general equation for the ketonic decarboxylation reaction

3

(Equation 1-4), which suggests that carboxylic acids can be converted into ketones, carbon dioxide and water.

$$2R\text{-}COOH \longrightarrow RCOR + CO_2 + H_2O \quad \text{(1-4)}$$
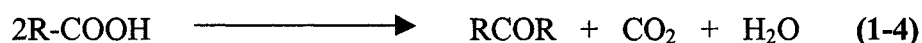
The catalysis of ketonic decarboxylation reactions has been extensively studied in order to favour the production of ketones. However, this reaction is also attractive to those interested in the conversion of carboxylic acids (corrosive compounds) into non-corrosive compounds such as the ketones.

The use of a suitable catalyst could facilitate the elimination of naphthenic acids from untreated oil and this process could be incorporated into the atmospheric distillation operation, which demands the study of the catalytic decarboxylation reaction in both the vapour and liquid phases. In particular, the use of alkali earth metal catalysts in the ketonic decarboxylation of carboxylic acids to produce ketones is well established. (Leung et al., 1995; Renz, 2005)

1.2. - Research Objectives

As a model study, the initial phase of this research consists of the vapour phase decarboxylation of butyric acid ($C_4H_8O_2$) by evaluating the oxides and carbonates of lithium (Li_2CO_3), magnesium (MgO, $MgCO_3$), calcium (CaO, $CaCO_3$), and barium ($BaCO_3$) as reagent powders. The specific reaction to be studied is shown in equation 1-5:

$$C_4H_8O_2 \longrightarrow \tfrac{1}{2}\,C_7H_{14}O + \tfrac{1}{2}\,CO_2 + \tfrac{1}{2}\,H_2O \quad \text{(1-5)}$$
(Butyric acid)   (4-Heptanone)
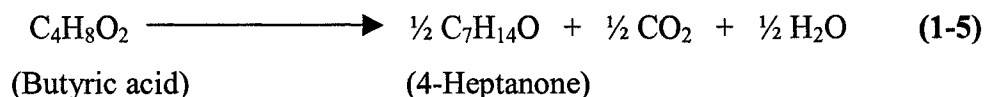
In this project, carbonates and oxides were prepared and screened through the use of a continuous reactor system in order to determine the reagent powder with the best potential performance under the specific operating conditions studied. Subsequently, further studies involving the use of a batch reactor system were carried out to analyse the

4

reagent powders in the post-reaction state, in order to determine the formation of butyrate as an intermediate in the reaction pathway.

Supplementary experiments at less severe operating conditions were also carried out to complement the reaction results and evaluate potential process schemes to remove naphthenic acids from crude oil. Further studies involving heavier naphthenic acids and eventually bitumen would be required to finalize this research.

A theoretical review of the different approaches to reduce or eliminate naphthenic acids from bitumen, different reaction mechanisms proposed by other researchers as well as different techniques of preparation of carbonates and oxides are contained in Chapter 2 of this work. Chapter 3 summarizes the different experimental techniques utilized to analyze the reagent powders before and after reaction, as well as it describes the continuous flow reaction system and the batch reaction system used to perform the study of the decarboxylation reaction of butyric acid.

The results obtained from this project are condensed in Chapter 4, while the discussion of these results is shown in Chapter 5. Chapter 6 presents the conclusions and recommendations suggested.

CHAPTER 2

LITERATURE REVIEW

2.1. -Approaches for the Removal of Naphthenic Acids from Crude Oil

There are several different approaches for the removal of naphthenic acids from crude oil in order to avoid corrosion problems; however, most of these proposals have not yet been applied in commercial industrial plants.

Moser et al. (1940) mentioned the use of a thermal liquid phase treatment for crude oil without a catalyst, in which the crude oil is heated to temperatures between 315 and 400 °C in order to crack the naphthenic acid molecules into neutral compounds. The usefulness of this method is limited because the cracking of the carboxylic acids is a slow and incomplete reaction; while on the other hand, crude oil cracks significantly when exposed to such high temperatures.

Varadaraj et al. (2000) claimed that treating crude oil with alkoxylated amines and water under the optimal temperatures and contact time would form a water-in-oil emulsion of the amine, which would decrease the concentration of naphthenic acids in the crude by around 95%. The emulsion can be broken into different layers that could be separated by centrifuge, gravity settling or electrostatic separation, whereby the uppermost layer contains the crude oil free of the naphthenic acid. They also suggested that this process could be carried out in existing desalter units.

Michael et al. (2001; 2004) proposed to reduce the concentration of carboxylic acids in crude oil by adding sufficient alcohol and a group IA or IIA metal carbonate, hydroxide or phosphate to the crude in order to form the ester of the alcohol, which is a non-corrosive compound. Information related to the use of this technology at a commercially-scaled plant has not been found.

Varadaraj et al. (2002) also studied mixing water, solids and crude oil in order to form a water-in-oil emulsion which could be broken, and subsequently the resulting layers could be separated by conventional separators with minor modifications. The solids may be selected from alumina, clays, coke, silica, etc. Varadaraj et al. (2002)

6

mentioned that sonic energy could be required to break the resulting interfacial film present in the water-in-oil emulsion. At the time of this writing, no information on the commercial use of this technology has been found.

Sartori et al. (2000) and Blum et al. (2004) stated that naphthenic acids contained in crude oil can be neutralized by adding sufficient amounts of a group IA or IIA metal oxide, hydroxide, or hydroxide hydrate. In some cases, water may also be required, yet some crude oils contain enough water such that this would not be necessary. Blum et al. (2004) claimed that this process did not involve the formation of water-in-oil or oil-in-water emulsions, and between 1 to 20 hours would be required to obtain oil with a low concentration of naphthenic acid.

On the other hand, Moser et al. (1940) studied the vapour-phase decarboxylation reaction of naphthenic acids from crude oil. According to these authors, upon passing hydrocarbon vapours through alkaline earth metal oxides at 200 °C, naphthenates form. These naphthenates then subsequently decompose to earth oxides, ketones and CO_2. Operational difficulties were reported in this process. Moser et al. (1940) also used carbonates and oxides of calcium, magnesium, lithium, manganese, iron, cadmium, thorium and other metals in the study of the decarboxylation reaction of naphthenic acids. They reported that calcium, lithium and magnesium carbonates gave very good results. Additionally, lithium seemed to increase the activity of other earth alkaline oxides.

Furthermore, Moser et al. (1940) also claimed that cracking crude oil at temperatures around 400 and 450 °C requires a contact time of around 3 to 4 seconds, while the elimination of 95% of the naphthenic acids contained in crude oil requires a contact time of only 1/25 seconds at the same temperature. Thus, according to Moser et al. (1940), naphthenic acids can be removed from crude oil if this is heated in the presence of lithium, calcium or other earth alkaline carbonates to sufficiently high temperatures with limited contact time.

2.2. - Ketonic Decarboxylation Reaction

The ketonic decarboxylation of carboxylic acids could also be an alternative to achieve the reduction of the naphthenic acid content in bitumen. A reaction mechanism able to satisfactorily explain the ketonic decarboxylation has not yet been reported.

7

However, several different reaction mechanisms have been proposed (Pestman et al., 1997).

2.2.1. - Reaction Mechanism via β-Keto Acid Intermediate

In 1939, Neunhoeffer and Paschke proposed a β-keto acid intermediate as an explanation for the reaction mechanism. The β-keto acid intermediate implies the abstraction of an α-hydrogen atom from the acid (Pestman et al. 1997).

It has been proposed that ketones are formed from carboxylic acids via formation of anhydrides. Apparently, α-hydrogen atoms are more loosely held in anhydrides than in acids, so decarboxylation would follow the rearrangement of the anhydride to the β-keto acid (equation 2-1) (Patai 1966).

$$2RCH_2COOH \xrightarrow{-H_2O} \begin{array}{c} RCH_2C=O \\ \diagdown O \\ \diagup \\ RCH_2C=O \end{array} \longrightarrow RCH_2COCHCO_2H \underset{R}{|}$$

$$\longrightarrow RCH_2COCH_2R + CO_2 \qquad (2\text{-}1)$$
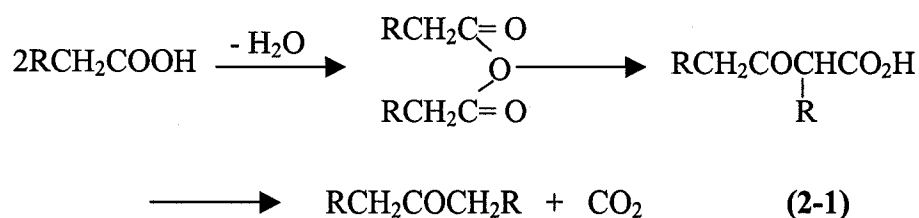
The formation of an intermediate β-keto acid is consistent with the observation that aliphatic acids without an α-hydrogen lead to the production ketones (Patai, 1966).

Curtis et al. (1947) used several metallic oxides and carbonates to study the preparation of ketones from fatty acids and it was found that magnesium oxide was the most suitable. The ideal temperature range was 330–360 °C. These results agreed with the proposed formation of keto-acid compounds as intermediates in the formation of ketones. It was suggested that the formation of the salts of the keto-acids is the rate determining step in the reaction, and this step is catalyzed by the metallic oxide / carbonate. (Patai, 1966)

Two reactions were proposed for the formation of ketones by using MgO.

$$2RCH_2COOH + MgO \longrightarrow (RCH_2COO)_2Mg + H_2O \qquad (2\text{-}2)$$

8

$$(RCH_2COO)_2Mg \longrightarrow (RCH_2)_2CO + MgO + CO_2 \quad \textbf{(2-3)}$$
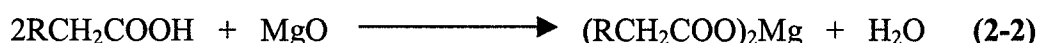
However, reaction (2-3) is not sufficient since there is some evidence explaining the formation of ketones through β-keto-acids, so reaction (2-3) must be replaced by reactions (2-4) through (2-8), as shown in Figure 2-1 (Curtis et al., 1947).

$$(RCH_2COO)_2Mg \longrightarrow RCH_2COCHRCOOMgOH \quad \textbf{(2-4)}$$

$$RCH_2COCHRCOOMgOH + RCH_2COOH \longrightarrow RCH_2COCHRCOOMgOCOCH_2R + H_2O \quad \textbf{(2-5)}$$

$$RCH_2COCHRCOOMgOCOCH_2R + RCH_2COOH \longrightarrow RCH_2COCHRCOOH + (RCH_2COO)_2Mg \quad \textbf{(2-6)}$$

$$RCH_2COCHRCOOMgOH \longrightarrow (RCH_2)_2CO + MgO + CO_2 \quad \textbf{(2-7)}$$

$$RCH_2COCHRCOOH \longrightarrow (RCH_2)_2CO + CO_2 \quad \textbf{(2-8)}$$
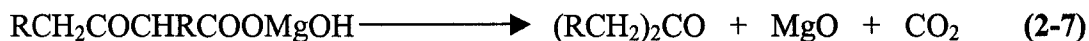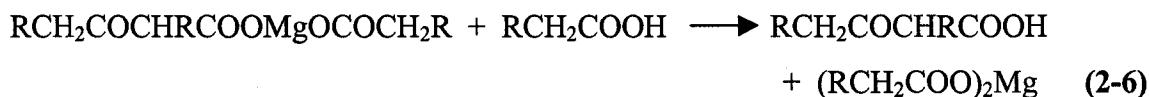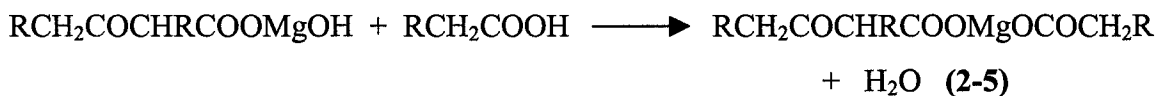
The formation of metallic acid (reaction 2-2) does not influence the rate of production of CO_2 (Curtis et al., 1947). Evidence of the formation of β-keto-acids was found by comparing the unchanged acid determined experimentally with that calculated from the amount of CO_2 formed at various stages of the reaction. If the formation of ketones occurred without the formation of β-keto-acids, these values would be identical. However, in all of the experiments made by Curtis et al. (1947), the amount of unreacted acid was lower than that from the carbon dioxide liberated.

9

2.2.2. - Reaction Mechanism via γ-Keto Acid Intermediate

Miller et al. (1950) studied the ketonic decarboxylation of trimethylacetic acid on thorium oxide (ThO_2) at 490 °C, finding that the main product was t-butyl isobutyl ketone and no evidence of di-t-butyl ketone. Besides CO_2, the other products of the reaction, such as t-butyl methyl ketone, t-butyl ethyl ketone, trimethylacetaldehyde, butanes, butylenes, etc, seem to be decomposition products of t-butyl isobutyl ketone. CO was also reported as a product of ketone decomposition due to the high temperature (490 °C) (Miller et al., 1950). They proposed the following reaction mechanism:

1. - Adsorption of the molecule of acid (trimethylacetic acid) in the gaseous phase over the basic catalyst (ThO_2).
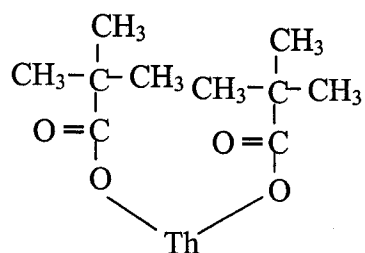
Figure 2-1: Adsorption of trimethylacetic acid in the gaseous phase over ThO_2

2. - Formation of a carboxylic salt between the thorium and the carboxylic acid (trimethylacetic acid). Apparently the function of the catalyst is to provide the right orientation to two or more molecules of acid.
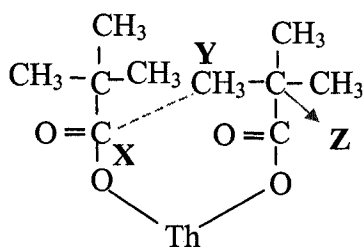
Figure 2-2: Carboxylic salt between ThO_2 and trimethylacetic acid.

10

Di-t-butyl ketone cannot be formed because carbon **Z** is saturated with methyl groups, and it cannot approach carbon **X**. Instead, carbon **Y** reacts with carbon **X** in order to form a seven-member ring intermediate through an aldol type of condensation. (Miller et al. 1950)

3. - The seven membered intermediate is not very stable and it decomposes to a thorium salt of a γ keto acid.

$$CH_3-\underset{\underset{CH_3}{|}}{\overset{\overset{CH_3}{|}}{C}}-\overset{\overset{O}{\diagup\!\!\!\diagup}}{\underset{\gamma}{C}}-CH_2-\underset{\underset{CH_3}{|}}{\overset{\overset{CH_3}{|}}{C}}-\overset{\overset{O}{\diagup\!\!\!\diagup}}{\underset{\alpha}{C}}-O-Th-$$
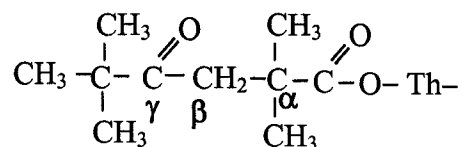
Figure 2-3: Thorium salt of the γ keto acid

4. - Thorium salt of a γ keto acid is decarboxylated.

$$CH_3-\underset{\underset{CH_3}{|}}{\overset{\overset{CH_3}{|}}{C}}-\overset{\overset{O}{\diagup\!\!\!\diagup}}{C}-CH_2-\underset{\underset{CH_3}{|}}{\overset{\overset{CH_3}{|}}{CH}} \quad + \quad CO_2 \quad + \quad Th$$
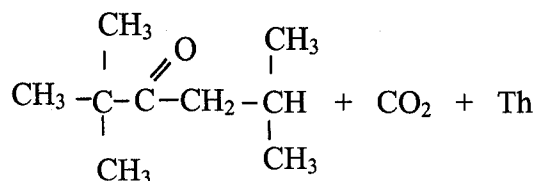
Figure 2-4: t-butyl isobutyl ketone as the main product

This reaction mechanism can also be applied to carboxylic acids containing α-hydrogen. This was confirmed by studying the reaction of isobutyric acid over ThO_2 at 490 °C, which produced 50% diisopropyl ketone and 5% of n-propyl isopropyl ketone. In this case, carbon **X** can approach carbon **Y** and also carbon **Z** since there is hydrogen attached to carbon **Z**. (Miller et al. 1950)

2.2.3. - Reaction Mechanism via Pyrolysis of Carboxylic Acids

Leung et al. (1995) studied the pyrolysis of neat saturated C_4, C_5, C_7, C_8, C_{10} and C_{12} carboxylic acids over alumina at 450 °C and a WHSV of ~0.46 h^{-1} in order to investigate the reaction pathway and mechanisms involved in the conversion of carboxylic acids to hydrocarbons. They reported that the lower the molecular weight of

the carboxylic acid, the higher the selectivity to production of symmetrical ketones, which degraded to methyl ketones and hydrocarbons likely via a γ-hydrogen transfer. After pyrolysis of each acid, the authors found two different liquid phases; organic and pyrolytic water. For the pyrolysis of butyric acid, the reported composition of the organic phase, which includes ketone products and subsequent γ-hydrogen transfer products, was 77.6 wt% 4-heptanone, 6.2 wt% 2-pentanone and 0.4 wt% acetone, while for the composition of the γ-hydrogen transfer products for the pyrolized ketone was 11.1 wt% heptene, and 2.1 wt% pentene.

The mass of coke reported by Leung et al. (1995) showed an increase in the deposition of coke with the increase in the molar mass of the acids, going from 10.3 wt% (C_4) to 25.6 wt% (C_{12}). The composition of the gas produced by the pyrolysis is mostly CO_2 and CO in a lower concentration. (Leung et al. 1995) In this work, a pathway reaction was postulated which proposes that symmetrical ketones are formed by the pyrolysis of the carboxylic acids, followed by a γ-hydrogen transfer mechanism involving rearrangement in order to form methyl ketones and alkenes (Figure 2-5). However, the results presented showed the presence of alkenes with the same number of carbon atoms as the ketones.

$$
\begin{array}{c}
\overset{\displaystyle O}{\underset{\displaystyle \|}{}} \\
R_1 - C - CH_2 - CH_2 - R_2
\end{array}
$$

$$
\begin{array}{ccc}
\overset{\displaystyle O - H}{\underset{\displaystyle |}{}} & & \overset{\displaystyle O}{\underset{\displaystyle \|}{}} \\
R_1 - C = CH_2 \quad + \quad CH_2 = CH - R_2 & \longrightarrow & R_1 - C - CH_3
\end{array}
$$
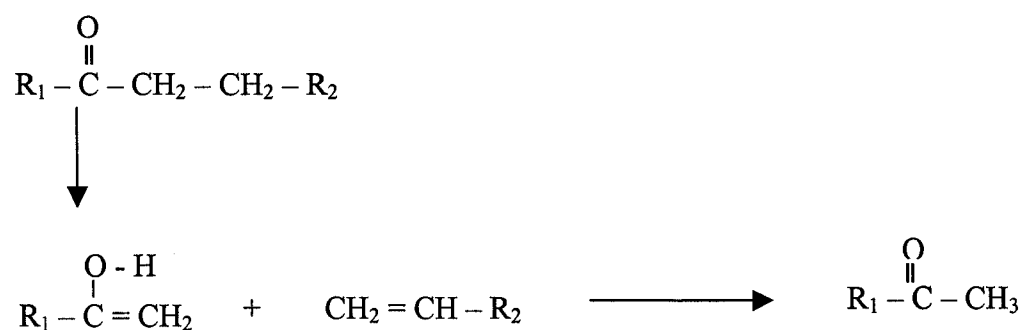
Figure 2-5: γ-hydrogen mechanism on symmetrical ketone and methyl ketone proposed by Leung et al. (1995).

Leung et al. (1995) also studied the pyrolysis of the ketones in order to compare with the pyrolysis of the carboxylic acids. It was found the gas and coke formation is

12

found mainly from the carboxylic acid before they are converted into ketones. Since the gas chromatograms of the products of the carboxylic acid pyrolysis and the products of the ketones pyrolysis were very similar, it was concluded that carboxylic acids convert into ketones very quickly, and these further degrade to methyl ketones and hydrocarbons.

2.2.4. - Reaction of Carboxylic Acids on Oxides

When a basic oxide catalyst is used in the ketonic decarboxylation of carboxylic acids, a carbonate is produced by the reaction of the acid with the catalyst. This carbonate is also catalytically active in the ketonization reaction. (Pestman et al., 1997)

Pestman et al. (1997) studied ketonic decarboxylation of acetic acid using different catalysts. They found that γ-alumina showed high catalytic activity for this reaction, and at temperatures above 300 $^{\circ}$C, the only products detected were acetone, carbon dioxide and water. TiO_2, Cr_2O_3 and ZrO_2 showed similar behaviour, but were less active unless the reaction temperature was higher, around 400 $^{\circ}$C. These authors also studied the behaviour of Bi_2O_3, PbO_2, MgO, MnO_2 in the ketonization of acetic acid. These catalysts showed a different performance from the catalysts mentioned above. When the reaction temperature is around 150 – 200 $^{\circ}$C (depending on the catalyst used), the concentration of carboxylic acid drops significantly without any evidence of the main product (acetone), accompanied by a small increase in the concentration of water. However, around 300 – 350 $^{\circ}$C (material specific) the concentration of carbon dioxide and acetone increase considerably. (Pestman et al. 1997)

Pestman et al. (1997) mention that the carboxylic acid likely reacts with the oxide to form an intermediate that is decomposed later at higher temperatures, to produce ketone, CO_2 and water. They used XRD to analyze the catalysts after reaction at low temperatures (150 – 200 $^{\circ}$C), and they found that the catalysts were converted from oxides to acetates. Since the oxides they used were basic and of low lattice energy (the energy required to separate a mole of the solid into its component ions in the gas phase), they proposed that the oxide was completely converted to its corresponding acetate. (Equation 2-9):

$$2CH_3COOH \ + \ MO \ \longrightarrow \ Me(CH_3COO)_2 \ + \ H_2O \qquad (2\text{-}9)$$

13
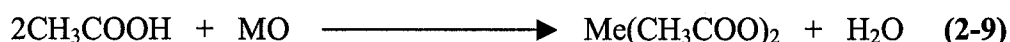
Subsequently, it was postulated that this salt could be decomposed at high temperature as shown:

$$M(CH_3COO)_2 \longrightarrow CH_3COCH_3 + CO_2 + MO \qquad \textbf{(2-10)}$$

Or

$$M(CH_3COO)_2 \longrightarrow CH_3COCH_3 + MCO_3 \qquad \textbf{(2-11)}$$

Pestman et al. (1997) concluded that when oxides with low lattice energy are used as catalysts, the acetate, not the oxide, is the real catalyst. Catalysts with high lattice energy, such as alumina, zirconia, titania or vanadia, which do not present a similar behaviour as the basic oxide catalysts, remain macroscopically unchanged in the reaction. In other words, ketonization occurs via bulk acetates when the oxide has low metal–oxygen bond strength, but via a surface reaction if the oxide has high metal–oxygen bond strength. High basicity can also favour the formation of acetates.

Pestman et al. (1997) also reported the selectivity to the production of ketones of different carboxylic acids with different numbers of α-hydrogen atoms (acetic acid, propionic acid, isobutyric acid and pivalic acid) in the ketonic decarboxylation using different catalysts, such as iron oxide, vanadia and titania. The results showed that the lower the number of α-hydrogen atoms, the lower the selectivity of ketones. These authors studied the formation of ketenes and ketones in the ketonization of acetic acid with varying contact times. They found that the shorter the contact time, the higher the production of the ketene and the lower the production of acetone. Based on this, they suggested that ketene could be an intermediate in the formation of ketone, which demands the abstraction of α-hydrogen atoms (Pestman et al., 1997).

Ketonization of a mixture of pivalic acid and C^{13} – labelled acetic acid was studied using titania as catalyst in a range of temperature of 370 – 450 °C by Pestman et al. 1997. Acetone and unlabeled 2,2-dimethyl-3-butanone were detected, which are the products of the reaction between two molecules of acetic acid and between one molecule of acetic acid with on molecule of pivalic acid. Since no product from the reaction of two molecules of pivalic acid was found, pivalic acid did not form its corresponding ketone.

14

Because the 2,2-dimethyl-3-butanone was unlabelled, the carbonyl group required to form this ketone should have come from the pivalic acid, which cannot form any ketene. Pestman et al. (1997) also suggested that the α-carbon of the alkyl group could also be part of an intermediate in the ketonization reaction, which requires the abstraction of a α-hydrogen atom.

Sugiyama et al. (1992) reported conversion of acetic acid to acetone using magnesium, calcium, barium, zinc and sodium oxides on SiO_2 at 400 °C with space velocity equal to 3600 h^{-1}. Mg and Zn showed high activity, while Ca, Ba and Na showed low activity. They concluded that the activity of the catalysts correlated with the decomposition temperature of the acetates, but did not correlate with those of the carbonates. The following reaction sequence was proposed.

$$MgO + 2CH_3COOH \longrightarrow (CH_3COO)_2Mg + H_2O \quad \textbf{(2-12)}$$

$$(CH_3COO)_2Mg \longrightarrow MgCO_3 + (CH_3)_2CO \quad \textbf{(2-13)}$$

$$MgCO_3 + 2CH_3COOH \longrightarrow (CH_3COO)_2Mg + CO_2 + H_2O \quad \textbf{(2-14)}$$

Sugiyama et al. (1992) also reported that Li_2CO_3/SiO_2 showed a low conversion in the ketonic decarboxylation of benzoic acid, giving selectivity to benzophenone of 8% at 500 °C. Alkaline earth catalysts supported on active carbon demonstrated a higher activity than those supported on silica (Sugiyama et al., 1992).

Zhang et al. (2004) studied the catalytic decarboxylation reactions of several carboxylic acid systems, both neat, as mixtures and within crude oil. The catalysts studied were the oxides of Mg, Ca, Sr, Ba, Ag and Cu. When using only one carboxylic acid or a mixture of carboxylic acids, Zhang et al. (2004) found that MgO showed the highest activity at temperatures around 150 – 250 °C. Although very high conversions of the carboxylic acids were reported (80%), comparatively low yields for CO_2 were also found (18%) at 300 °C using MgO. When small amounts of Ni and Cu were added to

15

MgO, the conversion improved significantly. Discrepancies between carboxylic acid conversions and the yield of CO_2 could be explained by the formation of carboxylic salts due to acid-base reaction, or by the adsorption of CO_2 on the metal oxides in order to form alkaline earth metal carbonates (Zhang et al., 2004).

In studies of acidic crude oil, Zhang et al. (2004) reported that CaO showed the highest activity at 300 °C while MgO did not show significant reactivity. In later work, Zhang et al. (2006) studied the decarboxylation reaction of naphthoic acid in the presence of different oxides such as magnesium, calcium, strontium and barium oxide at 250 °C, finding the calcium oxide gave the highest conversion of the carboxylic acid followed by magnesium oxide. However, because magnesium oxide was the only catalyst which produced CO_2, it was used it to carry out further studies in the removal of naphthenic acids from crude oil.

According to Zhang et al. (2006), the reactivity of magnesium oxide does not depend on the structure of the acid. Experiments using crude oil in a continuous flow reactor system showed that MgO removed more than 30% of the naphthenic acid at 250 °C, deactivating after 9 hours. At 300 °C, the removal of naphthenic acids was between 50 and 64%, deactivating in a time ranging from 12.5 to 20.5 hours. They claimed that magnesium oxide could be used as a catalyst in the removal of naphthenic acids from crude oil at temperatures around 150 and 250 °C. The reaction mechanism suggested could involve acid-base neutralization reactions, oxidative decarboxylation and ketonization of carboxylic acids.

On the other hand, Glinski et al. (1995) studied a series of 20 different oxide catalysts on alumina, silica and titania. They reported insignificant activity at 325 °C for all the catalysts studied, which included SiO_2, B_2O_3, MoO_3, WO_3, P_2O_5, V_2O_5, Bi_2O_3, NiO, Al_2O_3, CuO, ZnO, PbO, Cr_2O_3, Fe_2O_3, CoO, MgO, Nd_2O_3, La_2O_3, MnO_2, CdO, CeO_2, for the catalytic ketonization of acetic acid. Yields of acetone higher than 90 % were reported for MnO_2, CdO, and CeO_2 at 400 °C. CO and methane are reported as products in addition to the rapid formation of coke on the surfaces of many of the catalysts at 350 °C or higher temperatures.

Glinski et al. (1995) reported the influence of the concentration of the active phase within the catalysts on the activity dependence of the yield of acetone on the LHSV

16

(Liquid Hourly Space Velocity). In addition, the activity profile over extended periods was reported for CeO_2 supported on SiO_2. They found that the higher the concentrations of the active phase in the catalyst, the higher the yields of acetone. The range of concentrations of CeO_2 on SiO_2 used in the study was between 5 wt% and 20 wt% (Glinski et al., 1995). A considerable drop in the yield of acetone was reported when the LHSV was increased (from 1 to 4 ml $g^{-1}h^{-1}$) over a temperature range between 300 – 350 °C for 20 wt% CeO_2/SiO_2. At higher temperatures, a very high conversion of the acid is reported despite of the LHSV (Glinski et al., 1995). They reported the yield of acetone over 20 wt% CeO_2 supported on SiO_2 at 350 °C and LHSV of 3 ml g^{-1} h^{-1} for 15 h, finding a very small decrease in the activity of the catalyst in the first 5 hours, and then, the activity was essentially constant. They also noted that alumina supported catalysts exhibited the highest activity among the silica, alumina and titania supported catalyst (Glinski et al., 1995).

2.2.5. - Thermal Decomposition of Carboxylic Salts

As suggested by Sugiyama et al. (1992) and Zhang et al. (2004), the formation of carboxylic salts could be an intermediate in the decarboxylation reaction of carboxylic acids. It has been reported that the thermal decomposition of carboxylic salts produces ketones, carbonates, oxides or the metal depending on the salt (Afzal et al., 1991).

Hites et al. (1972) reported that thermal decomposition of carboxylic salts produces symmetrical ketones, as in the case of calcium acetate, which yields acetone and calcium carbonate when heated. They also studied the thermal decomposition of calcium decanoate at 500 °C, finding various ketones, alkanes, alkenes and CO_2 as the products of the pyrolysis. They proposed the formation of free radicals such as alkyl and acyl radicals from the salt. These radicals are believed to react with each other to form the symmetrical ketone (10-nonadecanone), but also a variety of alkenes, alkanes and other symmetrical and non-symmetrical ketones. The alkyl radicals are also believed to form fragments of carbon chains due to hydrogen rearrangements and β-scission reactions. Figure 2-6 shows a summary of the possible reactions occurring between the formed free radicals in order to generate the final products.

17

$(C_9H_{19}COO)_2Ca$

CaCO$_3$ $C_9H_{19}C \bullet$ $C_9H_{19} \bullet$ $CH_3(CH_2)_n$-CH

     $\overset{\|}{O}$ CH_2 — $(CH_2)_m$-$\overset{\bullet}{C}H_2$

$C_9H_{19}C$ C_9H_{19} $CH_3(CH_2)_n$-CH=CH$_2$

CaO + CO$_2$ $\overset{\|}{O}$ + $CH_3(CH_2)_m \bullet$

         $C_9H_{20} + C_9H_{18}$ $n + m = 5$; n or m=0, 1 ...

**Hydrogen rearrangement +
β scission**
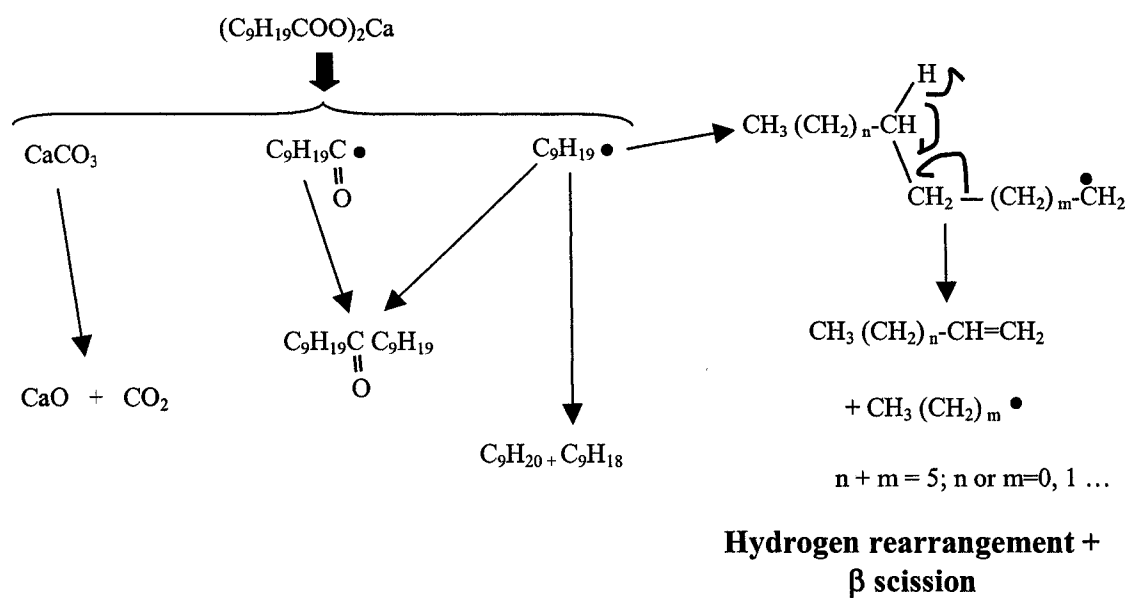
Figure 2-6: Pyrolytic decomposition of calcium decanoate via formation of both alkyl and acyl radicals from the salt proposed by Hites et al. (1972).

Varma et al. (1997) studied the decomposition reaction of zirconium butyrate. Zirconium butyrate began to decompose at 303.5 °C until a temperature of 428.9 °C. It was suggested that zirconium soaps decompose into zirconium carbonate and ketone, as shown in equation 2-15.

$$(C_4H_7O_2)_4Zr \longrightarrow Zr(CO_3)_2 + 2C_3H_7COC_3H_7 \quad (2\text{-}15)$$
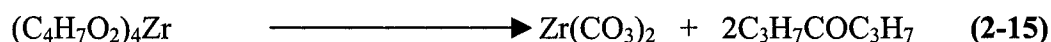
Wiberg (1952) studied the thermal decomposition of deuterated barium butyrate, finding that it decomposes to dipropyl ketone and barium carbonate at around 365 °C.

2.3. - Preparation of Carbonates

As mentioned by Pestman et al. (1997), basic oxides and carbonates could be used in the decarboxylation reaction of carboxylic acids. Carbonates can be prepared by different methods such as precipitation of salts, thermal decomposition of acetates, and thermal decomposition of oxalates.

Choudhary et al. (1994) studied the influence of different preparation conditions (precipitation conditions) of basic magnesium carbonate on its thermal decomposition behaviour and specific surface area. They found that the thermal decomposition of precipitated magnesium carbonate and the surface area of the resulting magnesium oxide are strongly influenced by the following preparation conditions:

- The magnesium salt used particularly magnesium nitrate, sulfate, acetate or chloride.
- The precipitating agent employed, such as sodium carbonate, potassium carbonate, sodium bicarbonate or potassium bicarbonate.
- The concentration of magnesium salt.
- The pH.
- The temperature.
- The method of mixing the magnesium salt and the precipitating agent.
- The aging period of the precipitate (Choudhary et al. 1994).

Choudhary et al. (1994) stated that the nucleation and growth of the crystals of magnesium carbonate are affected by the different concentrations of the salts, as well as the pH, temperature and the time of ageing of the precipitate. The resulting specific surface areas of magnesium oxide reported to vary between 7.5 and 113.6 m^2/g.

2.3.1. - Precipitation of Salts

Carbonates can be prepared by precipitation of different salts. The preparation of carbonates of calcium, magnesium, lithium and barium is described as follows:

- Calcium Carbonate: $CaCO_3$ is obtained and purified from limestone by precipitation (Patnaik et al., 2003). Richards et al. (1910) reported the production of $CaCO_3$ by mixing a solution of calcium nitrate [$Ca(NO_3)_2$] with ammonium carbonate [$(NH_4)_2CO_3$]. The precipitation was conducted at 100 °C and the precipitate was washed several times with hot, pure water.

19

$$Ca(NO_3)_2\text{-}4H_2O_{(aq)} + (NH_4)_2CO_{3\,(aq)} \longrightarrow CaCO_{3\,(p)} + 2NH_4NO_{3\,(aq)} \quad (2\text{-}16)$$
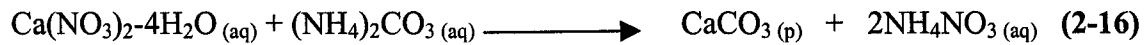
Calcium carbonate can have three different crystal structures (calcite, aragonite and vaterite), depending on the arrangement between the atoms of carbon, oxygen and calcium. These different crystals structures have different morphologies, symmetries and shapes, such as rhombohedral, scalenohedral, prismatic and spherical (Figure 2-7). (Minerals Technologies, 2006)
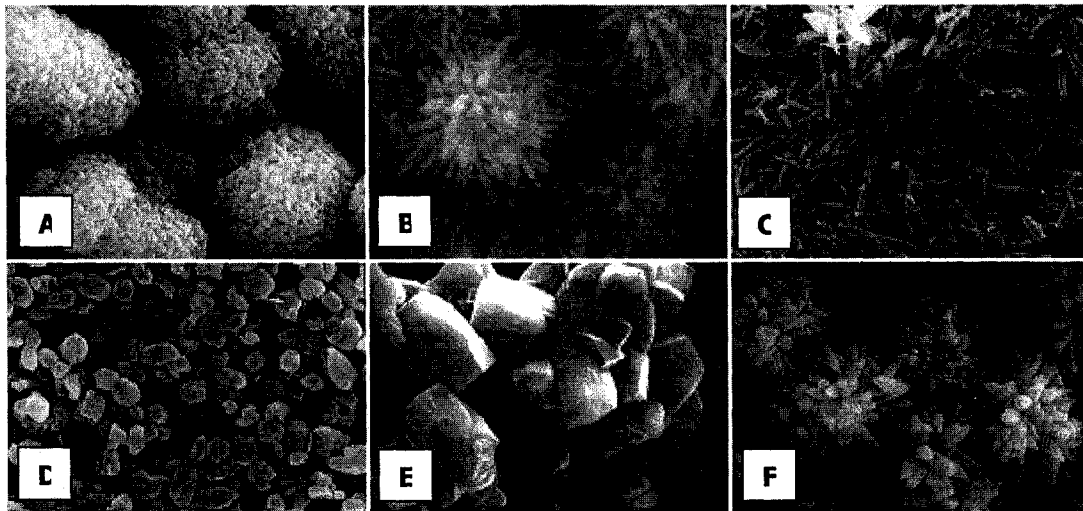
Figure 2-7: Different morphologies for precipitated calcium carbonate: (A) spherical calcite, (B) clustered acicular aragonite, (C) discrete acicular aragonite, (D) prismatic calcite, (E) rhombohedral calcite, and (F) scalenohedral calcite.

From http://www.mineralstech.com/products.html accessed on March 8th 2006

- Lithium Carbonate: Li_2CO_3 can be obtained from mixing a solution of lithium, such as lithium chloride (LiCl) or sulphate (Li_2SO_4) with a hot concentrated solution of sodium carbonate (Na_2CO_3) (equation 2-17) (Patnaik et al., 2003). Pure lithium carbonate can be prepared from mixing a concentrated solution of lithium chloride and a hot solution of ammonium carbonate alkalised with ammonia (equation 2-18).

$$Li_2SO_4\ _{(aq)}\ +\ Na_2CO_3\ _{(aq\ or\ solid)}\ \longrightarrow\ Li_2CO_3\ _{(p)}\ +\ Na_2SO_4\ _{(aq)} \quad \textbf{(2-17)}$$

$$2\ LiCl\ _{(aq)}\ +\ (NH_4)_2CO_3\ _{(aq\ or\ solid)}\ \xrightarrow{NH_4^+}\ Li_2CO_3\ _{(p)}\ +\ 2\ NH_4Cl\ _{(aq)} \quad \textbf{(2-18)}$$
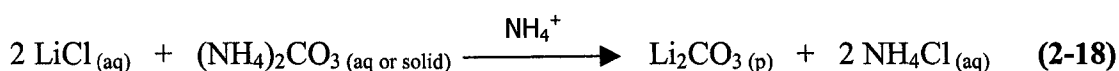
Lithium carbonate can also be obtained by treating a hot solution of lithium nitrate with a solution of ammonium carbonate. The precipitate (lithium carbonate) is collected and washed with distilled water four times, and then the precipitate is heated at 400 °C (Archibald, 1932)

- Magnesium Carbonate: $MgCO_3$ is obtained by mixing a solution of magnesium nitrate with a solution of sodium carbonate. Magnesium carbonate can also be prepared by carbonation of magnesium hydroxide [$Mg(OH)_2$] slurry with carbon dioxide (CO_2) under a pressure of around 5 atmospheres. Anhydrous magnesium carbonate can only be prepared under a very high pressure of carbon dioxide. However, magnesium carbonate trihydrate ($MgCO_3-3H_2O$) can be prepared by precipitation of salts under ordinary conditions (equation 2-19), and this gives anhydrous magnesium carbonate when dried at about 100 °C (equation 2-20). Magnesium carbonate can also form mixed salts with alkali salts, alkaline earth metal salts, and ammonia salt such as $MgCO_3-Na_2CO_3$ (Patnaik et al., 2003).

$$Mg(NO_3)_2.6H_2O\ _{(aq)}\ +\ Na_2CO_3\ _{(aq\ or\ solid)}\ \longrightarrow\ MgCO_3-3H_2O\ _{(p)}\ +\ 2NaNO_3\ _{(aq)}$$
$$\textbf{(2-19)}$$

$$MgCO_3.3H_2O\ _{(p)}\ \longrightarrow\ MgCO3\ _{(p)}+\ H2O\ _{(g)} \quad \textbf{(2-20)}$$

21
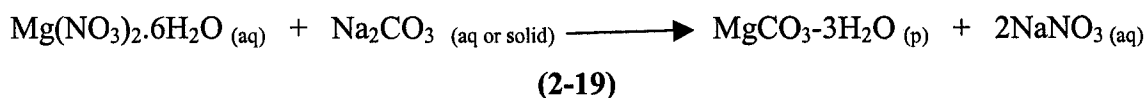
- Barium Carbonate: $BaCO_3$ is obtained commercially from treating barium sulphide (BaS) with sodium carbonate at 60 – 70 °C, resulting in a precipitate of barium carbonate (equation 2-21). Barium carbonate can also be prepared by passing CO_2 through barium sulphide at 40 – 90 °C (equation 2-22) (Patnaik et al., 2003).

$$BaS \ + \ Na_2CO_3 \ \xrightarrow{\text{heat}} \ BaCO_3 \ + \ Na_2S \qquad \textbf{(2-21)}$$

$$BaS \ + \ CO_2 \ + \ H_2O \ \xrightarrow{\text{heat}} \ BaCO_3 \ + \ H_2S \qquad \textbf{(2-22)}$$

2.3.2. - Thermal Decomposition of Acetates to Carbonates

Machinaga et al. (1989) studied the thermal decomposition of calcium acetate. Calcium carbonate was obtained from calcium acetate after it was heated for 210 minutes in an air atmosphere at a calcining temperature of 400 °C. Differential thermal analyses (DTA) of calcium acetate carried out in nitrogen showed one endothermic peak from 398 °C. It was concluded that the weight loss found in the analyses agreed quantitatively with the complete conversion of calcium acetate to acetone and calcium carbonate (Machinaga et al., 1989). The calcium carbonate prepared by Machinaga et al. (1989) showed an X-ray diffraction pattern for calcite (calcium carbonate) and it also showed a small peak that suggests the existence of carbon (graphite) in the sample.

The specific surface area of the untreated acetate was about 1 m^2/g, which increased rapidly to 28 m^2/g upon dehydration. Variations in the acetate decomposition temperature produced carbonates of varying specific surface areas. For example, Patnaik et al. (2003) reported specific surface areas ranging from 2 to 7 m^2/g for decomposition temperatures ranging from 400 to 600 °C. Starting with white calcium acetate, a grey coloured carbonate was reported by Machinaga et al. (1989). The grey colour was explained in terms of pale yellow and red components, (graphite and trace organics). Calcium acetate calcined at 700 °C decomposed to calcium oxide, which has a higher specific surface area than the calcium carbonate because of increased porosity that develops at such a high temperatures (Machinaga et al., 1989).

2.3.3. - Thermal Decomposition of Oxalates to Carbonates

It is known that oxalates decompose to carbonates, and subsequently to oxides, when heated to sufficiently high temperature (Celis et al., 2001). These authors studied the thermal decomposition of calcium oxalate, strontium oxalate and a mixture of these substances. They reported three reaction steps that can be detected by TGA upon increasing heating:

$$CaC_2O_4\text{-}2H_2O_{(s)} \longrightarrow CaC_2O_{4\,(s)} + H_2O_{(g)} \quad \textbf{(2-23)}$$

$$CaC_2O_{4\,(s)} \longrightarrow CaCO_{3\,(s)} + CO_{(g)} \quad \textbf{(2-24)}$$

$$CaCO_{3\,(s)} \longrightarrow CaO_{(s)} + CO_{2\,(g)} \quad \textbf{(2-25)}$$

Based on the TGA data presented by Celis et al. (2001), calcium oxalate forms the carbonate at 450 °C, while strontium oxalate forms the carbonate at 480 °C. Dollimore et al. (1971) studied the thermal decomposition of lithium oxalate. Decomposition of lithium oxalate to carbonate was reported at temperatures between 469 and 492 °C, with higher temperatures leading to higher rates of decomposition.

2.4. - Preparation of Oxides

- Calcium Oxide: CaO is obtained from combusting calcium carbonate or calcium oxalate at around 800 °C. CaO is commercially produced from limestone, which is heated to temperatures below 1200 °C in order to release the CO_2 (Patnaik et al., 2003).

$$CaCO_{3\,(s)} \xrightarrow{\quad heat \quad} CaO_{(s)} + CO_{2\,(g)} \quad \textbf{(2-26)}$$
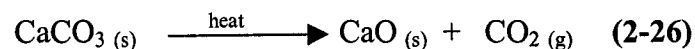
- Lithium Oxide: Li_2O is a very porous compound used as an absorbent for carbon dioxide. It can be obtained from heating lithium metal in dry oxygen at around 100 °C (equation 2-27). Thermal decomposition of lithium peroxide also leads to the production of lithium oxide (equation 2-28). Another method for producing lithium oxide is the

23

heating of lithium hydroxide at around 800 °C under vacuum (equation 2-29) (Patnaik et al., 2003).

$$2Li_{(s)} + O_{2\,(g)} \xrightarrow{\text{heat}} Li_2O_{(s)} \qquad \textbf{(2-27)}$$

$$Li_2O_{2\,(s)} \xrightarrow{\text{heat}} Li_2O_{(s)} + \tfrac{1}{2}O_{2\,(g)} \qquad \textbf{(2-28)}$$

$$2Li(OH)_{(s)} \xrightarrow{\text{heat / vacuum}} Li_2O_{(s)} + H_2O_{(g)} \qquad \textbf{(2-29)}$$
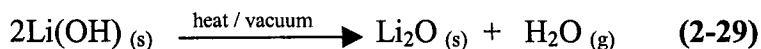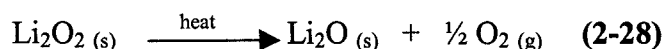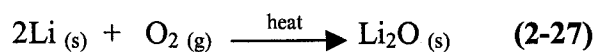
- <u>Magnesium Oxide</u>: MgO can be obtained from calcining magnesium salts such as nitrate, hydroxide, oxalate, etc., but magnesium oxide is produced mainly from calcining magnesium carbonate at 600 °C for about one hour (equation 2-30 and 2-31) (*Handbook of preparative inorganic chemistry* 1963).

According to the same authors, the temperature of the calcination process is very important since it affects significantly the particle size, purity and reactivity of the resulting oxide. Light grade reactive magnesium oxide can be produced at calcination temperatures around 600 °C, while a denser form of a heavier grade of magnesium oxide is obtained when calcined at around 800 to 900 °C.

$$MgCO_{3\,(s)} \xrightarrow{\text{calcination}} MgO_{(s)} + CO_{2\,(g)} \qquad \textbf{(2-30)}$$

$$Mg(OH)_{2\,(s)} \xrightarrow{\text{calcination}} MgO_{(s)} + H_2O_{(g)} \qquad \textbf{(2-31)}$$

- <u>Barium Oxide</u>: BaO can be obtained from heating barium carbonate with coke or black carbon (equation 2-32) (Patnaik et al., 2003). Thermal decomposition of barium nitrate, iodate or peroxide lead to the production of barium oxide (Handbook of preparative inorganic chemistry 1963).

$$BaCO_{3\,(s)} + C_{(s)} \xrightarrow{\text{heat}} BaO_{(s)} + 2CO_{(g)} \qquad \textbf{(2-32)}$$

24

2.5. - Summary

Different approaches to reduce the content of naphthenic acids from bitumen have been proposed, such as thermal treatment of crude, use of alkoxylated amines, alcohols or solids to form emulsions and layers of different densities in the crude, which could be separated to remove the naphthenic acids. The use of alkaline and alkaline earth metal compounds to achieve the decarboxylation reaction of the naphthenic acids in addition to other alternatives has been also proposed.

Other works regarding the study of the decarboxylation reaction aiming the reduction of carboxylic acids or the production of ketones have led to the proposal of different reaction mechanisms such as β-keto acid intermediate, γ-keto acid intermediate and formation of carboxylic salt as an intermediate.

Additionally, different techniques of preparation of carbonates such as precipitation of inorganic salts, thermal decomposition of acetates and thermal decomposition of oxalate were also described.

CHAPTER 3

EXPERIMENTAL DETAILS

3.1. - Preparation of the Carbonates and Oxides

Unsupported oxides and carbonates of lithium (Li_2O, Li_2CO_3), magnesium (MgO, $MgCO_3$), calcium (CaO, $CaCO_3$), and barium ($BaCO_3$) were prepared for the study of the gas-phase ketonic decarboxylation of butyric acid. The chemicals employed in the preparation of the different reagent powders are shown in Table 3-1.

Table 3-1: Reactants used in the preparation of carbonates and oxides

Reactant	Formula	% Purity	Supplier
Sodium carbonate	Powder, anhydrous	Na_2CO_3	100	Fisher Scientific
Lithium nitrate	Reagent grade, granular	Li_2NO_3	> 99	Fisher Scientific
Lithium sulfate	Anhydrous	Li_2SO_4	99	Acros Organic
Calcium nitrate	Reagent grade, granular	$Ca(NO_3)_24H_2O$	> 98	Fisher Scientific
Barium nitrate	Certified A.C.S., crystal	$Ba(NO3)2$	99.3	Fisher Scientific
Magnesium nitrate	Hexahydrate, reagent A.C.S.	$Mg(NO_3)_26H_2O$	100	Acros Organic
Lithium acetate	Pure	$C_2H_3LiO_2$	100	Acros Organic
Calcium acetate	Hydrated	$C_4H_6CaO_4H_2O$	99	Acros Organic
Lithium oxalate	Powder	$C_2O_4Li_2$	100	MP Biomedicals

Different preparation methods of carbonates, such as precipitation of salts, and oxalate/acetate thermal decomposition to carbonates were studied as factors that are known to affect the morphology of these materials (Choudhary, 1994). The hypothesis was made that differences in morphology would lead to differences in activity.

3.1.1. - Preparation of Carbonates by Precipitation

Carbonates of lithium, calcium, magnesium and barium were prepared by precipitation. Soluble salts of lithium, magnesium, calcium or barium were used as the precursors of the carbonates (Table 3-2).

Table 3-2: Preparation of carbonates by precipitation

Carbonate	Precursor		Na_2CO_3
	Salt	g / 100 ml de-ionized water	g / 100 ml de-ionized water
Li_2CO_3	Li_2SO_4	15.2287	15.2497
$MgCO_3$	$Mg(NO_3)_2$-6H2O	36.0979	15.0750
Mg/Li_2CO_3	$Mg(NO_3)_2$-6H$_2$O	31.9121	15.0366
	Li_2SO_4	3.39410	
$CaCO_3$	$Ca(NO_3)_2$-4H$_2$O	33.6820	15.1400
$BaCO_3$	$Ba(NO_3)_2$	5.1349	2.1316
Ba/Li_2CO_3	$Ba(NO_3)_2$	12.1150	6.0489
	Li_2SO_4	3.3777	

The procedure employed in the preparation of the carbonates is described as follows:

- Each precursor was dissolved in de-ionized water. If required, the solution was heated in order to completely dissolve the salt.

- A second precursor was added to the solution in the case of mixed metal carbonates.

- The precipitating agent (sodium carbonate) was added to the solution of the precursor(s).

- The mixture was heated until boiling with continuous stirring.

- When lithium carbonate is prepared, $LiHCO_3$ is formed at this point. This compound is soluble in water and decomposes to Li_2CO_3 when heated. The solubility of Li_2CO_3 decreases with temperature (Archibald, 1932).

- Upon the formation of a precipitate, the mixture was filtered to collect the solids.

- The precipitate was washed three times with hot de-ionizied water.

- The precipitate was dried at 110 °C for 24 hours and then stored in a glass vial.

3.1.2. - Preparation of Carbonates by Thermal Decomposition of Acetates

Lithium, calcium and a mixture of lithium and calcium carbonates were prepared from the thermal decomposition of lithium and calcium acetates. The acetates were heated at 450 °C for 4 hours (Appendix A.1).

3.1.3. - Preparation of Carbonates by Thermal Decomposition of Oxalates

It is known that oxalates decompose to carbonates at high temperatures (Celis et al., 2001; Dollimore et al., 1971). A sample of lithium oxalate (initially white) was heated at 500 °C for 2 hours (Appendix A.1).

3.1.4. Preparation of Oxides from Carbonates

Lithium, calcium, magnesium, a mixture of calcium/lithium and a mixture of magnesium/lithium oxides were prepared from their carbonates. The carbonates were calcined at 950 °C for 24 hours (Appendix A.1).

28

3.2. – Development and Tuning of the Continuous Flow Reactor System

A continuous flow reactor system for the study of the vapour-phase decarboxylation reaction of the butyric acid was constructed, and is represented schematically as shown in Figure 3-1. Due to the corrosive nature of butyric acid, the tubing and all connection elements of the reaction system were made of stainless steel.
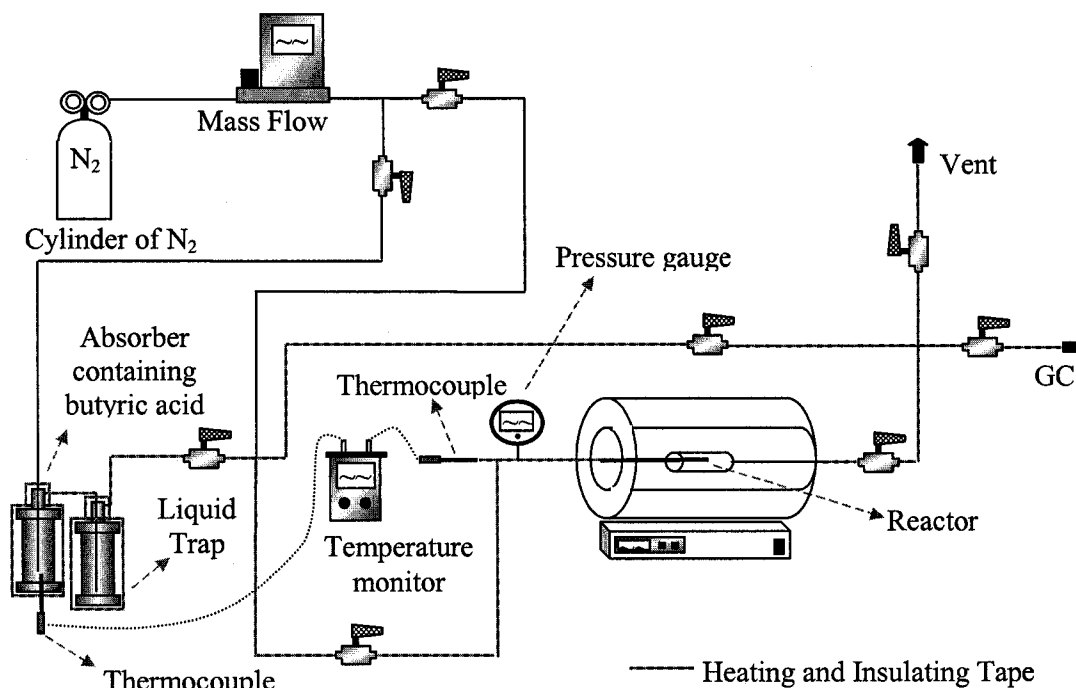
Figure 3-1: Reaction system employed in the study of the vapour-phase decarboxylation of butyric acid.

Nitrogen served as an inert and inexpensive carrier gas. The flow rate was fixed by a mass flow controller (*Omega – FMA 2617A*) located between the N_2 cylinder and the reaction system. The system allowed the flow of N_2 to be initially directed to the absorber and then to a gas chromatograph (GC), which determined the inlet concentration of butyric before flowing through the reactor (Figure 3-1).

Butyric acid (99 %, Aldrich) was incorporated into the gas flow by using the absorber connected in series to a liquid trap, which avoided the flow of liquid from the absorber to the tubing. The liquid butyric acid (b.p. 163 °C) contained in the absorber was

29

maintained at a temperature of 45 °C during the complete experiment. For most of the experiments, the concentration of butyric acid in the gas flow leaving the absorber was between 0.140 and 0.185 mmol/L, although concentrations of 0.478 mmol/L were also found. The gas phase concentration of butyric acid could be varied by controlling the absorber temperature. The temperature in the absorber and in the liquid trap were controlled by a direct current temperature controller, and because different heating tapes were used for the absorber and the liquid trap, the temperature in the absorber was fixed at around 45 °C and in the liquid trap was fixed at around 60 °C. A K-type thermocouple inserted at the bottom of the absorber measured the temperature of the butyric acid inside the absorber. In order to avoid condensation in the reaction system, the temperature in the rest of the tubing (Figure 3-1) was controlled by an alternate current temperature controller, which kept the temperature between 120 and 130 °C. The effluent of the absorber could be sent either to the reactor or to the GC, through the use of a 6-port gas-sampling valve. Figure 3-2 shows an overview of the 6-port gas-sampling valve.

The gas chromatograph used was a *Hewlett Packard - 5890* with a flame ionization detector (FID). The software employed to calculate the area and determine the retention time of the peaks detected was the software ChemStation of Agilent Technologies. The GC was equipped to handle both liquid samples by manual injection or gas samples through the 6-port gas-sampling valve. (Figure 3-2)
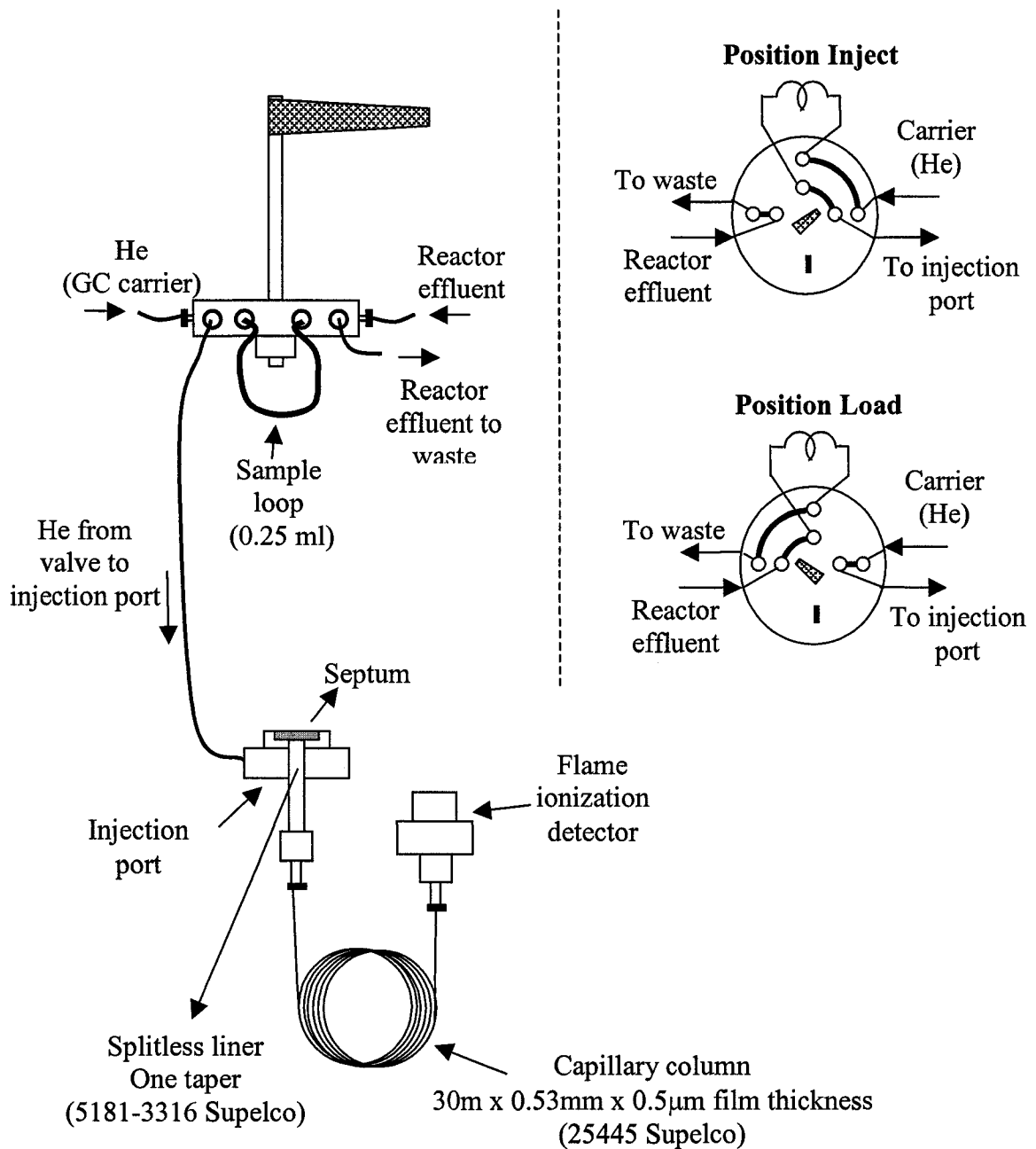
Figure 3-2: Schematic of the 6-port gas sampling valve and the liquid injection port in used in the GC.

The continuous flow reactor was a ¾" internal diameter stainless steel tube, 2.8-inch in length. This tube was installed horizontally within a tube furnace featuring a

31

temperature controller to maintain the reactor temperature at the desired setting. The internal temperature of the reactor was measured directly using a K-type thermocouple located inside the reactor, which was connected to an *Omega HH306 T-HH-CTR thermologger*. The reactor inlet pressure was measured by a pressure gauge *Omega DPG1000B-300G*.

Before using the continuous flow reactor system to test all the different reagent powders, N_2 was directed to the absorber heated at 45 °C and then to the GC bypassing the reactor to measure the peak area of the butyric acid at the reactor inlet. Subsequently, the N_2 was directed to the absorber (45 °C) and then to the GC through the reactor filled with Pyrex glass wood in order to measure the peak area of butyric acid at the outlet. These two peak areas were compared and it was determined that they were similar enough to conclude that the concentrations of the butyric acid at the inlet and outlet of the reactor were practically the same. This led to the conclusion that there was no condensation of butyric acid in any of the pathway of the continuous flow reactor system.

In addition, other preliminary experiments were performed in order to study the thermal stability of butyric acid and 4-heptanone. A gas stream containing butyric acid, 4-heptanone or a mixture of these was directed to the reactor (heated to 400 °C) filled with only Pyrex glass wood in order to establish the thermal stability of these compounds. Based on agreement in the peak areas detected by GC at the inlet and outlet of the reactor for the butyric acid and the 4-heptanone were proved to be thermally stable and non-reactive with each other in the vapour phase up to at least 400 °C

Preliminary studies in the reaction system were performed in order to determine suitable operating conditions. A low gas flow rate facilitates a more stable temperature and a more stable concentration of butyric acid. It was also observed that high gas flow rates favour the condensation of butyric acid in the reaction system. Therefore, a low gas flow rate of 10 sccm was chosen.

The temperature of the absorber was selected in order to achieve a low concentration of butyric acid in the gas stream, but high enough to be detected by the GC. A low concentration of butyric acid is desired in order to avoid condensation in the system and to delay deactivation of the potential catalysts. A temperature in the absorber

of 45 °C resulted in a butyric acid molar flow rate of 1.50x10^{-6} mol/min, and a concentration of 0.150 mmol/L at standard conditions.

Three runs with the reactor filled only with Pyrex glass fibre wool and no reagent powder were carried out in order to determine the thermal stability of the reactant (butyric acid) and the expected product (4-heptanone). In the first run, the absorber was filled with butyric acid only and the reactor was heated at 400 °C. The concentrations of butyric acid in the inlet and in the outlet of the reactor were very similar, which demonstrated that butyric acid is stable at temperatures as high as 400 °C. The second run was exactly as the first one, but instead of using butyric acid, 4-heptanone was employed. The result demonstrated that 4-heptanone is stable at temperatures as high as 400 °C. In the third run, the absorber was filled with a mixture of butyric acid and 4-heptanone and the reactor was heated at 400 °C. The concentrations of butyric acid and 4-heptanone in the inlet and in the outlet of the reactor were very similar, which demonstrated that butyric acid and 4-heptanone do not react with each other at temperatures as high as 400 °C.

Moser (1940) reported a high activity for lithium carbonate in the ketonic decarboxylation reaction. On the other hand, some literature has reported MgO as one of the best catalysts for the catalytic ketonic decarboxylation reaction (Curtis, 1947; Sugiyama et al., 1992; Zhang et al., 2004). Based on these results, several runs using first lithium carbonate (Li$_2$CO$_3$), and subsequently magnesium oxide (MgO) were carried out in order to define the amount of the potential catalyst and the reaction temperature to use in each experiment. The reaction temperatures used in the first runs using lithium carbonate includes values between 155 °C and 305 °C. A reduction in the concentration of butyric acid was observed, but no product was detected in the GC. Afterwards, magnesium oxide was used in other preliminary runs, which were performed at temperatures between 330 °C and 380 °C. The GC detected 4-heptanone when the temperature reaction was above 360 °C. A temperature around 385 °C was chosen as the reaction temperature in order to detect product when using other catalysts. Finally, different amounts of MgO were employed in order to obtain a conversion between 20 and 80%, which is considered to be a good range of conversion to compare activity for different catalysts. Conversion is defined by equation 3-1 and 3-2.

33

$$X_{(BA)} = \frac{F_{C(BA)}}{F_{I(BA)}} \tag{3-1}$$

$$F_{C(BA)} = F_{I(BA)} - F_{O(BA)} \tag{3-2}$$

Several arrangements of reagent powder in the reactor were tested such as using pellets of the reagent powders and the reactor filled with Pyrex glass fibre wool, or using the potential catalyst in powder and the reactor filled with Pyrex glass fibre wool. Figure 3-3 shows how the reagent powder was loaded and located in the reactor.

Figure 3-3 diagram showing labels: Pyrex glass fibre wool, Thermocouple, Silica carbide (SiC), Silica carbide (SiC), ~ 0.050 g reagent powder, ~1 cm^3 (reagent powder + SiC)
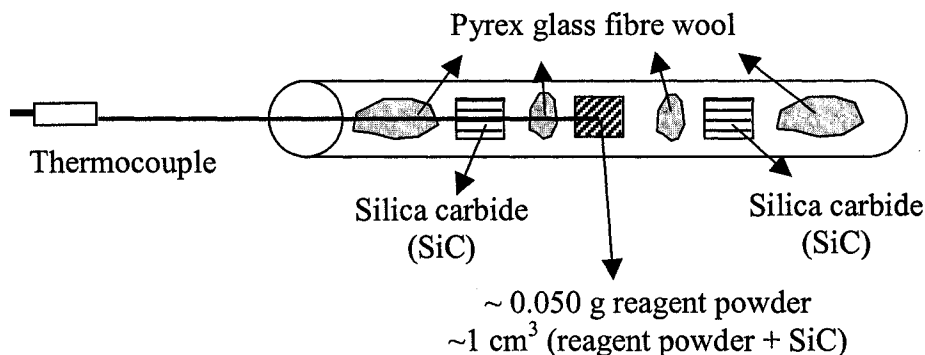
Figure 3-3: Reagent powder loaded to the reactor.

This arrangement is thought to provide a good distribution of the gas flowing through the reactor and a good contact between the gas and the potential catalyst. In this preparation, around 0.050 grams of ground potential catalyst were mixed with sufficient silica carbide (SiC) to give 1 cm^3 of mixture. The mixture of the reagent powder and SiC is isolated from the rest of the SiC by the glass wool because this mixture will be analysed by x-ray photoelectron spectroscopy (XPS) before and after reaction in order to determine any oxidation state change that could occur in the reagent powder.

3.2.1. - GC Operation and Calibration

The GC did not only detect 4-heptanone as a product during the initial studies, but also detected acetone (C_3H_6O). Therefore, a temperature ramp is employed to operate the GC in order to achieve a good resolution of the peaks of the different products observed. An initial temperature of 75 ^{o}C was held for 5 minutes, next the temperature was increased to 175 ^{o}C at a rate of 10 ^{o}C/min, and then the temperature was held for 15 minutes. A low temperature at the beginning of the measurement benefits the separation of the different products. A high temperature at the end of the measurement facilitates the elution of butyric acid through the column, reducing the tail of the peak for the butyric acid and therefore the time required to achieve the original baseline.

In order to determine the concentration of butyric acid in the stream before and after the reactor, a calibration curve was developed. Several solutions of butyric acid and methylene chloride (solvent) were prepared and then analyzed in the GC in order to relate moles of butyric acid with peak area (Appendix A.2).

Based on the calibration curve, the moles of butyric acid in the sample loop in the 6-port valve installed in the GC were defined by equation 3-3 and R^2 was 0.9908:

$$N_{SL\,(BA)} = 7*10^{-15}*A_{(BA)} \qquad\qquad \textbf{(3-3)}$$

The same procedure was followed to elaborate the calibration curve for the 4-heptanone (Appendix A.2). In this case, the solvent employed was hexadecane because its retention time is quite different from the retention time for the 4-heptanone.

Based on the calibration curve, the relationship between peak area and the moles of heptanone in the sample loop is defined by equation 3-4 with an associated R^2 value of 0.9996:

$$N_{SL\,(H)} = 5*10^{-15}*A_{(H)} \qquad\qquad \textbf{(3-4)}$$

The solvent employed in the construction of the calibration curve for the acetone was 4-heptanone, because its retention time is quite different from the retention time for the acetone (Appendix A.2). The acetone showed more than one peak in the

35

chromatograms due to its decomposition upon injection. The largest peak, with a retention time around 2.3 minutes, was used to generate the calibration as well as to analyze experimental results.

A reaction temperature of around 385 °C was used to evaluate the activity of the reagent powders. The conversion of butyric acid, the molar ratio of 4-heptanone produced ($C_7H_{14}O$) per mol of butyric acid consumed, and molar ratio of acetone (C_3H_6O) produced per mol of butyric acid consumed were determined by gas chromatography. Here, since the precise reaction stoichiometry is not known, the term 'selectivity' is avoided.

Based on the calibration data, the moles of acetone in the sample loop were defined by equation 3-5 with and R^2 value of 0.9996:

$$N_{SL\ (A)} = 5*10^{-15}*A_{(A)} \qquad (3\text{-}5)$$

The ratio of 4-heptanone produced to butyric acid consumed was defined by equation 3-6:

$$R_{P\ (H)\ /\ C\ (BA)} = \frac{F_{P\ (H)}}{F_{C\ (BA)}} \qquad (3\text{-}6)$$

The ratio of acetone produced to butyric acid consumed was defined by equation 3-7:

$$R_{P\ (A)\ /\ C\ (BA)} = \frac{F_{P\ (A)}}{F_{C\ (BA)}} \qquad (3\text{-}7)$$

3.3. – Characterizing the Reagent Powder Before and After Reaction

Several analytical methods were used to characterize the physical and chemical properties of the catalysts used in this study. These characterization methods are described in the following sections.

36

3.3.1. - Infrared (IR) Spectroscopy

In order to characterize the prepared reagent powders, Fourier transform infrared spectroscopy (FTIR) was used to identify their chemical structure. The instrument used was a *Nicole 8700 FT − IR* manufactured by *Thermo Electron Corporation* and the software employed to analyse the data was *OMNIC*.

Infrared (IR) spectroscopy is an analytical technique used to measure the ability that a material has to absorb, transmit and reflect infrared radiation. Infrared radiation describes the electromagnetic spectrum with a wavelength of 0.78 μm to 1000 μm. In IR, the wavelength is reported as wavenumber in cm^{-1}, which is defined as the inverse of the wavelength. The most useful range of wavenumber in IR is 4000 to 670 cm^{-1}. Molecules whose vibrations and rotations cause a net change in the dipole moment of the molecule are able to absorb infrared radiation. A molecule will absorb the radiation frequency that matches the vibrational and rotational frequencies of the molecule. In IR spectroscopy, infrared radiation is passed through a sample, part of the radiation is absorbed, reflected and the rest is transmitted. The resultant spectrum of the sample represents the molecular transmission and absorption of the sample creating an exclusive fingerprint, since each compound with a unique structure exhibits a unique spectrum. In this way, IR spectroscopy is a very useful technique to identify unknown compounds. Additionally quantitative compositional analysis can be carried out because the amplitude of the component peaks in the spectrum is determined by the amount of the characteristic group or compound in the sample.

The original instrument employed in IR spectroscopy required the use of a prism or grating to separate the different frequencies of infrared energy. The detector measured the amount of energy per each frequency that passed through the sample, and then the spectrum, a plot of intensity vs. frequency, was generated. This spectrometer was known as a dispersive type. Later, the Fourier transform infrared spectrometry (FTIR) was developed to improve the dispersive instrument. The FTIR permits to measure all the different frequencies of energy at the same time, which makes the process significantly faster. FTIR equipment is also more sensitive than dispersive equipment. Figure 3-4 shows a schematic of a FTIR spectrometer.

37

Samples of potassium bromide (KBr) containing between 1 and 5wt% of the reagent powders were prepared, ground and analysed. Based on the typical IR spectrum for each carbonate and oxide, the reagent powders were identified. The method employed when recording the data was the Kubelka–Munk conversion. Kubelka–Munk transforms the absolute reflectance of the sample into a signal such as a linear relationship between the spectral intensity and the concentration of the sample is created, and this is usually used to analyse powder samples. Typical infrared wavenumbers for carbonates are 1410 – 1450 cm^{-1} and 800 – 880 cm^{-1}. (Alpert, 1970)
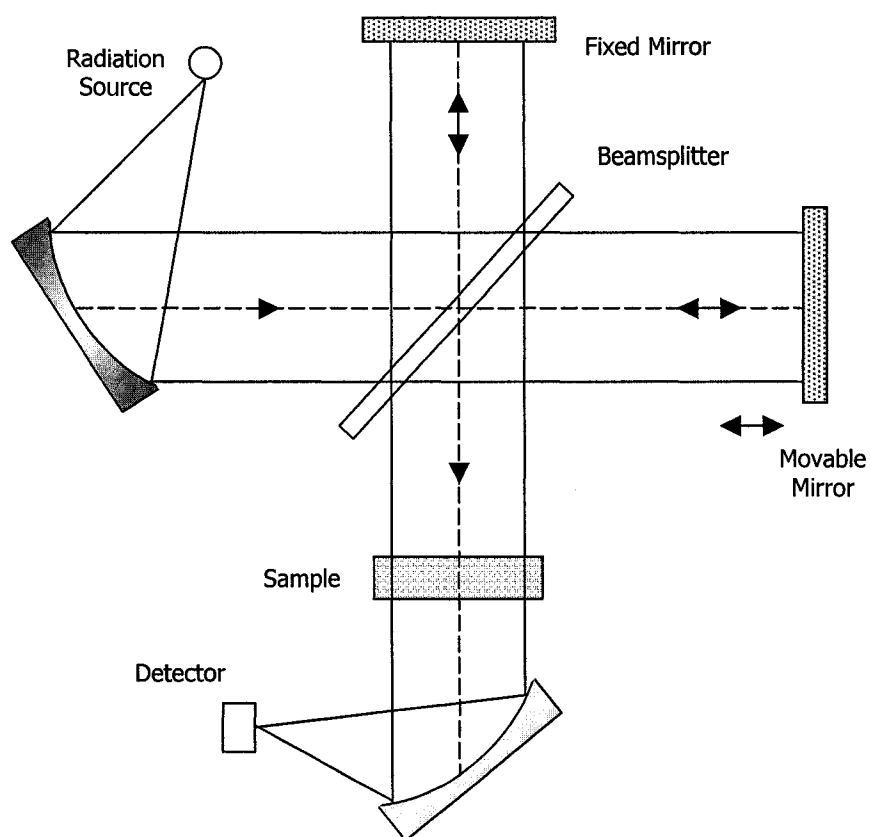
Figure 3–4: Schematic diagram of a Fourier Transform spectrometer with a classical Michelson interferometer. Adapted from Gunzler et al. 2002.

3.3.2. - X-Ray Photoelectron Spectroscopy (XPS)

Quantitative composition of the surface of each reagent powder before and after reaction was established by x-ray photoelectron spectroscopy (XPS). The reagent was analyzed after reaction in order to determine any significant change in the chemistry of the carbonates and oxides tested. The instrument used was the *AXIS 165* manufactured by *Kratos*.

XPS is one of the most widely used techniques in catalysis. It is employed to determine the chemical composition and the oxidation state of a sample surface down to 1 nm of depth. It can also be used to determine the dispersion of one surface phase over another. When an atom is bombarded by a photon (excited by x-rays radiation), the atom gains an amount of energy equal to $h\nu$ that ejects a core electron from the atom to vacuum (photon electron). The photoelectron leaving the atom has a kinetic energy that is measured by the equipment. The difference between the energy of the x-ray bombarding the atom, the kinetic energy measured by the equipment and the instrument work function, is known as the binding energy, which depends on the nature of the element (see Figure 3-5).

The instrument is calibrated to account for the work function and $h\nu$ is known for a given anode; 1253.6 eV for magnesium $K\alpha$ and 1486.6 eV for aluminium $K\alpha$ sources. The binding energy depends on the element and its chemical state, and this is used to identify an element and its oxidation state. The binding energy is calculated with the following energy balance equation:

$$h\nu = E_{kinetics} + E_{binding} + \phi \qquad (3\text{-}8)$$

Because an electron has left the atom, there is an electron vacancy at a specific level of energy, which is filled by an electron from a higher level of energy. This is known as an Auger transition, which causes an Auger electron to be ejected. The kinetic energy of the Auger electron is also measured by the instrument, and Auger peaks are also reported in the XPS spectra.
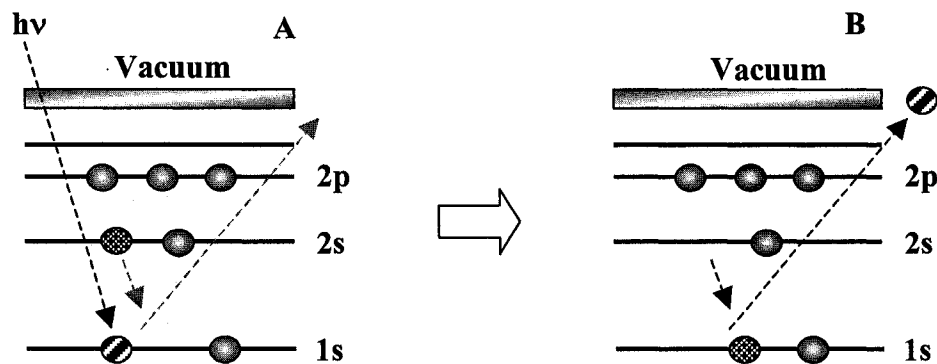
Figure 3-5: Photoemission principle. Taken and adapted from http://www.lasurface.com/xps/niveau2.php (Accessed on May 24th 2006). A: Atom bombarded by a photon. B: Photoelectron ejected from the atom and electron from a higher level of energy filling the electron vacancy.

The XPS samples were prepared by filling an aluminium sample holder with a small amount of powder, which was then transferred into the XPS instrument and pumped down to a pressure of 1×10^{-9} torr.

Table 3-3 shows the parameters used to analyze the reagent powders using XPS.

Table 3-3: Parameters used in the XPS analyses

Scan	Start energy (eV)	End energy (eV)	Dwell (ms)	Step (eV)	Number Sweet	Anode
Wide	1100	0	60	0.3	2	Mg
Narrow (C 1s)	292	280	300	0.1	8	Mg

3.3.3. – Particle Size Distribution

The surface area of the powders could have not been not successfully measured by the available instrument (BET) due to the very low surface area of the samples. Each

reagent powder was ground and then its particle size distribution before reaction was determined by laser diffraction. The instrument used was the Mastersizer 2000.

Table 3-4 exhibits the parameters used in the measurement of the particle size distribution of the reagent powders.

Table 3-4: Parameters used in the measurement of the particle size distribution of the reagent powders

Reagent Powder	Dispersant	Reflectance Index		Concentration (%Vol)
		Particle	Dispersant	
Li_2CO_3 (p)	Acetone	1.563	1.320	0.0128
Li_2CO_3 (a)	Acetone	1.563	1.320	0.0956
Li_2CO_3 (o)	Acetone	1.563	1.320	0.0257
$MgCO_3$ (p)	Acetone	1.563	1.320	0.0690
Mg/Li_2CO_3 (p)	Acetone	1.563	1.320	0.0288
MgO (p)	Water	1.710	1.330	0.0409
Mg/Li_2O (p)	Water	1.735	1.330	0.0473
$CaCO_3$ (p)	Water	1.570	1.330	0.0129
$CaCO_3$ (a)	Water	1.570	1.330	0.0615
Ca/Li_2CO_3 (a)	Water	1.570	1.330	0.0311
CaO (p)	Water	1.838	1.330	0.0466
CaO (a)	Water	1.838	1.330	0.0644
Ca/Li_2O (a)	Water	1.838	1.330	0.1386
$BaCO_3$ (p)	Water	1.603	1.330	0.0052
Ba/Li_2CO_3 (p)	Water	1.603	1.330	0.0081
Na_2CO_3 (f)	Acetone	1.500	1.320	0.2730

p: Prepared by precipitation of salts

a: Prepared by thermal decomposition of acetate

o: Prepared by thermal decomposition of oxalate

41

The particle size distribution of the powders was not used to estimate the surface area of the samples because the morphology of carbonates and oxides are very diverse and different from spherical shape (Minerals Technologies, 2006).

3.3.4. – Thermal Gravimetric Analysis (TGA)

The thermal stabilities of the lithium, magnesium, calcium and barium carbonates prepared by precipitation were studied by thermal gravimetric analysis. The instrument used was the *TG – DSC 111* manufactured by *SETARAM* and the software employed to analyse the data was *Setsoft 2000*.

Thermal gravimetric analysis is the branch of thermal analysis that studies changes in mass of a material or substance as a function of temperature, or as a function of time when the temperature is constant (isothermal mode) (Hatakeyama et al., 1999). In thermal gravimetric analysis, the sample is heated at a fixed rate, usually quite slowly, (between 5 to 20 °C/min), while measuring the mass. As a result, the thermal stability of the sample can be described as the loss of mass at specific temperatures. Phenomena as absorption, desorption, sublimation, vaporization, oxidation, reduction and decomposition can be studied by TGA. How the mass of the sample changes strongly depends on the conditions of the experiments (Hatakeyama et al 1999). In TGA, the mass registered by the instrument is graphed as a function of time. The mass loss is calculated by the area of the peaks found when the change of mass is graphed as a function of time as shown in Figure 3-6.
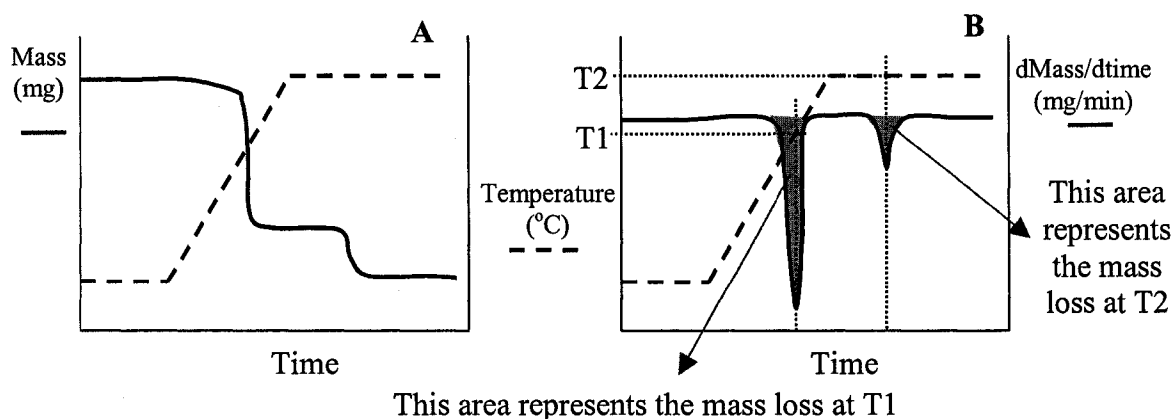
Figure 3-6: A: Mass of the sample vs. time when heated in TGA. B: Change of mass of the sample vs. time when heated in TGA.

A thermobalance records the thermal gravimetric curves. A thermobalance consists of an electronic microbalance, a furnace, a temperature controller and a computer that records the outputs coming from these devices. Figure 3-7 shows a typical scheme of a TGA instrument.
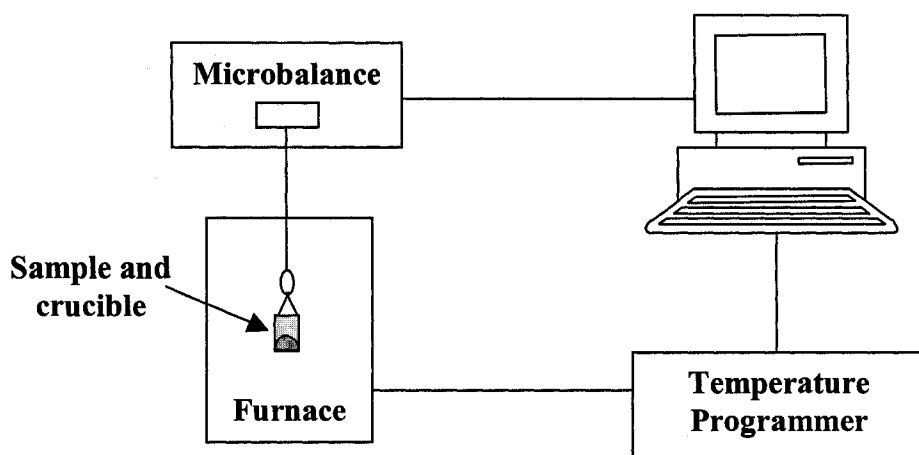
Figure 3-7: Scheme of a thermobalance. (Taken and adapted from "Thermal Analysis. Fundamentals and Applications to Polymer Science". (Hatakeyama et al. 1999). Figure 4.2, page 47).

The temperature programs used in the TGA analyses performed on the different reagent powders before and after reaction are described in chapters 4 and 5.

3.4. – Reaction Experiments in the Continuous Flow Reactor System

Each of the reagent powders prepared was tested in the continuous flow reactor system in order to compare their activities in the removal of butyric acid. Additionally, two commercial precipitated calcium carbonates with known morphologies were tested in order to compare performance of these with the prepared precipitated calcium carbonate, and in order to attempt to relate morphology and performance of the reagent powders. The reaction system was run at the same operating conditions each time. In each experiment, the peak area measured by the GC was used to determine the amount of butyric acid, acetone, and 4-heptanone. The peak areas were measured every 35 minutes.

At the beginning of each experiment, N_2 was directed through the absorber to the gas chromatograph bypassing the reactor until the temperature in the absorber was constant and three consecutive peak areas for butyric acid were in agreement (around 10% difference between each area was taken to be acceptable). After the concentration of butyric acid was stabilized, the N_2/butyric acid stream exiting the absorber was directed through the reactor (this was taken to be time = 0 for the experiment). Again, GC sampling of the reactor effluent was continued until three consecutive peak areas of butyric acid were observed (with 10% deviation as above).

It was desired to have temperature of the absorber the same (45 °C) for all the experiments, so that the initial concentration of butyric acid would also be the same in each run. However, because the absorber temperature was not directly controlled, there were some slight differences in the temperatures of the absorber between experiments. Also, the temperature in the reactor was intended to be 385 °C for all the tests. However, the temperature in the reactor varied slightly in each run because the temperature controller in the tube furnace responded to the temperature in the internal walls of the furnace, instead of the temperature inside of the reactor itself.

The pressure inside the reactor was 1 atm (abs.) for all the experiments. The volume of the mixture of reagent powder and silica carbide was 1 cm^3 in each run. The gas hourly space velocity was calculated following equation 3-9.

$$\text{GHSV}_{(BA)} \, (h^{-1}) = \frac{Q_{I\,(N2)} * (60 \text{ min/h})}{V_{RP} * [1 - y_{(BA)}]} \qquad (3\text{-}9)$$

The molar fraction of butyric acid feeding the reactor was calculated using equation 3-10.

$$y_{(BA)} = \frac{N_{SL\,(BA)}}{N_{SL\,(T)}} \qquad (3\text{-}10)$$

The total moles contained in the sample loop attached to the 6-port valve were calculated using equation 3-11.

$$N_{SL\,(T)} = \frac{V_{SL} * P_{SL}}{(T_{SL} + 273) * [0.082 \text{ atm}*L/ (K*mol)]} \qquad (3\text{-}11)$$

44

The volume of the sample loop (V_{SL}) was 0.25 ml, the absolute pressure in the sample loop (P_{SL}) was assumed to be 1 atm and the temperature of the sample loop (T_{SL}) was assumed to be equal to the temperature of the oven of the GC, which was 75 °C when the effluent of the reactor was sampled. The space-time was calculated at operating conditions using equation 3-12.

$$\tau = \frac{V_{RP} * 298 \text{ K} * [1 - y_{(BA)}] * (60 \text{ s/min})}{Q_{I(N2)} * (T_{RX} + 273)} \qquad (3\text{-}12)$$

The weight hourly space velocity (WHSV) based only on butyric acid was calculated in each case as shown in equation 3-13.

$$WHSV_{(BA)} (\text{h}^{-1}) = \frac{F_{I(BA)} * MW_{(BA)} * (60 \text{ min/h})}{M} \qquad (3\text{-}13)$$

The molar flow rate of butyric acid fed to the reactor was calculated using equation 3-14.

$$F_{I(BA)} = \frac{y_{(BA)} * F_{I(N2)}}{[1 - y_{(BA)}]} \qquad (3\text{-}14)$$

The molar flow rate of N_2 at the inlet of the reactor was determined as shown in equation 3-15.

$$F_{I(N2)} = \frac{Q_{I(N2)} * 1 \text{ atm}}{(1000 \text{ cm}^3/\text{L}) * (298 \text{ K}) * [0.082 \text{ atm*L/ (K*mol)}]} \qquad (3\text{-}15)$$

Tables 3-5 and 3-6 show the operating conditions as well as the different reagent powders tested in each case.

Table 3-5: Reactor pressure, volume of the reagent powder, GHSV and space-time in the continuous flow reactor system for all the reagent powders tested.

Reactor absolute pressure (atm)	1 ± 1
Volume of reagent powder (cm^3) (VRP)	1.0 ± 0.2

GHSV (h^{-1})	602
Space time (s) (τ)	2.7

Table 3-6: Temperature conditions and WHSV$_{BA}$ in the continuous flow reactor system for each reagent powder tested.

Reagent Powder		Temperature (°C)		WHSV$_{BA}$ (h^{-1})
Preparation technique	Mass (g) (+/- 0.0001 g)	Absorber	Reactor	
Li$_2$CO$_3$ — Precipitation	0.0527	60.8 ± 0.1	387.0 ± 0.1	0.4845
Li$_2$CO$_3$ — Precipitation	0.0500	44.4 ± 0.2	384.7 ± 1.6	0.1475
Li$_2$CO$_3$ — Precipitation	0.0508	44.9 ± 0.2	387.0 ± 1.3	0.1572
Li$_2$CO$_3$ — From acetate	0.0519	47.4 ± 0.1	385.8 ± 1.4	0.1455
Li$_2$CO$_3$ — From oxalate	0.0563	45.5 ± 0.1	386.2 ± 1.0	0.1319
MgCO$_3$ — Precipitation	0.0523	43.8 ± 0.2	383.6 ± 1.3	0.1487
Mg/Li$_2$CO$_3$ — Precipitation	0.0526	45.7 ± 0.5	382.3 ± 1.6	0.1858
MgO — Precipitation	0.0508	60.1 ± 0.2	385.3 ± 1.3	0.0931
MgO — Precipitation	0.0519	44.8 ± 0.1	386.8 ± 0.4	0.1669
Mg/Li$_2$O — Precipitation	0.0506	43.3 ± 0.1	383.3 ± 1.8	0.1478
CaCO$_3$ — Precipitation	0.0530	44.7 ± 0.1	386.0 ± 0.7	0.1597
CaCO$_3$ — From acetate	0.0531	44.8 ± 0.4	385.2 ± 1.0	0.1442
Ca/Li$_2$CO$_3$ — From acetate	0.0540	43.8 ± 0.7	384.5 ± 1.5	0.1394
CaO — Precipitation	0.0518	50.6 ± 0.2	381.0 ± 3.0	0.1734
CaO — Precipitation	0.0530	44.0 ± 0.2	385.8 ± 2.2	0.1382
CaO — From acetate	0.0514	49.2 ± 0.1	384.5 ± 0.5	0.1852
Ca/Li$_2$O — From acetate	0.0529	44.5 ± 0.1	387.0 ± 1.0	0.1467
PCC (1) * — Precipitation	0.0539	42.5 ± 0.1	383.5 ± 1.5	0.1126
PCC (2) ** — Precipitation	0.0526	43.9 ± 0.1	383.7 ± 2.9	0.1453
BaCO$_3$ — Precipitation	0.0532	42.4 ± 0.1	384.3 ± 3.1	0.1183
Ba/Li$_2$CO$_3$ — Precipitation	0.0525	44.4 ± 0.1	383.3 ± 1.1	0.1398

46

Na$_2$CO$_3$	Fisher reagent	0.0502	42.6 $\pm$ 0.1	384.5 $\pm$ 3.0	0.1631

Precipitation: from precipitation of salts

From acetate: thermal decomposition of acetate

From oxalate: thermal decomposition of oxalate

   *: Commercial precipitated calcium carbonate (1)

  **: Commercial precipitated calcium carbonate (2)

3.5. – <u>Analyses of the Products and Reagent Powders used in the Continuous Flow Reactor System Experiments</u>

3.5.1. – Analysis of the Products by Gas Chromatography (GC)

In order to confirm the identity of the products detected by the GC, a sample of the condensed products from the reaction system was collected and sent to the Department of Chemistry of the University of Alberta.

The carrier used in the system was helium (He) and a trap of liquid nitrogen was placed at the outlet of the reactor, as shown in Figure 3-8. The reagent powder when collecting the sample was precipitated calcium carbonate prepared in the laboratory.
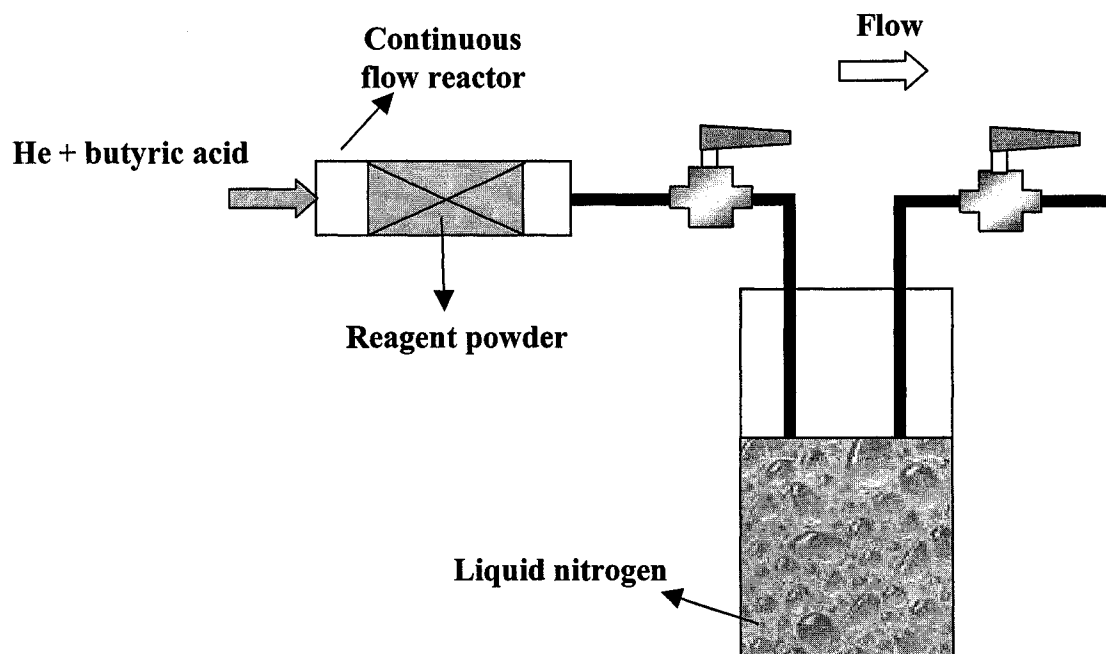
Figure 3-8: Liquid nitrogen trap used at the outlet of the continuous flow reactor.

47

3.6. – <u>Batch Reactor Experiments</u>

Subsequent detailed analyses of the reagent powder after reaction were not feasible when the continuous flow reactor system was employed because the amount of reagent powder used was very small and this was mixed with silica carbide before testing. In order to analyse the reagent powder after reaction, batch reactor experiments were run at the operating conditions shown in Table 3-7.

Table 3-7: Operating conditions of the batch reactor experiments *

Reagent powder			Butyric acid		Reaction conditions	
Sample	(g)	Mol**	(ml)	Mol	Temperature (°C)	Time (h)
$CaCO_3$ (PCC 1)	1.4655	0.0132	4	0.0470	385	3
$CaCO_3$ (PCC 2)	1.4105	0.0127	4	0.0470	385	3
Li_2CO_3	1.3188	0.0161	4	0.0470	385	3
MgO	0.7049	0.0159	4	0.0470	385	3
$BaCO_3$	2.1219	0.0100	3	0.0352	385	3

*: The absolute pressure of the reactor before reaction at room temperature was 1 atm in each experiment.

** 90 % purity was assumed.

Each batch reactor was built from a ¾" stainless steel tube, a ¾" cap and a 1/8" – ¾" reducing union which joined the reactor to a 1/8" stainless steel valve. This valve allowed the reactor to be isolated from the flow path, (see valve on top of the batch reactor in Figure 3-9). The reagent powder and the butyric acid were loaded into the reactor at room temperature in the fumehood, subsequently, the reactor was purged ten times using pure N_2. A fluidized sand bath was used to keep the reaction temperature

48

constant. The reactor was agitated within the bath so that a good contact between the reagent powder and the butyric acid was achieved (Figure 3-9). Each reactor was loaded into the sand bath after the temperature of the bath was stabilized at 385 °C.
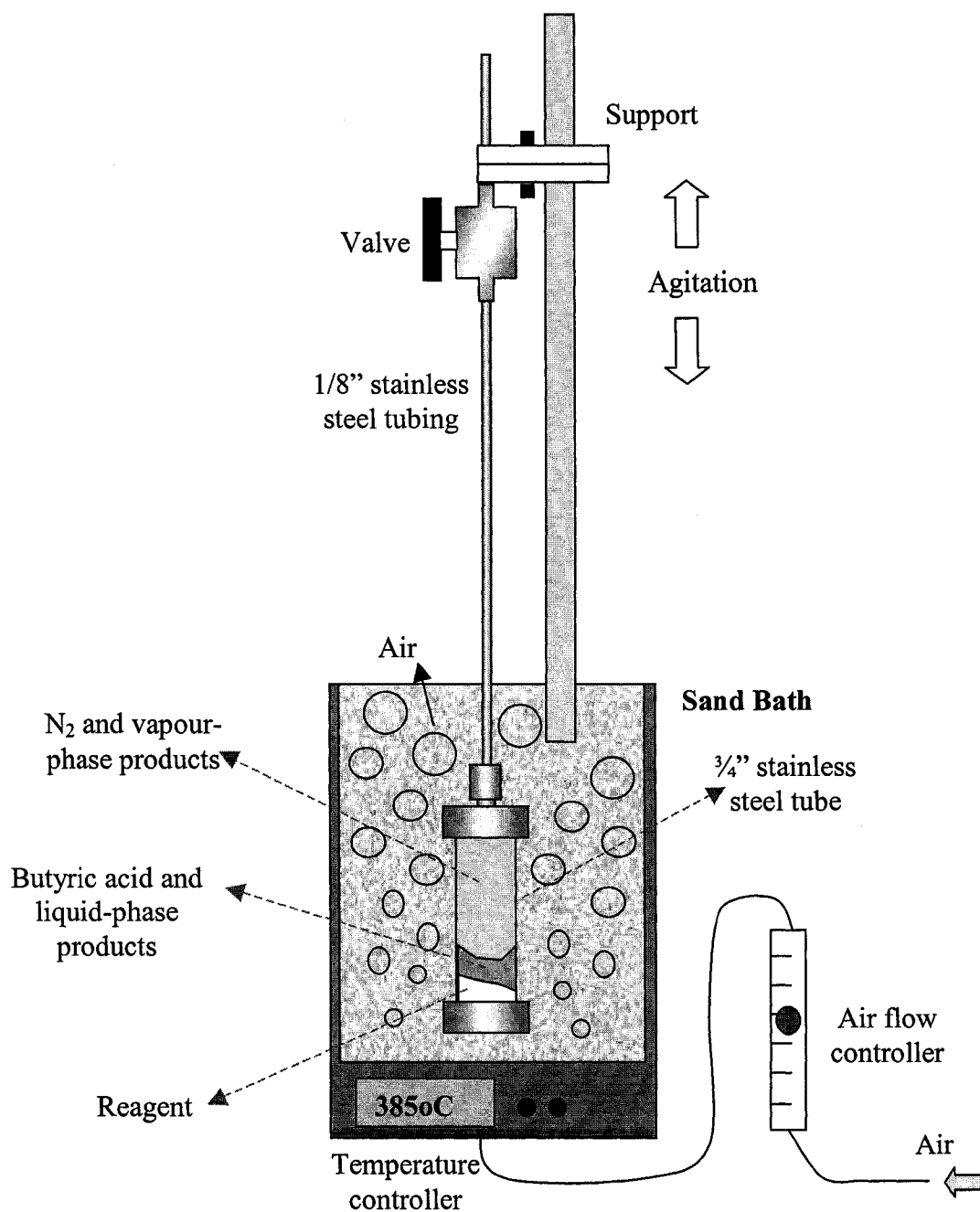
Figure 3-9: Batch reactor/fluidized sand bath system used.

3.7. – Analyses of the Products of the Batch Reactor System Experiments

3.7.1. – Analyses of the Vapour-phase and Liquid-phase Products by Gas Chromatography and Mass Spectrometer (GC – MS)

Vapour and liquid phase samples were collected from the batch reactor experiments. In some cases no liquid was found in the reactor. Table 3-8 shows the type of sample collected from each batch reactor experiment. The gas phase samples were collected using gas-sampling bags. The samples were analysed by the Department of Chemistry of the University of Alberta using GC-MS.

Table 3-8: Vapour and liquid phase samples collected from the batch reactors.

Sample	Vapour-phase sample	Liquid-phase sample	Analysis technique
$CaCO_3$ (PCC 1)	No	No liquid found	---
$CaCO_3$ (PCC 2)	Yes	No liquid found	GC
Li_2CO_3	Yes	No liquid found	GC-MS
MgO	No	Yes	GC-MS
$BaCO_3$	No	Yes	GC-MS

GC – MS is a very useful combination of techniques that allows simultaneous qualitative and quantitative compositional analysis of an unknown sample. Chromatography consists of a mobile phase (gas, liquid or supercritical liquid) forced to flow through a stationary phase, (called a chromatographic column). In gas chromatography (GC) the mobile phase is a gas and the stationary phase is either a liquid or a solid usually contained in a column. The sample flows through the column by continuous addition of the mobile phase. This process is known as elution. The

50

different compounds contained in the mobile phase have different interactions with the stationary phase, which cause that each of these compounds flow at dissimilar velocities.

Because of these differences in the elution rate, the various components of the sample are separated as they move through the column.

On the other hand, mass spectrometry is used to identify unknown compounds. This technique makes use of the fragmentation of molecules that accompanies ionization. In the mass spectrometer, the sample is vaporized and a beam of energetic electrons bombards the molecules in the gas phase. Usually the energy of the bombarding electrons is much higher than the energy of some of the bonds of the molecule, which causes that positive and negative ions as well as neutral species are formed. When electrons with high energy interact with the molecules of the sample, not only the ionization process occurs but also some bonds are broken and then, fragments from the molecule are formed and detected by the instrument. The instrument measures the masses of individual charged fragments. In fact, the mass spectrometer measures the mass-to-charge ratio of such fragments, reporting this an m/z value. The combination of GC-MS is very useful to determine the composition of unknown samples because the different compounds contained in the sample can be separated by the gas chromatograph and subsequently, these can be analysed by the mass spectrometer to determine their identification as shown in Figure 3-10.

Sample

Gas Chromatographer

Chromatogram

Mass Spectrometer

A   B   C

m/z

A   B   C
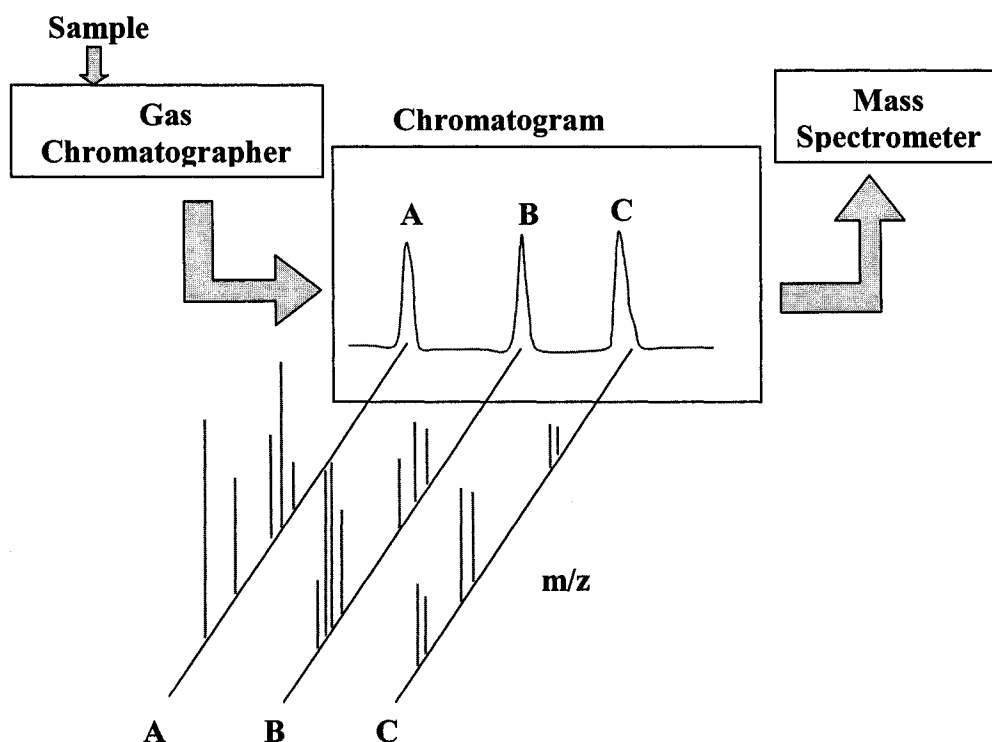
Mass spectra of the individual GC peaks

Figure 3-10: Scheme of a chromatography – mass spectrometry system. (Adapted from http://www.asms.org/whatisms/p13.html Figure 15. Accessed on May 31st 2006).

3.7.2. – Analyses of the Reagent Powder After Reaction by TGA and IR

All of the reagent powders tested using the batch reactors were dried at 200 °C overnight after reaction in order to evaporate any remaining butyric acid contained on the surface of the solids, so that any interference of this acid with the analysis of the post reaction powders could have been eliminated. Subsequently, the solids were analysed by TGA using the following temperature program:

- Temperature ramp from 18 °C to 105 °C at a rate of 5 °C/min
- Isothermal at 105 °C for 1 hour
- Temperature ramp from 105 °C to 180 °C at a rate of 5 °C/min
- Isothermal at 180 °C for 2.5 hours
- Temperature ramp from 180 °C to 650 °C at a rate of 5 °C/min

52

- Isothermal at 650 °C for 2 hours

- Temperature ramp from 650 °C to 18 °C at a rate of 15 °C/min

Also, the post-reaction powders were analysed using IR in order to determine the formation of butyrate. Each reagent powder was ground and mixed with potassium bromide (KBr) (1 – 5 %wt of sample in the mixture) before analysed using IR. The method employed when recording the data was Kubelka – Munk.

3.8. – Experimental Procedure to Study the Formation of Butyrate at Low Temperature

Several experiments mixing butyric acid and calcium compounds at room temperature were performed. Calcium hydroxide, calcium oxide and two different commercial precipitated calcium carbonates were used in the tests as shown in Table 3-9.

Table 3-9: Compounds used in the study of butyrate formation from butyric acid.

Reagent powder			Butyric acid		Water		Temperature
Sample	(g)	Mol*	(ml)	Mol	(ml)	Mol	(°C)
Ca(OH)$_2$	2.4094	0.0335	8	0.0940	0	0	25
CaO	2.0080	0.0335	8	0.0940	4	0.2222	25
CaCO$_3$	3.4251	0.0336	8	0.0940	7	0.3889	25
(PCC 1)	3.4806	0.0341	8	0.0940	2	0.1111	50
CaCO$_3$	3.3087	0.0324	8	0.0940	1	0.0556	25
(PCC 2)	3.5264	0.0346	8	0.0940	2	0.1111	50

*: Purity of calcium compounds were: 98% wt for calcium carbonate, 100% for calcium hydroxide and 90% calcium oxide (assumed).

In each experiment, the powder was physically mixed with liquid butyric acid in a mortar until the solid took up significant amount of the liquid. When calcium oxide and calcium carbonates were tested, some water was required to use so that some liquid was taken up by the solid. When both calcium carbonates were tested at room temperature, the solid did not take up any liquid. The resultant mixture of the solid and liquid was

53

filtered and washed with chloroform (4x20mL). It is known that chloroform can dissolve any the remaining butyric acid but not the butyrate (Valor et al., 2002). After being filtered and washed, the solid was dried at room temperature for 24 hours in the fumehood. Subsequently, this was dried at 200 °C overnight and then it was stored in a glass vial.

3.8.1. – Analyses of the Resultant Solids by TGA and IR

All of the resultant powders were analysed by TGA. In these TGA analyses, the temperature was increased at a rate of 5 °C/min, then subsequently held at 105 °C to eliminate the remaining chloroform (b.p. 80 °C), and subsequently the temperature was raised at a rate of 5 °C/min and held at 180 °C to remove the butyric acid (b.p. 163 °C) still present in the solids. Finally the temperature was increased at 5 °C/min and held at 650 °C.

The solids were also analysed by IR in order to determine the formation of butyrate. Each post-reaction reagent powder was ground and mixed with potassium bromide (KBr) (1 – 5 %wt of sample in the mixture) before analysed by IR. The method employed when recording the data was Kubelka – Munk.

CHAPTER 4

RESULTS

4.1. - Characterization of the Reagent Powders before Reaction

4.1.1. - Infrared (IR) Spectroscopy

The carbonates and oxides prepared using different techniques were characterized by IR spectroscopy. The prepared and commercial carbonates showed very strong peaks with the typical wavenumbers for carbonates, such as $800 - 880$ cm^{-1} and particularly $1410 - 1450$ cm^{-1}. However, some of the prepared oxides also exhibited these peaks, which were much weaker than the corresponding peaks observed in the carbonates.

Lithium carbonate prepared by thermal decomposition of lithium acetate also showed wavenumbers of 2498 and 2567 cm^{-1}, which are distinctive for carboxylic acid, while calcium carbonate prepared by thermal decomposition did not show them. Table 4-1 shows the different wavenumbers reported for each reagent powder analyzed. Appendix B shows the IR spectra for each one of the carbonates and oxides.

55

Table 4-1: IR wavenumbers of the different reagent powders analyzed

Reagent Powder	CO_3 (cm^{-1})		Others (cm^{-1})	
Theoretical	800 – 880	Strong 1410 – 1450	---	---
Li$_2$CO$_3$ (p)	866	Strong 1447	Strong 1548	---
Li$_2$CO3 (a)	867	Strong 1444	Strong 1536	2498, 2567
MgCO$_3$ (p)	793, 853, 885	Strong 1425	Strong 1511	1119, 2905
Mg/Li$_2$CO$_3$ (p)	848, 886	Strong 1483	1122	---
MgO (p)	Weak 884	Weak 1441	---	---
Mg/Li$_2$O (p)	---	---	Weak 667	---
CaCO$_3$ (p)	878	Strong 1447	713	1798, 2512
CaCO$_3$ (a)	874	Strong 1416	Strong 1517	---
Ca/Li$_2$CO$_3$ (a)	876	Strong 1441	672	1798, 2512
CaO (p)	Weak 876	Weak 1441	Strong 3642	---
CaO (a)	---	Weak 1413	673	3654
Ca/Li$_2$O (a)	---	Weak 1409	557	671
PCC (2)*	873	Strong 1483	713	1794, 2512
BaCO$_3$ (p)	856	Strong 1462	694	---

*: Commercial precipitated CaCO$_3$ (2)

p: Prepared by precipitation of salts

a: Prepared by thermal decomposition of acetate

o: Prepared by thermal decomposition of oxalate

56

4.1.2. - X-Ray Photoelectron Spectroscopy (XPS)

Surface compositions of the different reagent powders were determined by XPS, which are shown in Table 4-2. Wide scans of each sample were performed from which the elemental composition was estimated by calculating the area of the characteristic peak of the individual elements. Narrow scans for carbon for each one of the samples analyzed were performed in order to confirm the existence of carbonate and to determine the extent of carbonate decomposition in the preparation of oxides decomposition of the acetates in the preparation of carbonates.

Table 4-2: Surface composition of the prepared carbonates and oxides determined by XPS

Sample	Experimental atomic composition (%)							
	C	O	Li	Mg	Ca	Ba	Na	S
Li_2CO_3 (p)	28.3	42.7	28.1	0.0	0.0	0.0	0.5	0.4
Li_2CO_3 (a)	31.6	43.7	24.7	0.0	0.0	0.0	0.0	0.0
Li_2CO_3 (o)	26.3	44.8	28.9	0.0	0.0	0.0	0.0	0.0
$MgCO_3$ (p)	28.5	56.0	0.0	13.4	0.0	0.0	2.1	0.0
Mg/Li_2CO_3 (p)	23.3	40.4	22.6	9.1	0.0	0.0	4.6	0.0
MgO (p)	17.2	49.5	0.0	28.5	0.0	0.0	4.7	0.0
Mg/Li_2O (p)	12.4	40.7	21.0	22.0	0.0	0.0	3.4	0.5
$CaCO_3$ (p)	30.3	51.2	0.0	0.0	13.6	0.0	4.9	0.0
Ca/Li_2CO_3 (a)	28.7	44.2	14.5	0.0	12.6	0.0	0.0	0.0
CaO (p)	32.6	50.4	0.0	0.0	15.6	0.0	1.4	0.0
CaO (a)	32.5	52.0	0.0	0.0	15.5	0.0	0.0	0.0
Ca/Li_2O (a)	24.7	37.4	25.5	0.0	12.4	0.0	0.0	0.0
$BaCO_3$ (p)	35.2	45.9	0.0	0.0	0.0	14.2	4.7	0.0
Ba/Li_2CO_3 (p)	30.0	44.5	10.1	0.0	0.0	13.1	2.2	0.0

(p): Prepared by precipitation

(a): Prepared from acetate

(o): Prepared from oxalate

The XPS analyses showed the presence of sodium in all the carbonates and oxides prepared by precipitation of salts, ranging from 0.5 % for Li_2CO_3 to 4.9 % for $CaCO_3$. The lowest concentration of sodium in the lithium carbonate could be explained by the fact that high temperatures favour the precipitation of this carbonate, but on the contrary, low temperatures favour the precipitation of the rest of the carbonates, including sodium carbonate (Patnaik et al., 2003). In addition, according to Patnaik et al. (2003), some carbonates such as $MgCO_3$ tend to form mixed salts with alkaline metal salts, such as $MgCO_3.Na_2CO_3$. Another impurity detected by the XPS analyses in the precipitated carbonates and oxides was sulphur (S), which was present in an atomic percentage of 0.4 % and 0.5 % in the Li_2CO_3 and the Mg/Li_2CO_3 samples respectively. This sulphur was due to the use of lithium sulphate as a precursor in the preparation of lithium carbonate.

The atomic compositions of the lithium carbonates prepared by precipitation of salts, thermal decomposition of acetate or thermal decomposition of oxalate reported in Table 4-2 are very consistent, ranging from 24.7 % to 28.9 % for lithium, 42.7% to 44.8 % for oxygen and 26.3 % to 31.6 % for carbon. The atomic compositions of the calcium oxides obtained from the decomposition of the carbonate prepared by precipitation and the carbonate prepared by thermal decomposition of acetate are also very coherent, ranging from 15.5 % to 15.6 % for calcium, 50.4 % to 52.0 % for oxygen and 32.5 % to 32.6 % for carbon.

In all the samples analysed using XPS, the atomic percentage of carbon is higher than the expected due to the presence of adventitious carbon, which represented around 45 % and 58 – 87 % of the carbon detected for the carbonates and oxides respectively.

The binding energies found for the C 1s peak for all the carbonates prepared agreed with the theoretical binding energies found in the literature, as shown in Table 4-3. Binding energies for adventitious carbon are also shown. Adventitious carbon is always observed on the surface of oxides or metals, and this type of carbon could be originated from carbon-containing compounds existing in the atmospheric air such as CO_2, CO, hydrocarbon (C-H), etc. Another source of adventitious carbon in the sample could also be contamination in the analysis chamber by vacuum pump oil.

Table 4-3: Binding energy (eV) for the C 1s for some of the prepared carbonates and oxides

Binding Energy (eV)	Adventitious Carbon		O-C=O	CO_3
Theoretical *	284.8	284.8	289	289.4-290.0
Li_2CO_3 (p)	284.8	285.9	---	289.8
% Area	33.4	13.1	---	53.5
Li_2CO_3 (a)	284.7	285.8	289.5	289.9
% Area	30.5	15.6	16.8	37.1
Mg/Li_2CO_3 (p)	284.7	285.5	---	289.7
% Area	26.5	18.9	---	54.6
Mg/Li_2O (p)	285.3	286.1	---	290.0
% Area	66.1	20.6	---	13.3
$CaCO_3$ (p)	285.2	286.3	---	289.5
% Area	36.6	8.5	---	54.9
CaO (a)	283.5	284.7	288.4	290.0
% Area	37.9	20.4	40.9	0.8
$BaCO_3$ (p)	285.0	286.3	---	289.5
% Area	33.6	14.1	---	52.3

*: http://srdata.nist.gov/xps/ and http://lasurface.com (accessed on June 26th 2006)

(p): Prepared by precipitation

(a): Prepared from acetate

Table 4-3 presents two C 1s peaks for adventitious carbon, which could be due to the presence of CO_2 and hydrocarbons (C-H) impurities on the surface of the samples coming from the atmospheric air. Because XPS is a technique used to analyze the surface of the samples and not the bulk, and because some of the samples were not supposed to contain any carbon, the percentage of adventitious carbon reported for some of the samples were very high. However, the percentage of adventitious carbon based on

the bulk composition of the sample could be neglected. The binding energies reported are referenced to the binding energy found in the literature for O 1s.

The C 1s peak for the Li_2CO_3 prepared by thermal decomposition of acetate also showed a binding energy of 289.5 eV, which is very similar to the binding energy found in the literature for the bond O-C=O (289 eV), which is typical for carboxylic salts. In addition, a peak with a binding energy of 288.4 eV was found for the CaO prepared from the thermal decomposition of calcium acetate and subsequent calcination. Therefore, evidence of the presence of acetate was found on the surface of Li_2CO_3 and CaO prepared from their corresponding acetates. On the other hand, the oxides prepared from carbonates that were analyzed using XPS showed C 1s peaks whose binding energies are characteristic of carbonates. For example, as shown in Table 4-3, Mg/Li_2O prepared from the precipitated Mg/Li_2CO_3, and CaO prepared from the acetate, evidenced peaks for C 1s with a binding energy of 290.0 eV, which is key feature of carbonates.

Selected XPS spectra obtained from the prepared carbonates and oxides are shown in Appendix C.1.

4.1.3. – Particle Size Distribution

In this study, the result were reported using the quantity $d(z)$, which is defined such that when the particles are arranged from smallest to largest diameter, the fraction z of them are of size $d(z)$ or smaller. For example, $d(0.1) = 5$ μm implies that of such a sample, 10 % of the particles are of a size 5 μm or less. In Table 4-4, $d(0.1)$, $d(0.5)$ $d(0.9)$, as well as the average particle size of the different samples, are reported. Appendix D shows the particle size distributions of each one of the carbonates and oxides analyzed. The average particle size was calculated using Equation 4-1, where f_i is the fraction of the particles whose diameter is d_i.

$$d(ave) = \Sigma d_i \times f_i \qquad (4\text{-}1)$$

Based on the results obtained, there was not obvious trend between the particle size and the technique used in the preparation of the sample or its chemistry. However, it is important to consider that for most of the samples analyzed, the particle size varied in less than one order of magnitude. The average particle sizes of almost all of the samples were between 40 μm and 170 μm. The prepared $BaCO_3$ and Ba/Li_2CO_3 showed the lowest average particle size, 14.59 μm and 3.72 μm respectively, while Ca/Li2O prepared by thermal decomposition of acetate exhibited the highest average particle size of 170.74 μm (Table 4-4).

Table 4-4: Particle size distribution of the different reagent powders analyzed

Reagent Powder	d(0.1) (μm)*	d(0.5) (μm)**	d(0.9) (μm)***	d(ave) (μm)****
Li_2CO_3 (p)	4	18	106	40
Li$_2$CO3 (a)	41	86	187	110
Li$_2$CO3 (o)	9	40	189	89
$MgCO_3$ (p)	39	76	155	96
Mg/Li_2CO_3 (p)	9	56	187	81
MgO (p)	15	34	77	46
Mg/Li_2O (p)	14	63	232	97
$CaCO_3$ (p)	6	16	68	28
$CaCO_3$ (a)	14	143	289	153
Ca/Li_2CO_3 (a)	6	82	277	117
CaO (p)	10	75	548	167
CaO (a)	26	81	184	98
Ca/Li_2O (a)	63	158	300	171
$BaCO_3$ (p)	1	3	46	15
Ba/Li_2CO_3 (p)	1	3	6	4
Na_2CO_3 (f)	98	288	641	333

*: Maximum diameter of the 10 % smallest particles

**: Maximum diameter of the 50 % smallest particles

***: Maximum diameter of the 90 % smallest particles

****: Average particle size

p: Prepared by precipitation of salts   f: Fisher reagent

a: Prepared by thermal decomposition of acetate

o: Prepared by thermal decomposition of oxalate

61

4.1.4. – Thermal Gravimetric Analysis (TGA)

The thermal stabilities of lithium, calcium, magnesium and barium carbonates prepared by precipitation of salts were established by thermal gravimetric analysis (TGA). The temperature ramp employed was from 25 °C to 650 °C at 20 °C/min. Subsequently, the temperature was held for 30 minutes at 650 °C and then the sample was cooled down to 25 °C at 20 °C/min. The percent mass loss for each carbonate when the temperature reached 385 °C and 650 °C, are reported in Table 4-5. Appendix E.1 contains the TGA studies for these carbonates before reaction.

Table 4-5: Mass loss for precipitated lithium, calcium, magnesium and barium carbonates due to thermal decomposition

	% Mass loss at 385 °C	% Mass loss at 650 °C
Li_2CO_3	~ 0.8	~1.0
$CaCO_3$	~ 2.0	~ 40
$MgCO_3$	~ 45	~ 65
$BaCO_3$	~ 0.6	~ 1.0

The thermal gravimetric analyses performed on the lithium and barium carbonates prepared by precipitation indicated that these materials have a high stability up to 650 °C, since they only lost 1 % of their mass under such conditions. Therefore, these carbonates should be very stable at 385 °C, which is the temperature used in the reaction experiments. In contrast, magnesium carbonate lost 45 % and 65 % of its mass when the temperature reached 385 °C and 650 °C, respectively, which indicates that what is assumed to be magnesium carbonate is more likely a mixture of magnesium carbonate/oxide at the reaction temperature. Since MgO represents 47.6 % of the mass of $MgCO_3$, the carbonate/oxide mixture should be mainly magnesium oxide.

In another TGA study of two different commercial precipitated calcium carbonates, PCC (1) and PCC (2), a mass loss of 2.0 % and 1.5 % (respectively) was observed when the temperature reached 385 °C, and 6.0 % and 7.5 % (respectively) when the temperature reached 650 °C. Based on these results, the two commercial precipitated

carbonates showed to be very stable at the reaction conditions. On the other hand, calcium oxide prepared from precipitated calcium carbonate was also studied and mass losses of 1.3 % and 7.0 % are reported when the temperature reached 385 °C and 650 °C, which revealed a very high thermal stability of this oxide at the reaction conditions.

4.2. - <u>Continuous Flow Reactor System Experiments</u>

4.2.1. - Reduction of Butyric Acid Concentration and Production of Ketones

As discussed in Section 3.2, the possibility of butyric acid condensation in the gas stream (saturated with butyric acid at 45 °C) in any of the pathways of the continuous flow reactor system can be ruled out. The condensation of butyric acid or any of the products at the conditions after reaction would be even less probable since the concentration of butyric acid (b.p. 163 °C) should be lower than the initial concentration, and the detected products 4-heptanone and acetone have boiling points of 145 °C and 56.5 °C, respectively. These boiling points indicate that these ketones are more volatile than butyric acid and the dew point at the reactor outlet should be lower than the dew point at the inlet of the reactor.

Each carbonate and oxide was tested in the continuous flow reactor system, as mentioned in section 3.2. The concentration of butyric acid was measured before and after reaction by GC analysis. The temperatures in the absorber and in the reactor were fixed at 45 °C and 385 °C, respectively. In order to determine the initial concentration of butyric acid (before reaction), N_2 was directed to the absorber bypassing the reactor and into the GC. When the areas of three consecutive peaks of butyric acid were in agreement (within 10% of each other), the N_2 was directed from the absorber, through the reactor and then to the GC. The experiment was timed, with the start of the experiment defined as the time when the gas stream started flowing through the reactor. The peak areas of butyric acid and the ketones (products) were measured at least every 35 minutes, as the GC run-time was 30 minutes, with 5 minutes required to return to a stable baseline. The reactor effluent was repeatedly sampled until the areas of three consecutive butyric acid peaks were constant (a difference less than 10% from each other). Figures 4-1 and

4-2 show the percent decrease of butyric acid and the production of ketones as a function of time. This data represents a comparison between Li_2CO_3 prepared from precipitation and a commercial precipitated $CaCO_3$, PCC (2).

As shown in both of the figures, there is a discrepancy between the production of ketones and the disappearance of butyric acid. The percent decrease in butyric acid and the moles of ketone produced per mole of butyric acid consumed, are shown in Table 4-6 and Figures 4-3, 4-4 and 4-5 for each reagent powder tested in the continuous flow reactor system. Appendix F contains the percent decrease of butyric acid and the production of ketone as a function of time for each carbonate and oxide studied. The values reported in Table 4-6 corresponded to the average of the last three data points observed as a function of time, and the standard deviation between these points was also reported.

64

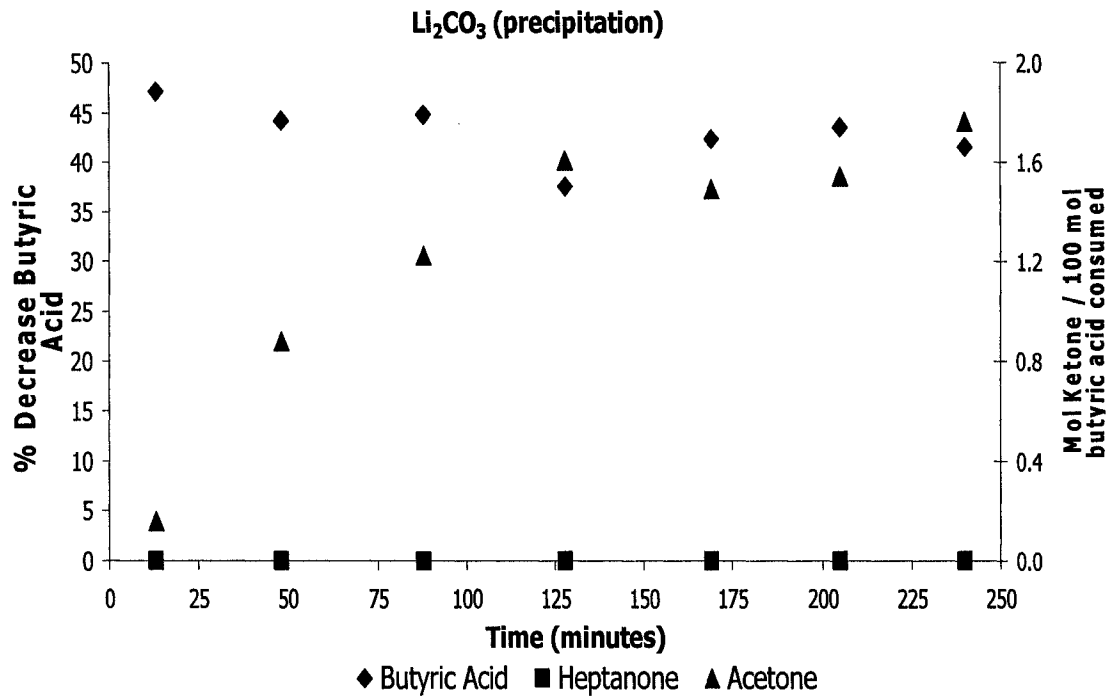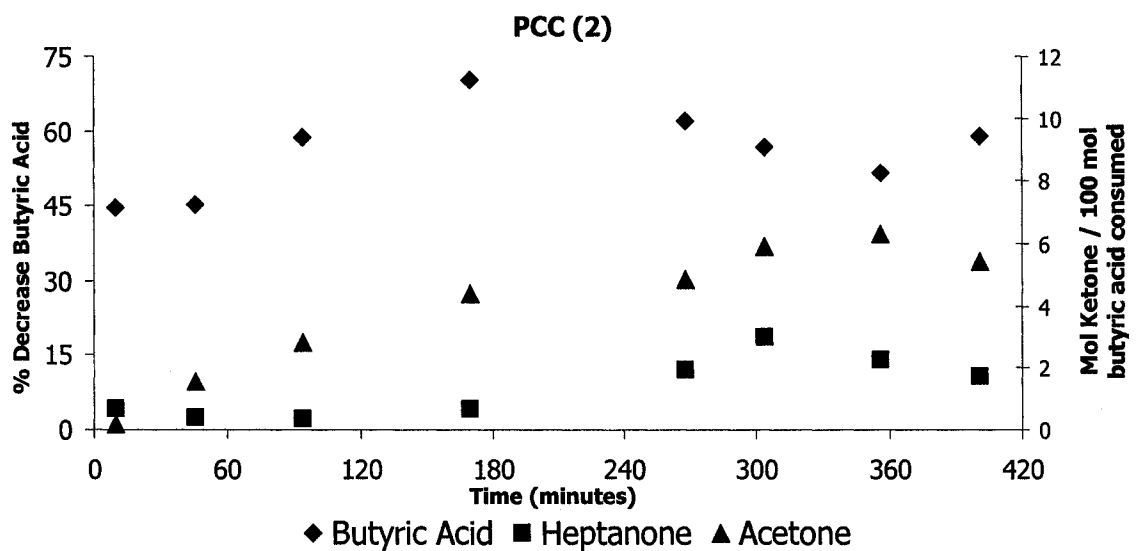**Figure 4-1:** Li_2CO_3 prepared by precipitation with a WHSV = 0.1572 h^{-1}

Figure 4-2: Commercial precipitated $CaCO_3$ (2) with a WHSV = 0.1453 h^{-1}

65

As shown in Figures 4-1 and 4-2, the reduction of butyric acid exceeded the amount of ketone produced, which is evidenced by the ratio ketone produced to butyric acid consumed. According to Figure 4-1, Li_2CO_3 prepared by precipitation showed no production of 4-heptanone and a production of acetone less than 2 mol per 100 mol of butyric acid consumed. Even though the stoichiometry of the production of acetone from butyric acid is not clear, it is very unlikely that only 0.02 moles of acetone (the only ketone formed) would be produced per mol of butyric acid consumed. Similar behaviour was observed for the commercial precipitated calcium carbonate (2), [PCC (2)], which exhibited a production of acetone less than 8 mol per 100 mol of butyric acid and a ratio of mol of 4-heptanone produced to 100 mol of butyric acid consumed less than 4. Based on these results for PCC (2), less than 0.12 mol of ketones were produced per mol of butyric acid consumed. It is important to consider, that no other product was detected by the GC.

Because the same behaviour was observed in all of the reagent powders analyzed, it was evident that some portion of the butyric acid was not reacting to form ketones and that probably this portion remained inside the reactor. Since it was not clear how the butyric acid was consumed in the reaction system, the term *conversion* was avoided, and in instead, the term *reduction* or *decrease* of butyric acid was used.

As shown in Table 4-6, commercial precipitated calcium carbonate (2) gave the highest percent of reduction of butyric acid. Calcium carbonate prepared by precipitation also showed one of the highest decrease of butyric acid, as well as the highest ratio of 4-heptanone to butyric acid consumed. The lowest percent of decrease of butyric acid was exhibited buy precipitated barium carbonate. $BaCO_3$, Ba/Li_2CO_3, Na_2CO_3, some of the Li_2CO_3, PCC (1) and $CaCO_3$ prepared from acetate did not show production of 4-heptanone. On the contrary, all the reagent powders tested exhibited production of acetone.

66

Table 4-6: Decrease of butyric acid and production of ketones in the continuous flow reactor system.

| Carbonate /Oxide	WHSV (h^{-1})	% Decrease Butyric acid	Mol 4-Heptanone / 100 mol Butyric acid consumed	Mol Acetone / 100 mol Butyric acid consumed
Li_2CO_3 (p)	0.4845	48.6 ± 0.4	8.8 ± 0.3	3.1 ± 0.1
Li_2CO_3 (p)	0.1475	44.2 ± 2.7	0.0	1.7 ± 0.1
Li_2CO_3 (p)	0.1572	42.5 ± 0.7	0.0	1.6 ± 0.1
Li_2CO_3 (a)	0.1455	26.2 +/- 0.9	2.3 ± 0.4	9.2 ± 0.4
Li_2CO_3 (o)	0.1319	41.2 ± 2.0	9.8 ± 0.9	7.8 ± 0.5
$MgCO_3$ (p)	0.1487	37.2 ± 1.5	20.9 ± 2.7	7.3 ± 0.5
Mg/Li_2CO_3 (p)	0.1858	41.0 ± 0.2	7.2 ± 0.1	6.0 ± 0.1
MgO (p)	0.1669	46.0 ± 1.0	3.0 ± 0.1	6.3 ± 0.5
MgO (p)	0.0931	43.8 ± 2.4	16.7 ± 1.8	7.2 ± 0.5
Mg/Li_2O (p)	0.1478	18.3 ± 1.7	14.1 ± 0.5	13.4 ± 1.5
$CaCO_3$ (p)	**0.1597**	**53.3 ± 0.6**	**38.6 ± 2.3**	**8.6 ± 0.6**
$CaCO_3$ (a)	0.1442	33.3 ± 2.0	0.0	6.4 ± 0.8
Ca/Li_2CO_3 (a)	0.1394	28.3 ± 4.0	21.5 ± 1.9	10.9 ± 1.1
CaO (p)	0.1382	34.5 +/- 2.4	0.0	3.9 ± 0.5
CaO (a)	0.1852	33.9 ± 0.2	26.8 ± 1.9	8.8 ± 0.2
Ca/Li_2O (a)	0.1467	49.5 ± 1.3	32.0 ± 0.6	8.5 ± 0.4
PCC (1)	0.1126	33.1 ± 2.8	0.0	10.8 ± 2.1
PCC (2)	**0.1453**	**55.9 ± 2.9**	**4.6 ± 0.9**	**5.9 ± 0.3**
$BaCO_3$ (p)	0.1183	22.6 ± 0.6	0.0	9.6 ± 1.5
Ba/Li_2CO_3 (p)	0.1398	38.3 ± 2.4	0.0	4.6 ± 0.4
Na_2CO_3 (f)	0.1631	40.1 ± 0.8	0.0	2.8 ± 0.5

p: Prepared by precipitation of salts

a: Prepared by thermal decomposition of acetate

o: Prepared by thermal decomposition of oxalate

f: Fisher reagent

Figure 4-3: Percentage of decrease of butyric acid for the carbonates and oxides tested in the continuous flow reactor
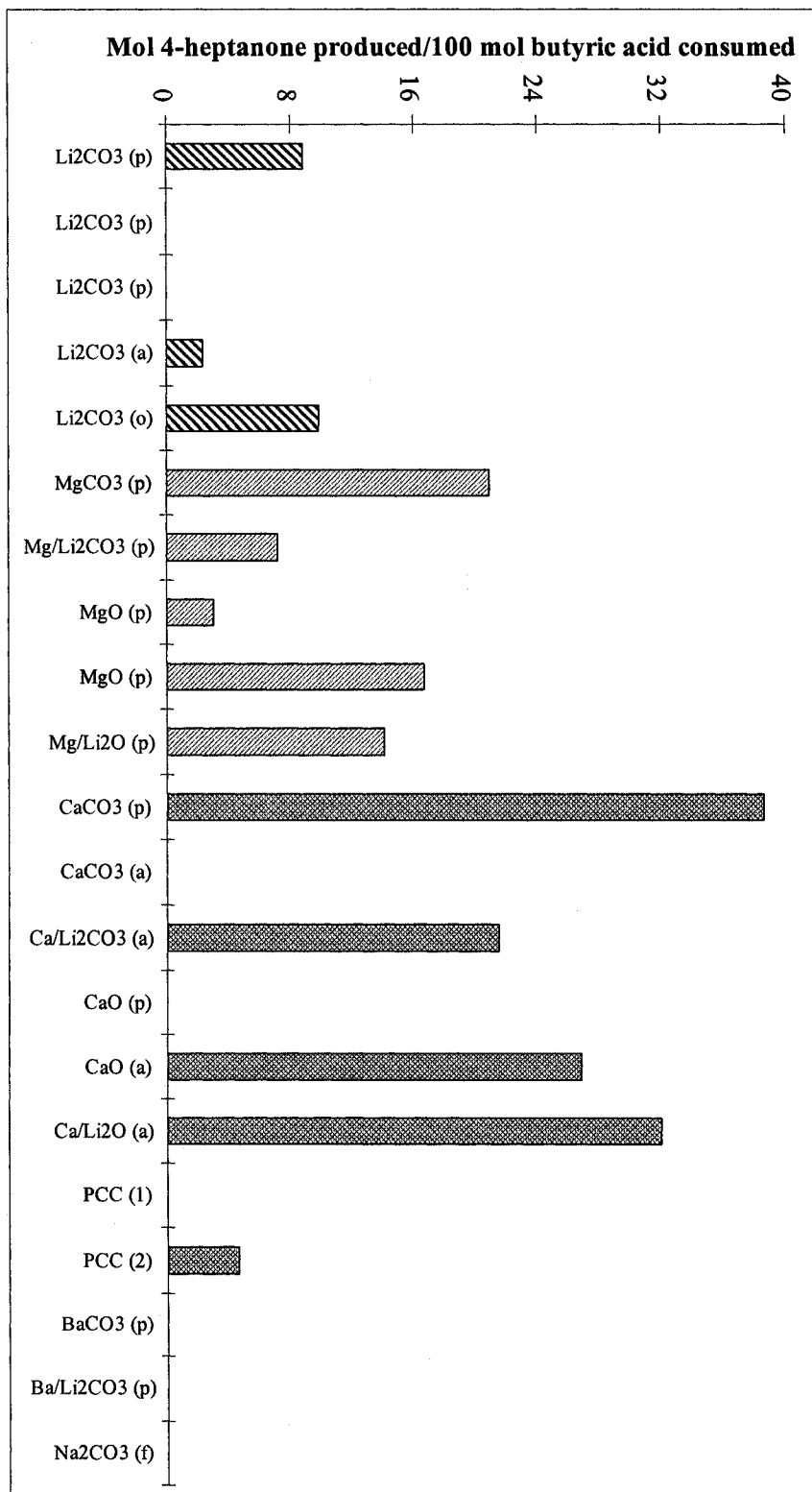
68
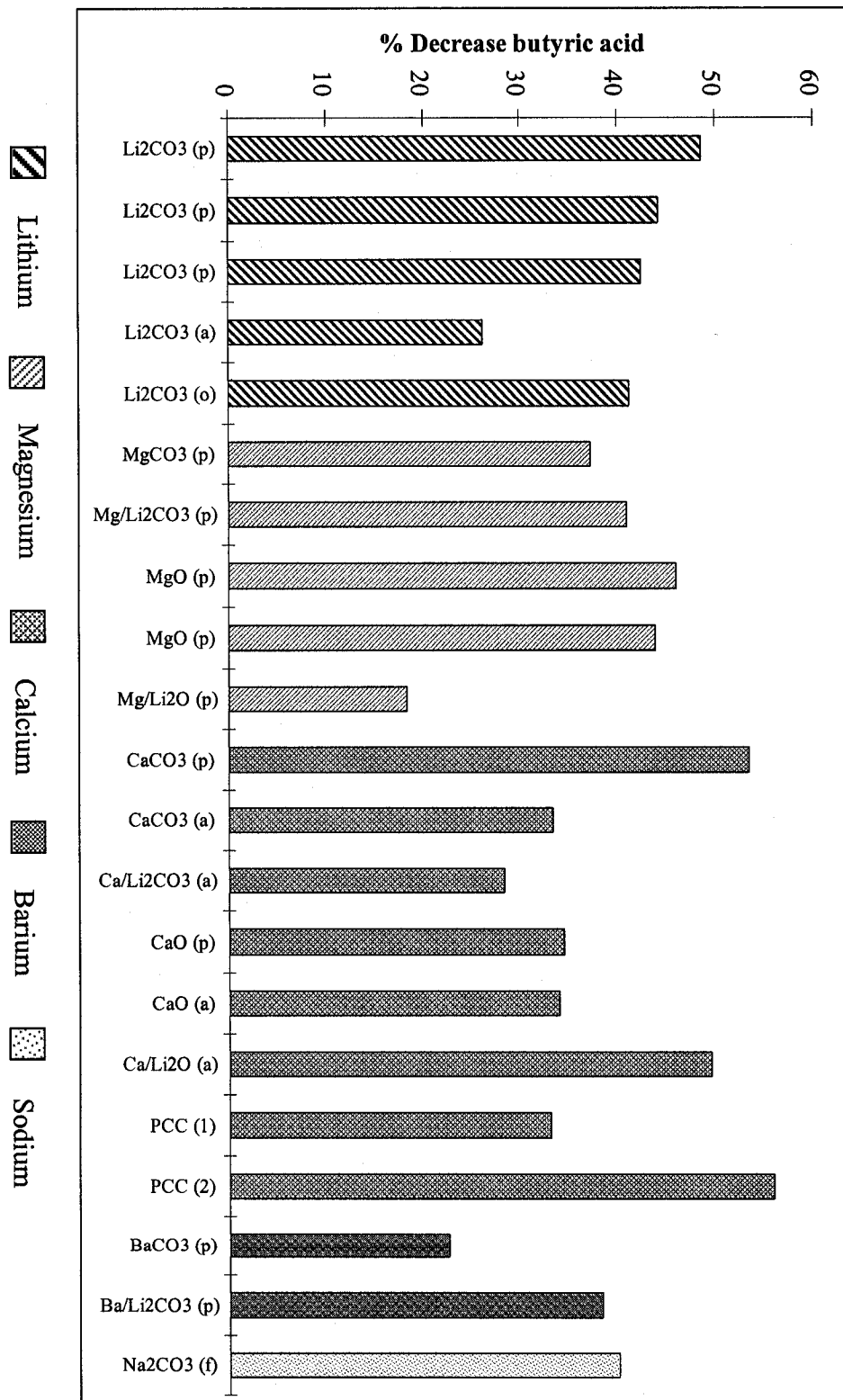
Figure 4-4: Production of 4-heptanone for the carbonates and oxides tested in the continuous flow reactor system.
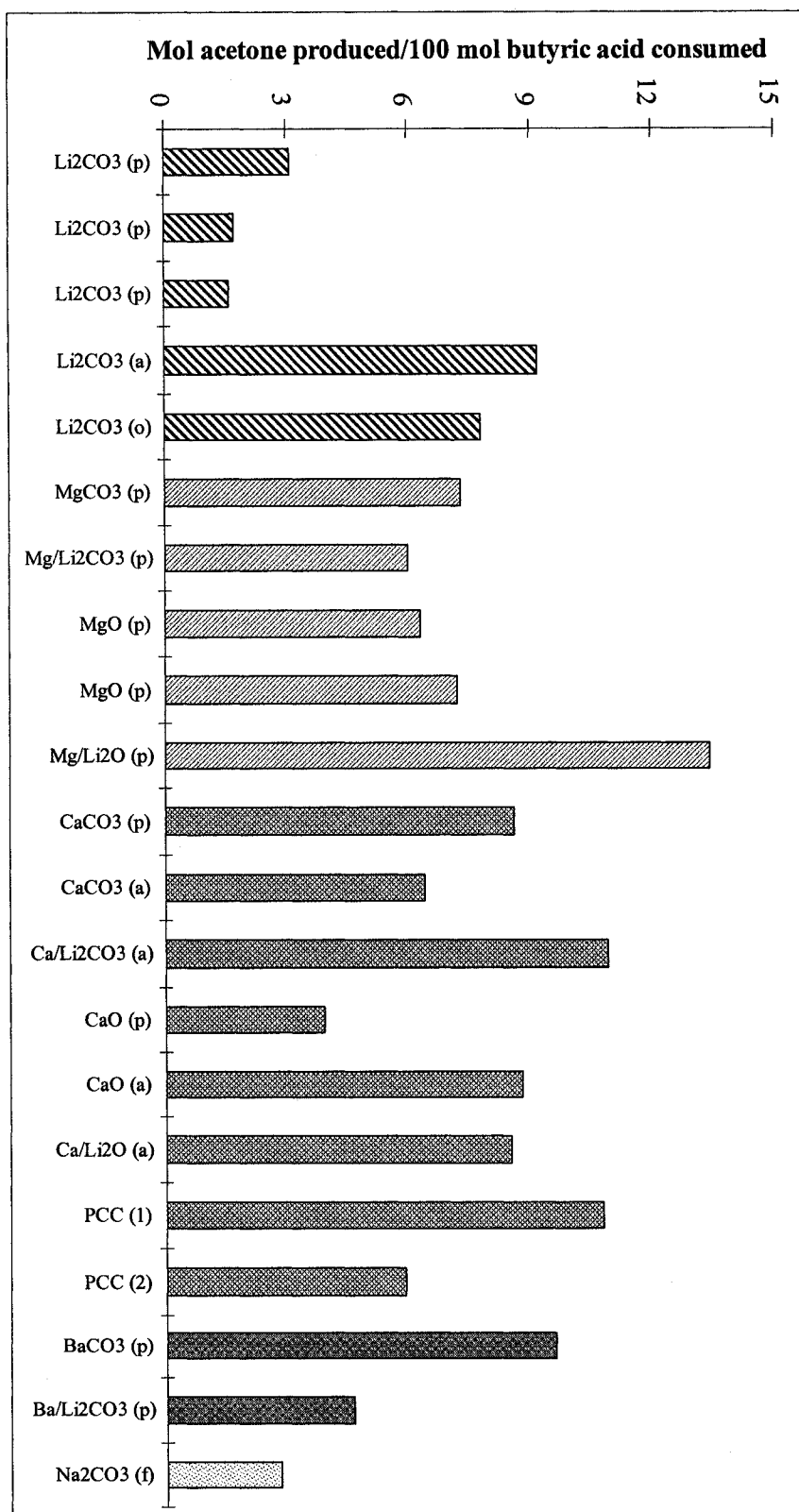
69

Figure 4-5: Production of acetone for the carbonates and oxides tested in the continuous flow reactor system.

70

4.2.2. - Analysis of the Reagent Powders by XPS before and after Reaction

The carbonates and oxides tested in the continuous flow reactor system were mixed with silicon carbide in order to achieve a good distribution of the powder in the reactor, as discussed in Section 3.2. The mixture of silicon carbide and each reagent powder was analyzed using XPS, and wide and narrow scans were performed in order to determine the oxidation states of the carbon atoms before and after reaction.

The oxidation states were determined using the software *CasaXPS* v.2.3.5, which uses peak fitting to resolve the binding energy of the data reported. XPS spectra are typically referenced to 285.0 eV; adventitious carbon, (http://srdata.nist.gov/xps/). However, due to the complexity of the multiples detected for the various carbon species on the surface, (carbonates, butyrates, etc) the reported binding energies are referenced to O 1s, 531.5 eV for Li_2CO_3. Once the binding energies were corrected, the different peaks found for the carbon were identified by comparing with the binding energies found in the literature. C 1s binding energies found in the samples agreed with literature values for carbonates, silicon carbide, adventitious carbon, the C-H bonds and O-C=O bonds present in carboxylic salts. This was confirmed by analyzing a sample of pure lithium butyrate supplied by Sigma Aldrich, using XPS.

Because pure lithium butyrate was commercially available, and previous experiments at low temperature were performed in the continuous flow reactor system using Li_2CO_3 (see Section 3.2), further analyses using XPS were completed in order to determine any possible change in the Li_2CO_3 structure or composition before and after reaction. The C 1s binding energies for pure lithium butyrate were compared with those detected in the pre- and post-reaction Li_2CO_3, (prepared by precipitation) before and after reaction at a temperature in the range of 150 and 220 °C for 625 minutes. In addition, a mixture of Li_2CO_3 - SiC before and after reaction at 385 °C for 308 minutes was also studied. This data is shown in Table 4-7 and Figure 4-6.

Similar analyses for selected carbonates and oxides tested at 385 °C were performed using XPS. A similar trend was observed, in that pre-reaction carbonates exhibit a C 1s peak with a binding energy around 289 eV. The post-reaction samples showed this same peak, plus the addition of a C 1s peak with a binding energy around 288 eV. This peak corresponds to a O-C=O bond characteristic of carboxylic acid salts.
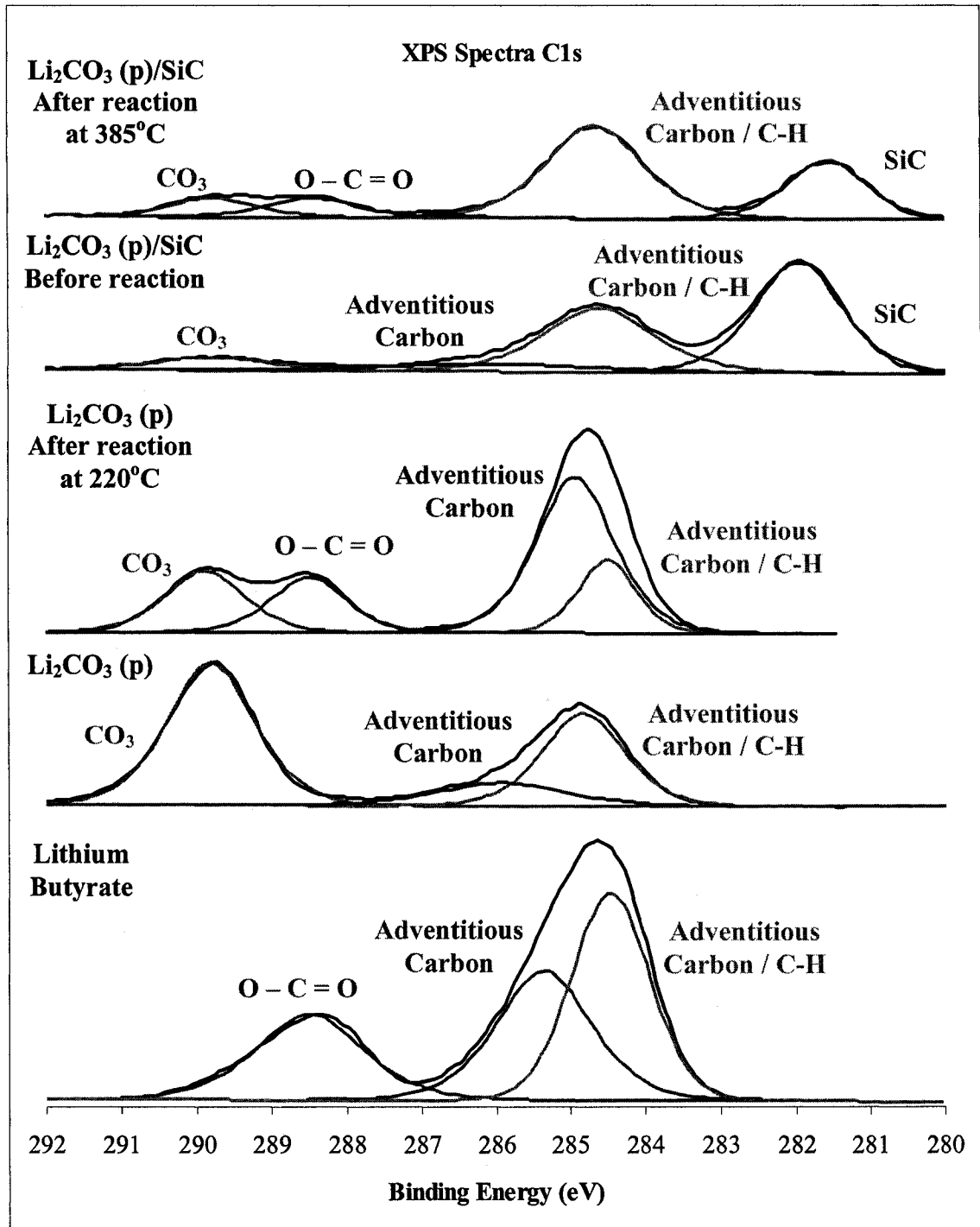
71

The pre-reaction mixture of MgO and SiC did not exhibit any peaks corresponding to carbonates or carboxylic acid salts. However, this sample in the post-reaction state showed evidence of a carboxylic acid salt, which indicates that butyrate could be formed on the surface of the reagent powder. This data can be found in Appendix C.2.

Table 4-7: Binding energy (eV) for the C 1s of Li_2CO_3 prepared by precipitation before and after reaction at different conditions

Binding Energy (eV)	SiC	Adventitiuos Carbon	C-H	O-C=O	CO$_3$
Theoretical *	281.5 283.8	284.8	284.8	289	289.8
Lithium Butyrate (C$_4$H$_7$O$_2$Li)	---	284.5	285.4	288.5	---
Li$_2$CO$_3$ Before Reaction	---	284.8	285.9	---	289.8
Li$_2$CO$_3$ After Reaction at 220°C	---	284.5	284.9	288.5	289.9
Li$_2$CO$_3$/SiC Before Reaction	281.9	284.6	286.1	---	289.8
Li$_2$CO$_3$/SiC After Reaction at 385°C	281.6	284.7	286.6	288.4	289.8

*: http://srdata.nist.gov/xps/ and http://lasurface.com (accessed on June 26th 2006)

72

Figure 4-6: XPS spectra for Li_2CO_3 prepared by precipitation before and after reaction at different conditions

XPS Spectra C1s

Li₂CO₃ (p)/SiC After reaction at 385°C — CO₃, O – C = O, Adventitious Carbon / C-H, SiC

Li₂CO₃ (p)/SiC Before reaction — CO₃, Adventitious Carbon, Adventitious Carbon / C-H, SiC

Li₂CO₃ (p) After reaction at 220°C — CO₃, O – C = O, Adventitious Carbon, Adventitious Carbon / C-H

Li₂CO₃ (p) — CO₃, Adventitious Carbon, Adventitious Carbon / C-H

Lithium Butyrate — O – C = O, Adventitious Carbon, Adventitious Carbon / C-H

292 291 290 289 288 287 286 285 284 283 282 281 280

Binding Energy (eV)

4.3. - Batch Reactor Experiments

Selected reagent powders (section 3.6) were tested in a batch reactor system and analyzed post-reaction in order to determine the formation of butyrate as a step in the reaction pathway of the decarboxylation reaction of butyric acid.

4.3.1. - Analyses of the Vapour-phase and Liquid-phase Products by Gas Chromatography and Mass Spectrometer (GC – MS)

Vapour and liquid phase products from the batch reactor experiments were analyzed using GC-MS by the Department of Chemistry at the University of Alberta. The resulting products consist of ketones, alkenes, carboxylic acids, CO_2, H_2O and others. These are reported in Tables 4-8 and 4-9.

Table 4-8: Vapour phase products identified in batch reactor studies

Ketones	Carboxylic Acids	Alkenes	Others
4-Heptanone	Butyric acid	2-Methyl 1-Butene	CO_2
2-Pentanone	Acetic acid	3-Hexene	H_2O
2,4-Dimethyl 3 - heptanone	Propanoic acid	3-Heptene	Butanal
	2-Methyl Propanoic acid	4-Propyl 3-Heptene	Butyric acid butyl ester

Table 4-9: Liquid phase products identified after reaction batch reactor studies.

Ketones	Carboxylic Acids	Alkenes	Others
4-Heptanone	Butyric acid	2-Pentene	CO_2
2-Pentanone	Acetic acid	3-Heptene	H_2O
3-Hexanone	Propanoic acid	2-Heptene	Butanal
3-Methyl 4-Heptanone		4-Methyl 3-Heptene	
7-Methyl 4-Octanone		4-Propyl 3-Heptene	
		3-Hexene	

It is important to notice that the products identified from the batch reactor experiments are different from the products identified from the continuous flow reactor experiments. The column and GC used in the continuous flow reactor system were able to distinguish all the products identified in the batch reactor system but CO_2 and H_2O. On the other hand, these products are not described by the decarboxylation reaction proposed by Senderens in 1913, described in Equations 1-4 and therefore Equation 1-5. Appendix G shows the chromatograms and the MS results obtained from these analyses.

4.3.2. - Analyses of the Reagent Powders after Reaction by TGA

Following batch reaction at 385 °C for 3 hours and drying overnight at 200 °C, the reagent powders were analyzed using TGA. For comparison, pure lithium butyrate was also analyzed using TGA. The temperature program used in the analyses was as follows: The sample temperature was increased from 18 °C to 105 °C at 5 °C/min, next, the sample temperature was held for 1 hour, then ramped to 180 °C at 5 °C/min. Following a hold at 180 °C for 2.5 hours, the temperature was subsequently raised to 650°C at 5 °C/min and held for 2 hours. Finally, the temperature was decreased to 18 °C at 15 °C/min. The percent mass loss for each sample was estimated by calculating peak areas generated by graphing change in mass as a function of time; dTG/dt vs t. The software Origin version 7.5 was used to calculate the area of the peaks found.

75

The thermal decomposition of pure lithium butyrate and Li_2CO_3 following batch reaction are compared and shown in Figures 4-7 and 4-8. It is evident that both, pure lithium butyrate and Li_2CO_3 post-reaction, showed the same thermal decomposition path. On the other hand, the thermal decomposition of commercial precipitated $CaCO_3$ (2) before and after batch reaction are compared and shown in Figures 4-9 and 4-10. $CaCO_3$ (2) after reaction exhibited a thermal decomposition very similar to that for pure lithium butyrate, and very different from the thermal decomposition showed by the $CaCO_3$ (2) before reaction. Post- reaction TGA data of the different carbonates and oxides tested in the batch reactor are compared and shown in Figures 4-11 and 4-12.

Figure 4-7: Thermal decomposition of pure lithium butyrate and Li_2CO_3 tested in the batch reactor after reaction

Li Butyrate ——— Li2CO3 after reaction ——— Temperature

76
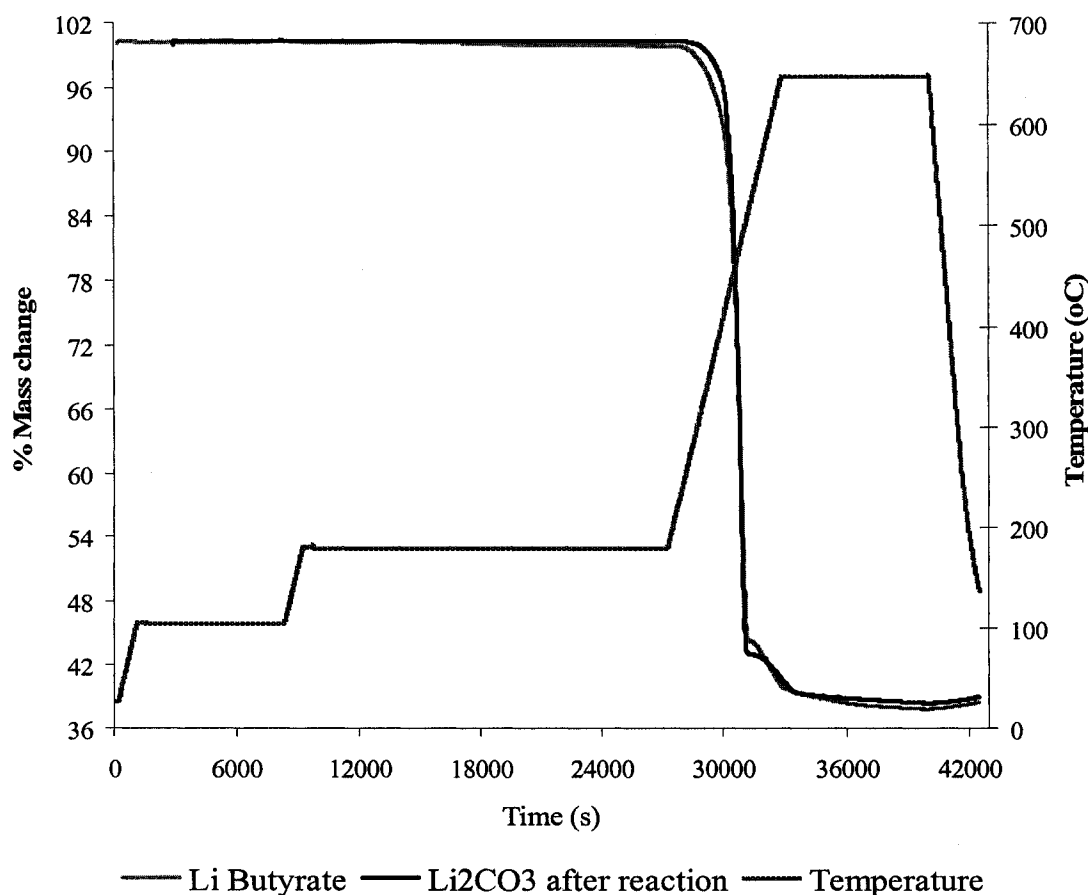
Figure 4-8: Rate of change in mass as a function of time (dTG/dt vs t) of pure lithium butyrate and Li_2CO_3 tested in the batch reactor after reaction

77
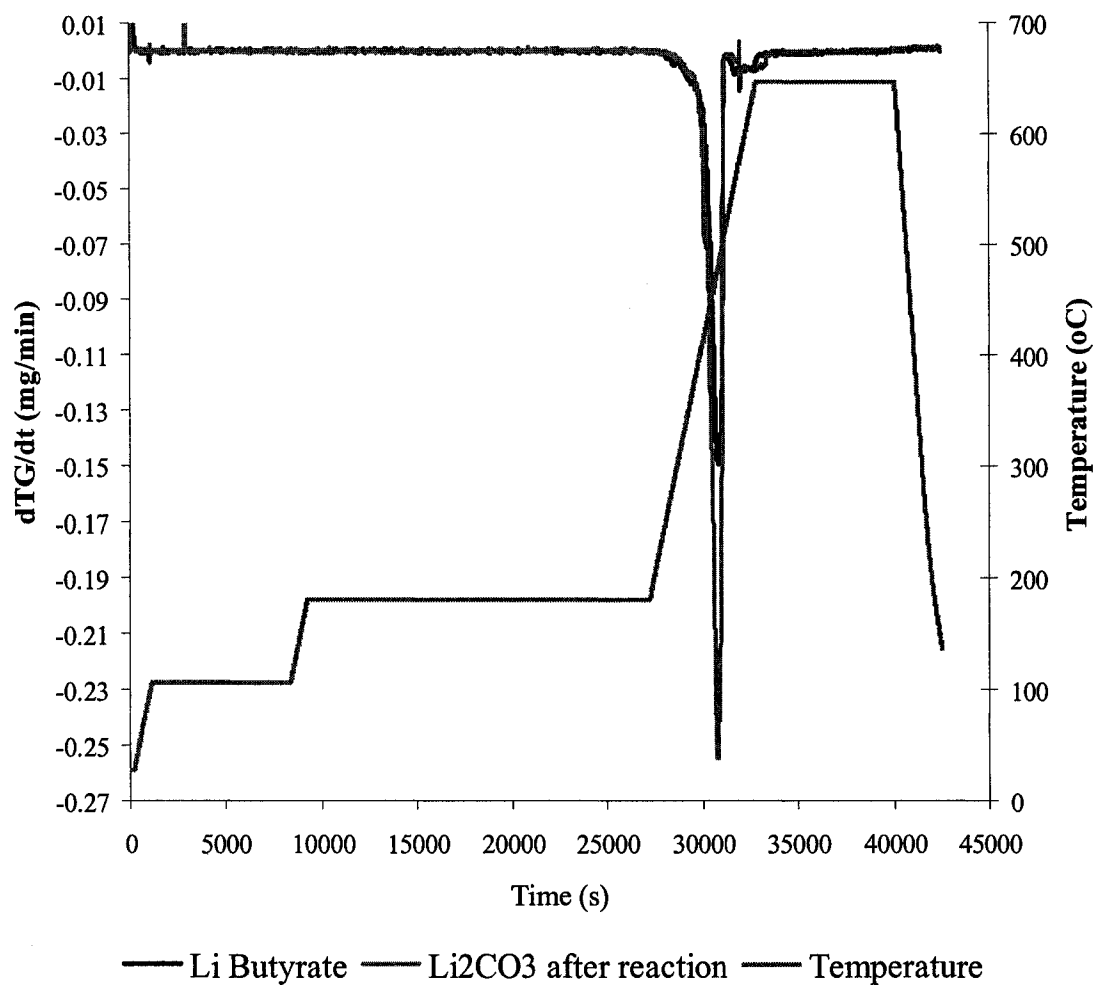
Figure 4-9: Thermal decomposition of commercial precipitated $CaCO_3$ (2) tested in the batch reactor, before and after reaction
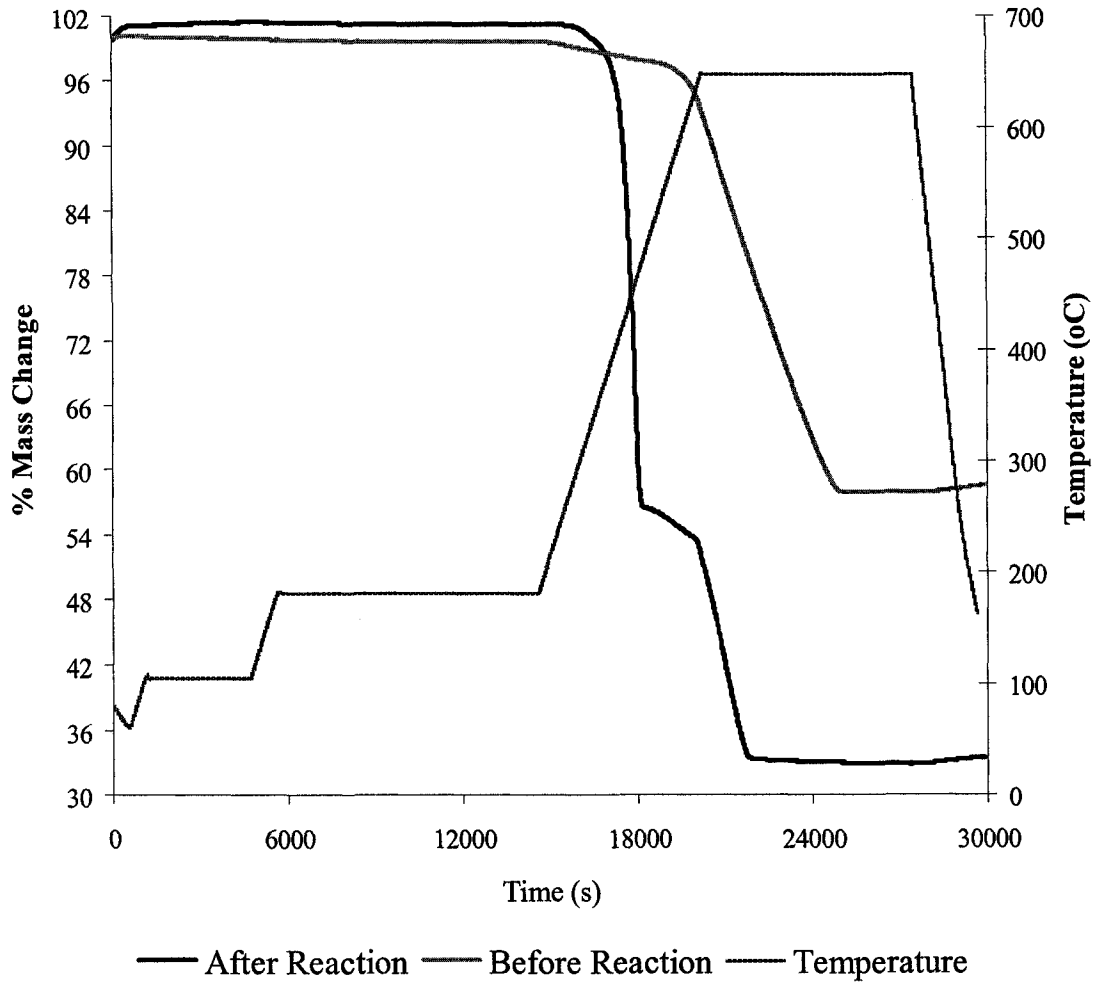
Figure 4-10: Rate of change in mass as a function of time (dTG/dt vs t) of commercial precipitated CaCO₃ (2) tested in the batch reactor, before and after reaction

——— After Reaction ——— Before Reaction ——— Temperature

79
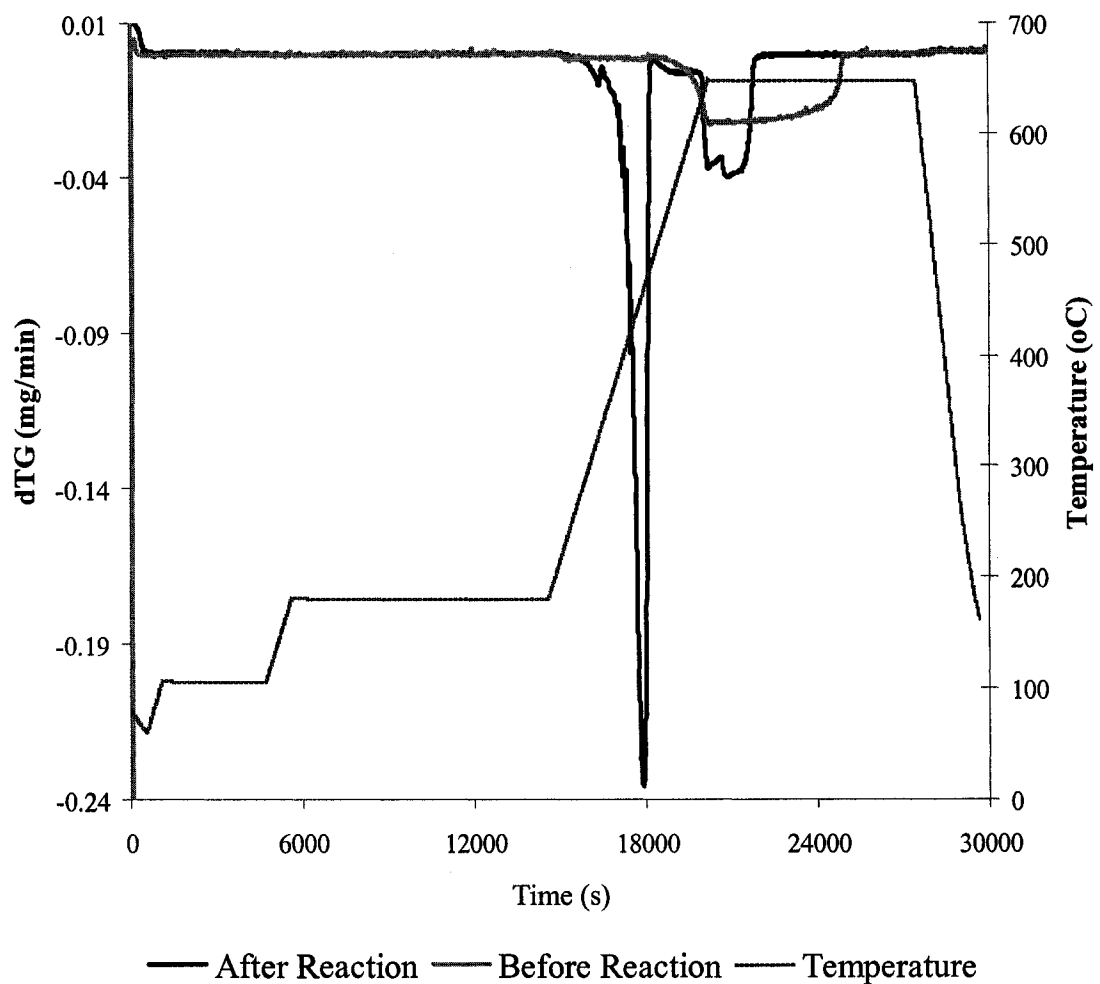
Figure 4-11: Thermal decomposition of carbonates and oxide tested in the batch reactor, after reaction

— PCC (1) — BaCO3 — MgO — PCC (2) — Li2CO3 — Temperature

80
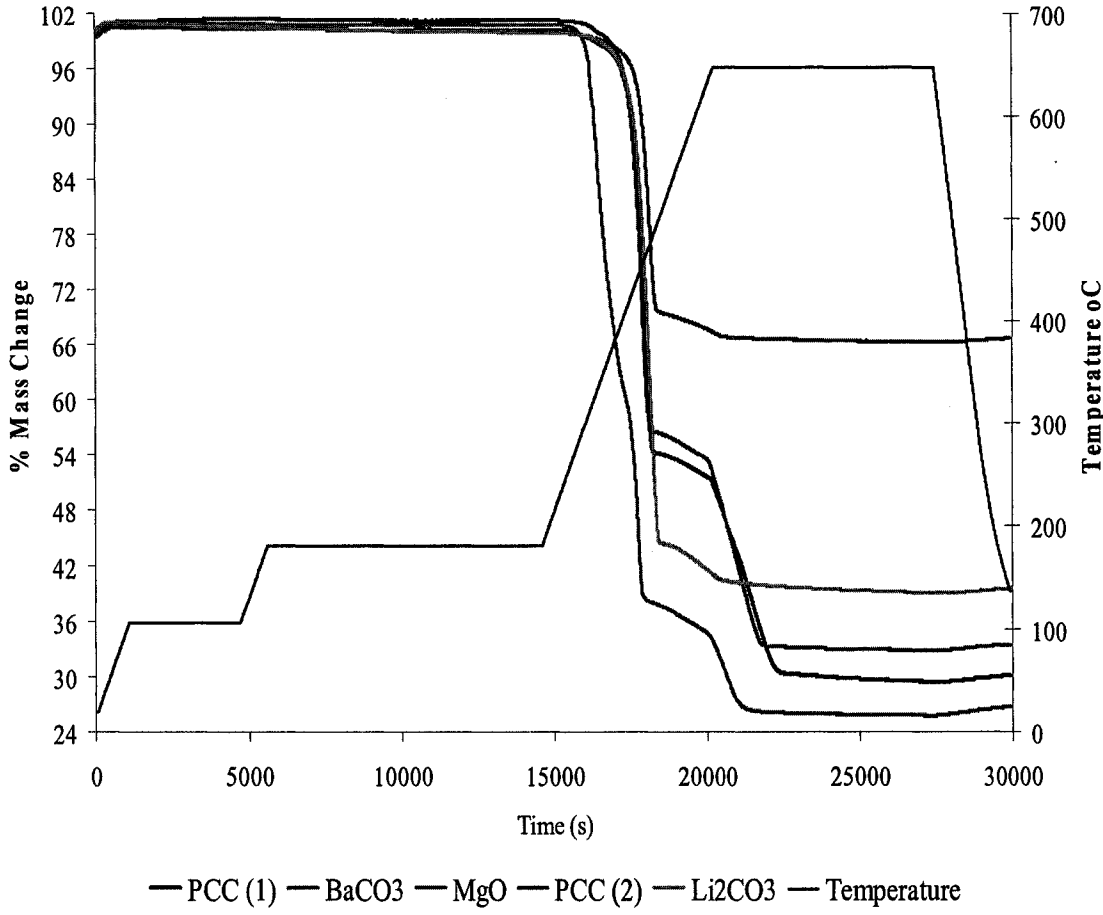
Figure 4-12: Rate of change in mass as a function of time (dTG/dt vs t) of the different carbonates and oxides tested in the batch reactor, after reaction

— PCC (1)　— BaCO3　— MgO　— PCC (2)　— Li2CO3　— Temperature
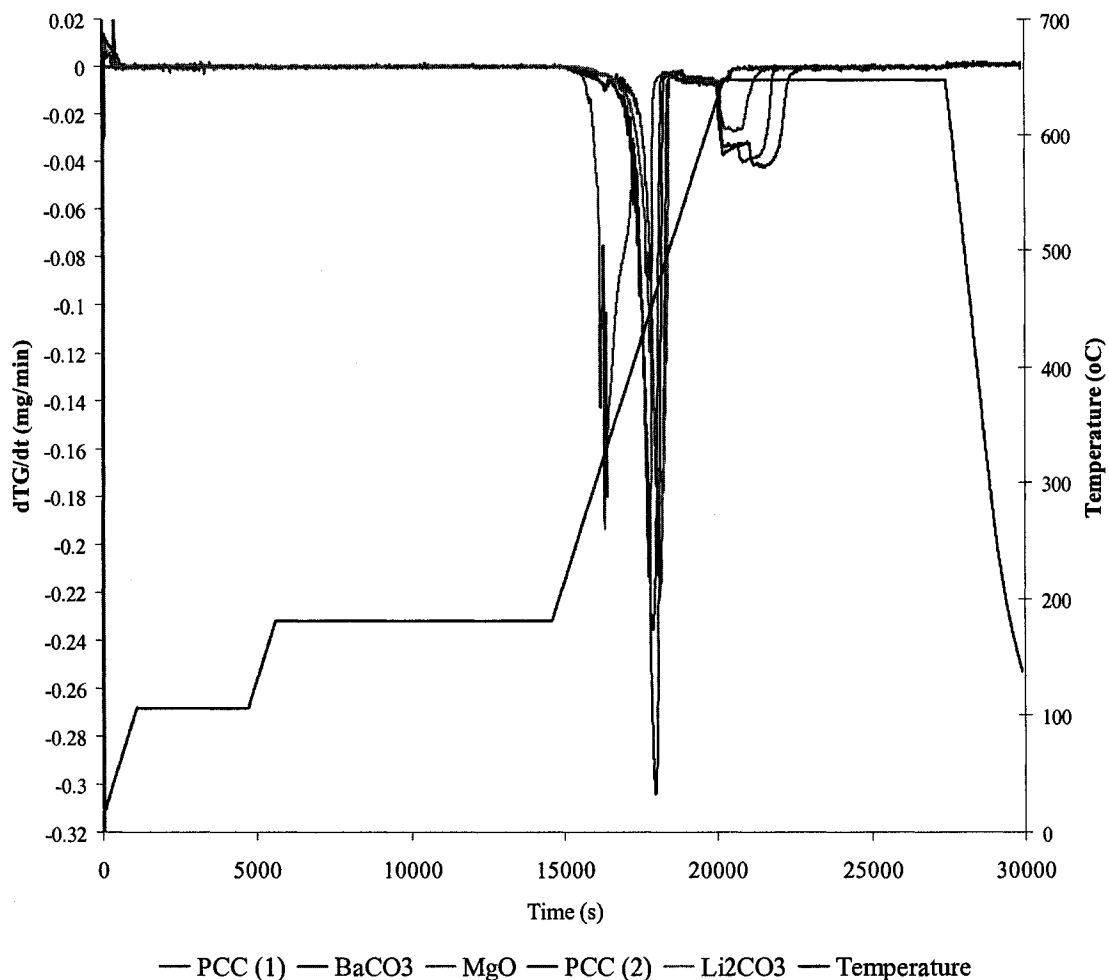
The percent mass lost for the reagent powders after reaction was calculated from the TGA studies. These results are shown in Table 4-10. The theoretical thermal decomposition of the butyrates is described in equation 4-2. A complete reaction (bulk reaction) between the carbonates or oxide and butyric acid was assumed in the calculation of the theoretical mass loss shown in Table 4-10.

$$\text{Metal}(C_4H_7O_2)_n \longrightarrow \text{Metal}(CO_3)_n + C_7H_{14}O \qquad \textbf{(4-2)}$$

Where n is the metal cation charge, (1 when for Li, 2 for Mg, Ca, Ba, etc).

Table 4-10: Experimental and theoretical thermal decomposition of the reagent powders tested in the batch reactor at 385°C for 3 hours, after reaction

Reagent Powder	Experimental % mass loss	Theoretical % mass loss	% Difference
PCC (1)*	46.0	53.3	-13.60
PCC (2)**	45.0	53.3	-15.53
Li_2CO_3	57.4	60.6	-5.31
MgO	62.6	57.6	8.75
$BaCO_3$	30.9	36.6	-15.60

*: Commercial precipitated $CaCO_3$ (1)

**: Commercial precipitated $CaCO_3$ (2)

The experimental percent of mass loss observed for the reagent powders tested are very similar to the theoretical percent of mass loss expected according to Equation 4-2, if a no complete contact between the reagent powder and the butyric acid is considered. The thermal decomposition of the post-reaction reagent powders and the percent of mass loss observed are evidence that the formation of butyrate could be a step in the reaction mechanism of the decarboxylation reaction of butyric acid.

4.3.3. - Analyses of the Reagent Powders after Reaction by IR

The reagent powders after reaction and after being dried at 200 °C overnight were analysed using IR in order to qualitatively determine their composition. The IR spectra obtained from these samples showed vibrational wavenumbers characteristic of carboxylic salts. This was confirmed by comparison with the IR spectrum measured for pure lithium butyrate. Figure 4-13 shows the IR spectrum obtained from pure lithium butyrate, while the IR spectra of the reagent powders tested in the batch reactor, after reaction, are shown in Figure 4-14. The wavenumbers reported in the different IR spectra are shown in Table 4-11. All the reagent powders analyzed after reaction in the batch reactor system exhibited wavenumbers corresponding to those showed by the pure lithium butyrate also analyzed.

Figure 4-13: IR spectrum for pure lithium butyrate
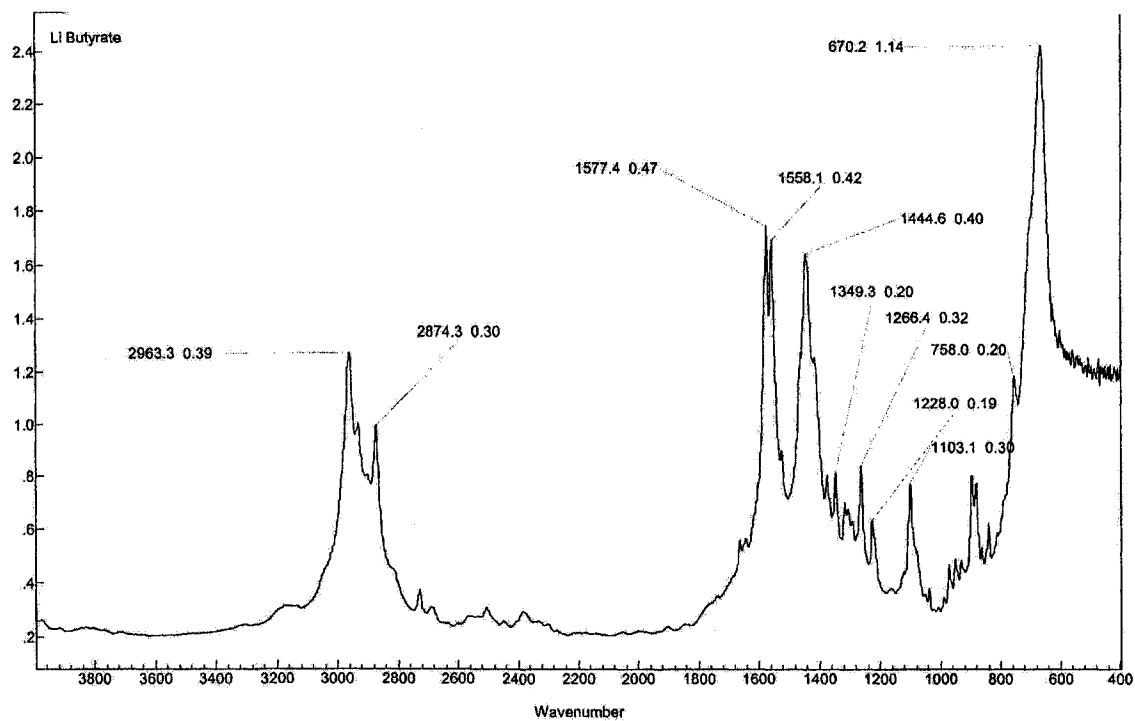
Figure 4-14: IR spectra of the reagent powders tested in the batch reactor, after reaction
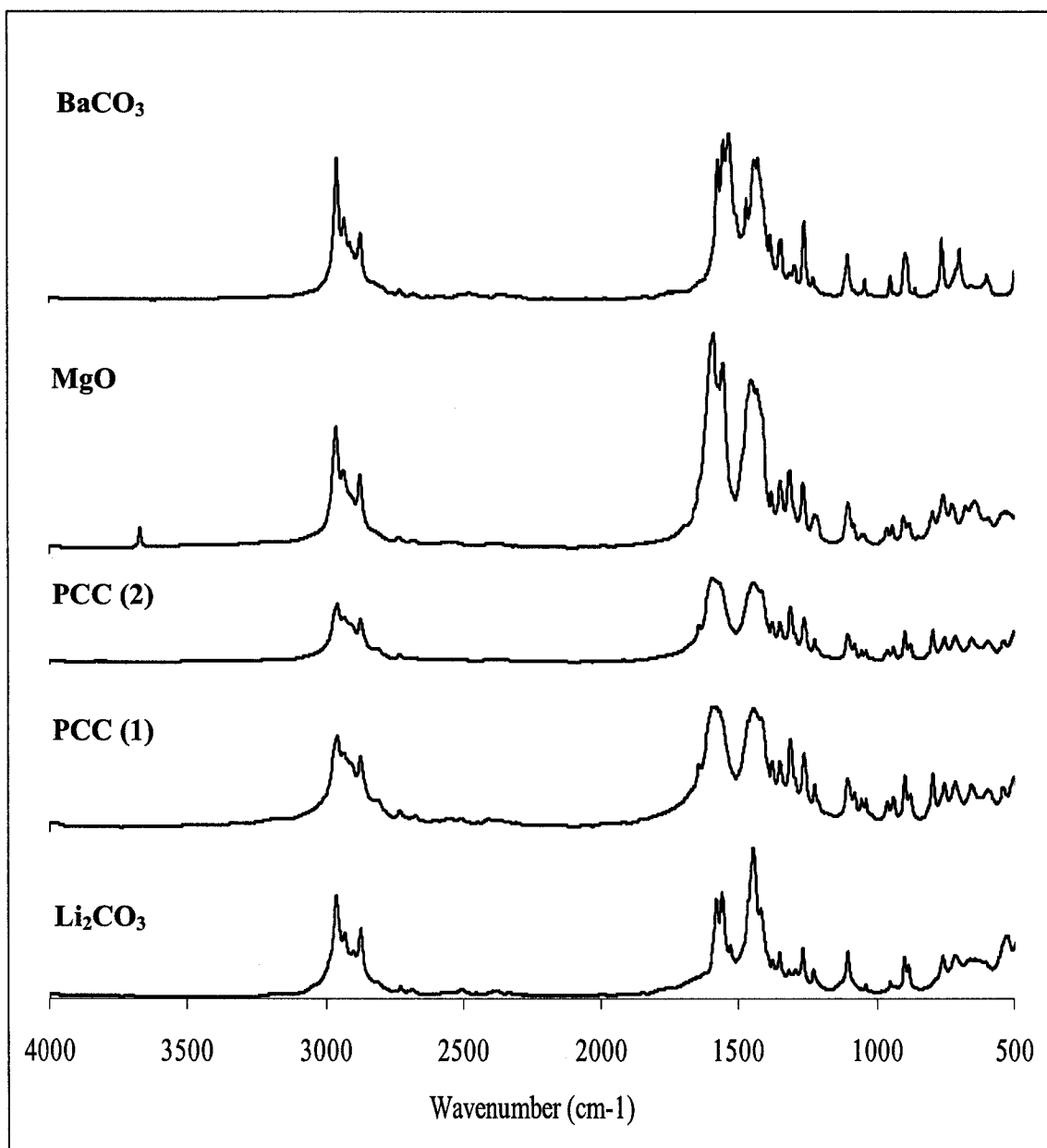
Table 4-11: IR wavenumbers of the different reagent powders analyzed after reaction

Reagent Powder	Wavenumber (cm^{-1})				
Lithium butyrate	**1445**	**1558**	**1577**	**2874**	**2963**
Li$_2$CO$_3$ (p)	1445	1557	1577	2874	2963
PCC (1)*	1443	---	1574	2874	2958
PCC (2)**	1443	---	1592	2874	2958
MgO (p)	1447	1552	1585	2874	2961
BaCO$_3$ (p)	1438	1550	1569	2871	2958

*: Commercial precipitated CaCO$_3$ (1)

**: Commercial precipitated CaCO$_3$ (2)

p: Prepared by precipitation of salts

Based on the clear agreement between the wavenumbers showed by the pure lithium butyrate and the wavenumbers exhibited by the post-reaction reagent powders analyzed using IR, it is evident that the carbonates/oxides tested and butyric acid reacted to form butyrate at the reaction conditions.

4.4. - Experimental Procedure to Study the Formation of Butyrate at Low Temperature

Low temperature experiments were performed to determine if butyrate could be formed at less severe conditions, so that potential process schemes and further studies could be suggested.

4.4.1. - Analyses of the Resultant Solids by TGA

Various calcium compounds were mixed with liquid butyric acid at low temperatures, (room temperature and 50 °C), after which the resulting solids were washed with chloroform and then dried at 200 °C. The resulting solids were studied by TGA to study their thermal decomposition. The percent mass loss for each sample was estimated as discussed in Section 4.3.2, and these results are reported in Table 4-12. The mass as a function of time and the rate of change of mass (dTG/dt) as a function of time of the samples are shown in Appendix E.2.

Table 4-12: Experimental and theoretical thermal decomposition of different reagent powders tested after mixing with butyric acid at low temperatures

Reagent Powder	Experimental % mass loss	Theoretical % mass loss	% Difference
Ca(OH)$_2$ (1)	45.4	53.3	-14.83
CaO (1)	44.0	53.3	-17.49
PCC (1)* (2)	32.7	53.3	-38.65
PCC (2)* (2)	8.8	53.3	-83.52

(1): At room temperature

(2): At 50°C

*: Commercial precipitated CaCO$_3$ (1)

**: Commercial precipitated CaCO$_3$ (2)

4.4.2. - Analyses of the Resultant Solids by IR

The calcium butyrate prepared by mixing liquid butyric acid with Ca(OH)$_2$ at room temperature was identified using IR spectroscopy. The typical vibrational wavenumbers for this carboxylic salt; 1443, 1594, 2874 and 2957 cm^{-1}, were identified in the IR spectrum, as shown in Table 4-13. The product of mixing CaO, liquid butyric acid and water at room temperature was also identified as calcium butyrate using IR spectroscopy. However, when the two commercial precipitated CaCO$_3$ were mixed with liquid butyric acid at room temperature, the solid did not take the acid up and no changes in the solid were observed, even after adding water. When the same experiment was repeated at 50 °C, the solids took some liquid up and the formation of a new solid was evident.

The IR analyses performed following mixing the carbonate, liquid butyric acid and water at 50 °C exhibited vibrational wavenumbers distinctive for carboxylic salts; 1462, 1592, 2874 and 2957 cm^{-1}, but also vibrational wavenumbers characteristic for carbonates such as 713, and 874 cm^{-1}. These results suggested that calcium carbonate did not convert completely into calcium butyrate. As shown in Figure 4-15, the vibrational wavenumber of 874 cm^{-1} for PCC (2) is notoriously stronger than that for PCC (1), which indicates a higher extent of conversion of carbonate to butyrate for PCC (1).

86

Figure 4-15: IR spectra of the different reagent powders tested after mixed with butyric acid at low temperatures
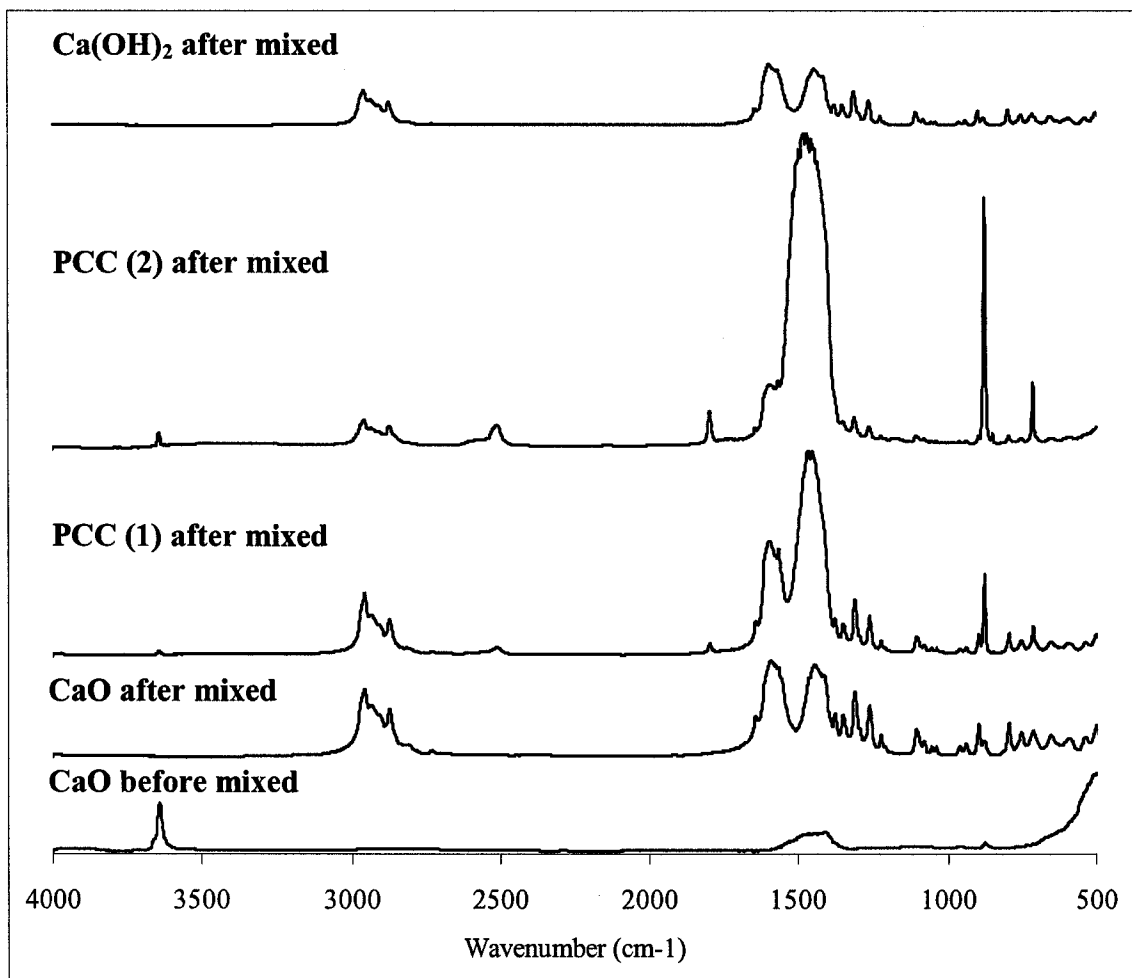
Table 4-13: IR wavenumbers of the different reagent powders tested after mixing with butyric acid at low temperatures

Reagent Powder	Wavenumber (cm^{-1})						
Ca(OH)$_2$ (1)	---	---	**1443, 1594** (3)	---	---	**2874**	**2957**
CaO (1)	---	---	**1443, 1574** (3)	---	---	**2874**	**2957**
PCC (1)* (2)	---	876	**1452, 1592** (3)	1795	2511	**2874**	**2957**
PCC (2)* (2)	713	874	**1462** (3)	1794	2512	**2874**	**2958**

(1): At room temperature

(2): At 50 °C

(3): Wide and strong peak

*: Commercial precipitated CaCO$_3$ (1)

**: Commercial precipitated CaCO$_3$ (2)

CHAPTER 5

DISCUSSION

5.1. - Characterization of the Reagent Powders

5.1.1. – IR and XPS Analyses

The carbonates and oxides prepared were identified using IR spectroscopy. The carbonates presented the distinctive vibrational wavenumbers of these compounds: 800 – 880 cm^{-1} and 1410 – 1450 cm^{-1} (See Table 4-1). However, the oxides also presented these wavenumbers although with a much lower intensity, which leads to the conclusion that the carbonates used to prepare the oxides were not completely converted. This is also suggested by the XPS analyses of these samples, since the oxides studied showed a peak whose binding energy was 290.0 eV, which is characteristic of the C 1s feature of carbonates. For these oxides, the percent area of the 290.0 eV peak was very low compared to the area of the remaining C 1s peaks. For example, for the sample of CaO prepared from acetate and the sample of Mg/Li$_2$O prepared by precipitation, the carbonate peak area represented only 0.80 % and 13.31 %, respectively, of the total carbon peak area (Table 4-3). The atomic percentages of carbon in these oxides were 32.5 % and 12.4 % (Table 4-2), corresponding to 0.26 % and 1.65 % of carbon due to carbonate in CaO and Mg/Li$_2$O respectively, which is an indication that the conversion of the carbonates was almost complete for the CaO prepared from acetate and the Mg/Li$_2$O.

On the other hand, IR analysis for Li$_2$CO$_3$ prepared by thermal decomposition of acetate showed vibrational wavenumbers characteristic of carboxylic acid salts. However, these were not detected in the CaCO$_3$ and Ca/Li$_2$CO$_3$ prepared from the acetates, which is an indication that the lithium acetate was not completely converted into carbonates.

Further XPS analyses showed that the carbonates prepared from the acetates contained some organic residue on their surfaces since peaks with a binding energy around 289 eV distinctive or a O-C=O surface species. These peaks represented a significant percentage of the C 1s signal; 40.84 % for the CaO and 16.84 % for the

89

Li_2CO_3, which added to the presence of adventitious carbon and explains the high atomic percentage of carbon contained on the surface of the samples. The high percentages of carbon contained on the surface of the samples caused that the percentages of the others elements were lower than expected.

In addition, the colour of these carbonates was a light grey and not white like the carbonates prepared by precipitation of salts. Machinaga et al. (1989) reported that the coloration of calcium carbonate prepared by thermal decomposition of acetate was a light grey due to the combination of pale yellow and red components coming from organic compounds (graphite carbon detected by XRD), which agrees with the observations and XPS results obtained in this study.

5.1.2. – Thermal Stability of the Prepared Carbonates

As shown in Table 4-5, Li_2CO_3 and $BaCO_3$ prepared by precipitation presented a high thermal stability at the reaction conditions, since these carbonates only lost around 1% mass when the temperature was held at 650 °C. Based on the percent of mass loss obtained from the TGA analyses, $CaCO_3$ prepared by precipitation showed a good thermal stability at the reaction conditions (2% mass loss at 385 °C) but it exhibited some decomposition at 650 °C (40% mass loss). In contrast, $MgCO_3$ also prepared by precipitation exhibited a very poor thermal stability at 385 °C, since the percent of mass loss is around 45% at this condition.

Regarding the thermal stability of the prepared calcium carbonate, a mass loss of 2 % and 40 % was reported when the temperature reached 385 °C and 650 °C, respectively, which showed a good stability of this carbonate at the reaction conditions but a thermal decomposition at 650 °C (probably to the oxide). The two commercial precipitated calcium carbonates analyzed by TGA exhibited a mass loss of less than 8 % when the temperature reached 650 °C, which leads to the conclusion that these are thermally more stable than the $CaCO_3$ prepared by precipitation. It is important to consider that the temperature programs used were different; the prepared carbonate was held for 30 minutes at 650 °C while the commercial carbonates were held for 2 hours at 650° C. The difference in thermal stability could have been caused by the different conditions used in the preparation of these carbonates. Choudhary et al. (1994) has

90

reported this phenomenon previously in the study of several magnesium carbonates prepared by precipitation using different preparation conditions.

5.2. - Continuous Flow Reactor System and Batch Reactor System Results

5.2.1. - Evidence of the Formation of Butyrate Salts

Preliminary tests performed at temperatures around 150 °C and 220 °C for Li_2CO_3 prepared by precipitation showed a lower concentration of butyric acid at the outlet of the reactor than at the inlet, even though the GC detected no products. This observation agrees with what Pestman et al. (1997) reported when they studied the ketonization of acetone using Bi_2O_3, PbO_2, MgO, MnO_2.

Additionally, if Equation 1-5 is assumed to describe the decarboxylation reaction of butyric acid, for all the prepared carbonates and oxides tested in the continuous flow reactor system at 385 °C the loss in butyric acid was higher than the butyric acid necessary to achieve the production of acetone and 4-heptanone. It was also observed that the percentage of butyric acid consumed appeared to be steady after a certain period of time, while the production of 4-heptanone and acetone was observed to increase continuously with time.

The observations mentioned previously may be explained by the reaction between the butyric acid and the reagent powder to form a carboxylic salt, which would decompose to generate the ketones as products. This possible reaction pathway agrees with what Pestman et al. (1997), Sugiyama et al. (1992), and Zhang et al. (2004) have reported for various oxides, such as MgO, CaO, BaO, NaO, in the study of the decarboxylation reaction of acetic acid, naphthoic acid and others carboxylic acids.

5.2.2. Analysis of Reagents Post-Reaction – Continuous Flow Reactor System

The Li_2CO_3 prepared by precipitation tested in the continuous flow reactor system at temperatures around 150 °C and 220 °C was analyzed before and after reaction using XPS. The XPS analyses shown in Figure 4-4 and Table 4-7 showed peaks with binding energies of 289.8 eV and 289.9 eV for the sample before and after reaction respectively,

which represent the typical C 1s peak for carbonates. A peak with a binding energy of 288.5 eV corresponding to the C 1s peak for the bond O-C=O distinctive of carboxylic salts was identified for the sample after reaction. This results leads to the assumption that at least on the surface of the carbonate, some butyrate intermediate was formed.

The XPS analyses performed for the carbonates and oxides tested in the continuous flow reactor system after reaction showed a C 1s peak corresponding to the O-C=O bond found in carboxylic acid salts. For example, as shown in Table 4-7, Li_2CO_3 prepared by precipitation and mixed with SiC showed C 1s peaks with binding energies of 281.9, 284.6, 286.1 and 289.8 eV, which are consistent with the binding energies found in the literature for the C 1s contained in SiC, adventitious carbon, the C-H bond and carbonate, respectively. When analysed after reaction, the binding energies estimated for the C 1s peaks were 281.6, 284.7, 286.6, 288.4 and 289.8 eV, corresponding to the C 1s contained in SiC, adventitious carbon, the bond C-H, the carboxylic O-C=O and carbonate, respectively. These results agree with the assumption that butyrate is formed as an intermediate in the reaction pathway in order to generate the ketones; however, these results are not decisive.

5.2.3. Analysis of Reagents Post-Reaction – Batch Reactor System

Because the amount of reagent powder used in the continuous flow reactor system was very small, around 0.050 grams, and this powder was mixed with more than 1 gram of SiC before be placed in the reactor, no further analyses were performed in order to confirm the formation of butyrate. Instead, as was discussed in Section 3.6, additional experiments were carried out in a batch reactor system. The carbonates and oxide tested, including PCC (1), PCC (2), MgO, Li_2CO_3 and $BaCO_3$ prepared by precipitation were analysed using IR and TGA after reaction.

The IR analyses suggested the formation of butyrate after reaction, since vibration wavenumbers around 1445, 1550, 1580, 2498 and 2960 cm^{-1} typical for carboxylic salts were found in the IR spectra. The complementary TGA studies also showed that the thermal decompositions of the reagent powders before and after reaction were very different, and therefore, a significant change in the structure and composition of the powders occurred as consequence of the reaction. For example, as shown in Figure 4-7

and 4-8, the commercial precipitate $CaCO_3$ (2) analyzed before and after reaction using the same temperature program lost around 2 % and 44 % of its mass when the temperature reach 500 °C, respectively.

In order to establish if the thermal decomposition of the powders after reaction correspond to the thermal decomposition of butyrate, pure lithium butyrate and Li_2CO_3 after reaction were analyzed using TGA and the same temperature program. Figures 4-5 and 4-6 exhibited a very similar behaviour between these two compounds; both samples lost around 55 % of their mass when the temperature reached 500 °C and the decomposition temperatures were 482.3 °C and 479.4 °C for the lithium butyrate and the lithium carbonate after reaction, respectively. Based on these results, it can be argued that butyric acid and the carbonates and oxide studied react to form butyrate.

5.2.4. Relative Reactivity of the Metal Carboxylic Salts

The difference between the mass loss calculated from the TGA analyses performed on the different reagent powders after reaction, and the theoretical mass loss for Li_2CO_3, the two commercial $CaCO_3$ and $BaCO_3$ were –5.31 %, -13.60 %, -15.53 %, and -15.60 %, respectively (Equation 4-2 and Table 4-10). These differences can be explained by considering that these reagent powders did not react *completely* to form the butyrate. However, the calculated difference for the MgO is +8.75 %, a positive number, which is an indication that the carbonate resulting from the thermal decomposition of the magnesium butyrate subsequently decomposed to generate magnesium oxide, which is consistent with the low thermal stability found for magnesium carbonate earlier in this study (Table 4-5). These differences could be due to an incomplete contact between the entire powder and the butyric acid inside the batch reactor.

The decomposition temperatures of each reagent powder after reaction in the batch reactor were determined from the graphs *dTG/dt* vs time shown in Figure 4-10. The decomposition temperatures of the butyrate formed from the prepared Li_2CO_3, the commercial $CaCO_3$ (1) and (2) and the prepared $BaCO_3$ were 479.4 °C, 462.0 °C, 455.1 °C, and 474.9 °C, respectively. The MgO analysed after reaction exhibited two different decomposition temperatures, 325.8 °C and 445.6 °C, which are thought to correspond to

the decomposition of butyrate to carbonate and the decomposition of carbonate to oxide respectively.

Based on the results obtained from the TGA and IR analyses performed on the reagent powders following batch reactions, the decrease of butyric acid reported in Table 4-6 and Figure 4-3 for the experiments carried out in the continuous flow reactor system can be attributed to the formation of butyrate between the butyric acid and the carbonate or oxide tested. In order to form the butyrate, the carbonate or oxide has to interact with the butyric acid; therefore, the more stable the carbonate or oxide is, the more difficult to form the butyrate should be. The oxides are expected to be more stable than the carbonates, and this is evidenced by the fact that the carbonates decompose to oxides at high temperatures. On the other hand, carbonates have different thermal stability depending on the cation contained in the carbonate. For example, for carbonates containing a cation within the same group in the periodic table, the heavier the cation, the more stable the carbonate is expected to be because a larger cation has less attraction strength towards electrons than a smaller cation. Therefore, a small cation will interact more strongly than a big cation with the electrons of the carbonate, destabilizing the bonds and favouring the decomposition to the metal oxide and CO_2.

Mg, Ca and Ba carbonates contain cations belonging to group IIA (the alkaline earth metal group). Because of the location of these cations on the periodic table, the trend in stability of these carbonates is expected to be: $BaCO_3 > CaCO_3 > MgCO_3$, which is in agreement with the TGA experiments performed on these reagent powders, as shown in section 4.1.4. Lithium carbonate contains a cation of group IA (the alkaline metal group). Carbonates with cations of group IA are expected to be more stable than carbonates with cations of group IIA, as long as the cations are located in the same period because the atomic radius of the group IIA cation should be smaller than the atomic radius of the group IA cation, and therefore group IIA cation should attract electrons more strongly than group IA and an analyses similar to what was explained previously would apply. Lithium carbonate is expected to be very stable and this is confirmed by the TGA analysis performed on Li_2CO_3, as shown in Section 4.1.4, which established a thermal stability for this carbonate comparable to that for $BaCO_3$.

94

Pestman et al. (1997) mentioned that basic oxides with low lattice energy are more likely to react with the carboxylic acid to form the carboxylic salt. If the lattice energy for inorganic compounds is understood as analogous to the bond energy for organic compounds, the higher the lattice energy, the more stable the compound will be. Therefore, according to Pestman et al. (1997), basic oxides with a "low stability" will tend to form the carboxylic salts, and this agrees with what was shown previously. The authors considered the oxides of bismuth, lead, magnesium and manganese to have low lattice energy, while the oxides of alumina, zirconia, titania or vanadia were considered to have high lattice energy.

The disappearance of butyric acid over by the carbonates prepared by precipitation tested in the continuous flow reactor system were 42.5 % to 48.6 % for Li_2CO_3, 37.2 % for $MgCO_3$, 53.3 % for $CaCO_3$ and 22.6 % for $BaCO_3$ (Table 4-6). The trend in decrease of butyric acid was $CaCO_3 > Li_2CO_3 > MgCO_3 > BaCO_3$, which did not agree with the expected behaviour based on the stability of the carbonates. The expected trend in the decrease of butyric acid was $MgCO_3 > CaCO_3 > Li_2CO_3 > BaCO_3$, and this differs from the actual trend. This difference could be due to the low thermal stability of $MgCO_3$ at 385 °C, as shown by the TGA analysis performed on this carbonate. This indicates that this particular carbonate likely decomposes partially to oxide. Therefore, this reagent powder at the reaction temperature would be a mixture of magnesium carbonate/oxide, but mainly oxide, which is more stable than the pure carbonate.

Analogously, because oxides are generally more stable than carbonates, the percentages of decrease of butyric acid achieved by the oxides are expected to be lower than those achieved by the carbonates. This is observed for the calcium carbonate prepared by precipitation of salts and its corresponding oxide, which exhibited a decrease of butyric acid of 53.3 % and 34.5 %, respectively. In contrast, the calcium carbonate prepared by the thermal decomposition of acetate and its corresponding oxide showed a different behaviour. Both compounds exhibited similar percentage of decrease of butyric acid, 33.3 % and 33.9 % respectively. This could be due to the presence of organic carbon on the surface of the carbonate and the oxide, which obviously decreases the purity of the samples.

95

However, even though it was mentioned previously that the decrease of butyric acid reached by the $MgCO_3$ was low because this material may exist as a mixture of the carbonate and the oxide at the reaction temperature, the percentage of decrease of butyric acid obtained from the prepared magnesium oxide was 43.8 % and 46.0 % in contrast to 37.2 % for $MgCO_3$. This indicates that the stability of the carbonates and oxides is not sufficient to explain the extent of decrease of butyric acid in the continuous flow reactor experiments.

The basicity of the carbonates and oxides is another factor that should be considered in this analysis. The carboxylic acid is more likely to interact with a basic compound to form a salt. Therefore, if there is any water in the reactor and the reagent powder is an oxide, the oxide will form a hydroxide, which is a stronger base than the corresponding carbonate. This could explain why the magnesium oxide showed a higher percentage of decrease of butyric acid than the magnesium carbonate. Magnesium hydroxide should be a more basic compound than calcium hydroxide, which could also explain why the magnesium oxide exhibited a higher reduction of butyric acid than all the calcium oxides. It is important to consider that one of the main products in the decarboxylation reaction is water.

Because the formation of butyrate is proposed as a step in the reaction pathway, the decarboxylation reaction would not only occur on the surface of the reagent powder but also in the bulk. Consequently, mass transfer processes are of considerable importance in the overall reaction, and therefore, the morphology and distribution inside the reactor of the reagent powder play a very considerable role in the consumption of butyrate. For example, the difference in the decrease of butyric acid over the two commercial precipitated calcium carbonates, 33.1 % and 55.9% for PCC (1) and PCC (2) respectively, is an evidence of the mass transfer effect in the reduction of butyric acid since the compositions of these two carbonates are practically the same; 97 % $CaCO_3$, 2 % $MgCO_3$ and <0.1 % Fe_2O_3. The only significant differences between these are the morphology; PCC (1) is prismatic and PCC (2) is scalenohedral, the median particle size for PCC (1) is 0.7 μm and for PCC (2) is 1.9 μm (Appendix H).

The prismatic morphology seems to be more ordered and to have a lower surface area than the scalenohedral morphology, even though the median particle size of the

96

prismatic carbonate is lower than the median particle size of the scalenohedral carbonate (0.7 μm and 1.9 μm respectively). Based on this observation and the performance of the carbonates PCC (1) and PCC (2), the higher of the surface area of the carbonate, the higher the probability of interaction between the butyric acid and the carbonate to form the butyrate. This could also explain the differences between the performance of the two commercial precipitated calcium carbonates, and therefore, the rest of the reagent powders tested. A morphology offering a high surface area should favour the formation of butyrate as a result of the higher probability of interaction between the carbonate/oxide and the butyric acid.

5.3. – Reaction Products and Mechanism

On the other hand, the production of 4-heptanone and acetone in the continuous flow reactor system may be partly due to the thermal decomposition of the butyrate formed on the surface of the reagent powder. According to the TGA analyses performed on the two commercial precipitated $CaCO_3$, precipitated Li_2CO_3, $BaCO_3$ and MgO analysed after reaction in the batch reactor, the percentage of mass loss at 385 °C is 10.1 %, 2.0 %, 2.7 %, 1.7 % and 34.5 %, respectively. Despite the 10.1% mass loss for the commercial precipitated $CaCO_3$ (1), the mass losses of the calcium, lithium and barium butyrates are practically the same and, therefore, the tendency to form ketones is expected to be very similar. Based on this analysis, the production of ketones was expected to be low and it should not close the mass balance with the consumed butyric acid reported in Table 4-6 and Figure 4-3.

Once again, Mg showed a different performance from what was expected. Due to the high mass loss (34.5 %) exhibited by the magnesium butyrate at 385 °C, a high production of ketone would be expected but the moles of 4-heptanone and moles of acetone produced per 100 mol of butyric acid consumed were 20.9 and 7.3 for $MgCO_3$ and 3.0 – 16.7 and 6.3 – 7.2 for MgO, respectively. However, the proportion of butyrate/carbonate or oxide in the continuous flow reactor system should have been very low due to the low concentration of butyric acid flowing through the reactor and the duration of each experiment. Therefore, the mass transfer phenomenon should have also

97

played a very important function in the production of the ketones, and this should not be only related to the decomposition temperature of the butyrates.

In the continuous flow reactor experiments, as shown in Table 4-6 and Figure 4-4, the GC showed the presence of 4-heptanone as a product for some of the lithium, calcium and magnesium reagent powders. In contrast, the GC exhibited the existence of acetone as a product for all the reagent powders tested. This was confirmed by the GC analysis of the condensed effluent of the reactor (Section 3.5.1) performed by the Department of Chemistry of the University of Alberta. For the batch reactor experiments, as shown in Table 4-8 and 4-9, the products were some ketones, alkenes, carboxylic acids, CO_2 and H_2O, and 4-heptanone was detected as a product of every reagent powder analysed. It is important to consider that the space-time for the continuous flow reactor experiments was 2.7 seconds and the concentration of butyric acid was very low. In contrast, for the batch reactor experiments, the reaction time was 3 hours and the butyric acid added to the reactor was 99 % pure.

The reaction mechanism is not well established yet (Pestman et al. 1997) and it is not the purpose of this research to propose a reaction pathway, however, the difference in the products detected between batch and continuous flow reactor system may be due to differences in contact time. In the batch reactor experiments, because the reaction time was longer, 4-heptanone was able to react with other intermediates of the reaction to form heavier ketones, and these intermediates may have reacted with one another to form lighter ketones and alkenes. The production of acetone in the continuous flow reaction system, but not in the batch reactor system, is not clearly understood.

Figure 5-1 proposes the formation of butyrate as an intermediate in the formation of ketones by the decarboxylation reaction of butyric acid. In this representation, step D could explain the difference in the products detected in the batch reactor experiments and the continuous flow reactor experiments, since the reaction between the intermediates and 4-heptanone, and the intermediates themselves could demand a longer reaction time. On the other hand, the molecules produced of 4-heptanone and/or possible intermediates in the continuous flow reactor are constantly leaving the reactor, which reduce very significantly the chance of interaction between them at the reaction conditions.

98

A: Butyric acid approach to the oxide or carbonate

$C_4H_8O_2$

$C_4H_8O_2$

Oxide / Carbonate

B: Reaction between butyric acid and the oxide/carbonate to form butyrate

$C_4H_8O_2$ $C_4H_8O_2$

Oxide / Carbonate   Butyrate

C: Thermal decomposition of butyrate to CO_2, H_2O, $C_7H_{14}O$ and intermediates

$C_4H_8O_2$

$C_4H_8O_2$

CO_2 $C_7H_{14}O$

H_2O

Butyrate   Carbonate   Butyrate   I   I

D: Reaction between $C_7H_{14}O$ and intermediates to form alkenes and other ketones

$C_4H_8O_2$

Other ketones

CO_2 $C_7H_{14}O$ Alkenes

$C_4H_8O_2$ H_2O

Butyrate   Carbonate   Butyrate   I ⟷ I

I   Intermediates

Figure 5-1: Formation of butyrate as an intermediate in the formation of ketones from butyric acid.

99

According to the literature, carboxylic acids decomposed thermally to carbonate and the symmetrical ketones [Wiberg (1952), Hites et al. (1972) and Varma et al. (1997)]. On the other hand, because the experimental mass loss and the theoretical mass loss of the post reaction powders tested in the batch reactors at 385 °C (Table 4-10) are reasonable very similar, the production of 4-heptanone is thought to be due to the thermal decomposition of the butyrate.

Based on the results obtained from the continuous flow reactor experiments and the batch reactor experiments, the reaction between the butyric acid and the carbonate or oxide is a bulk reaction. If two mol of butyric acid and one mol of carbonate are required to form a mol of butyrate, then the amount of butyric acid consumed in the continuous flow reactor experiments is enough to achieve the conversion of around 20% of the carbonate into butyrate, which would not be possible if the reaction occurred just on the surface of the powder. Additionally, regarding the batch reactor experiments, based on the similarity between the theoretical and experimental mass loss of the post reaction powders shown in Table 4-10, the reaction between butyric acid and carbonate or oxide does not seem to be occurring just on the surface but in the whole bulk of the powder.

5.4. - Formation of Butyrate at Low Temperature

As mentioned in section 4.4, low temperature experiments were performed to establish the formation of butyrate at less severe conditions. It is important to notice that addition of water was required to achieve the formation of butyrate from CaO. Calcium oxide and water reacted to form calcium hydroxide, which is a strong base, favouring the interaction with the carboxylic acid.

Based on the TGA and IR analyses performed on the post-reaction powders, partial formation of butyrate was achieved by the precipitated calcium carbonates and the prepared calcium oxide.

TGA results showed in Table 4-12, indicate that the conversion to butyrate from $Ca(OH)_2$ or CaO was higher than the conversion achieved by the carbonates due to the higher basicity of calcium hydroxide over calcium carbonate.

100

5.5. - Implications for Commercial Processes to Remove Naphthenic Acids from Bitumen

Based on the results obtained from the low temperature experiments, and the behaviour exhibited by the reagent powders studied, two different commercial processes are suggested for further studies.

5.5.1. - Low Temperature Process Using CaCO₃/CaO

Due to the high rate of disappearance of butyric acid found when precipitated $CaCO_3$ was tested, the ability to form butyrate from CaO at low temperature and because $CaCO_3$ is inexpensive and very easy to obtain, the process shown in Figure 5-2 is proposed for future studies. In this process, acidic bitumen would flow through a fixed bed of $CaCO_3$/CaO at low temperature and the naphthenic acid contained in the bitumen would react with the carbonate/oxide to form carboxylic salts. However, because the bed reactor would be at low temperature, the carboxylic salts would not decomposed but eventually the bed would saturate and therefore, no more naphthenic acids could be removed. At this stage of the process, the flow of acidic bitumen would be directed to an identical second bed reactor to continue removing the naphthenic acids until this is saturated. In the meantime, a very hot inert gas flow would be directed to the first reactor in order to heat the carboxylic salts and bring about their thermal decomposition to ketones and $CaCO_3$, which would decompose to oxide due to the high temperature. Because the naphthenic acids contained in the bitumen are expected to be much heavier than butyric acid, the decomposition temperature of their carboxylic salts are expected to be higher than the decomposition temperature of the butyrate and therefore, based on the TGA analyses, the decomposition temperature of the heavy carboxylic salts could be high enough to decompose the carbonate into oxide, at least partially.

101
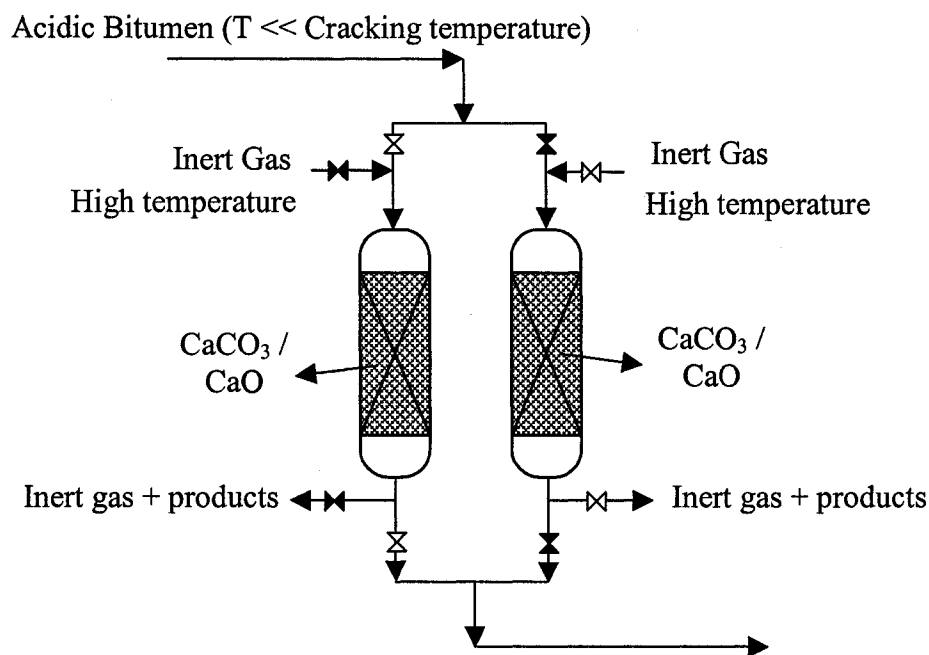
Figure 5-2: Proposed process for further studies in order to remove naphthenic acids from bitumen at low temperatures, using $CaCO_3/CaO$ as the reagent powder.

As mentioned in section 5.4, the formation of butyrate when CaO was tested at low temperature required the addition of water; therefore, the addition of water probably would be also necessary but it is important to consider that acidic bitumen could contain sufficient water obviating the need for specific addition. In this proposed process, the following aspects should be determined: the temperature required to form the carboxylic salts without decomposition, the ratio $CaCO_3$ - CaO to bitumen in order to remove satisfactorily the naphthenic acid content, the decomposition temperature of the carboxylic salts, the potential products, and how to place the carbonate/oxide in the reactor in order to maximize the physical contact between naphthenic acid and reagent powder, which would demand mass transfer limitation studies of the process.

5.5.2. - Process Schemes Using MgO

Because magnesium butyrate showed the lowest decomposition temperature between the butyrates, two options involving MgO are suggested in order to develop

102

further experiments. A process similar to that shown in Figure 5-2 could be considered, but in this case the temperature required to decompose the carboxylic salts would be much lower than the temperature required when $CaCO_3/CaO$ is used as the reagent powder.

On the other hand, since the decomposition temperature of the magnesium carboxylic salt would be much lower, the process shown in Figure 5-3 is proposed for consideration.
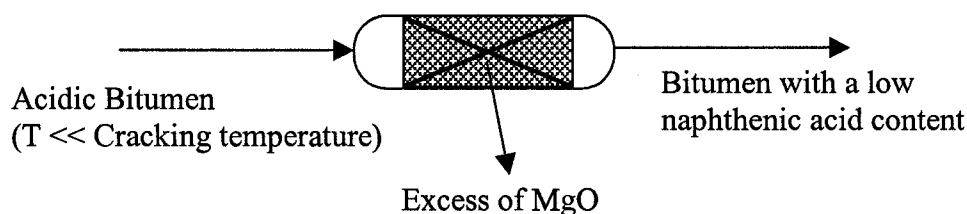
Figure 5-3: Proposed process for further studies in order to remove naphthenic acids from bitumen at low temperatures, using MgO as the reagent powder.

The temperature of this process would be high enough to partially decompose the magnesium carboxylic salt but low enough to prevent cracking of the bitumen. Then, if an excess of magnesium oxide were loaded into the reactor, while the carboxylic salt is constantly formed, a portion of this would be continuously decomposed to MgO, ketones and other products. In this case, variables such as ratio of MgO/acidic bitumen necessary to achieve satisfactorily the removal of naphthenic acid, temperature, and how to contact the bitumen with the MgO should be established.

CHAPTER 6

CONCLUSIONS AND RECOMMENDATIONS

6.1. – Conclusions

This work focused on the decarboxylation reaction of butyric acid using alkaline metal and alkaline earth metal carbonates and oxides such as Li, Mg, Ca and Ba in order to select the reagent powder with the best performance. Based on the results obtained, the following conclusions were drawn:

1. - $CaCO_3$ prepared by precipitation gave the highest rate of disappearance of butyric acid and the highest ratio of moles 4-heptanone produced to moles butyric acid consumed in the continuous flow reactor system.

2. - XPS, IR and TGA studies performed on the reagent powders before and after reaction, as well as GC-MS studies performed on the product mixtures collected, lead to the conclusion that the formation of butyrate due to the interaction between butyric acid and carbonate/oxide is an intermediate step in the decarboxylation reaction to produce ketones.

3. - Although the main products expected; 4-heptanone, CO_2 and H_2O were detected in both the continuous flow reactor and batch reactor systems, other products such as alkenes and lighter carboxylic acids were also identified in the batch reactor alone. The generation of other products in addition to 4-heptanone, CO_2 and H_2O, is an indication that the decarboxylation reaction does not only involve the formation of butyrate and the thermal decomposition to 4-heptanone, but obviously side reaction presumably involving reactions between intermediate compounds occurred at these reaction conditions.

4. - Magnesium oxide analysed after reaction using TGA showed a peculiar behaviour, since it decomposed at a much lower temperature (326 °C) than the rest of the reagent powders analyzed after reaction, which decomposed at temperatures between 455 °C and 479 °C.

5. - Li_2CO_3 and $CaCO_3$ prepared by precipitation exhibited a higher rate of disappearance of butyric acid than those prepared by thermal decomposition of acetates. Li_2CO_3 prepared by precipitation and prepared by thermal decomposition of oxalate showed similar rates of consumption of butyric acid

6. – As a result of the XPS studies, it was concluded the carbonates prepared by thermal decomposition of acetates contained organic carbon on their surface. On the other hand, IR analysis showed evidence of remaining acetate in the Li_2CO_3 prepared by thermal decomposition of acetate.

7. - Based on the TGA analyses, the trend in thermal stability of the precipitated carbonates was $BaCO_3 > Li_2CO_3 > CaCO_3 > MgCO_3$.

8. - IR and TGA studies also showed partial formation of butyrate from mixing $Ca(OH)_2$ or CaO with liquid butyric acid at room temperature, and a lower extent of conversion to butyrate is achieved when $CaCO_3$ is used.

.

6.2. – Recommendations

Based on the expertise gained in the progress of this work, the following recommendations are suggested for further studies:

1. – Due to the high rate of disappearance of butyric acid showed by precipitated $CaCO_3$, the formation of butyrate found when CaO was used at low temperature and the low cost of $CaCO_3$, the study of low temperature processes using $CaCO_3/CaO$ is strongly recommended. Parameter such as temperature formation and temperature decomposition of the calcium carboxylic salts, ratio $CaCO_3$ - CaO to bitumen required to reduce satisfactorily the naphthenic acid content and products obtained should be defined. In addition, experiments regarding how to expose the carbonate/oxide to the naphthenic acids contained in the bitumen would be also required to optimize their physical contact, which would demand mass transfer limitation studies of the process.

2. – Because MgO after reaction decomposed at a much lower temperature compared to the other post-reaction reagent powders (section 6.1), the use this oxide is also recommended for future studies. Potential commercial processes involving MgO as

shown in section 5.5.2 would require the study of parameters such as MgO/acidic bitumen necessary to accomplish the desired level of removal of naphthenic acid, formation temperature and decomposition temperature of the magnesium carboxylic salt, as well as the method required to achieve the optimal physical contact between the bitumen and the MgO, which would demand mass transfer limitations studies of the process.

3. – Because the potential commercial processes suggested involve the use of a continuous flow reactor, the use of a this type of reactor is recommended in order to establish the optimal physical contact between reagent powder and bitumen. A continuous flow reactor system is also desired to quantify the products obtained, as long as the analytical instruments to identified and quantify the products are available.

4. – Phenomena such as solubility of the reagent powder and solubility of the formed carboxylic salt in the bitumen should be also considered in the study of potential commercial processes to remove naphthenic acid from bitumen.

5. – The use of a batch reactor system is recommended in order to define the formation temperature and the decomposition temperature of the metal carboxylic salt generated from the acidic bitumen.

REFERENCES

Afzal, M.; Ahmad, H.; Mahmood, F. Decomposition kinetics of metal acetates. *Journal of the Chemical Society of Pakistan.* **1991**, *13 No 4*, pp 219 – 222.

Alpert, N. L.; Keiser, W. E.; Szymanski, H. A. *IR theory and practice of infrared spectroscopy.* 2nd edition. Plenum Press, New York, 1970; p 286.

Ambrose, D. Gas Chromatography. The Butterworth Group. 2nd edition, England, 1971; pp 2 – 3.

Archibald, E. H. *The preparation of pure inorganic substances.* John Wiley & Sons, Inc, New York, 1932; pp 35-36

Babaian-Kibala, E. Phosphate Ester Inhibitors Solve Naphthenic Acid Corrosion Problems. *Oil & Gas Journal,* **1994**, pp 31 – 35.

Blum, S. C.; Sartori, G.; Savage, D. W.; Gorbaty, M. L.; Ballinger, B. H.; Anderson, M. P.; Ramanarayanan, T. A.; Martella, D. J. Process for decreasing the acid content and corrosivity of crudes. *United States patent No 6679987,* **2004**, Patented January 20th.

Celis, K.; Van Driessche, I.; Mouton, R.; Vanhoyland, G.; Hoste, S. Kinetics of consecutive reactions in the solid state: Thermal decomposition of oxalates. *Measurement Science Review.* **2001**, *1 No 1*, pp 177 – 180.

Choudhary, V. R.; Pataskar, S. G.; Gunjikar, V. G.; Zope, G. B. Influence of preparation conditions of basic magnesium carbonate on its thermal analysis. *Thermochimica acta.* **1994**, *232*, pp 95 – 110.

Curtis, R. G.; Dobson, A. G.; Hatt, H. H. The ketonization of higher fatty acids with some observations on the mechanism of the reaction Part I.   Studies of waxes. *Journal of the Society of Chemical Industry London*, **1947**, *66 (11)*, pp 402 - 406.

Dollimore, D.; Tinsley, D. The thermal decomposition of oxalates. Part XII. The thermal decomposition of lithium oxalate. *Journal of the Chemical Society A – Inorganic Physical Theoretical.* **1971**, *19*, pp 3043 – 3047.

Glinski, M.; Kijenski, J.; Jakubowski, A. Ketones from monocarboxylic acids: catalytic ketonization over oxide systems.   *Applied catalysis A: General.* **1995**, *128*, pp 209 – 217.

Gunzler, H.; Gremlich, H.   *IR Spectroscopy. An Introduction.*   Wiley-VCH, Germany, 2002; p 53.

Handbook of preparative inorganic chemistry. 2nd edition. Academic Press Inc (London) Ltd, London, 1963; Vol 1, pp 911, 931, 933, 987.

Hatakeyama, T.; Quinn, F. X. *Thermal Analysis. Fundamentals and Applications to Polymer Science.* John Wiley & Sons, 2nd edition, England, 1999.

Hites, R. A.; Biemann, K. On the mechanism of ketonic decarboxylation. Pyrolysis of calcium decanoate. *Journal of the american chemical society.* **1972**, *94 No 16*, pp 5772 – 5777.

Laredo, G. C.; Lopez, C. R.; Alvarez, R. E.; Castillo, J. J.; Cano, J. L. Identification of Naphthenic Acids and other Corrositivity-Related Characteristics in Crude Oil and Vacuum Gas Oils from a Mexican Refinery. *Energy & Fuels*, **2004**, *18*, pp 1687 – 1694.

108

Leung, A.; David, G. B. B.; Konar, S. K. Pathway for the catalytic conversion of carboxylic acids to hydrocarbons over activated alumina. *Energy & Fuels*. **1995**, *9*, pp 913 – 920.

Machinaga, O; Kasai, J. Shape and properties of calcium carbonate obtained by thermal decomposition of calcium acetate. *Journal of the Ceramic Society of Japan*. **1989**, *97 No. 6*, pp 669-672.

Miller, A. L.; Cook, N. C.; Whitmore, F. C. The ketonic decarboxylation reaction: the ketonic decarboxylation of trimethylacetic acid and isobutyric acid. *J. Am. Chem. Soc.* **1950**, *72*, pp 2732 – 2735.

Moser, F. R. Process for removing naphthenic acids from hydrocarbon oils.   . *United States patent No 2186425*, **1940**, Patented January 9th.

Niemantsverdriet, J. W. *Spectroscopy in Catalysis. An Introduction.* VCH Publishers, New York, 1995; pp 39 – 45.

Patai, Saul. *The chemistry of the carbonyl group.   The chemistry of functional groups.* Interscience publishers. 1966.

Patnaik, P. *Handbook of inorganic chemistry.* McGraw-Hill. 2003; pp 82 – 83, 89 – 90, 159 - 160, 170 – 172, 497 – 498, 507 – 508, 518 – 520, 529 - 531.

Pestman, R.; Koster, R. M.; Duijne, A.; Pieterse, J. A. Z; Ponec, V. Reactions of carboxylic acids on oxides. Bimolecular reaction of aliphatic acids to ketones. *Journal of Catalysis*. **1997**, *168*, pp 265 – 272.

Piehi, R. L. Naphthenic acid corrosion in crude distillation units. *Materials Performance.* **1988**, *27*, pp 37 – 43.

Renz, M. Ketonization of carboxylic acids by decarboxylation: mechanism and scope. *Eur. J. Org. Chem.* **2005**, pp 979–988.

Richards, T. W; Honigschmid, O. A revision of the atomic weight of calcium. I. Analysis of calcium bromide. *J. Amer. Chem. Soc.* **1910**, *32*, pp 1577 – 1590.

Sartori; G.; Savage, D. W.; Gorbaty, M. L.; Ballinger, B. H.; Blum, S. C.; Anderson, M. P.; Ramanarayanan, T. A.; Martella, D. J. Process for decreasing the acid content and corrosivity of crudes. *United States patent No 6022494*, **2000**, Patented February 8th.

Siskin, M.; Manalastas, P. V.; Sartori, G. Process for treatment of naphthenic acids. *United States patent No 6767452*, **2004**, Patented July 27th.

Siskin, M.; Manalastas, P. V.; Sartori, G. Process for treatment of petroleum acids (LAW824). *United States patent No 6190541*, **2001**, Patented February 20th.

Slavcheva, E.; Shone, B.; Turnbull, A. Review of Naphthenic Acid Corrosion in Oil Refining. *British Corrosion Journal*, **1999**, *34 No 2*, pp 125 – 131.

Sugiyama, S.; Sato, K.; Yamasaki, S.; Kawashiro, K. Ketones from carboxylic acids over supported magnesium oxide and related catalysts. *Catalysis Letters*. **1992**, *14*, pp 127 – 133.

Supniewski, J. *Practical inorganic chemistry*. PWN Publishers, Warsaw, 1958; pp 382 – 383.

Tseng-Pu, F. Characterization of Naphthenic Acids in Petroleum by Fast Atom Bombardment Mass Spectroscopy. *Energy & Fuels*. **1991**, *5*, pp 371 – 375.

Valor, A.; Reguera, E.; Sanchez-Sinencio, F. Technical Articles – Synthesis and X-Ray Diffraction Study of Calcium Salts of Some Carboxylic Acids. *Powder Diffraction.* **2002**, *17 No 1*, pp 13 – 20.

Varadaraj, R.; Pugel, T. M.; Savage, D. W. Removal of naphthenic acids in crude oils and distillates. *United States patent No 6096196*, **2000**, Patented August 1st.

Varadaraj, R. Removal of acids from oil. *United States patent No 6454936*, **2002**, Patented September 24th.

Varma, R. P.; Singh, H.; Sharma, R. K.; Goel, H. Characterisation and thermal decomposition of zirconium (IV) soaps. *Tenside surfactants detergents: journal for theory, technology and application of surfactants.* **1997**, *34 No 3*, pp 195 – 198.

Wiberg, K. B. The thermal decomposition of deuterated barium butyrate. *Journal of the American Chemical Society.* **1952**, *74 No 17*, pp 4381 – 4382.

Zhang, A.; Ma, Q.; Tang, Y. Catalytic decarboxylation for naphthenic acid removal from crude oil. A theoretical and experimental study. *Division of petroleum chemistry of the american chemical society.* **2004**, *49 No 2*, pp 218 – 221.

Zhang, A.; Ma, Q.; Wang, K.; Liu, X.; Shuler, P.; Tang, Y. Naphthenic acid removal from crude oil through catalytic decarboxylation on magnesium oxide. *Applied Catalysis A: General,* **2006**, *303*, pp 103 – 109.

Websites:

Chromatography. Introductory Theory.
http://www.shu.ac.uk/schools/sci/chem/tutorials/chrom/chrom1.htm
(Accessed on May 31st 2006).

111

Infra – red absorption spectroscopy. Theoretical principles.

http://www.shu.ac.uk/schools/sci/chem/tutorials/molspec/irspec1.htm

(Accessed on May 19th 2006).

Introduction to Fourier transform infrared spectroscopy. Thermo Nicolet

Corporation.   http://mmrc.caltech.edu/mmrc_html/FTIR/FTIRintro.pdf

(Accessed on May 19th 2006).

Mass Spectrometry.   http://www.asms.org/whatisms/p4.html

(Accessed on May 31st 2006).

Naphthenic Acid Corrosion Mechanisms.

http://www.setlaboratories.com/naphthenic.htm

(Accessed on June 14th 2006).

XPS Database. http://lasurface.com (Accessed on June 26th 2006).

XPS Database. http://srdata.nist.gov/xps/ (Accessed on June 26th 2006).

Supplementary of Experimental Details

A.1. – Preparation of Carbonates / Oxides

Table A.1-1: Preparation of Li, Ca, Ca/Li carbonates from acetate

Sample	Mass of Ca Acetate (g)	Mass of Li Acetate (g)	Mass after heating (g)	Change of colour
Li_2CO_3	-----	4.8225	4.7955	From white to grey
$CaCO_3$	5.8177	-----	5.8014	From white to grey
Ca/Li_2CO_3	5.7782	0.1240	5.9143	From white to grey

Table A.1-2: Preparation of lithium carbonate from lithium oxalate (500 °C for 2 hours)

Sample	Mass of lithium oxalate (g)	Mass after heating (g)	Change of color
Li_2CO_3	6.5138	4.7695	From white to black

Table A.1-3: Preparation of Li, Mg, Mg/Li, Ca, Ca/Li oxides from carbonates

Sample	Mass of Carbonate	Mass after heating	Change of color
$LiCO_3 ---> Li_2O$	4.7633	3.9304	From black to white
$MgCO_3 ---> MgO$	3.9291	3.4872	No
$Mg/Li_2CO_3 ---> Mg/Li_2O$	4.7665	4.2077	No
$CaCO_3 ---> CaO$	13.3516	7.4741	No
$CaCO_3$ (from acetate)	8.4855	3.3280	From grey to white
Ca/Li_2CO_3 (from acetate)	7.9197	2.6364	From grey to white

A.2. – Calibration Curves for the Gas Chromatograph

Figure A.2-1: Calibration curve for the butyric acid relating peak area registered by the GC and number of moles of butyric acid injected.

114
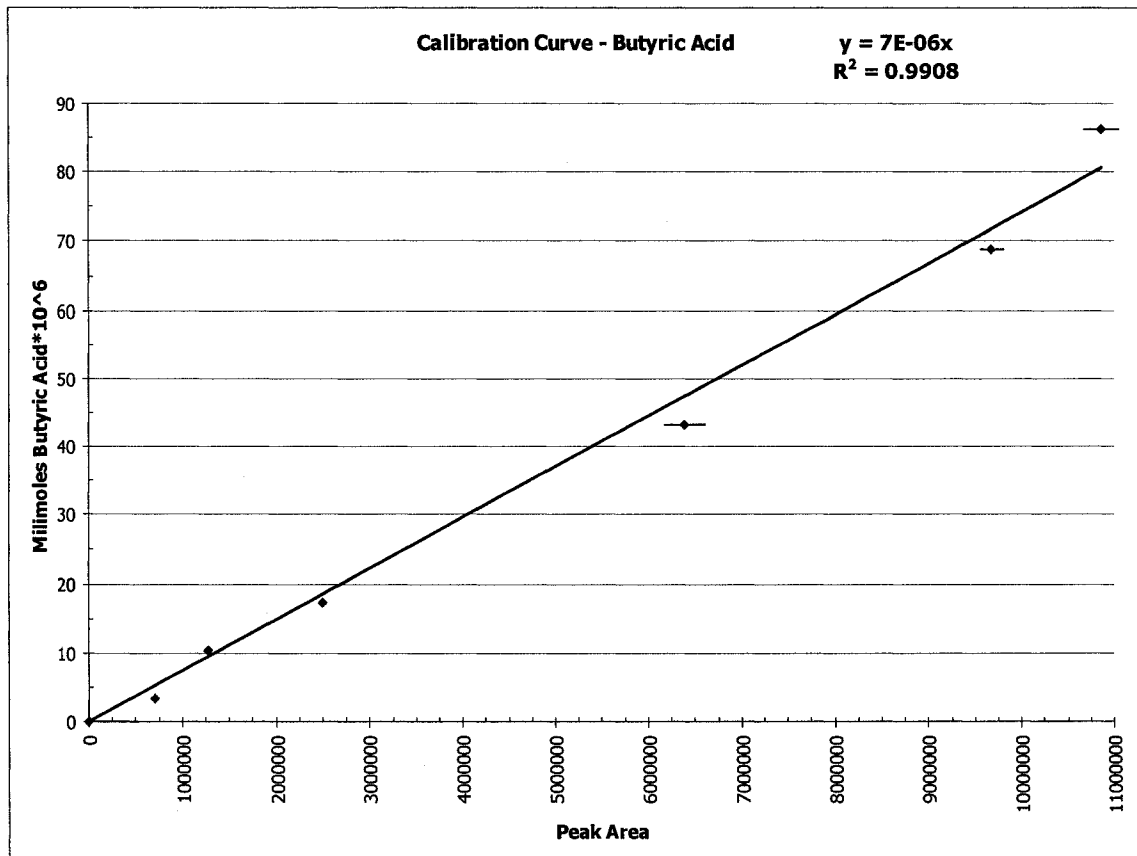
Figure A.2-2: Calibration curve for the 4-heptanone relating peak area registered for by the GC and number of moles of 4-heptanone injected.

Calibration Curve - Heptanone

$y = 5E\text{-}06x$
$R^2 = 0.9996$

115
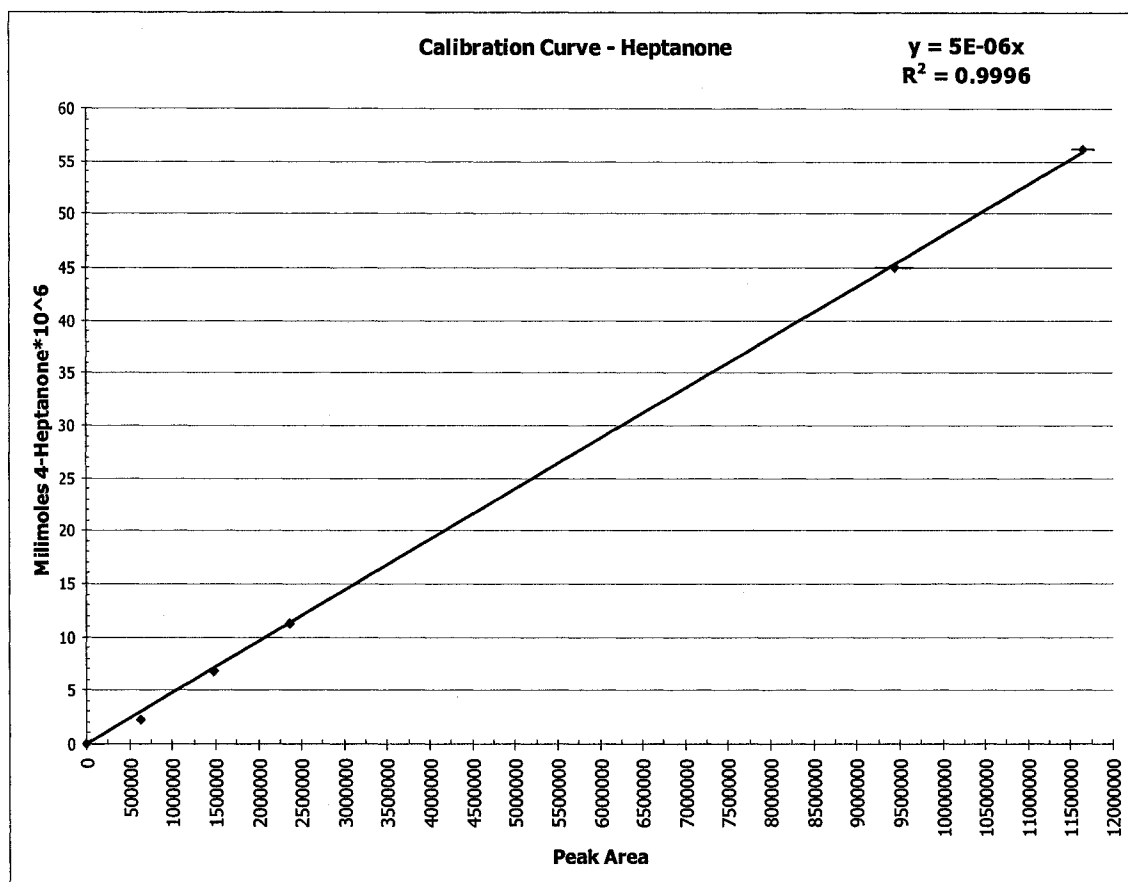
Figure A.2-3: Calibration curve for the acetone relating peak area registered for by the GC and number of moles of acetone injected.

116
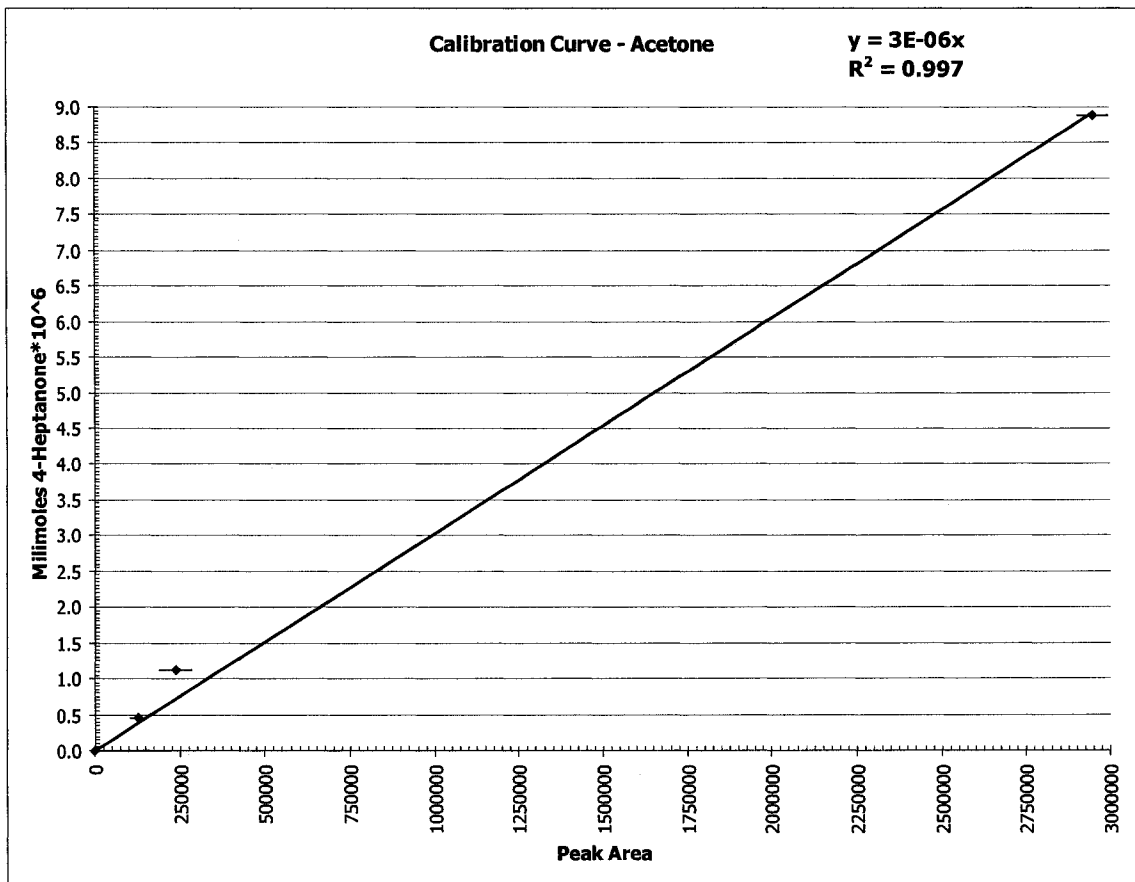
IR Spectra for the Prepared Carbonates and Oxides before Reaction

Figure B-1: IR spectrum for Li_2CO_3 prepared by precipitation
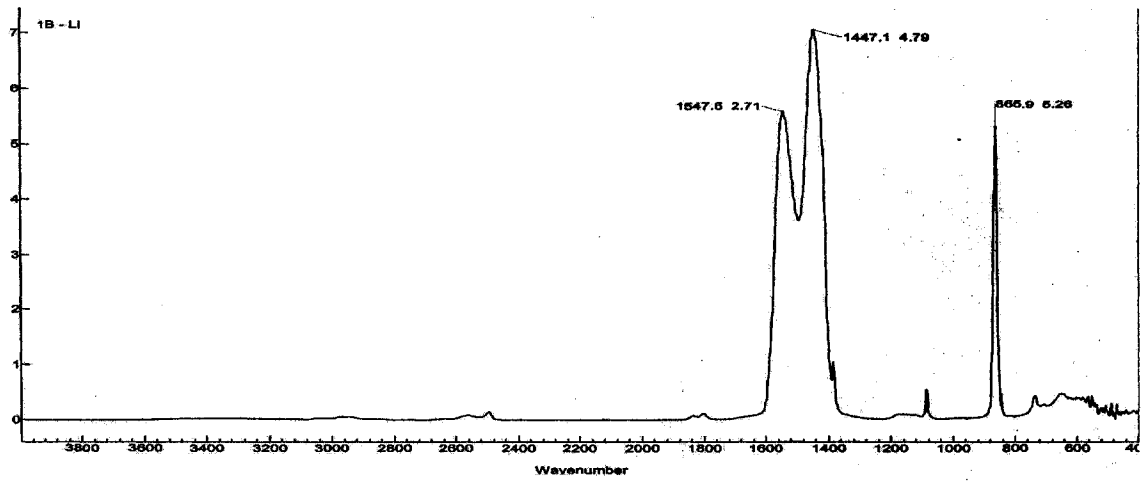
Figure B-2: IR spectrum for Li_2CO_3 prepared by thermal decomposition of acetate
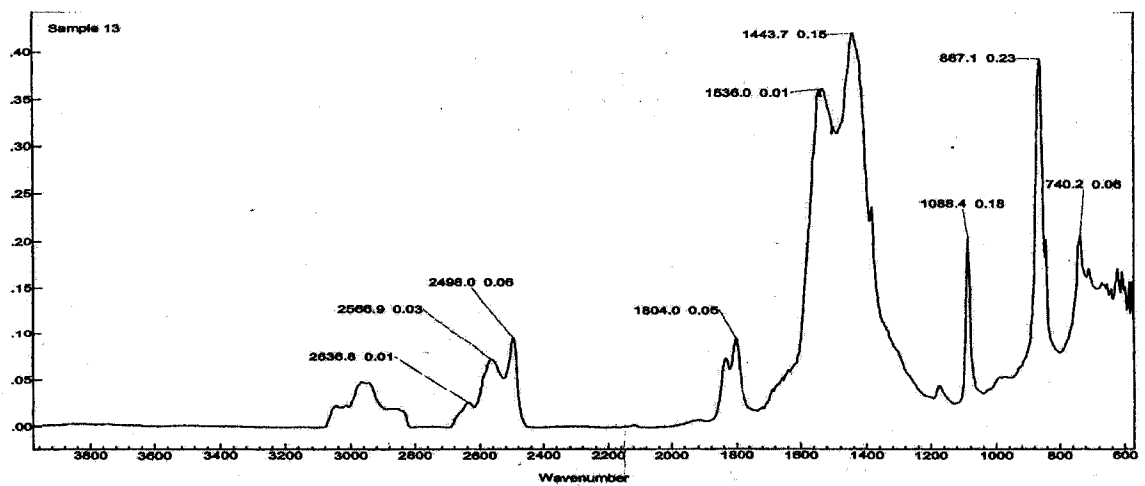
Figure B-3: IR spectrum for MgCO₃ prepared by precipitation
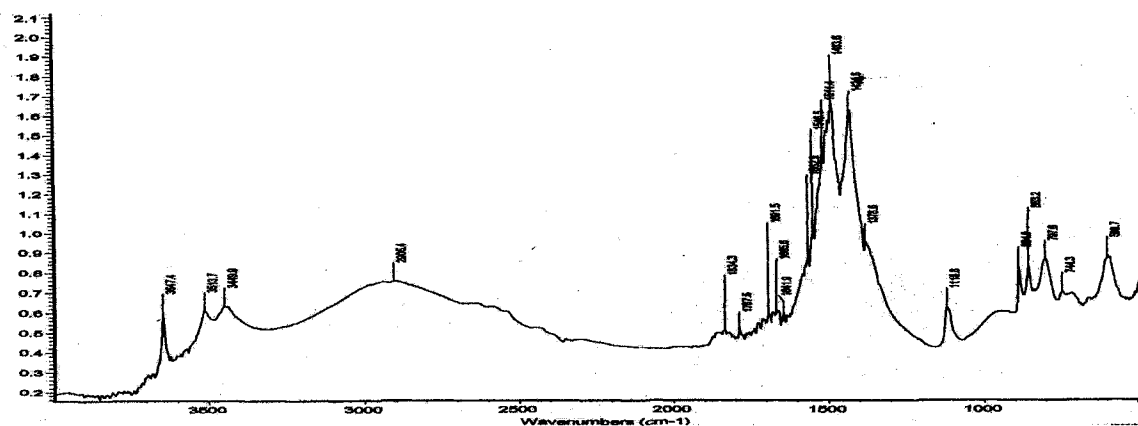
Figure B-4: IR spectrum for Mg/Li₂CO₃ prepared by precipitation
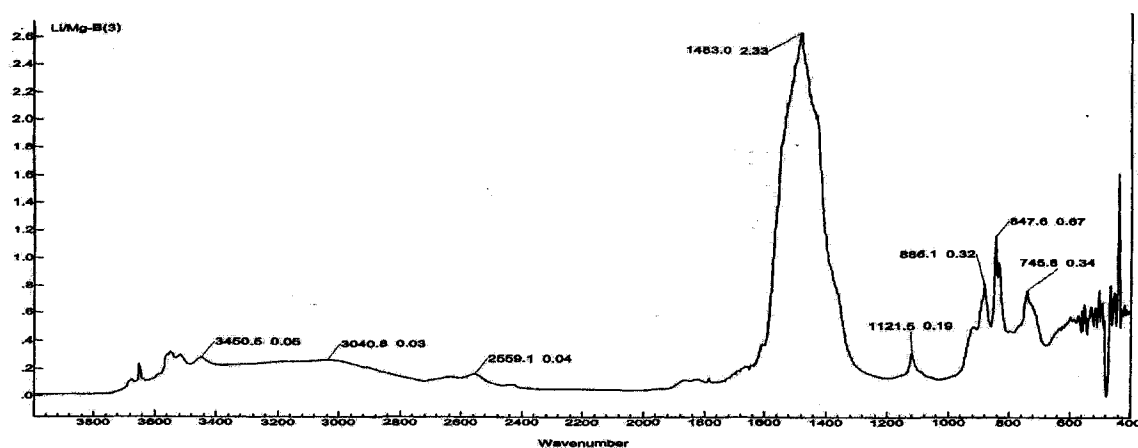
Figure B-5: IR spectrum for MgO

118
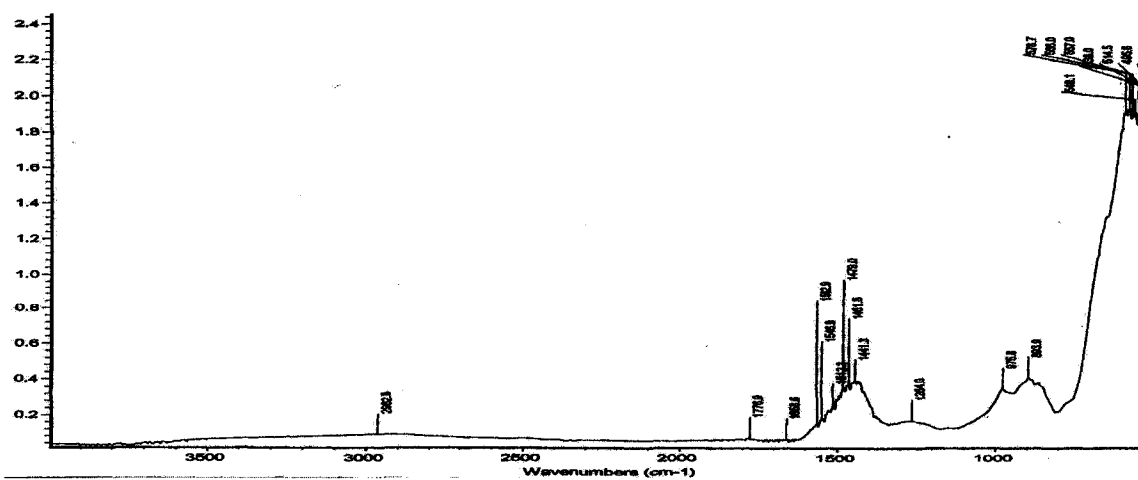
Figure B-6: IR spectrum for Mg/Li$_2$O
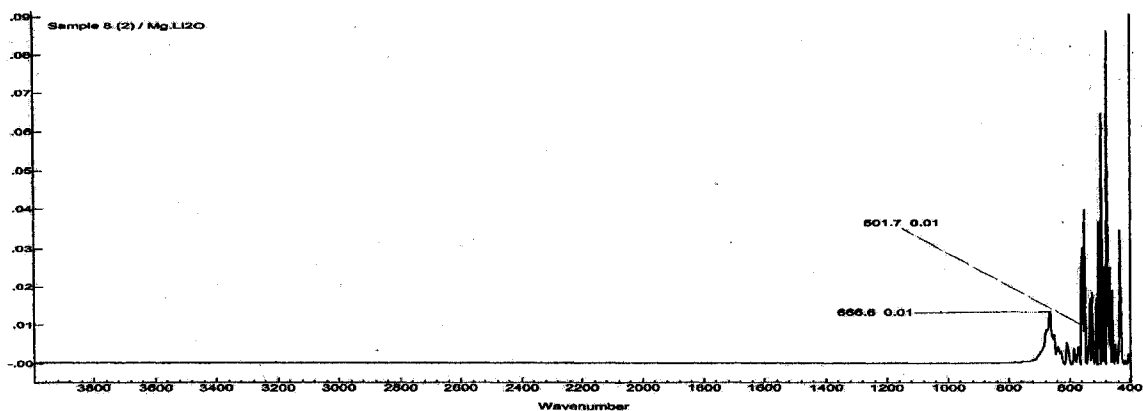
Figure B-7: IR spectrum for CaCO3 prepared by precipitation
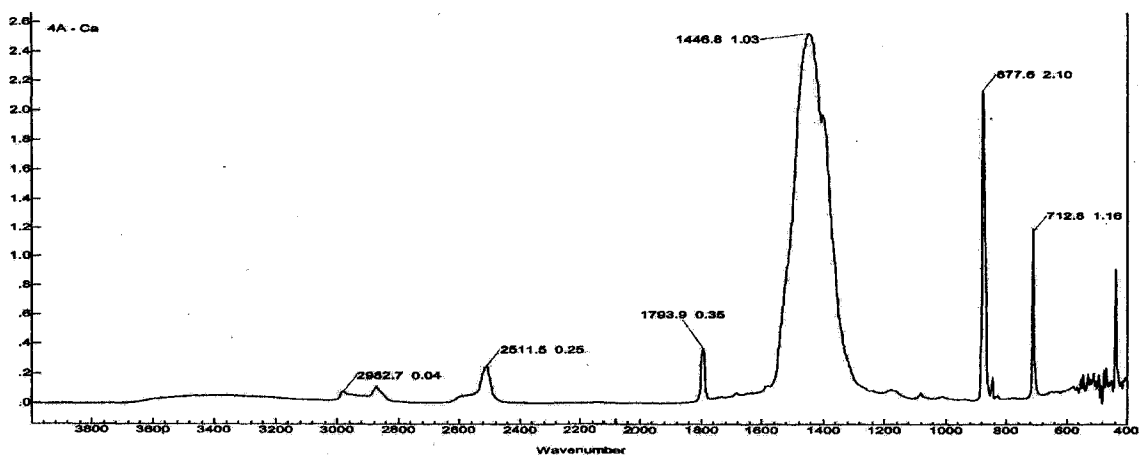
Figure B-8: IR spectrum for CaCO3 prepared by thermal decomposition of acetate

119
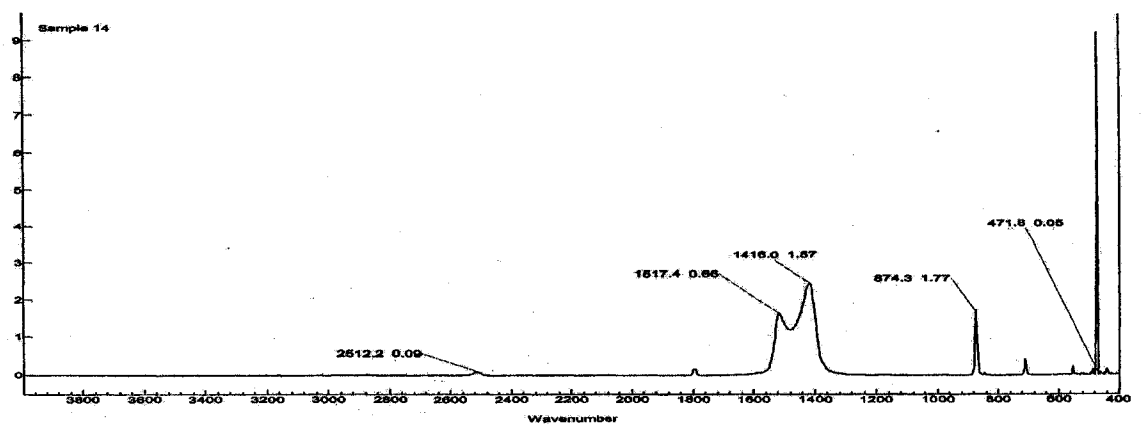
Figure B-9: IR spectrum for Ca/Li₂CO3 prepared by thermal decomposition of acetate
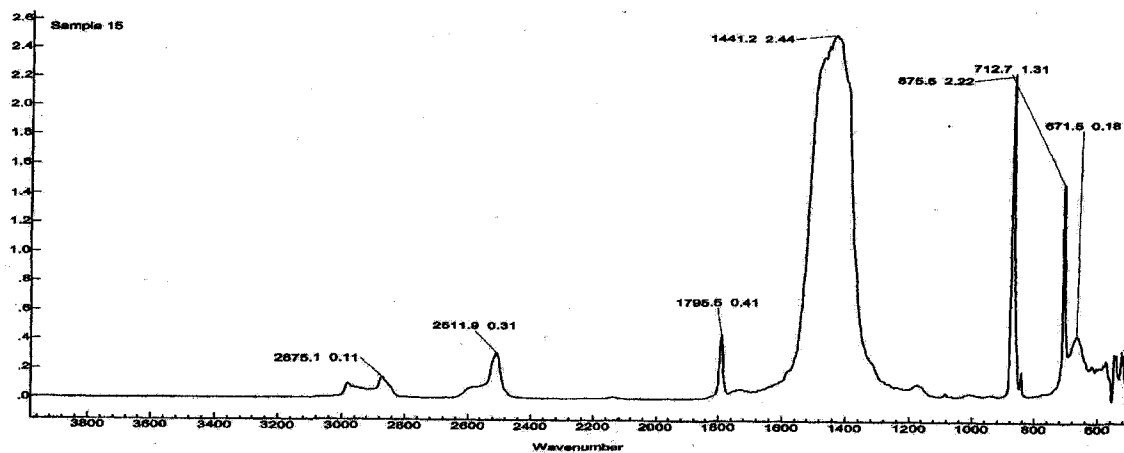
Figure B-10: IR spectrum for CaO from CaCO₃ prepared by precipitation
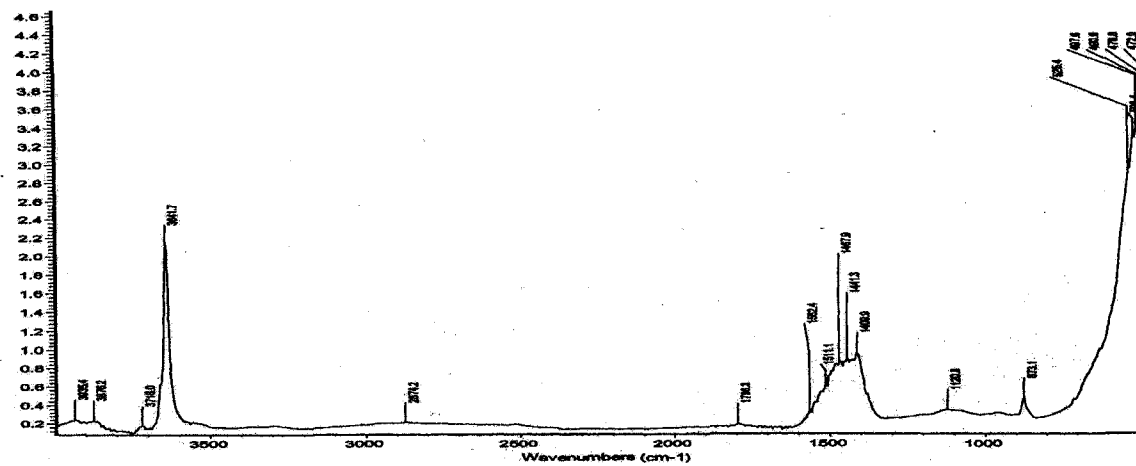
Figure B-11: IR spectrum for CaO from CaCO₃ prepared by thermal decomposition of acetate

120
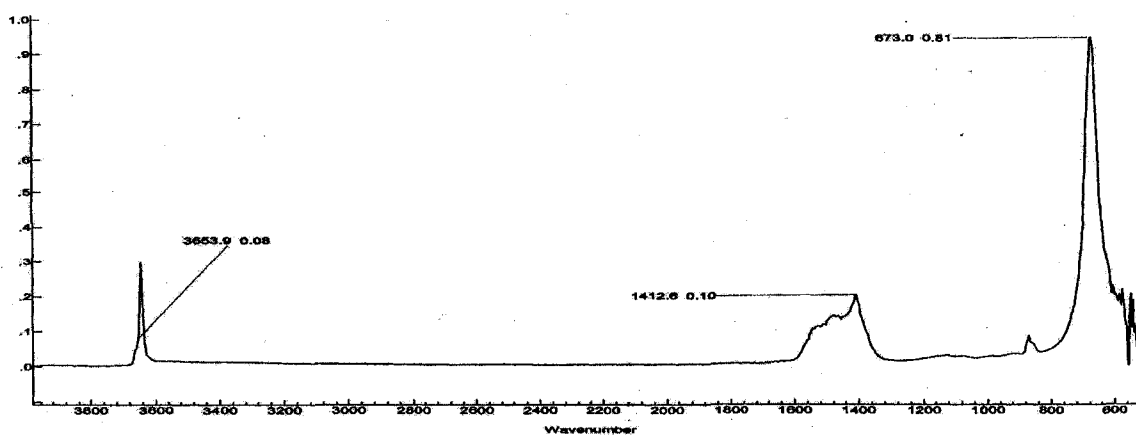
Figure B-12: IR spectrum for Ca/Li$_2$O from Ca/Li$_2$CO$_3$ prepared by thermal decomposition of acetate
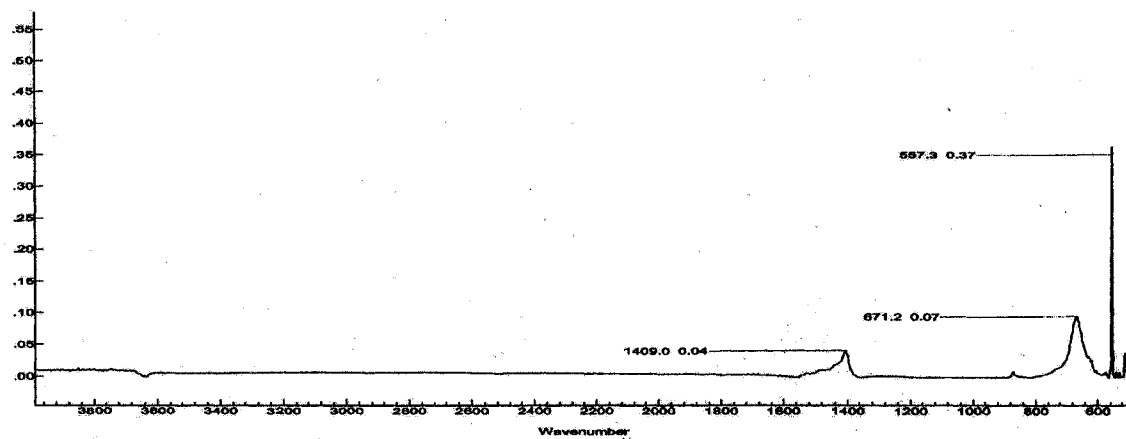
Figure B-13: IR spectrum for commercial precipitated CaCO$_3$ (2)
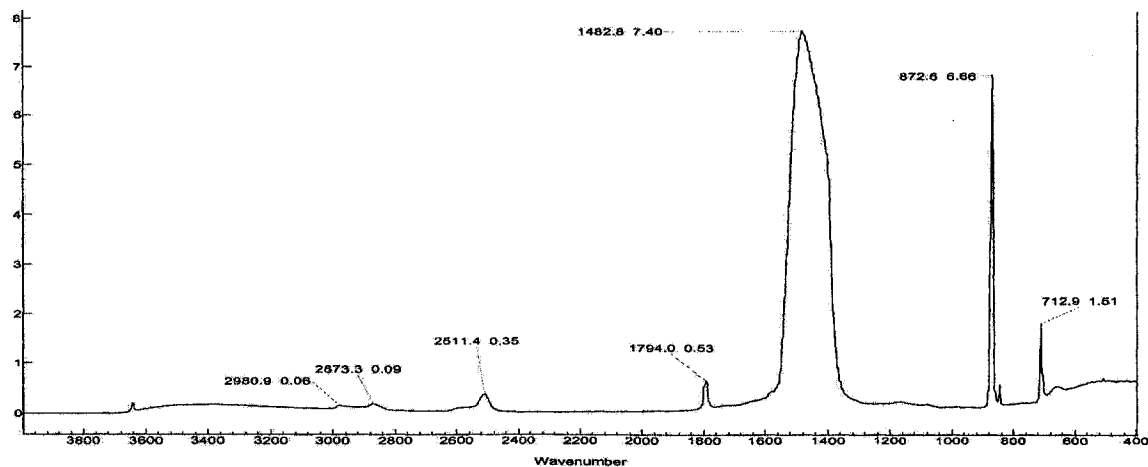
Figure B-14: IR spectrum for BaCO$_3$ prepared by precipitation

121
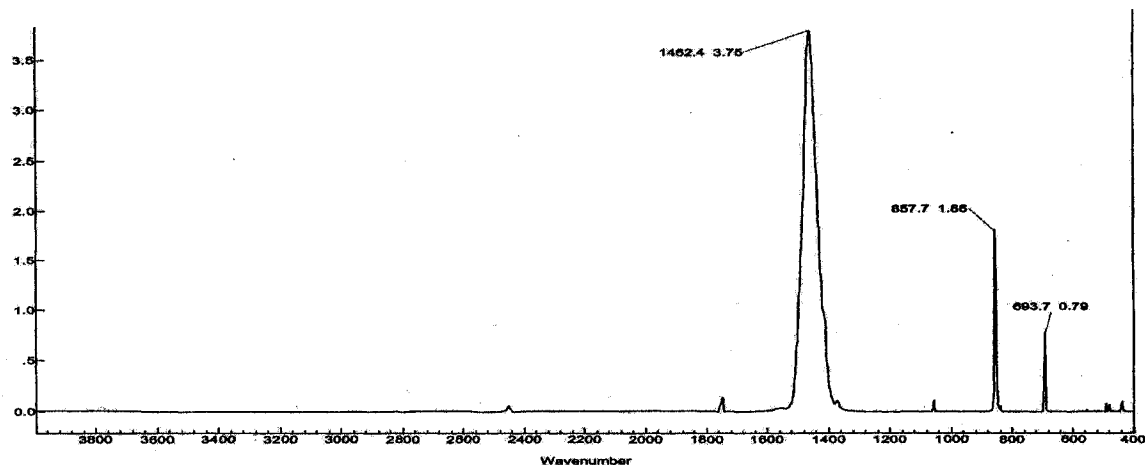
X-Ray Photoelectron Spectroscopy (XPS) Analyses

C.1. - XPS Studies for the Selected Carbonates and Oxides before Reaction

Figure C.1-1: A. - Wide scan for the $CaCO_3$ prepared by precipitation   B. – Narrow scan for the C 1s peak for the $CaCO_3$ prepared by precipitation

A

O 1s

Na 1s   Na KLL   Ca 2p

Ca 2s

C 1s

1100   1000   900   800   700   600   500   400   300   200   100   0

Binding Energy (eV)

B

CO_3

Adventitious
Carbon

292   291   290   289   288   287   286   285   284   283   282

Binding Energy (eV)

122
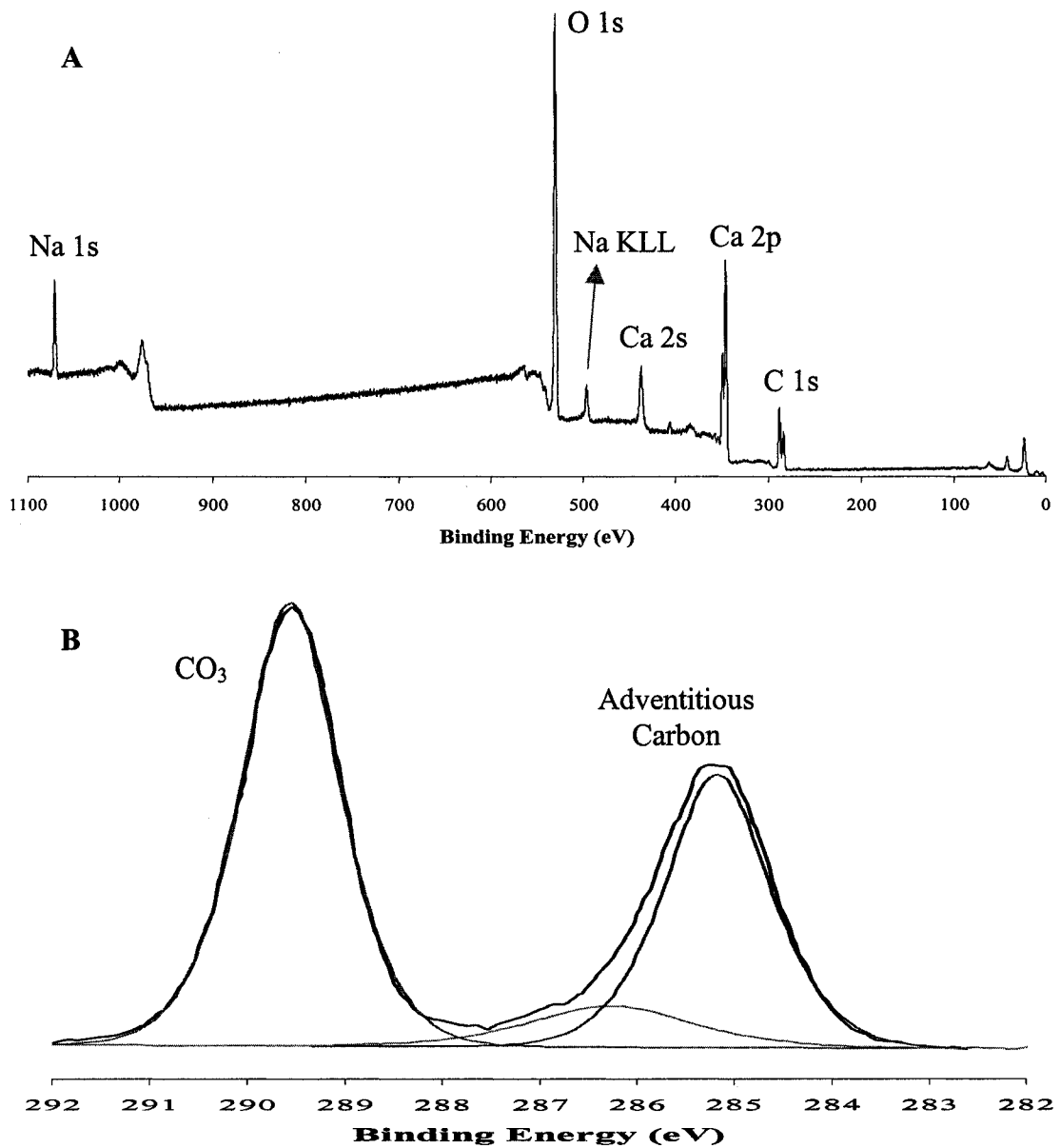
Figure C.1-2: A. - Wide scan for the Mg/Li$_2$O prepared by precipitation   B. – Narrow scan for the C 1s peak for the Mg/Li$_2$O prepared by precipitation
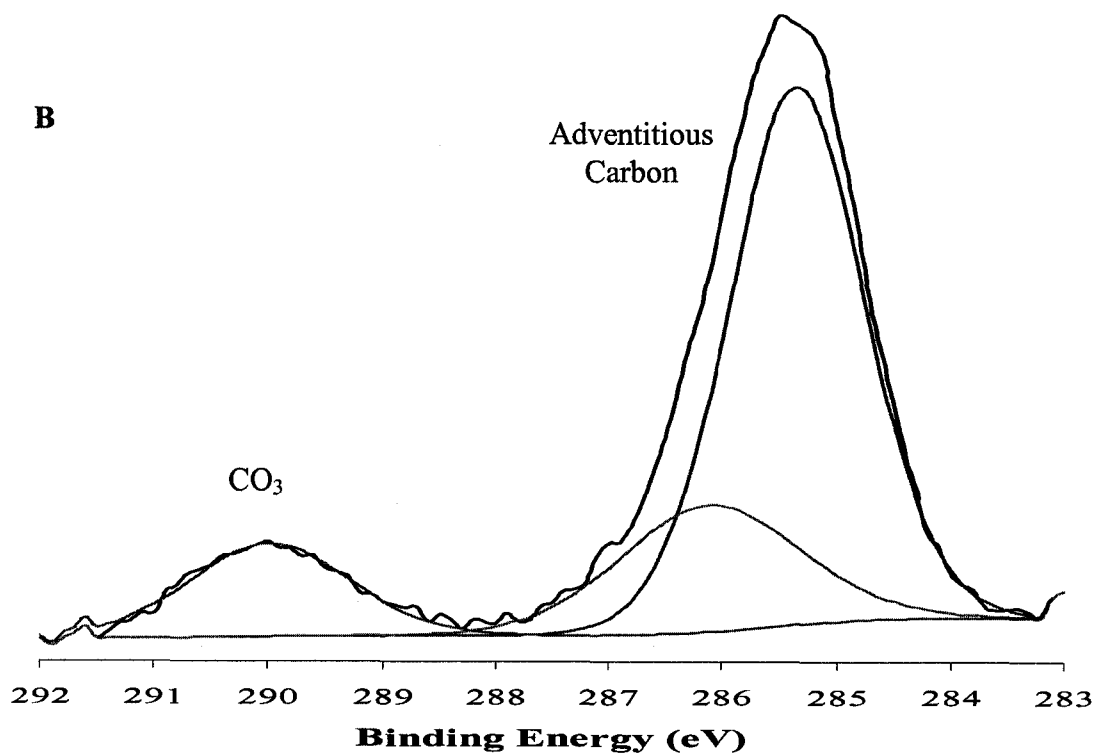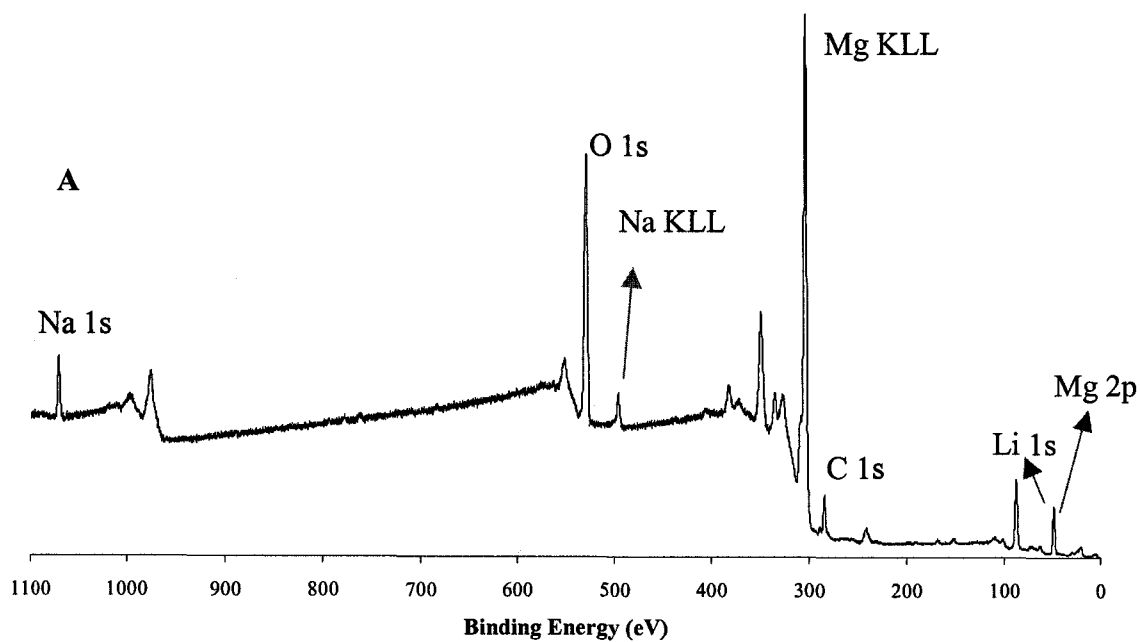
Figure C.1-3: A. - Wide scan for the Li_2CO_3 prepared by thermal decomposition of acetate   B. – Narrow scan for the C 1s peak for the Li_2CO_3 prepared from acetate

124
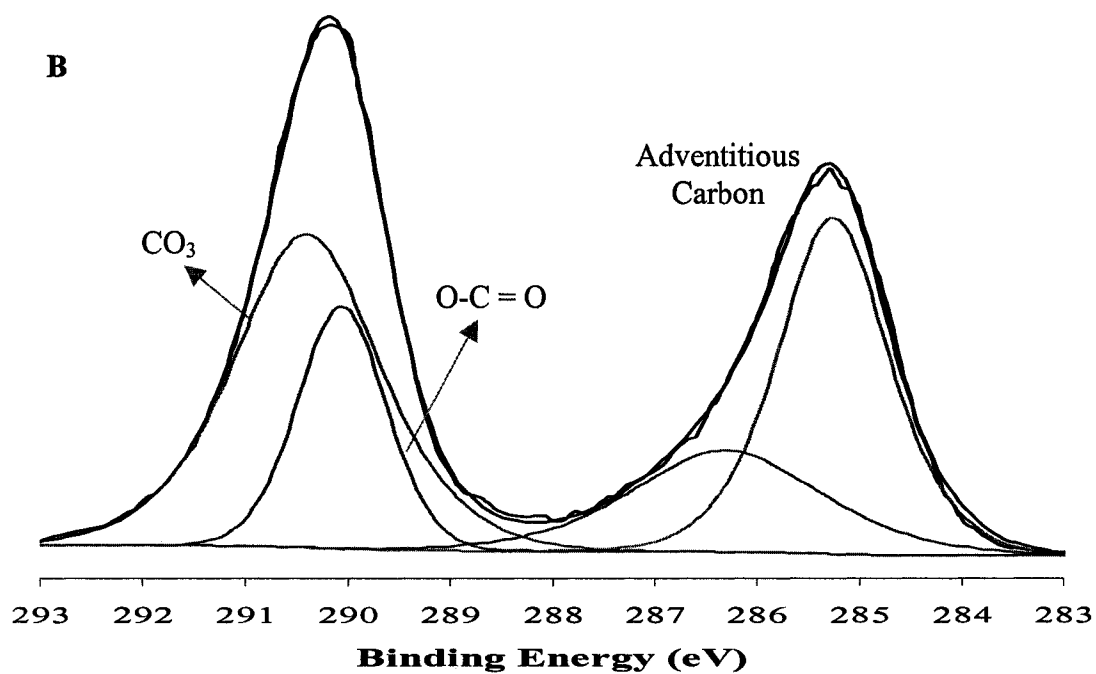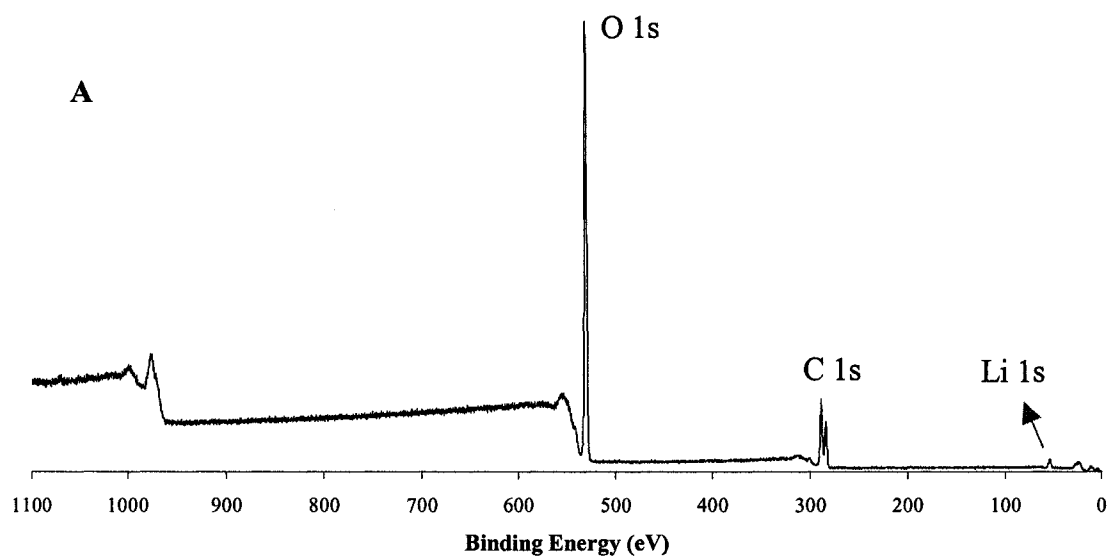
Figure C.1-4: A. - Wide scan for the CaO prepared by thermal decomposition of acetate
B. – Narrow scan for the C 1s peak for the CaO prepared from acetate

A

O 1s

Ca 2p

Ca 2s

C 1s

Ca 3p

Ca 3s

Binding Energy (eV)

B

O-C = O

Adventitious
Carbon

CO₃

Binding Energy (eV)

125
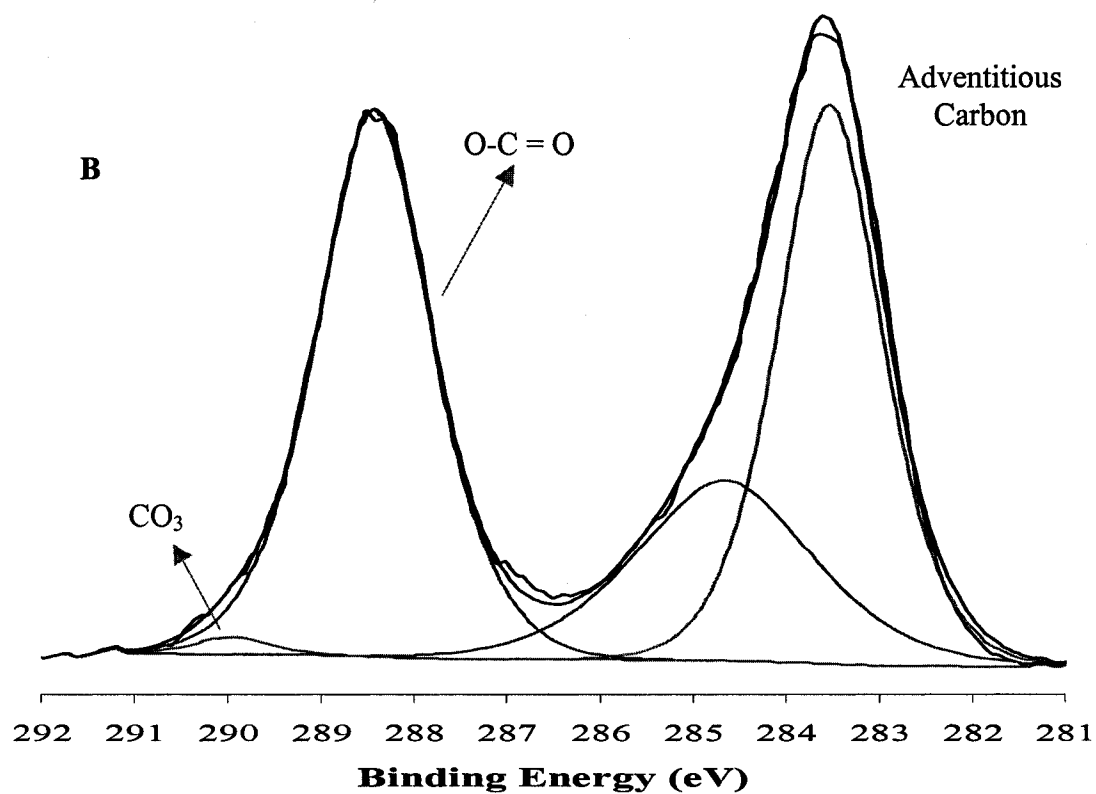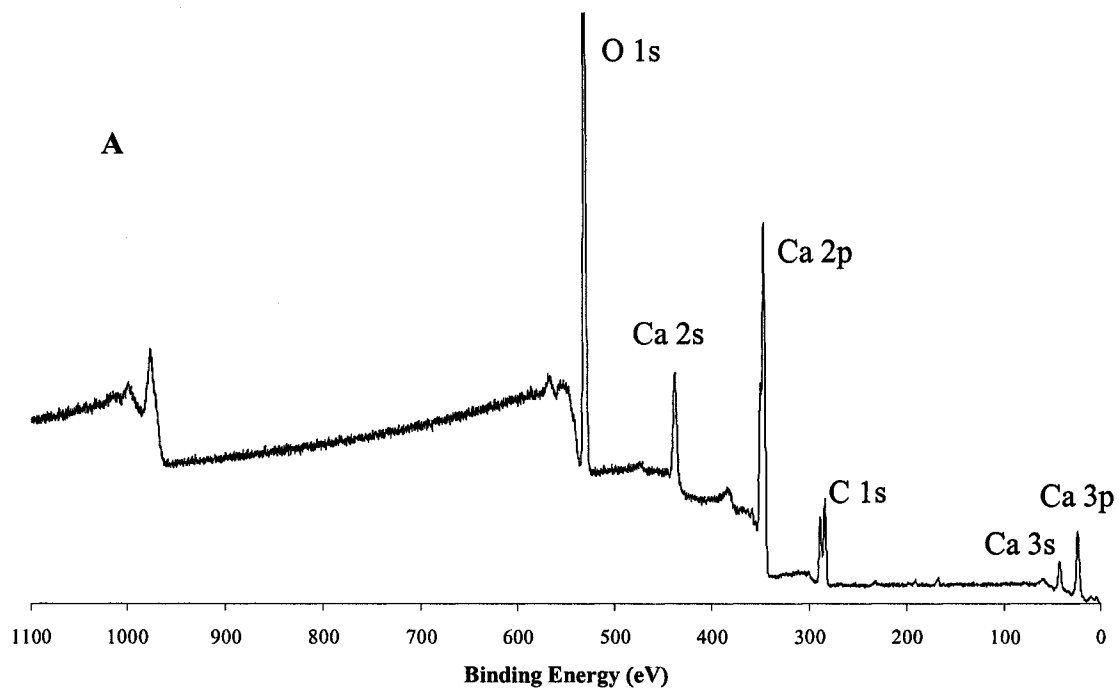
C.2. - XPS Studies for Selected Reagent Powders Mixed with SiC before and after Reaction at 385°C in the Continuous Flow Reactor System

Figure C.2-1: Narrow scan for C 1s peak for MgO mixed with SiC before an after reaction at 385°C in the continuous flow reactor system
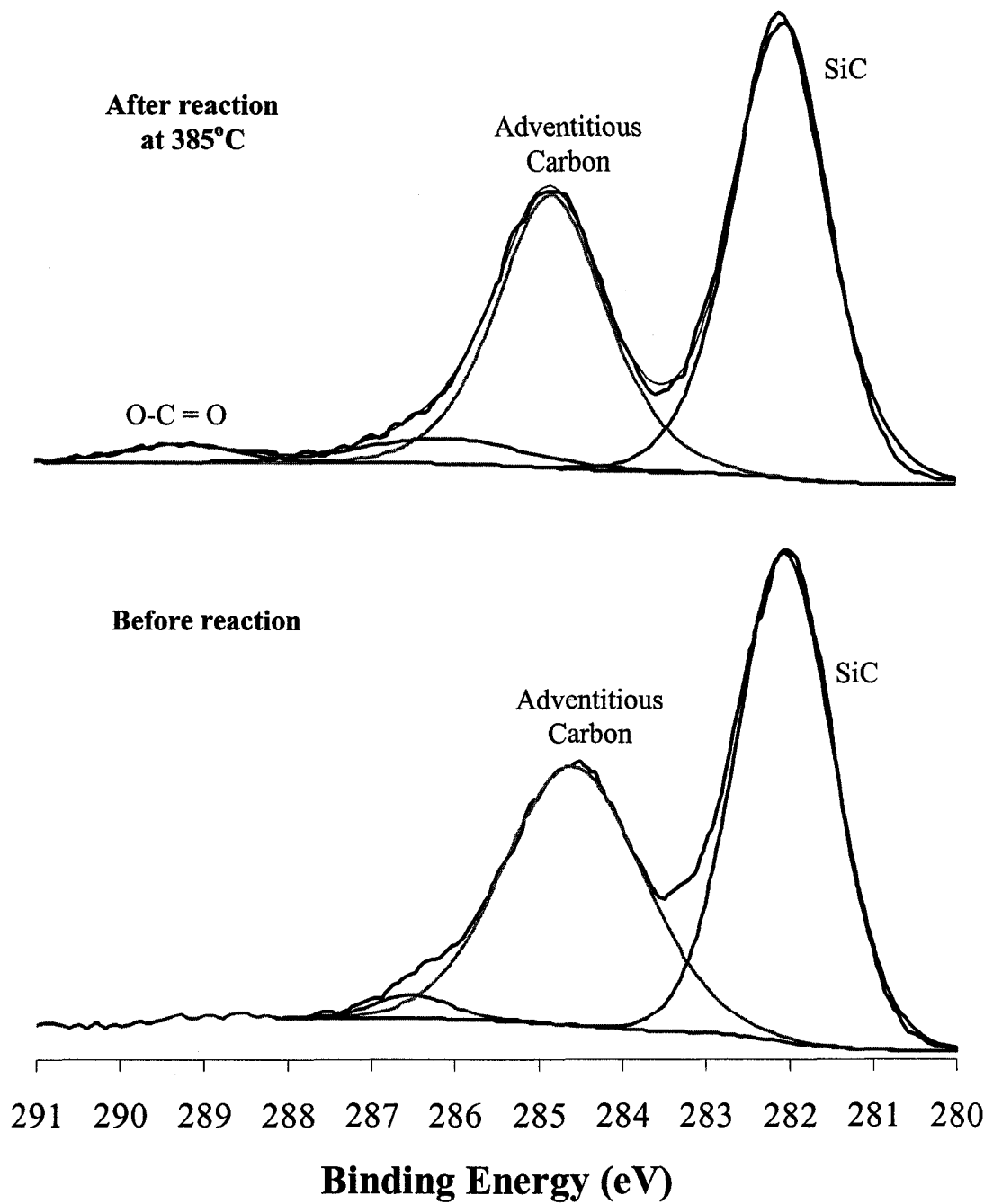
Particle Size Distribution of the Prepared Carbonates and Oxides before Reaction

Figure D-1: Particle size distribution of Li_2CO_3 prepared by precipitation

Li₂CO₃ (precipitation)
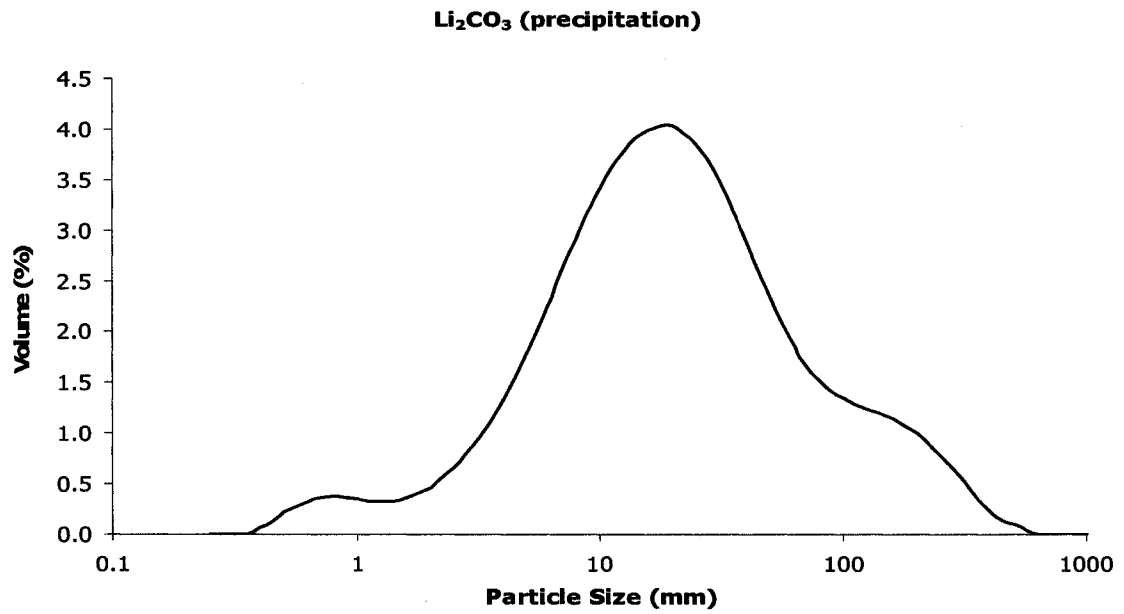
Figure D-2: Particle size distribution of Li_2CO_3 prepared by thermal decomposition of acetate

Li₂CO₃ (acetate)

127
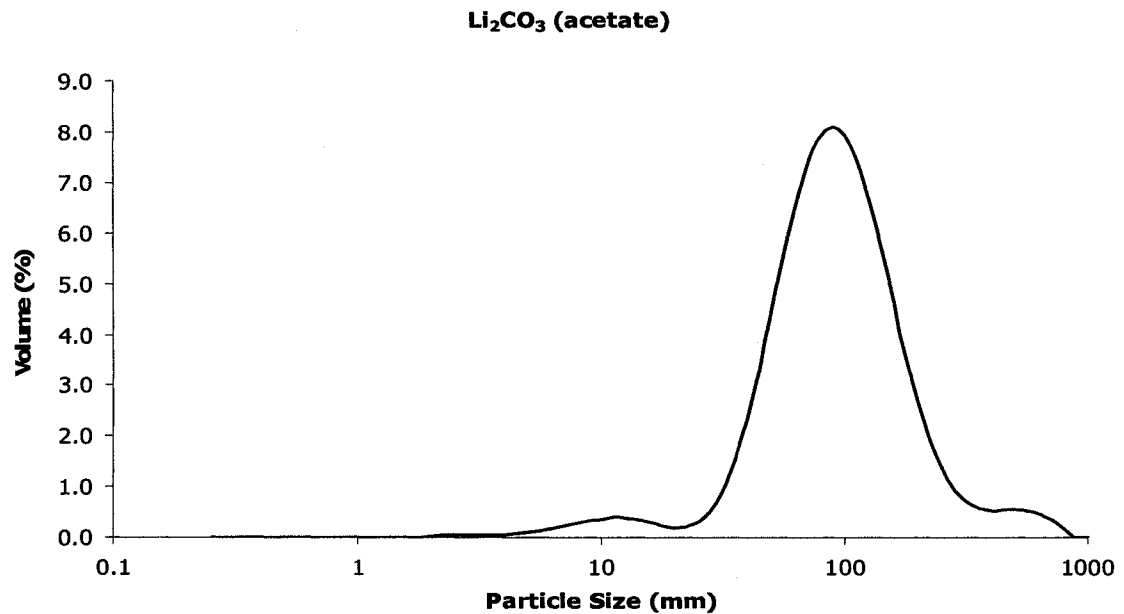
Figure D-3: Particle size distribution of Li_2CO_3 prepared by thermal decomposition of oxalate

Li_2CO_3 (oxalate)
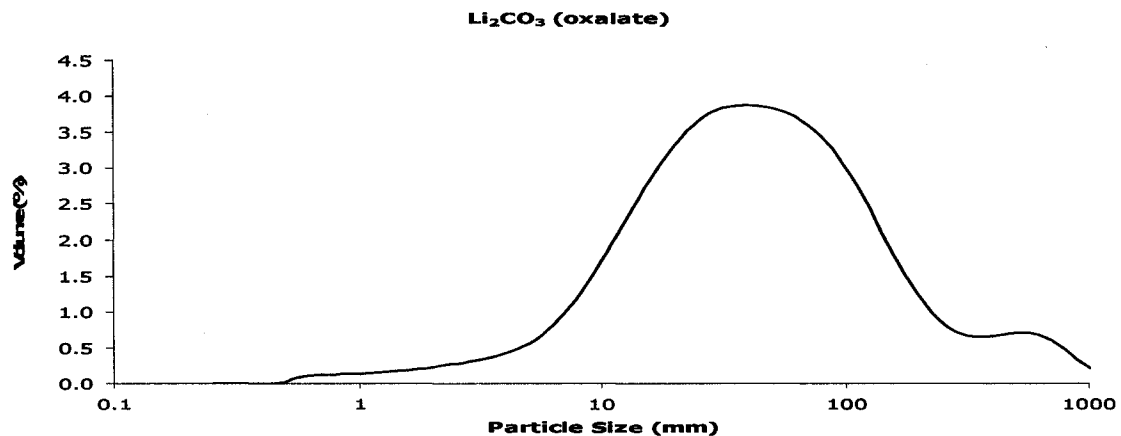
Figure D-4: Particle size distribution of $MgCO_3$ prepared by precipitation

$MgCO_3$ (precipitation)
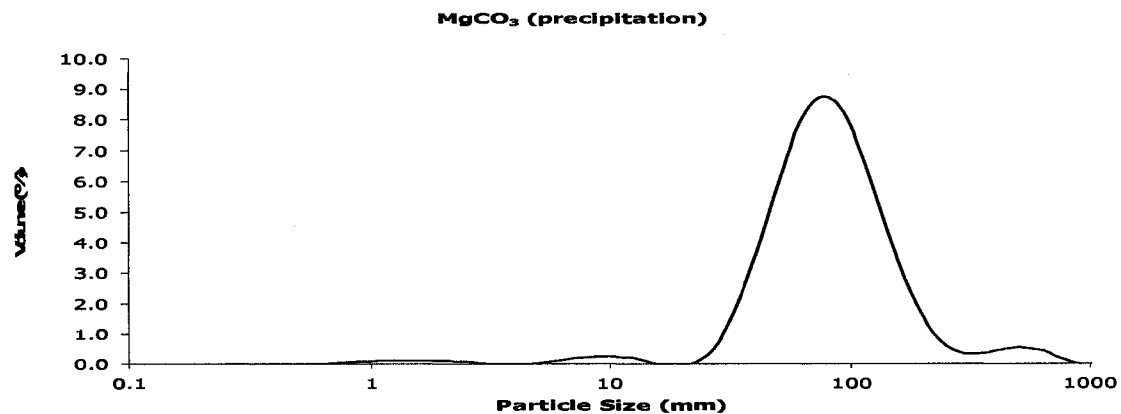
Figure D-5: Particle size distribution of Mg/Li_2CO_3 prepared by precipitation

Mg/Li_2CO_3 (precipitation)

128
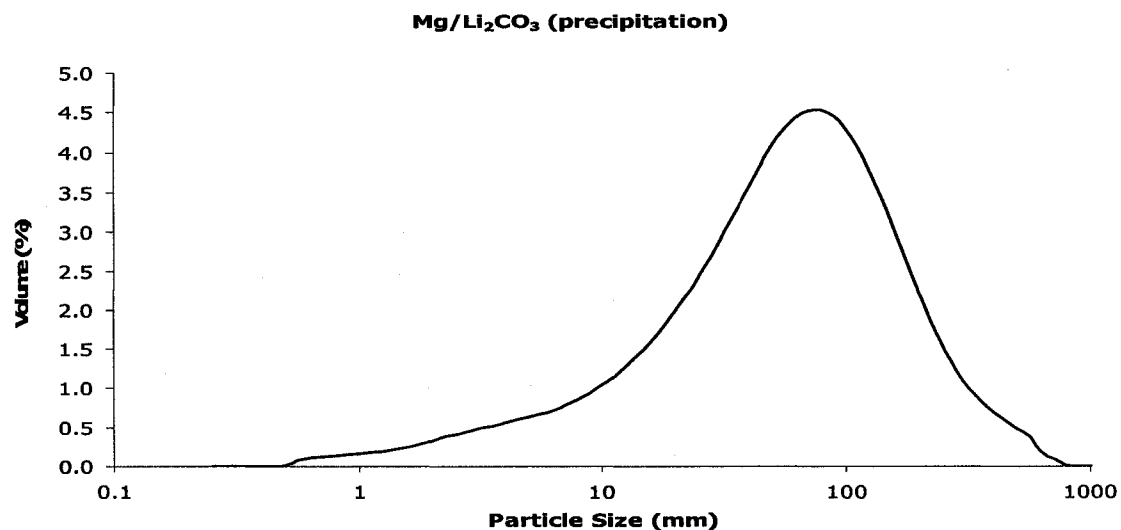
Figure D-6: Particle size distribution of MgO
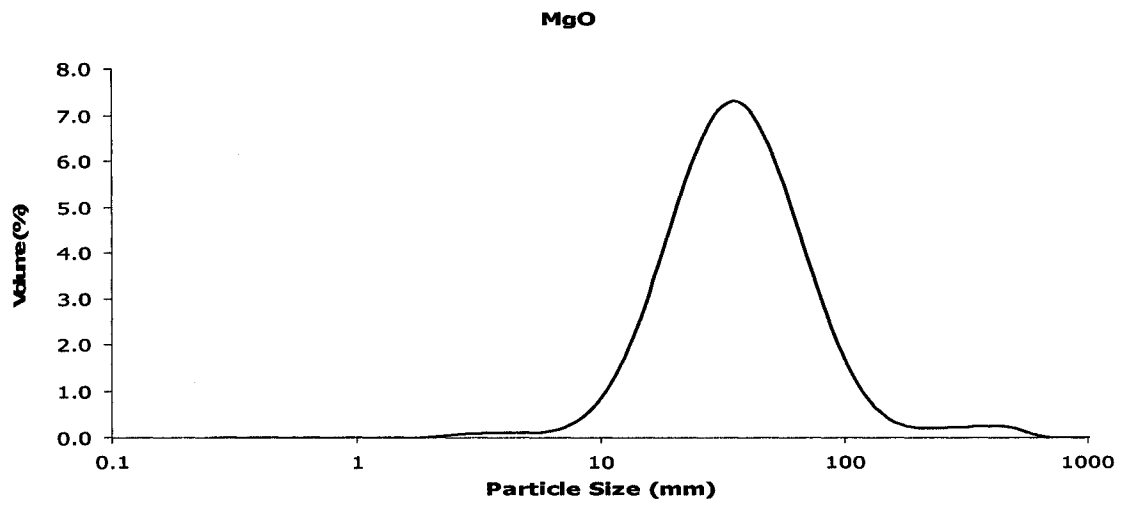
Figure D-7: Particle size distribution of Mg/Li$_2$O
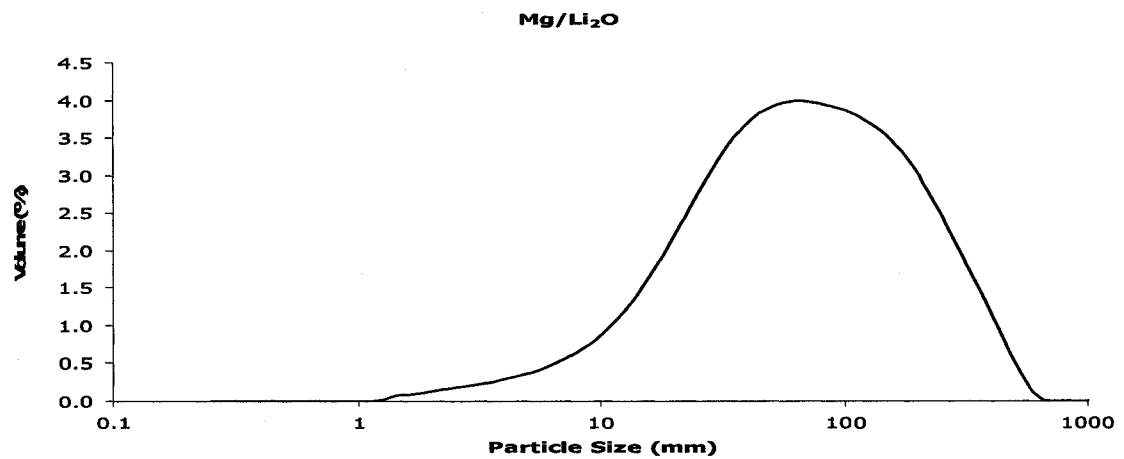
Figure D-8: Particle size distribution of CaCO$_3$ prepared by precipitation

129
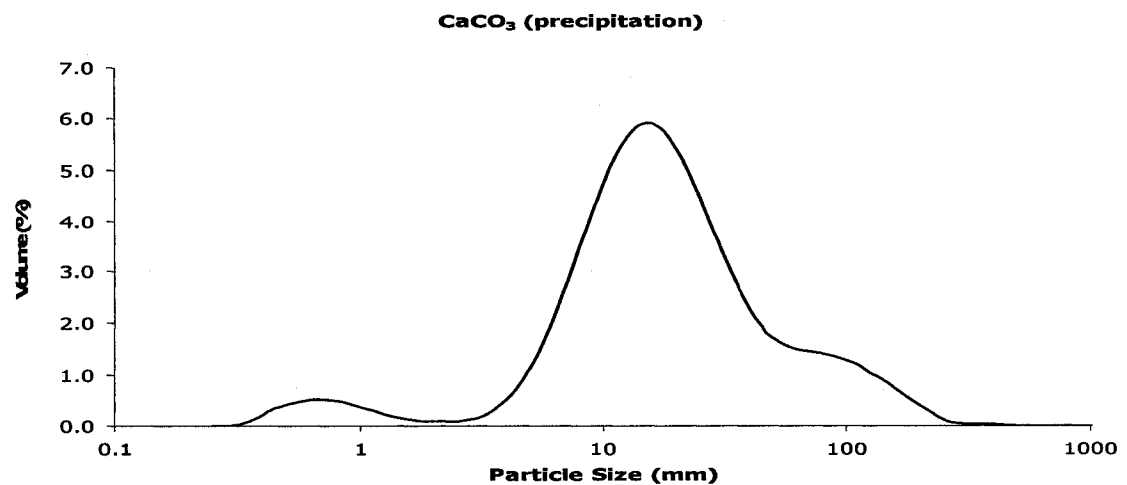
Figure D-9: Particle size distribution of $CaCO_3$ prepared by thermal decomposition of acetate
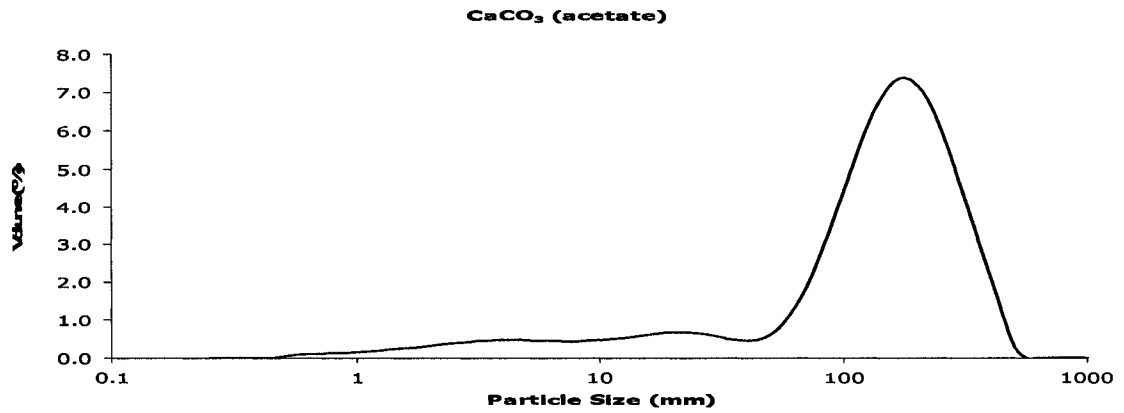
CaCO₃ (acetate)

Figure D-10: Particle size distribution of Ca/Li_2CO_3 prepared by thermal decomposition of acetate
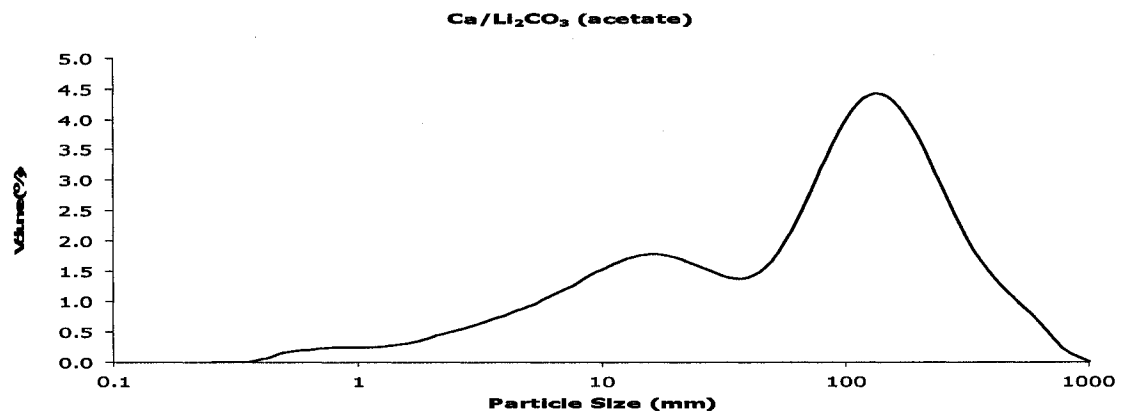
Ca/Li₂CO₃ (acetate)

Figure D-11: Particle size distribution of CaO from $CaCO_3$ prepared by precipitation

CaO (precipitation)

130
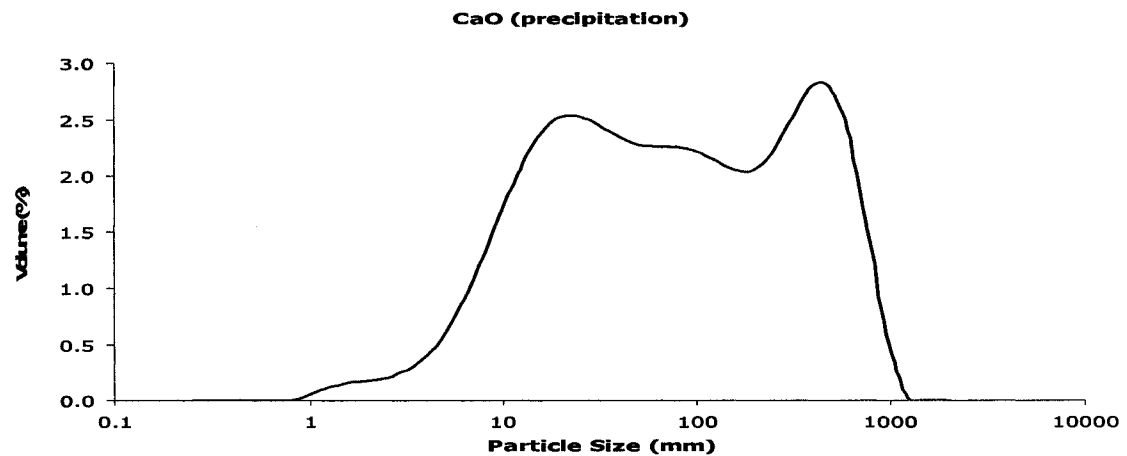
Figure D-12: Particle size distribution of CaO from $CaCO_3$ prepared from acetate

CaO (acetate)
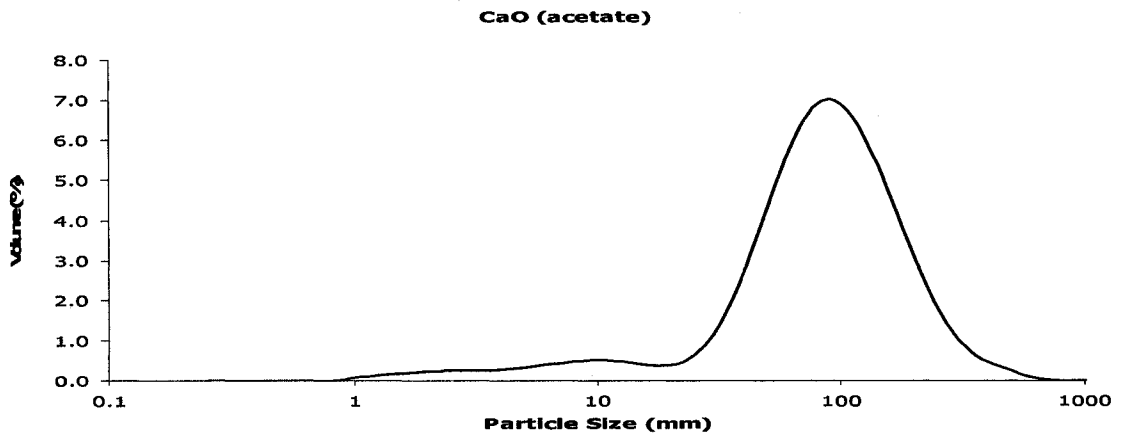
Figure D-13: Particle size distribution of Ca/Li_2O from Ca/Li_2CO_3 prepared from acetate

Ca/Li$_2$O (acetate)
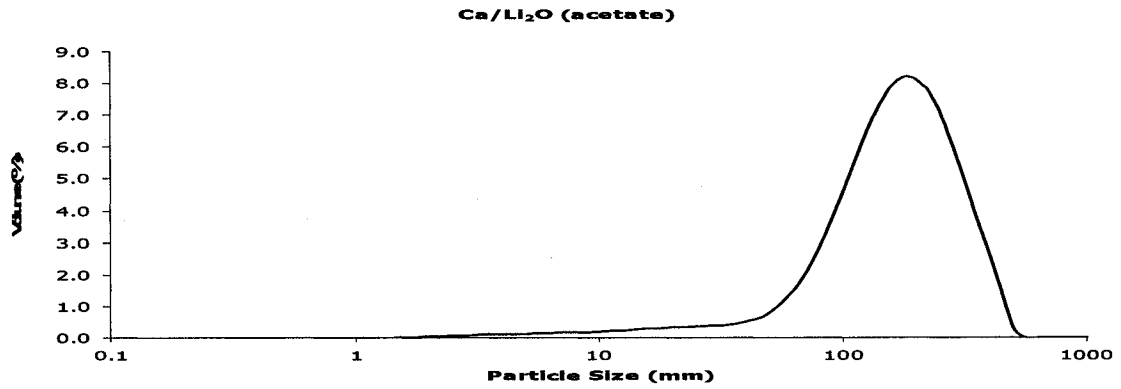
Figure D-14: Particle size distribution of $BaCO_3$ prepared by precipitation

BaCO$_3$ (precipitation)

131
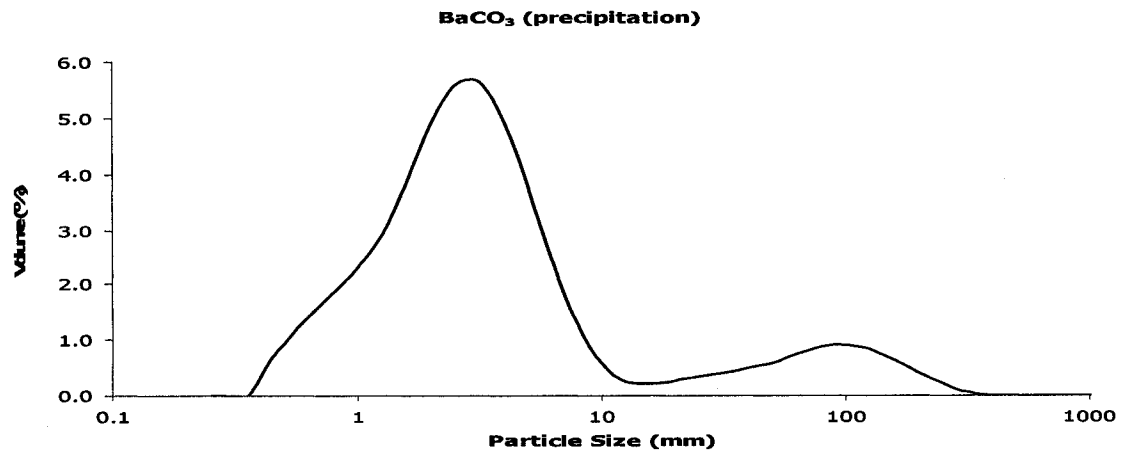
Figure D-15: Particle size distribution of Ba/Li$_2$CO$_3$ prepared by precipitation

Ba/Li$_2$CO$_3$ (precipitation)
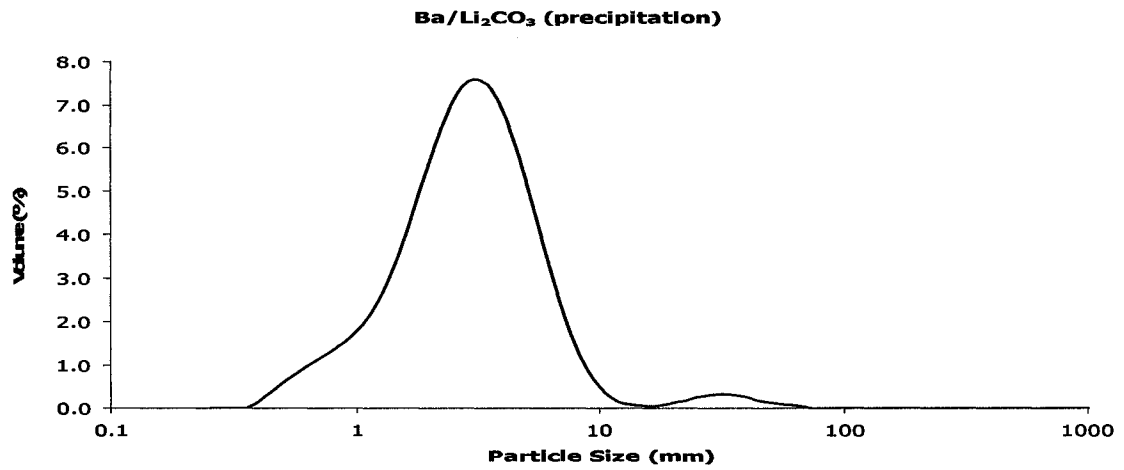
Figure D-16: Particle size distribution of Na$_2$CO$_3$ (Fisher reagent)

Na$_2$CO$_3$ (Fisher reagent)

132
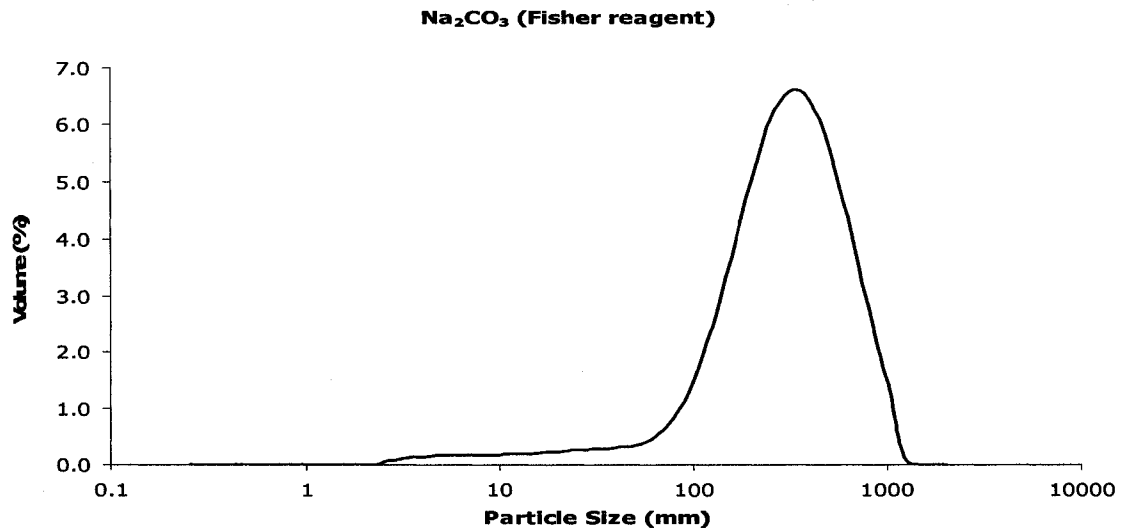
Thermal Gravimetric Analyses

E.1. - TGA Studies for the Carbonates Prepared by Precipitation before Reaction

Figure E.1-1: Mass as a function of temperature - Li_2CO_3 prepared by precipitation
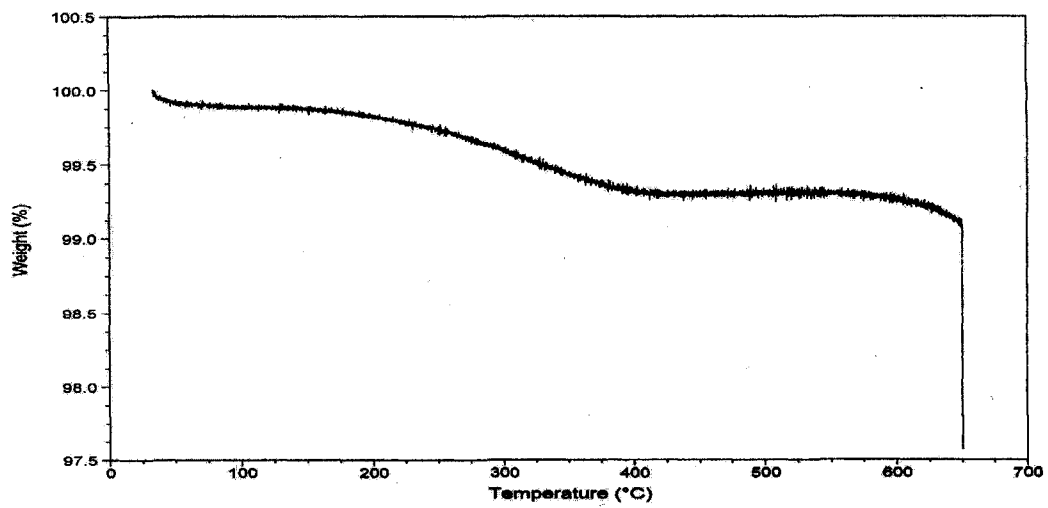
Figure E.1-2: Mass as a function of temperature - $CaCO_3$ prepared by precipitation
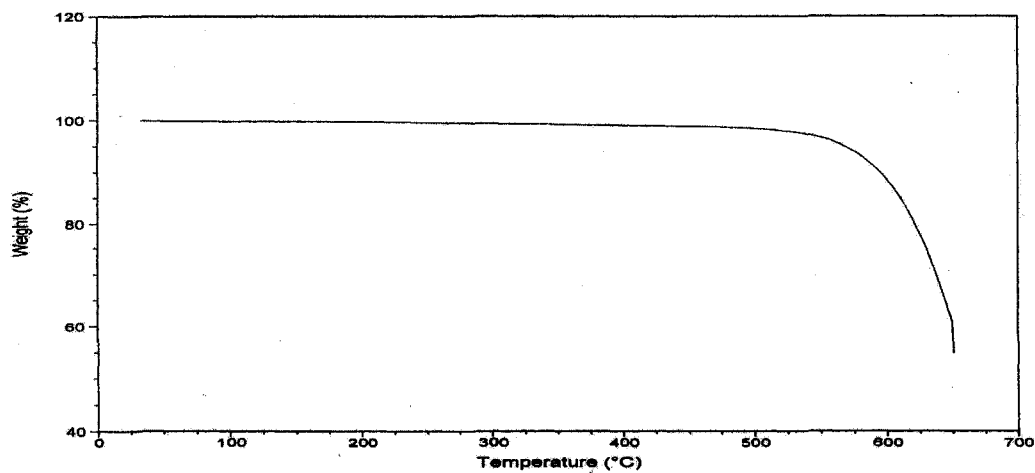
Figure E.1-3: Mass as a function of temperature - Commercial precipitated CaCO3 (1)

PCC (1)
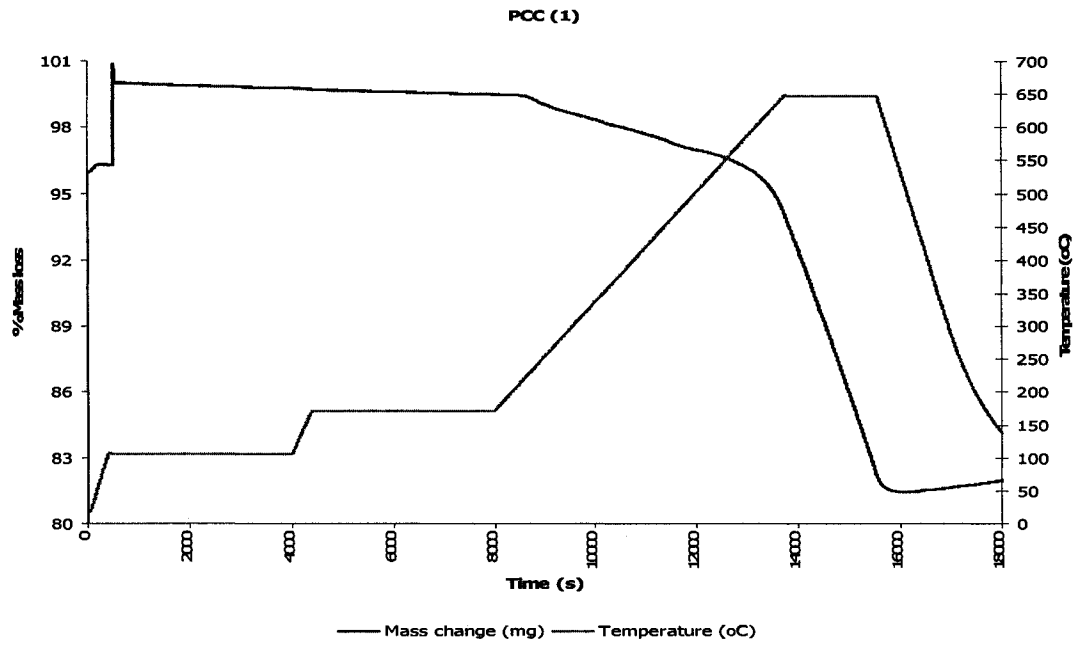
Figure E.1-4: dTG/dt - Commercial precipitated CaCO3 (1)

PCC (1)

134
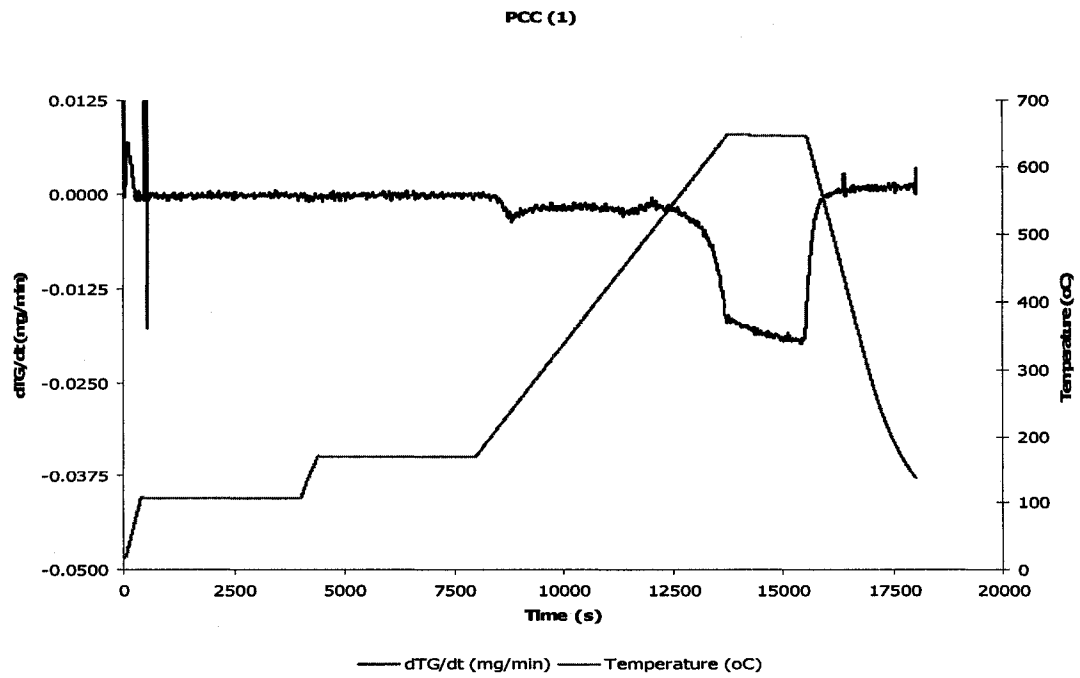
Figure E.1-5: Mass as a function of temperature - Commercial precipitated CaCO₃ (2)

PCC (2)
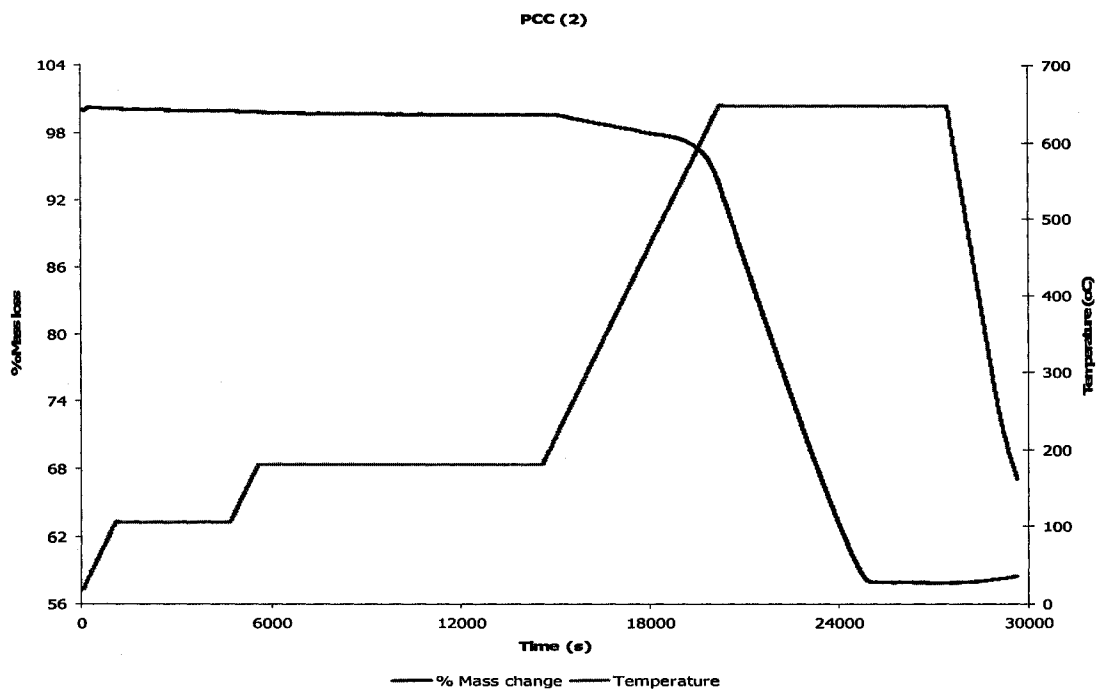
Figure E.1-6: dTG/dt - Commercial precipitated CaCO₃ (2)

PCC (2)

135
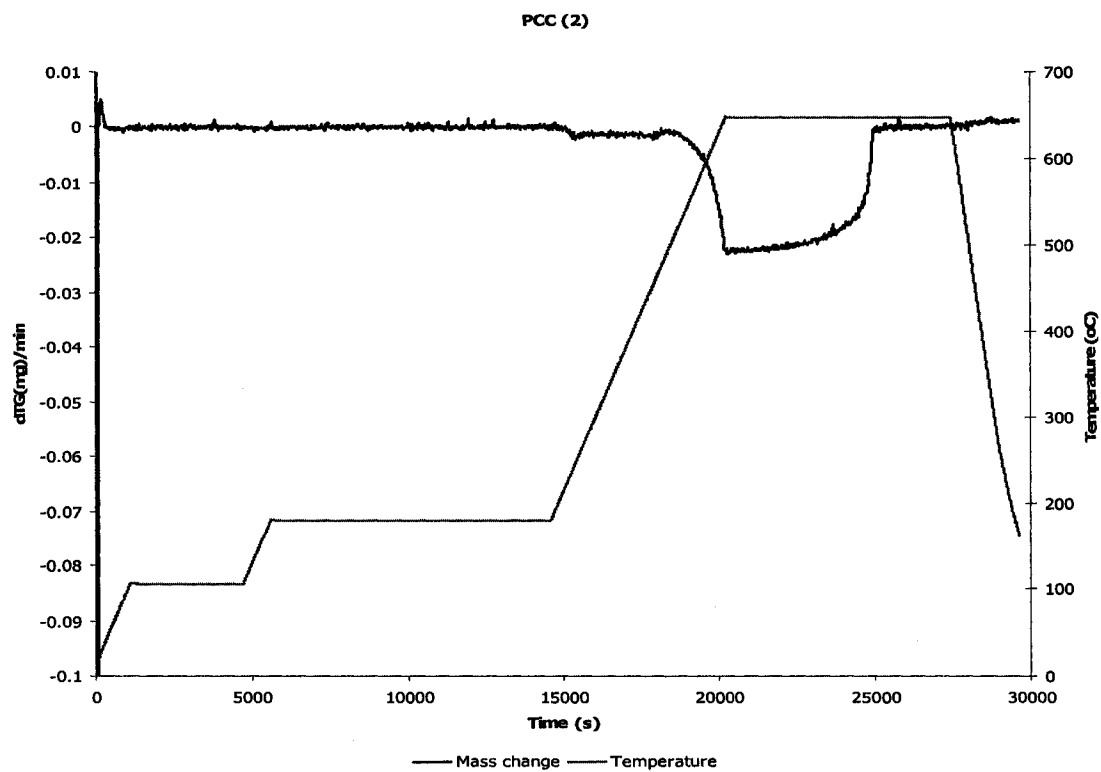
Figure E.1-7: Mass as a function of temperature - MgCO$_3$ prepared by precipitation
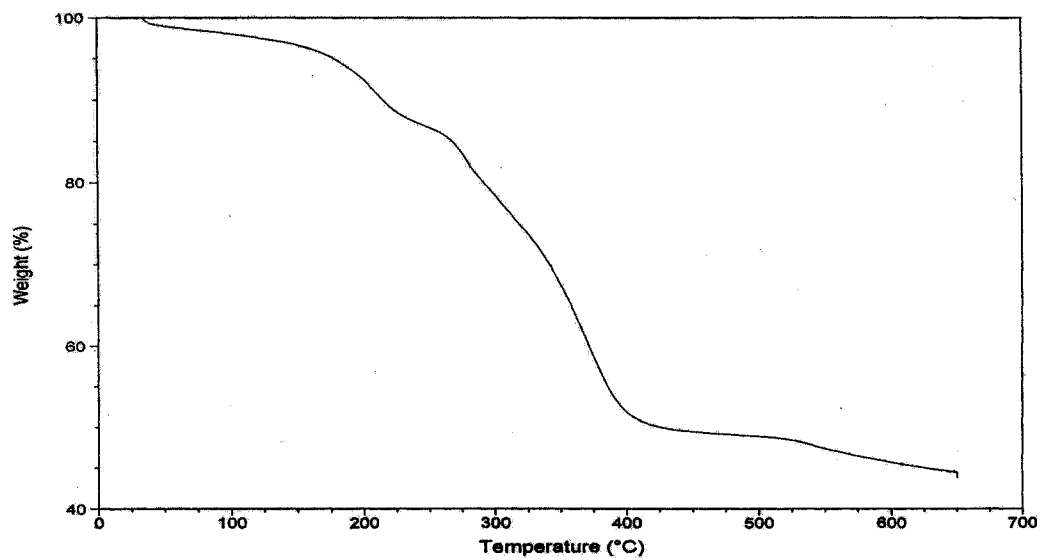
Figure E.1-8: Mass as a function of temperature - BaCO$_3$ prepared by precipitation

136
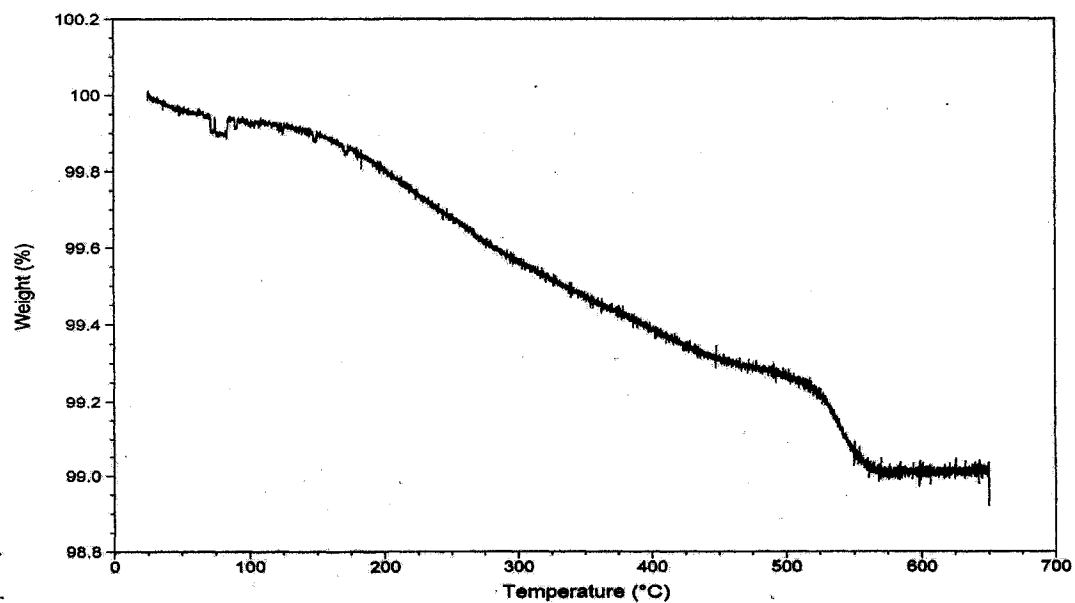
Figure E.1-9: Mass as a function of temperature – CaO

CaO
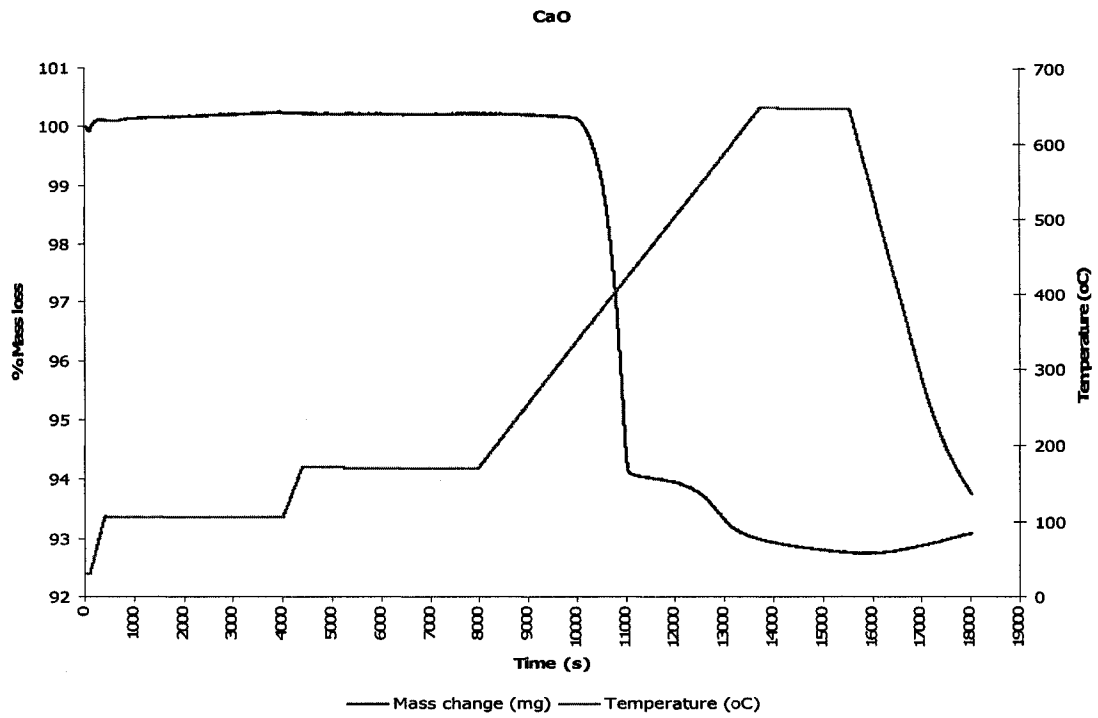
Figure E.1-10: dTG/dt - CaO

CaO

137
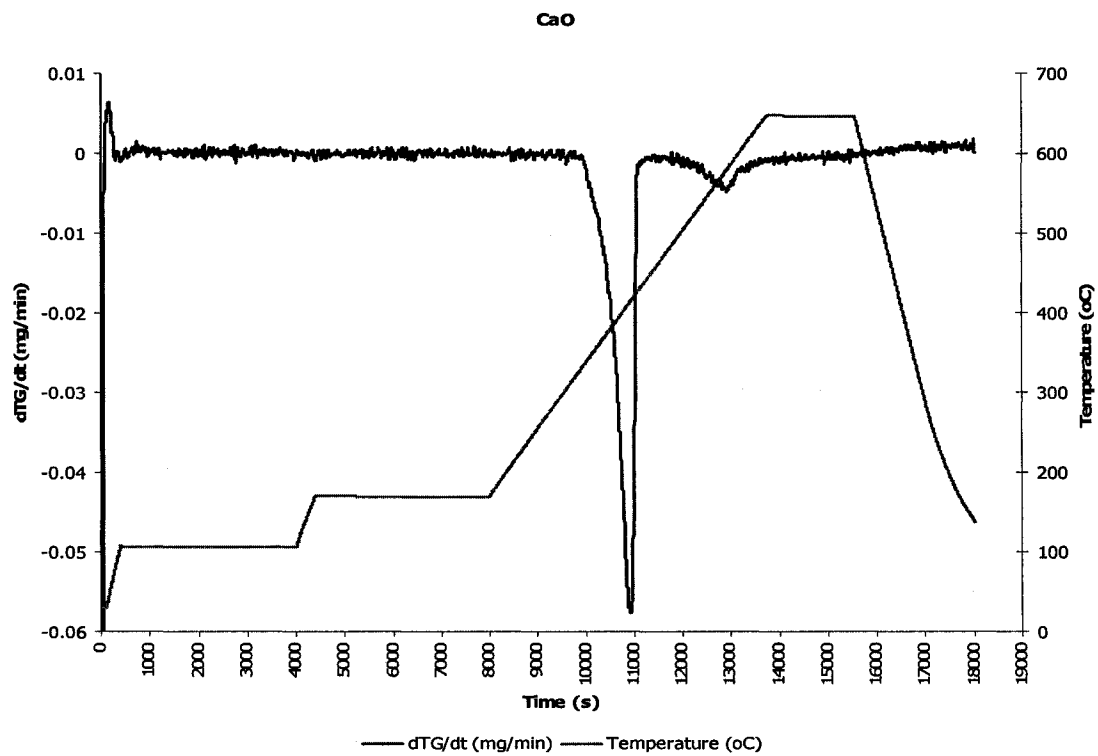
E.2. - TGA Studies for the Resultant Solids from the Low Temperature Tests

Figure E.2-1: Mass as a function of temperature – Ca(OH)$_2$ after mixed with butyric acid at room temperature. The resultant solid was not dried at 200°C
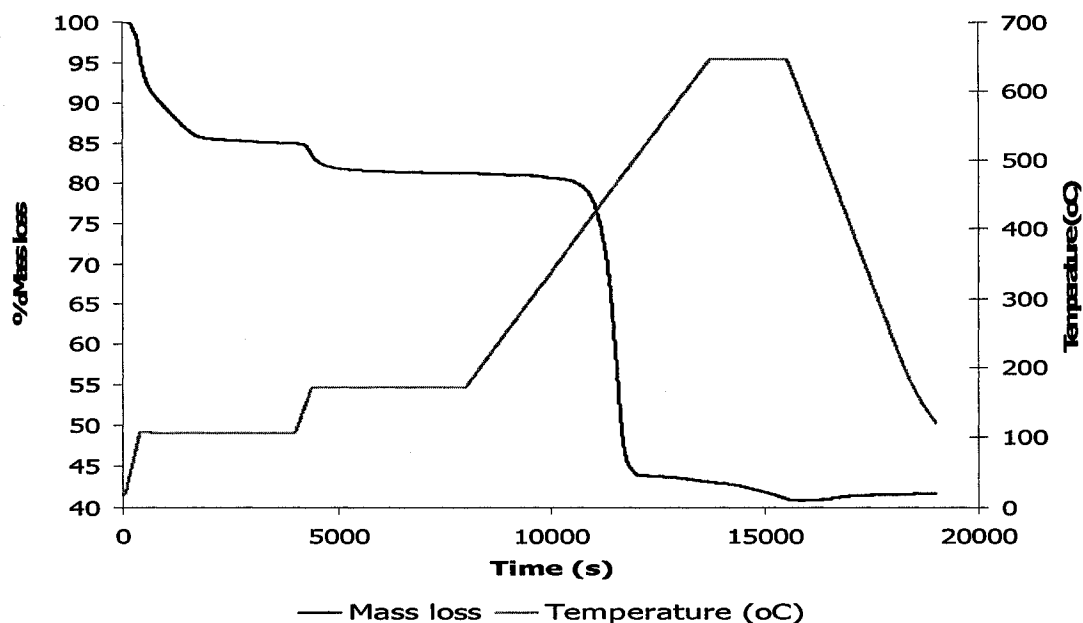
Figure E.2-2: dTG/dt – Ca(OH)$_2$ after mixed with butyric acid at room temperature. The resultant solid was not dried at 200°C

138
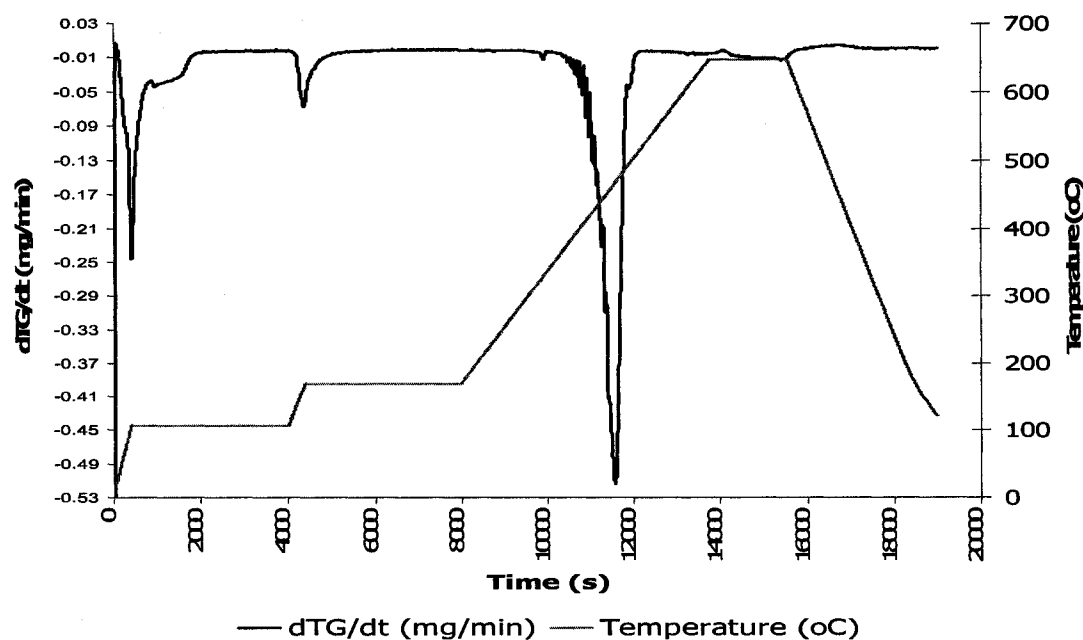
Figure E.2-3: Mass as a function of temperature – Commercial precipitated CaCO₃ (1) [PCC (1)] after mixed with butyric acid at 50°C and dried at 200°C
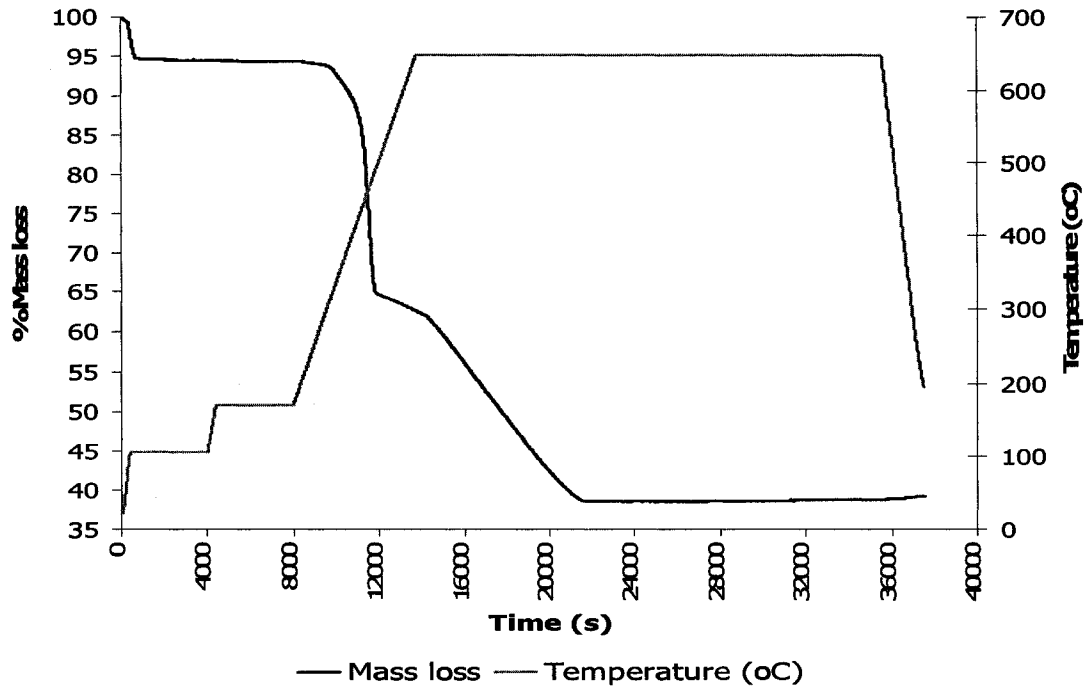
Figure E.2-4: dTG/dt – Commercial precipitated CaCO₃ (1) [PCC (1)] after mixed with butyric acid at 50°C and dried at 200°C

139
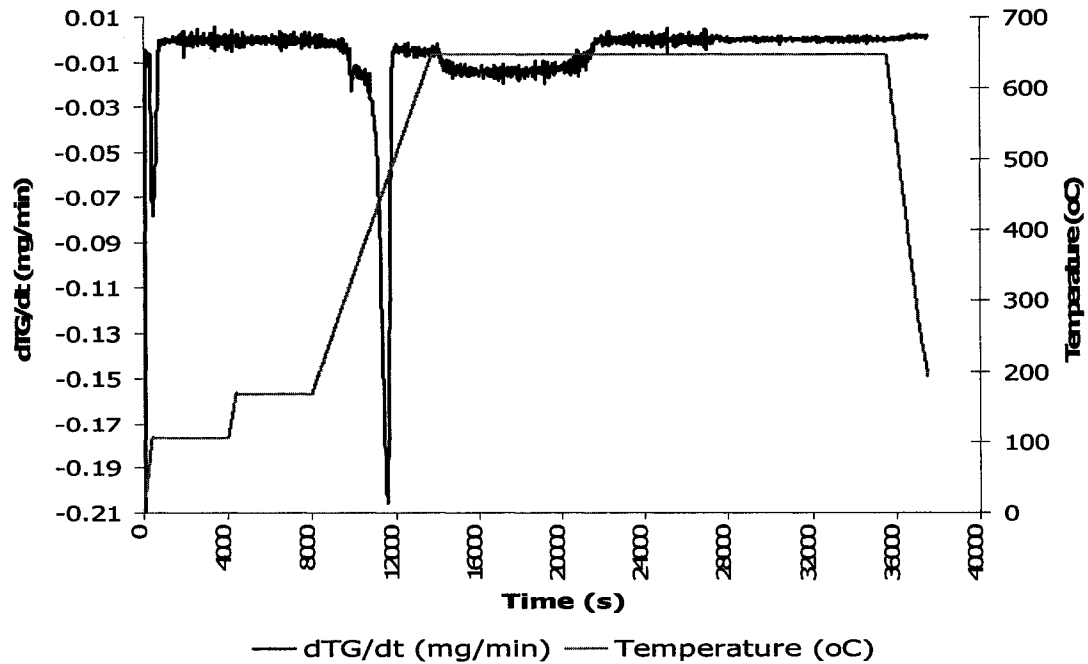
Figure E.2-5: Mass as a function of temperature – Commercial precipitated CaCO₃ (2) [PCC (2)] after mixed with butyric acid at 50°C and dried at 200°C
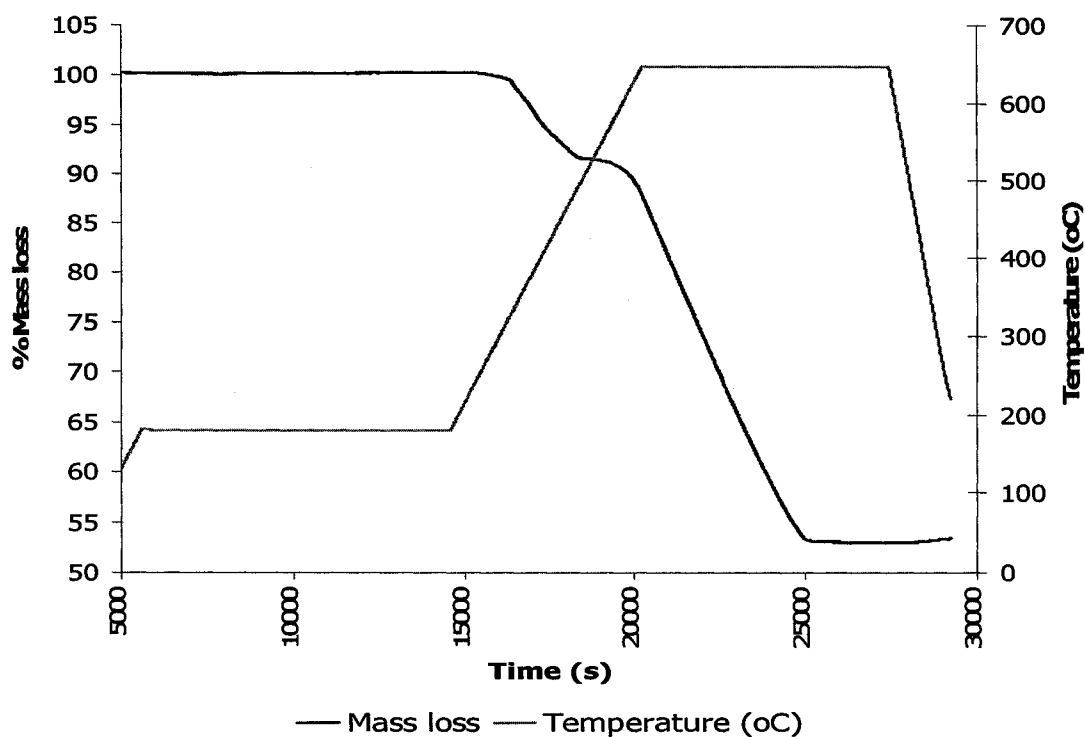
Figure E.2-6: dTG/dt – Commercial precipitated CaCO₃ (2) [PCC (2)] after mixed with butyric acid at 50°C and dried at 200°C

140
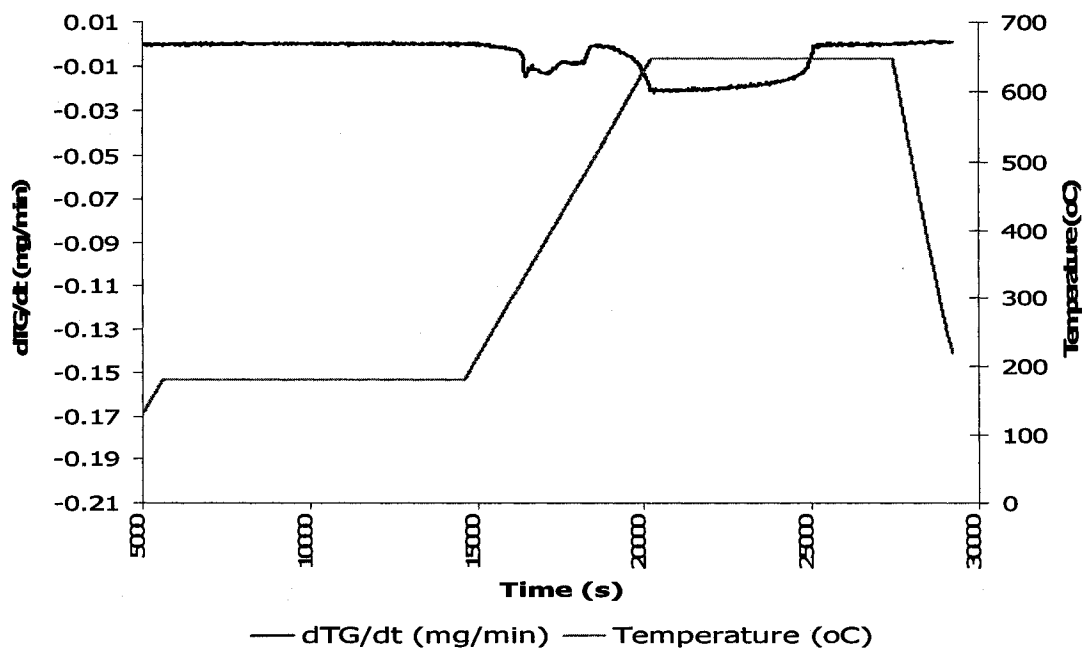
Figure E.2-7: Mass as a function of temperature – CaO from CaCO$_3$ prepared by precipitation after mixed with butyric acid at 50°C and dried at 200°C

— Mass loss — Temperature (oC)
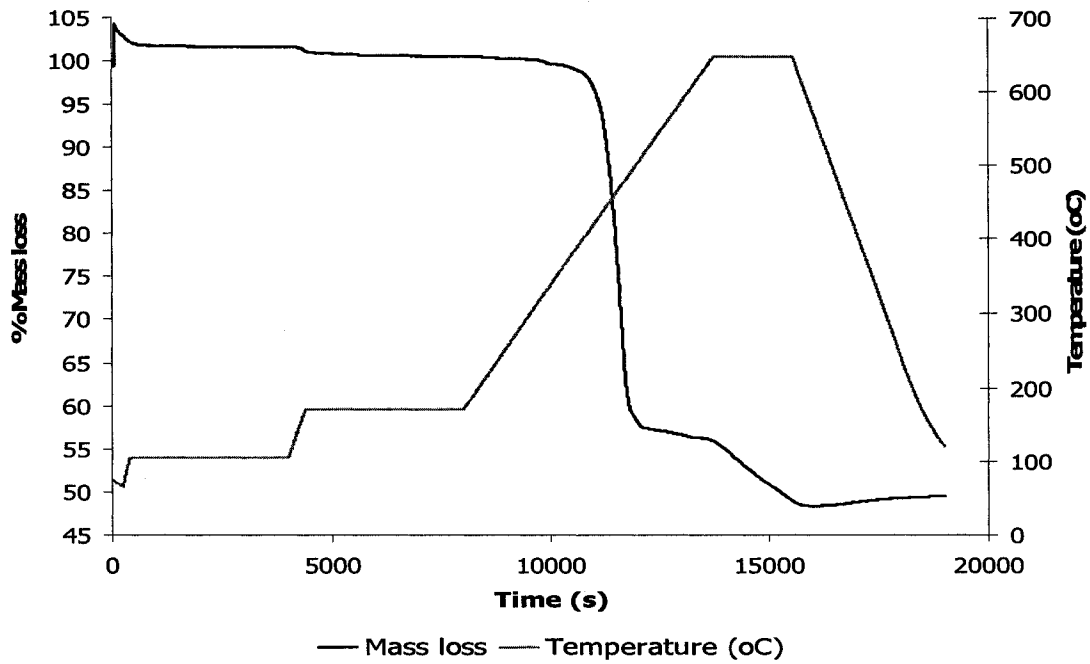
Figure E.2-8: dTG/dt – CaO from CaCO$_3$ prepared by precipitation after mixed with butyric acid at 50°C and dried at 200°C

— dTG/dt (mg/min) — Temperature (oC)

141
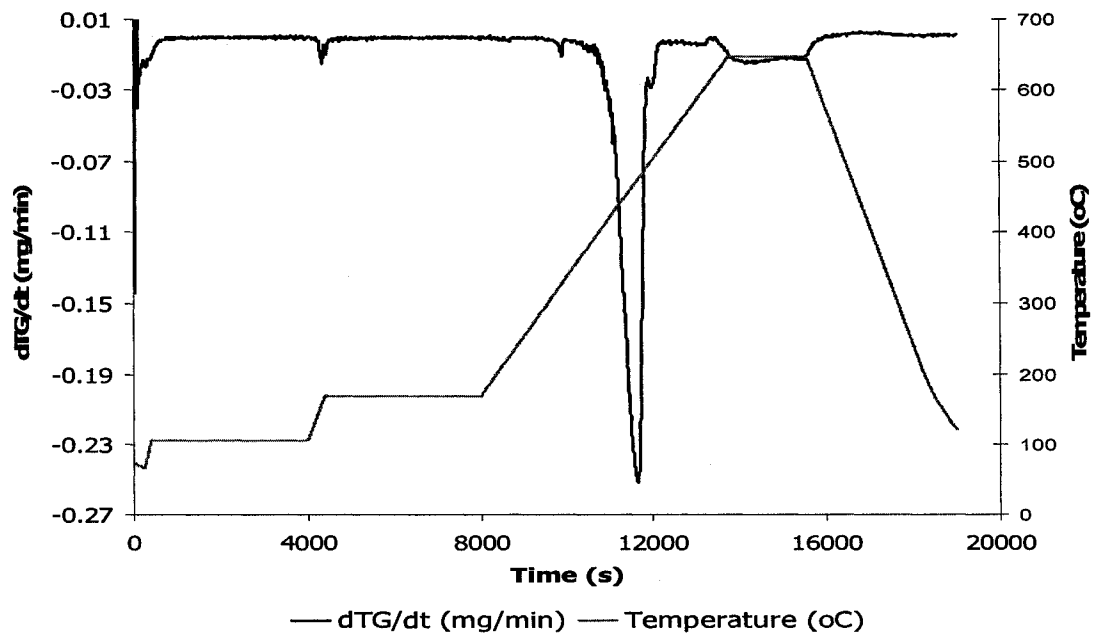
Appendix F

Decrease of Butyric Acid and Production of Ketones as a Function of Time

Figure F-1: Li_2CO_3 prepared by precipitation with a WHSV = 0.4845 h^{-1}
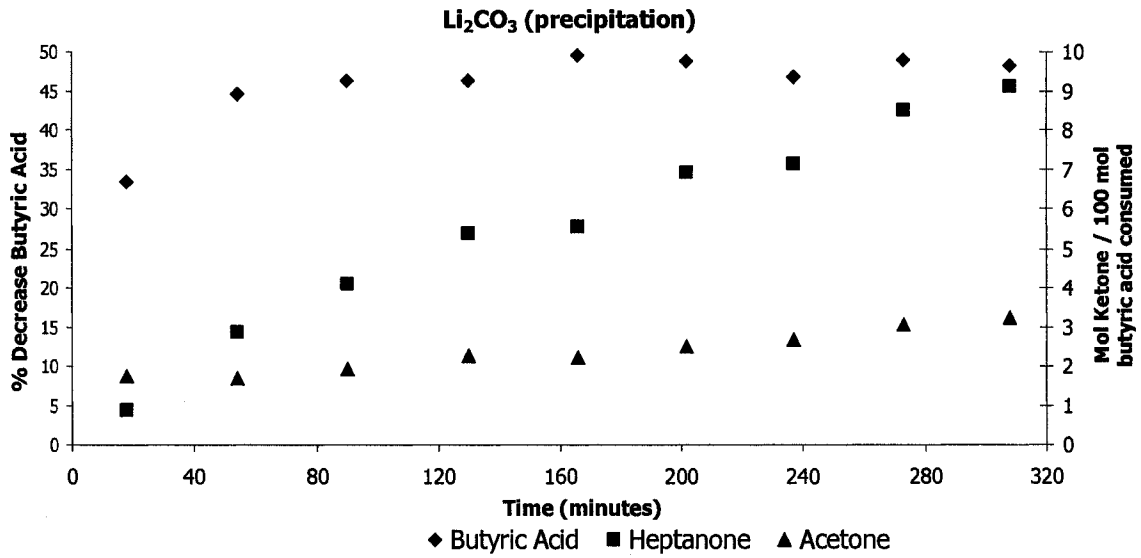
Figure F-2: Li_2CO_3 prepared by precipitation with a WHSV = 0.1475 h^{-1}

142
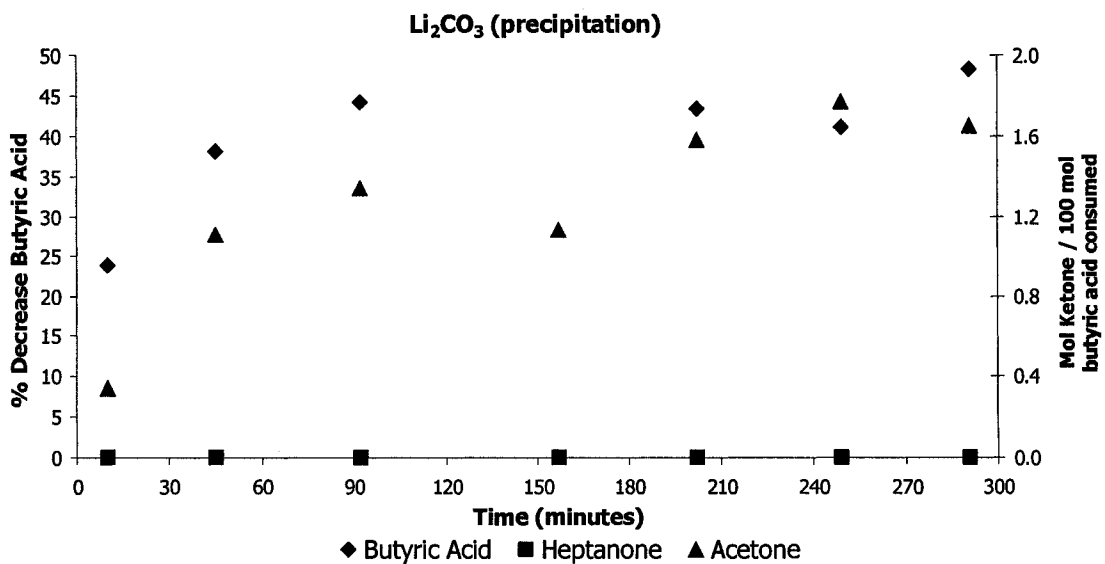
Figure F-3: Li_2CO_3 prepared by precipitation with a WHSV = 0.1572 h^{-1}

Li₂CO₃ (precipitation)

◆ Butyric Acid ■ Heptanone ▲ Acetone
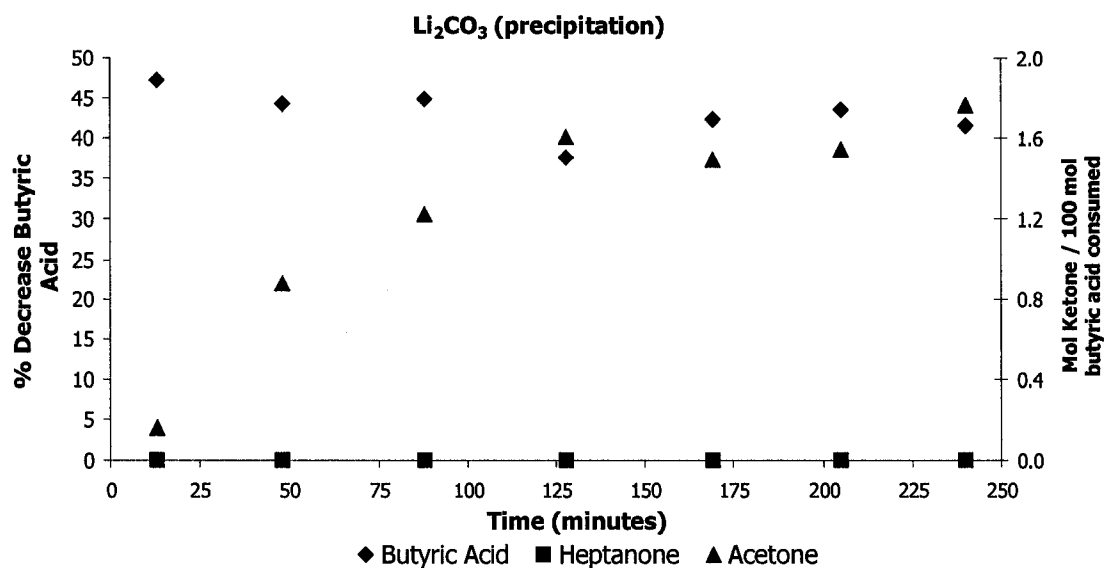
Figure F-4: Li_2CO_3 prepared by thermal decomposition of acetate with a WHSV = 0.1455 h^{-1}

Li₂CO₃ (acetate)

◆ Butyric Acid ■ Heptanone ▲ Acetone

143
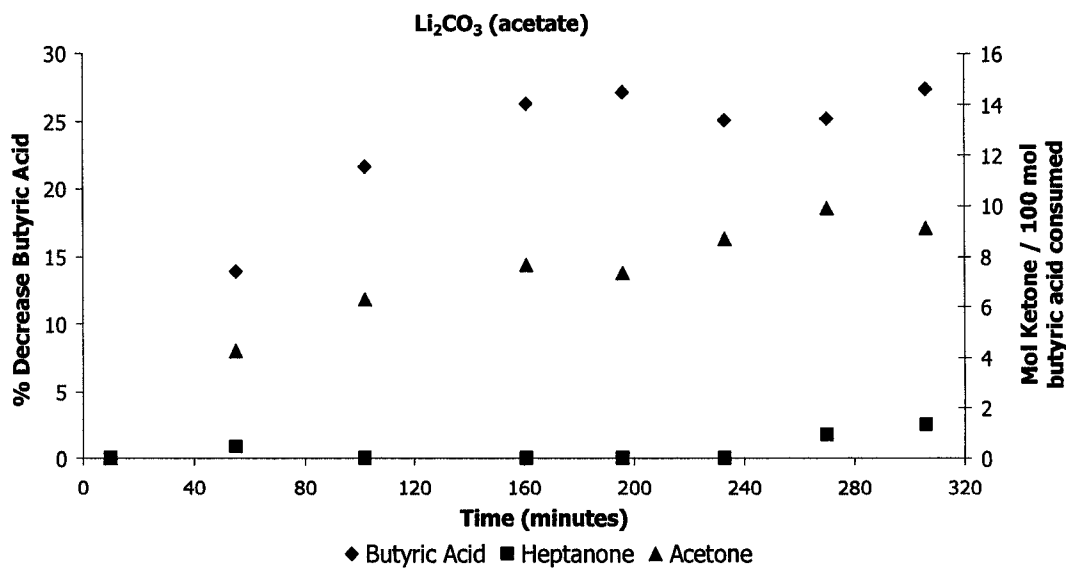
Figure F-5: Li$_2$CO$_3$ prepared by thermal decomposition of oxalate with a WHSV = 0.1319 h^{-1}

Li$_2$CO$_3$ (oxalate)

♦ Butyric Acid ■ Heptanone ▲ Acetone
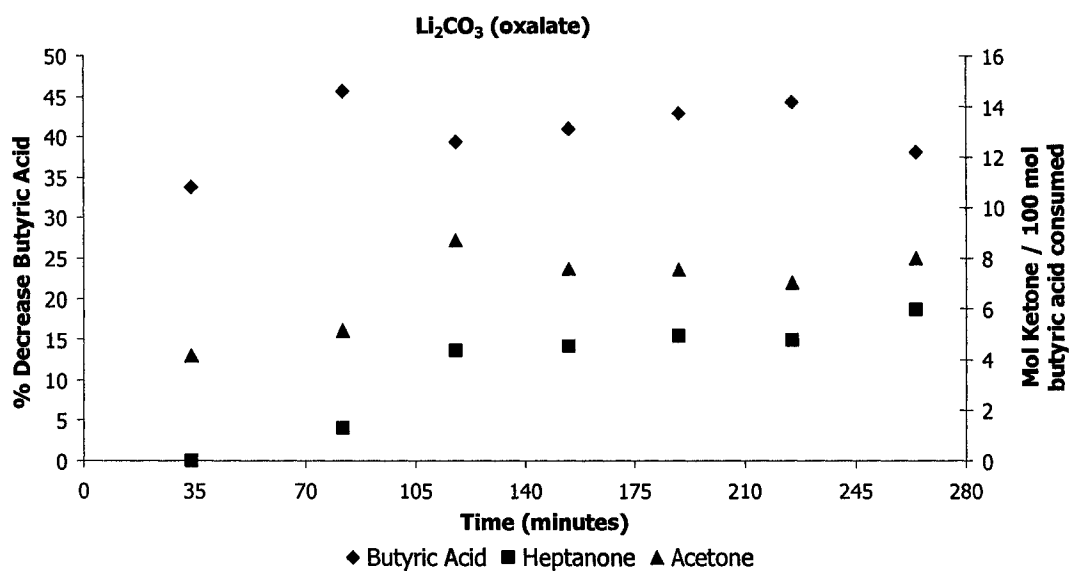
Figure F-6: MgCO$_3$ prepared by precipitation with a WHSV = 0.1572 h^{-1}

MgCO$_3$ (precipitation)

♦ Butyric Acid ■ Heptanone ▲ Acetone

144
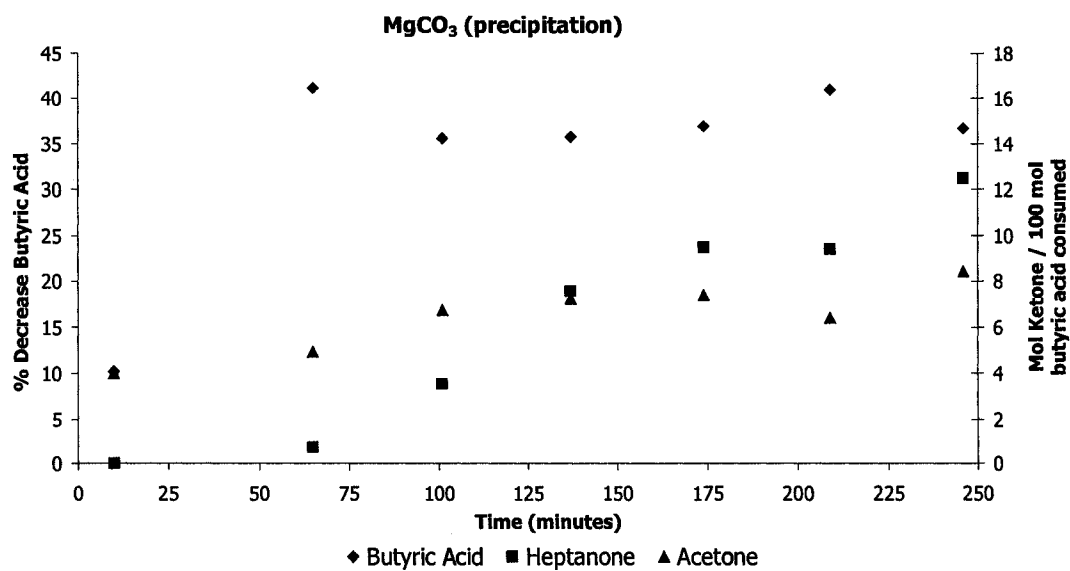
Figure F-7: Mg/Li$_2$CO$_3$ prepared by precipitation with a WHSV = 0.1858 h^{-1}

Mg/Li$_2$CO$_3$ (precipitation)

◆ Butyric Acid ■ Heptanone ▲ Acetone
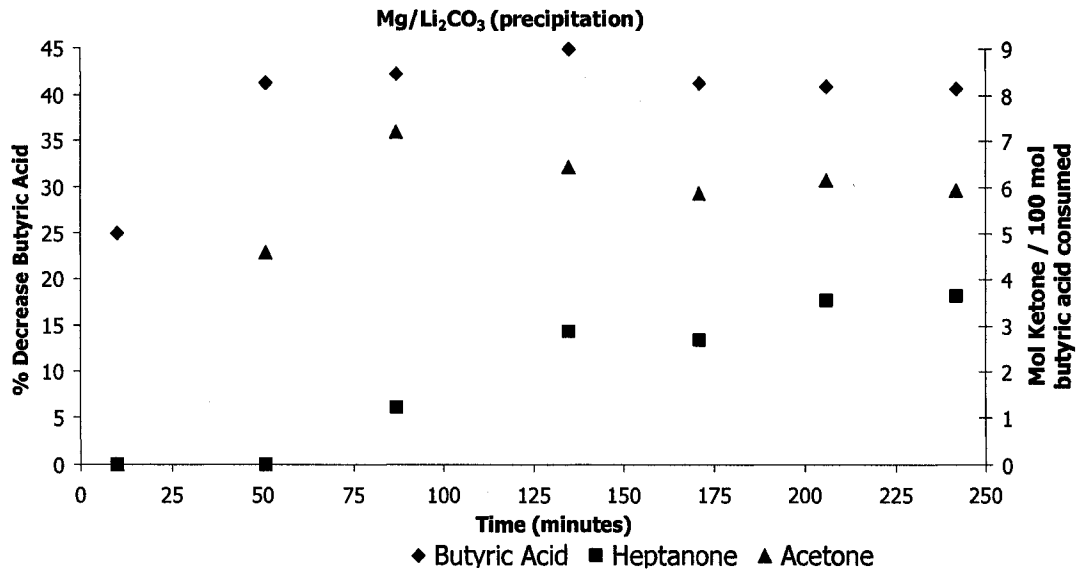
Figure F-8: MgO with a WHSV = 0.1669 h^{-1}

MgO

◆ Butyric Acid ■ Heptanone ▲ Acetone

145
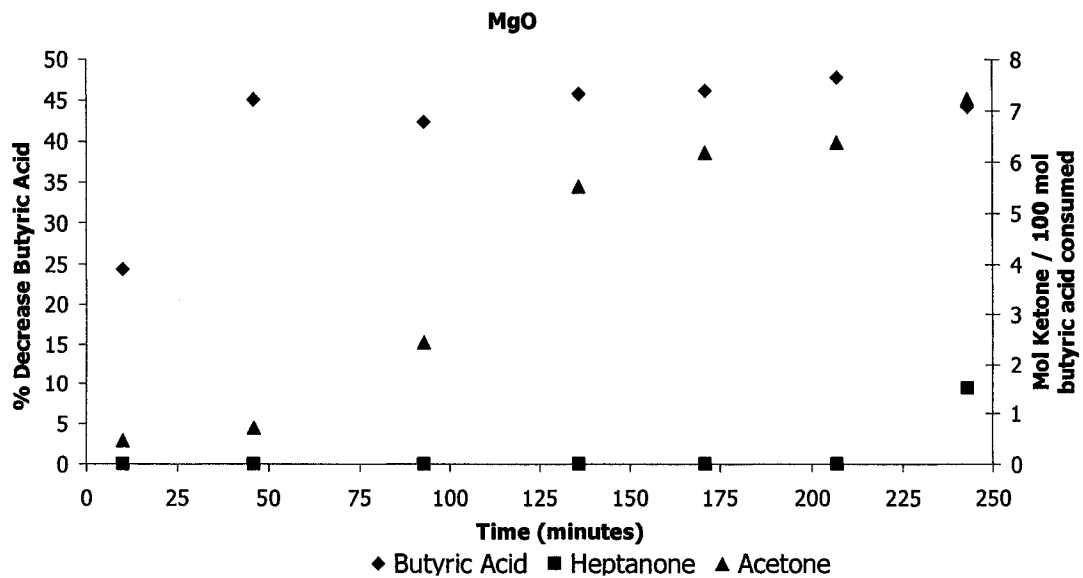
Figure F-9: MgO with a WHSV = 0.0931 h^{-1}

MgO

% Decrease Butyric Acid

Mol Ketone / 100 mol butyric acid consumed

Time (minutes)

♦ Butyric Acid ■ Heptanone ▲ Acetone
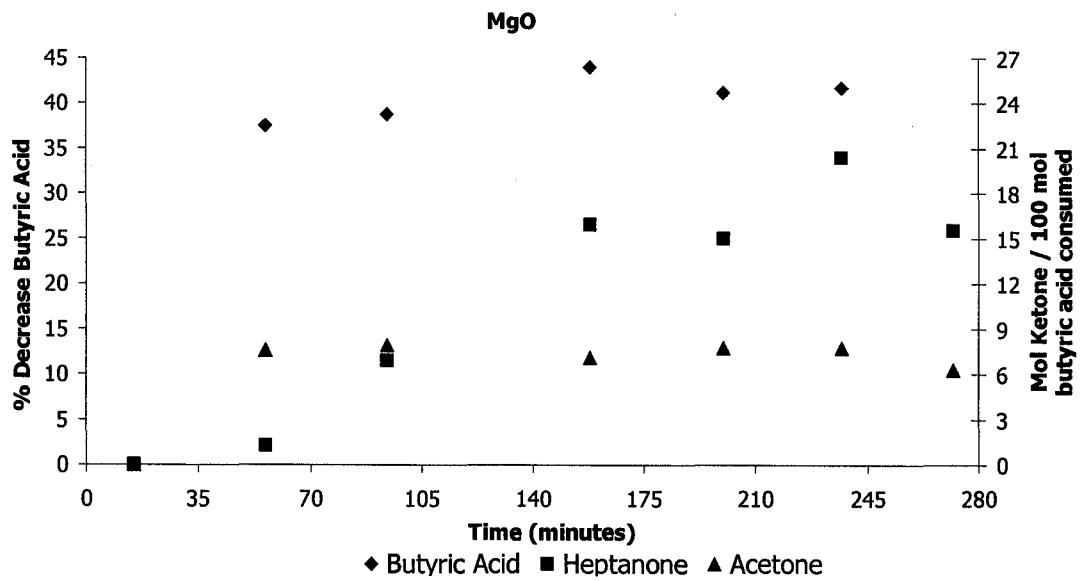
Figure F-10: Mg/Li$_2$O with a WHSV = 0.1478 h^{-1}

Mg/Li$_2$O

% Decrease Butyric Acid

Mol Ketone / 100 mol butyric acid consumed

Time (minutes)

♦ Butyric Acid ■ Heptanone ▲ Acetone

146
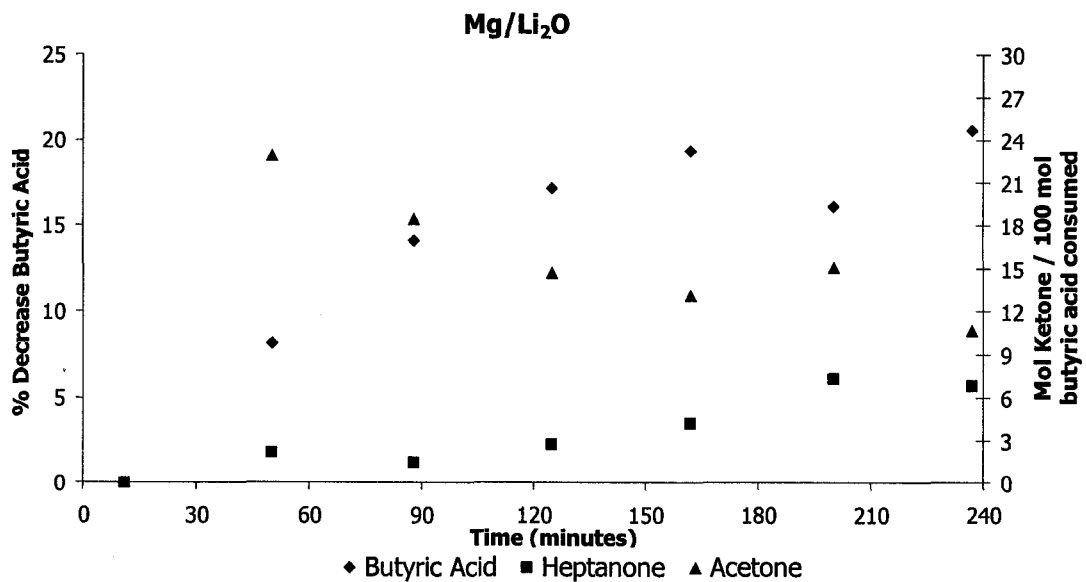
Figure F-11: CaCO₃ prepared by precipitation with a WHSV = 0.1597 h⁻¹

CaCO₃ (precipitation)

◆ Butyric Acid   ■ Heptanone   ▲ Acetone
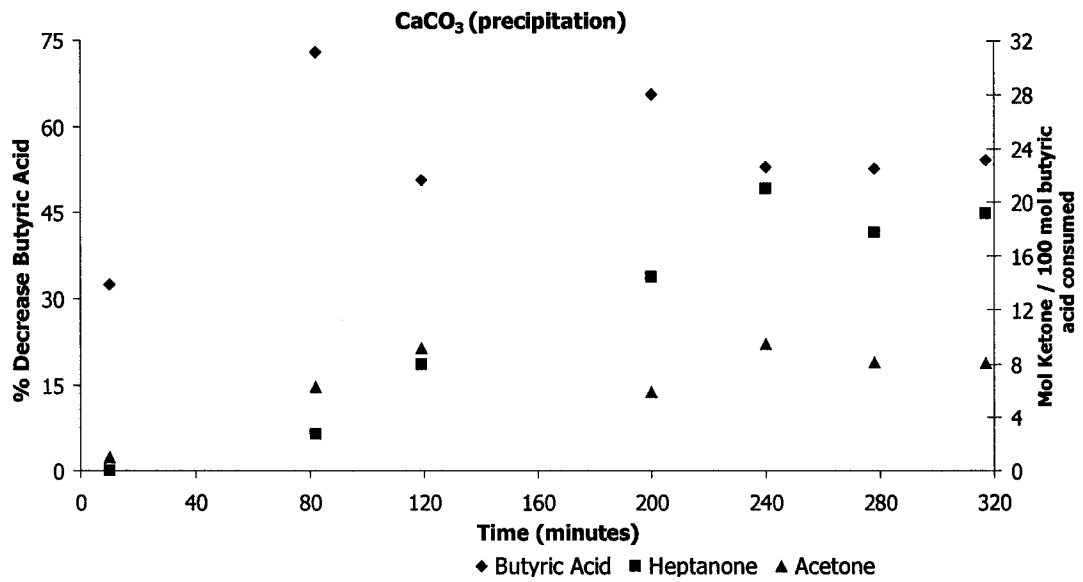
Figure F-12: CaCO₃ prepared by thermal decomposition of acetate with a WHSV = 0.1442 h⁻¹

CaCO₃ (acetate)

◆ Butyric Acid   ■ Heptanone   ▲ Acetone

147
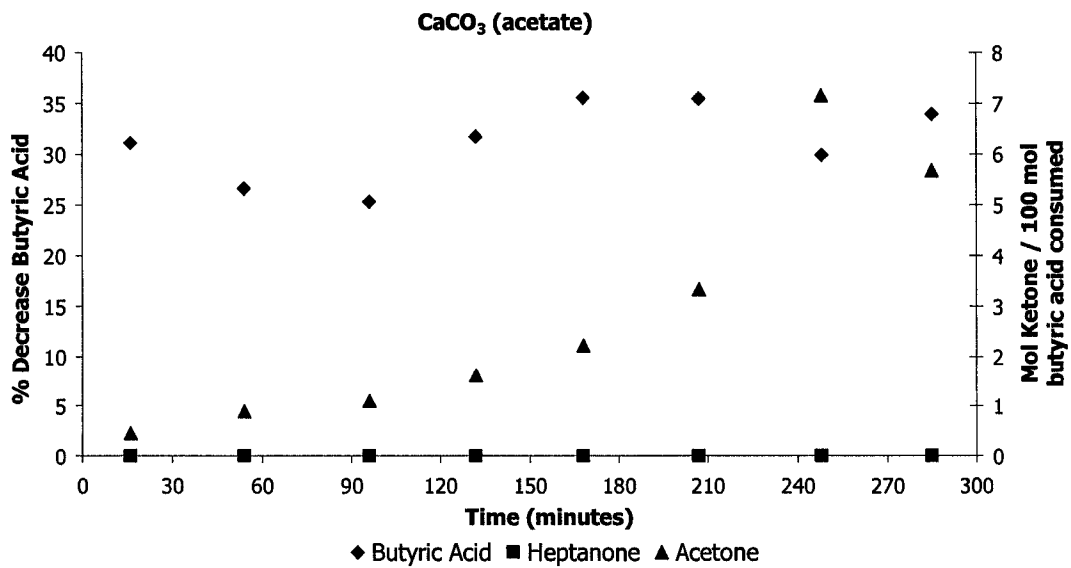
Figure F-13: Ca/Li$_2$CO$_3$ prepared by thermal decomposition of acetate with a WHSV = 0.1394 h^{-1}

Ca/Li$_2$CO$_3$ (acetate)

◆ Butyric Acid ■ Heptanone ▲ Acetone
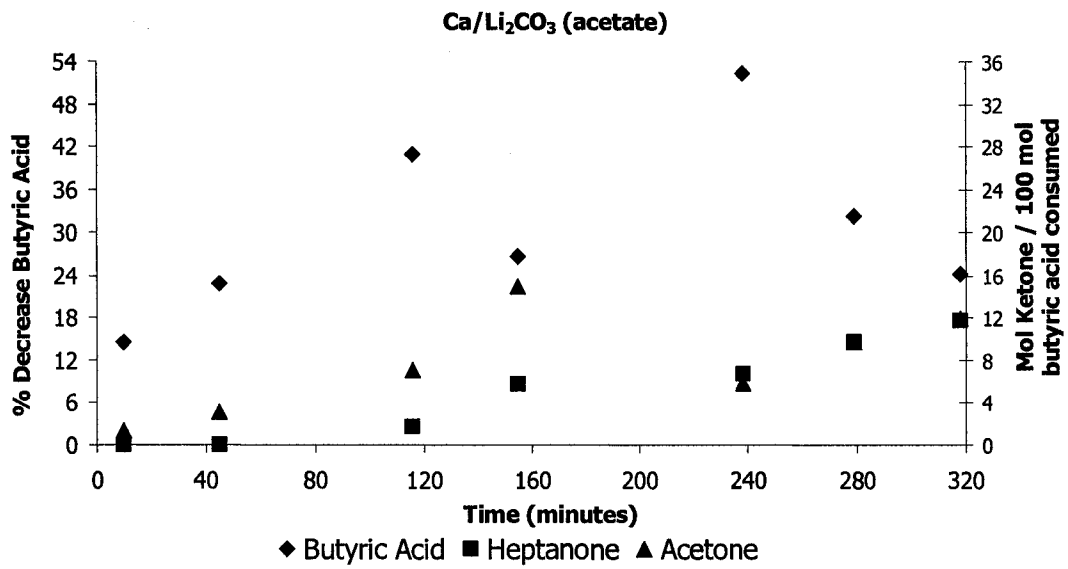
Figure F-14: CaO from precipitated calcium carbonate with a WHSV = 0.1382 h^{-1}

CaO

◆ Butyric Acid ■ Heptanone ▲ Acetone

148
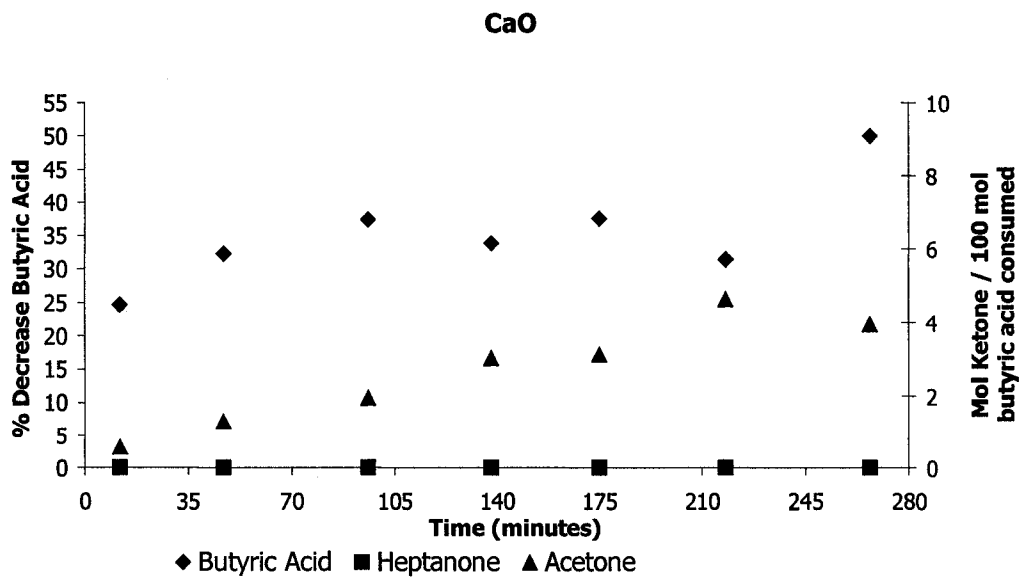
Figure F-15: CaO from $CaCO_3$ prepared from acetate with a WHSV = 0.1852 h^{-1}

CaO (acetate)
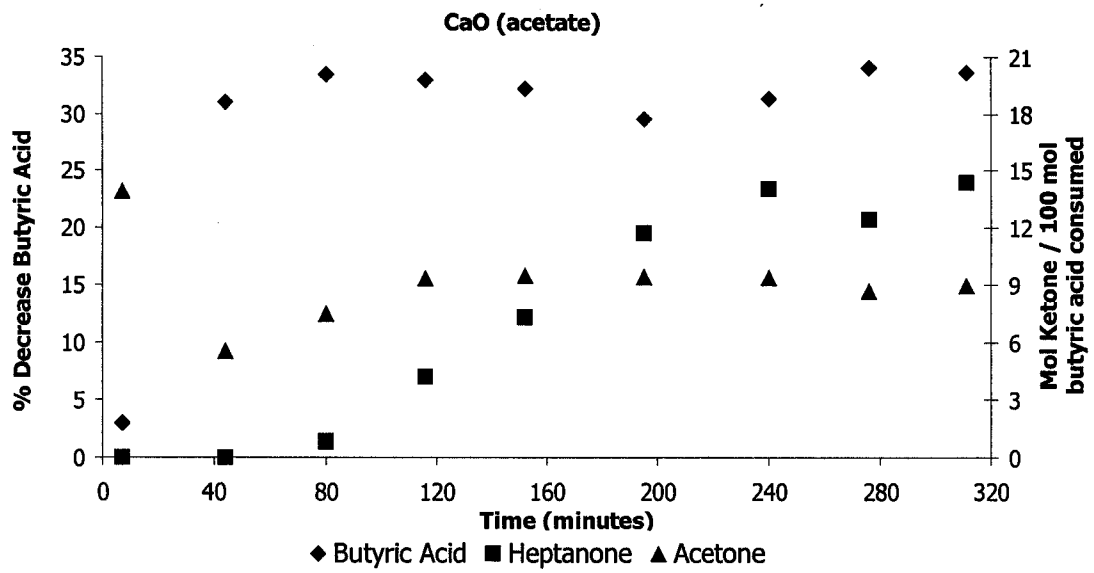
Figure F-16: Ca/Li_2O from Ca/Li_2CO_3 prepared from acetate with a WHSV = 0.1467 h^{-1}

Ca/Li₂O (acetate)

149
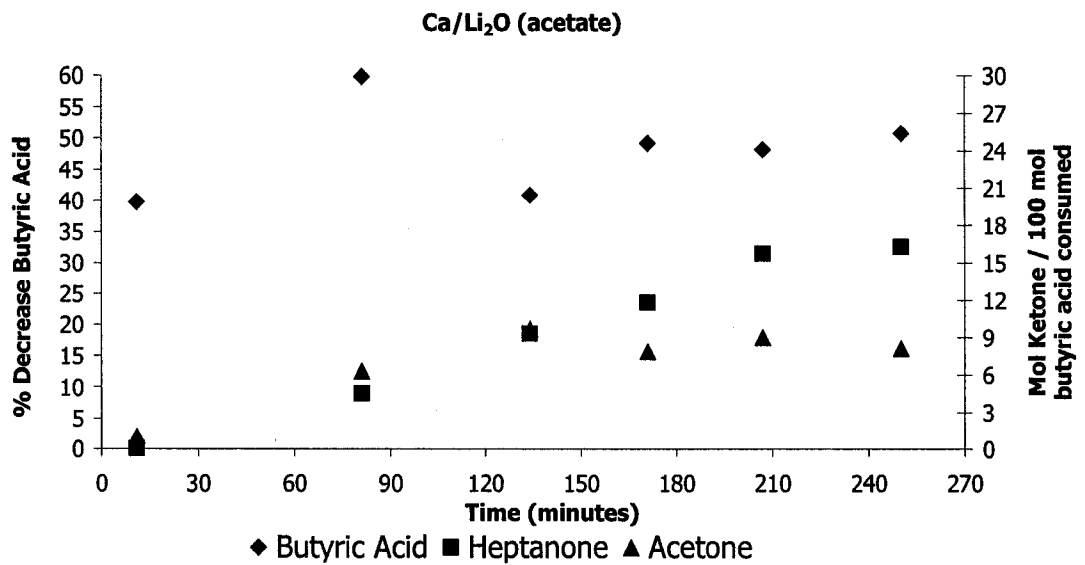
Figure F-17: Commercial precipitated $CaCO_3$ (1) with a WHSV = 0.1126 h^{-1}

PCC (1)

◆ Butyric Acid ■ Heptanone ▲ Acetone
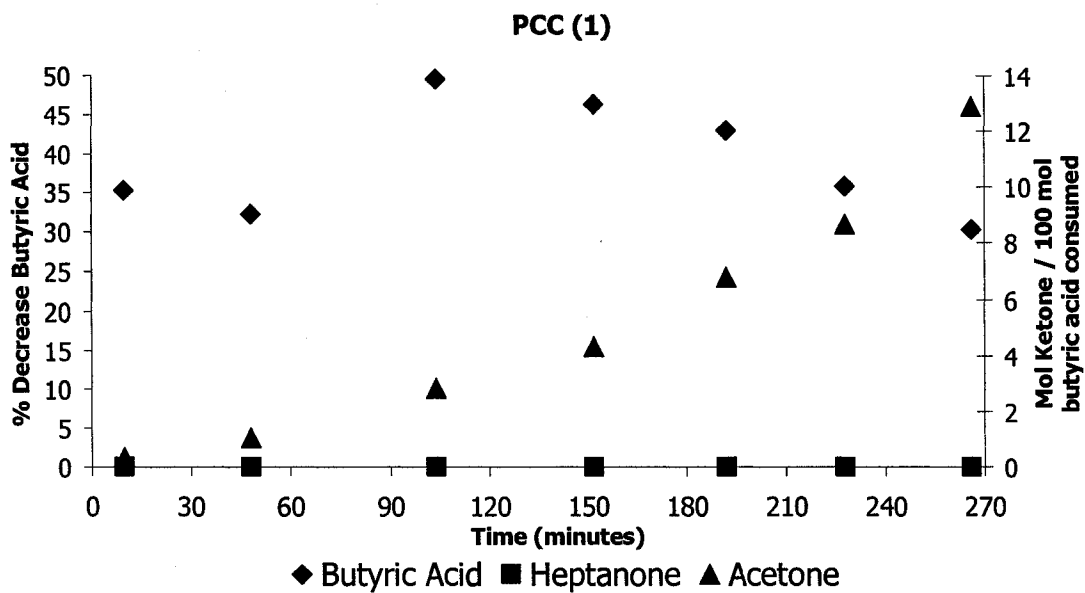
Figure F-18: Commercial precipitated $CaCO_3$ (2) with a WHSV = 0.1453 h^{-1}

PCC (2)

◆ Butyric Acid ■ Heptanone ▲ Acetone

150
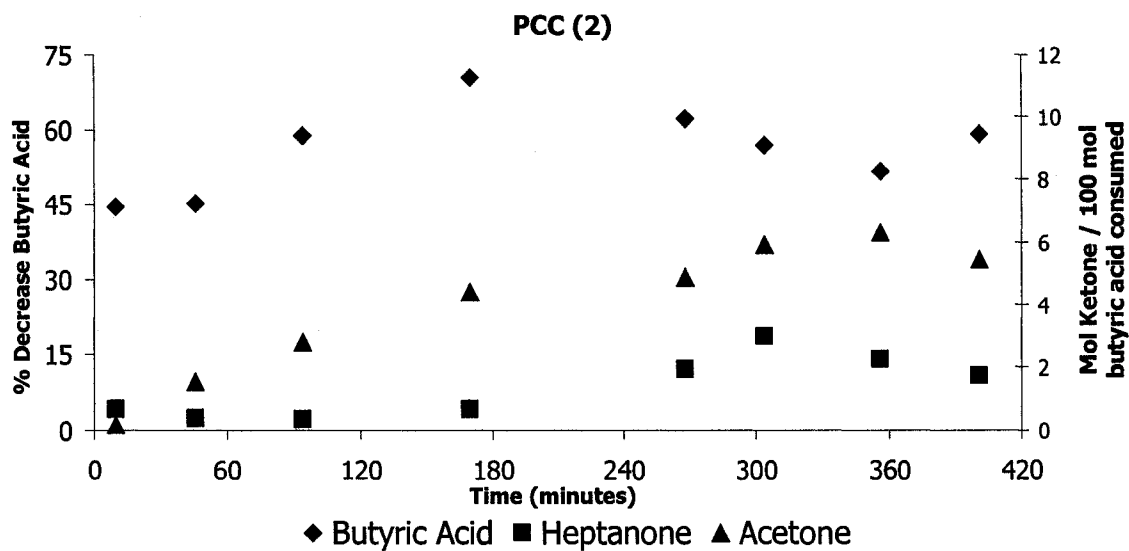
Figure F-19: BaCO₃ prepared by precipitation with a WHSV = 0.1183 h⁻¹

BaCO₃ (precipitation)

◆ Butyric Acid   ■ Heptanone   ▲ Acetone
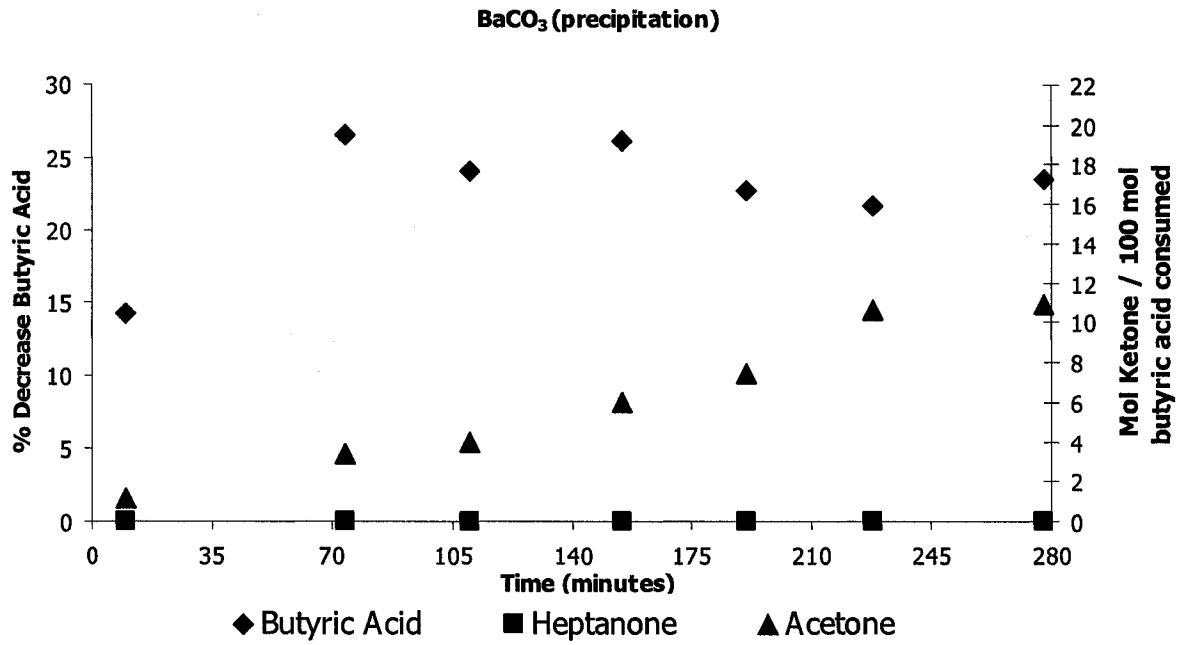
Figure F-20: Ba/Li₂CO₃ prepared by precipitation with a WHSV = 0.1398 h⁻¹

Ba/Li₂CO₃ (precipitation)

◆ Butyric Acid   ■ Heptanone   ▲ Acetone

151
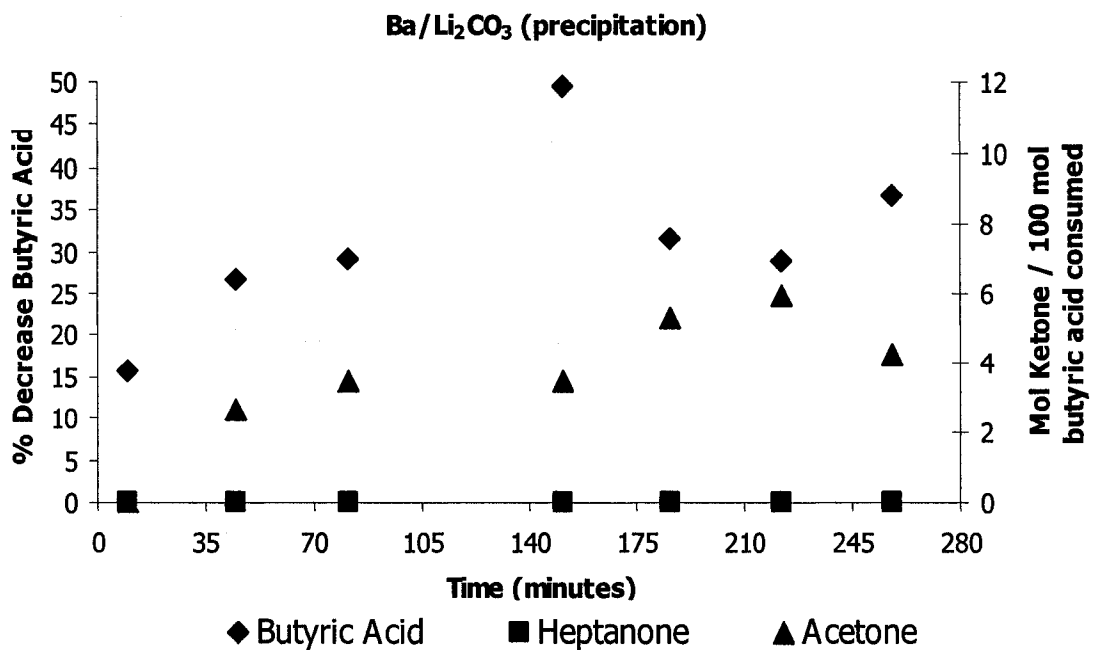
Figure F-21: Na_2CO_3 prepared by precipitation with a WHSV = 0.1631 h^{-1}

Na$_2$CO$_3$

◆ Butyric Acid   ■ Heptanone   ▲ Acetone

152
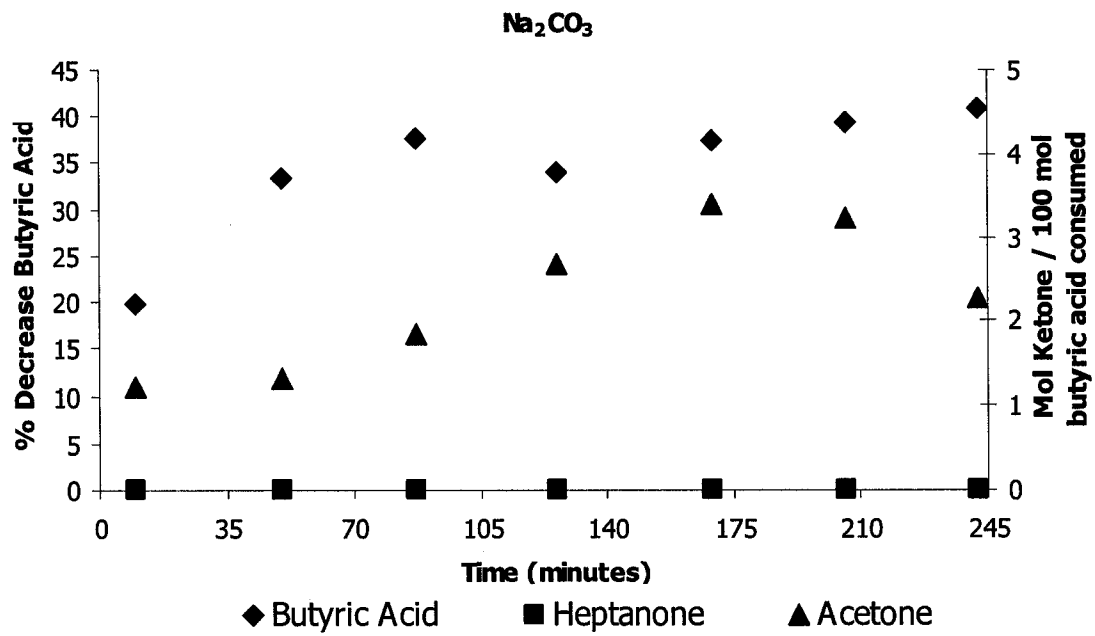
Appendix G

GC-MS Analyses of the Batch Reactor Experiment Products

Figure G.1-1: Chromatogram for the vapour-phase product obtained when the commercial precipitated $CaCO_3$ (2) was tested.
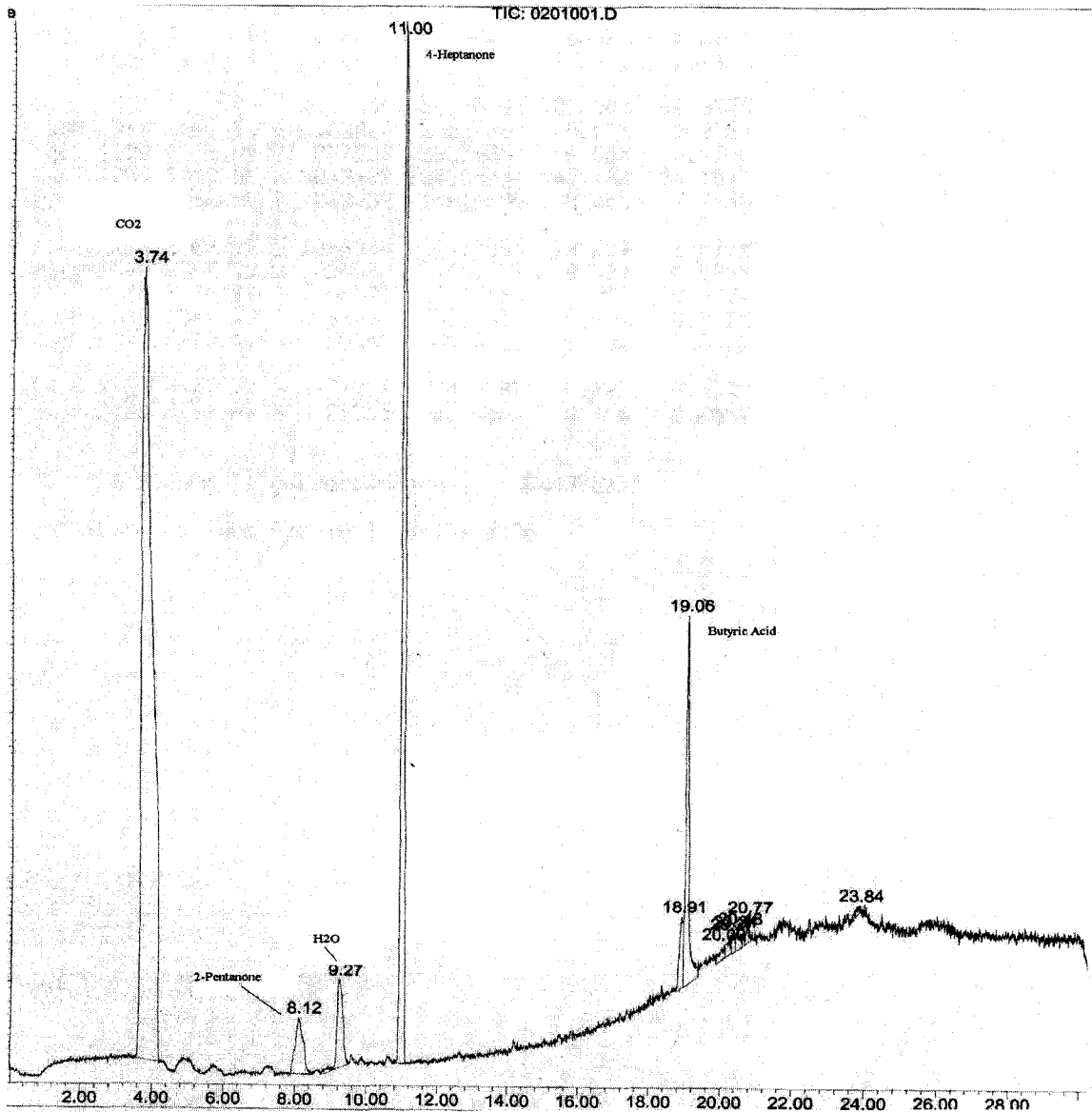
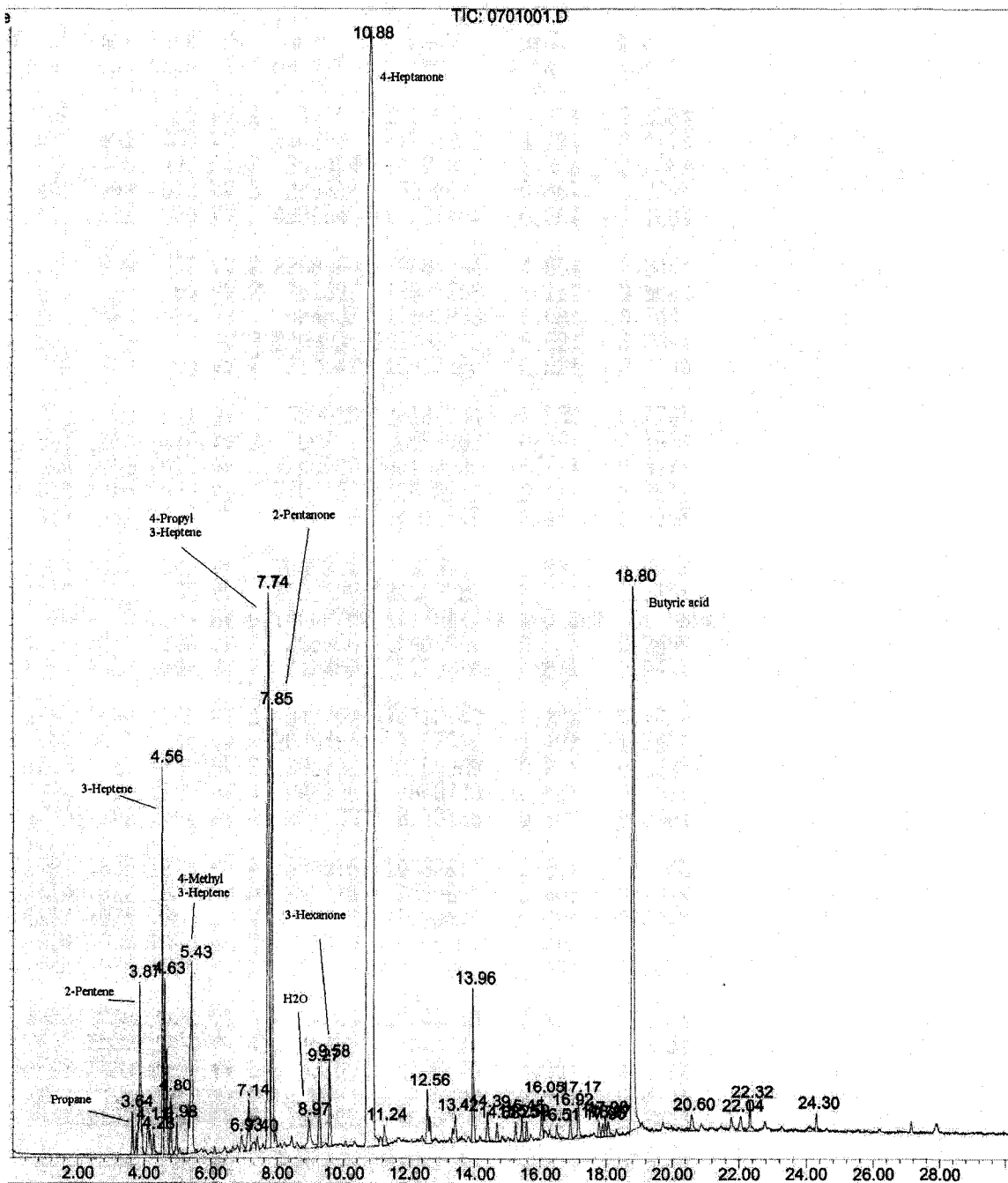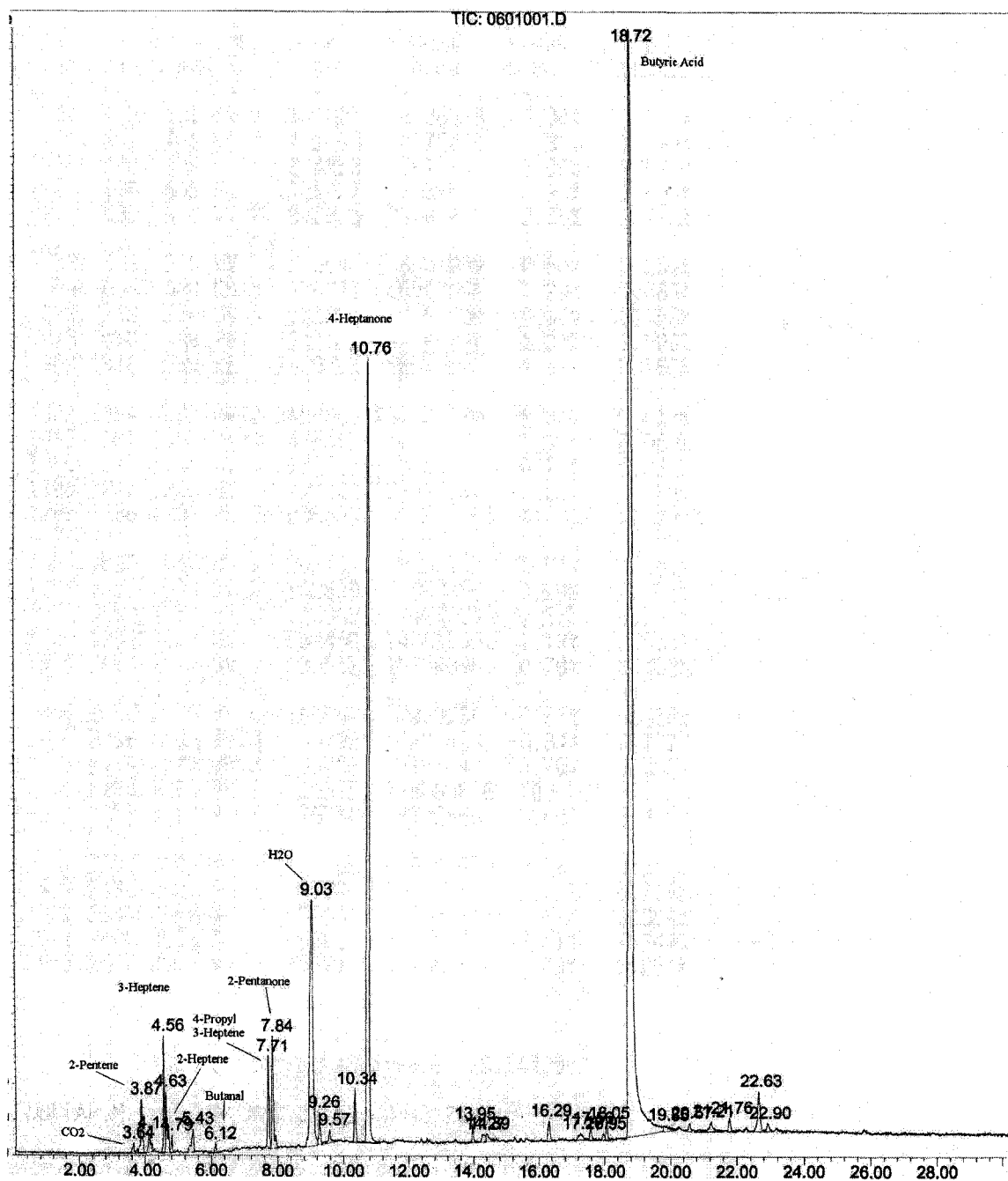**Figure G.1-2:** Chromatogram for the liquid-phase product obtained when the prepared MgO was tested.

154

Figure G.1-3: Chromatogram for the liquid-phase product obtained when the prepared $BaCO_3$ was tested.

155

Appendix H

Commercial Precipitated Calcium Carbonates Used

Figure H-1: Characteristics of the commercial precipitated CaCO₃ (1)

Typical Properties

Particle Shape .... Symmetrical

Median Particle Size, μm 0.7
(Sedigraph 5100)

+325 Mesh Residue, % 0.2
(Dispersed wet sieve)

Specific Gravity 2.7

Dry Brightness (Hunter Y, Rd value) 98

Bulk Density (pounds/ft³) 17
           (grams/cc) 0.27

Tap Density (pounds/ft³) 33
           (grams/cc) 0.53

Oil Absorption (grams/100 grams pigment) 30

Chemical Composition (typical)

Calcium Carbonate	$CaCO_3$	97%
Magnesium Carbonate	$MgCO_3$	2%
Iron as	Fe_2O_3	<0.1%
Moisture	H_2O	0.2%

PARTICLE SIZE DISTRIBUTION
SEDIGRAPH
% BY WEIGHT BELOW - MICRON SIZE

156
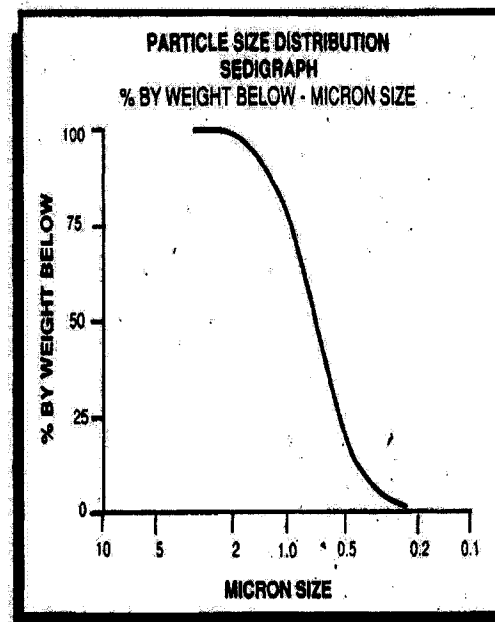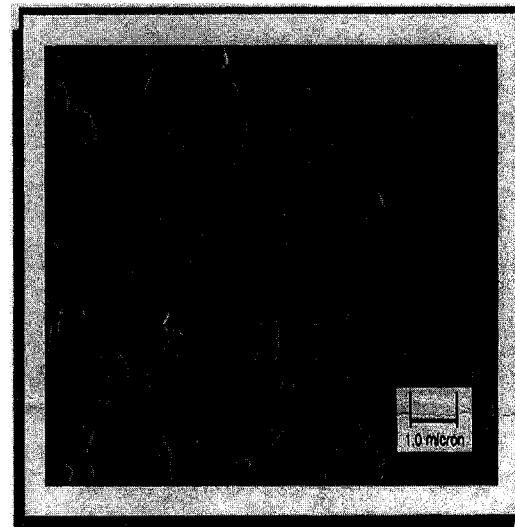
Figure H-2: Characteristics of the commercial precipitated CaCO$_3$ (2)

Typical Properties

Particle Shape .... Rosette

Median Particle Size, μm 1.9
(Sedigraph 5100)

+325 Mesh Residue, % .... <0.05
(Dispersed wet sieve)

Dry Brightness (Hunter Y, Rd value) 98

Einlehner Abrasion, mg 4
(Model AT-1000 at 174,000 rev., brass wire)

Form .... Dry Powder

Surface Area meters²/gram 7

Chemical Composition
(typical)

Calcium Carbonate	CaCO$_3$	97%
Magnesium Carbonate	MgCO$_3$	2%
Iron as	Fe$_2$O$_3$	<0.1%

PARTICLE SIZE DISTRIBUTION

157